Terms and Conditions of Use of Digitised Theses from Trinity College Library Dublin

Copyright statement

All material supplied by Trinity College Library is protected by copyright (under the Copyright and Related Rights Act, 2000 as amended) and other relevant Intellectual Property Rights. By accessing and using a Digitised Thesis from Trinity College Library you acknowledge that all Intellectual Property Rights in any Works supplied are the sole and exclusive property of the copyright and/or other IPR holder. Specific copyright holders may not be explicitly identified. Use of materials from other sources within a thesis should not be construed as a claim over them.

A non-exclusive, non-transferable licence is hereby granted to those using or reproducing, in whole or in part, the material for valid purposes, providing the copyright owners are acknowledged using the normal conventions. Where specific permission to use material is required, this is identified and such permission must be sought from the copyright holder or agency cited.

Liability statement

By using a Digitised Thesis, I accept that Trinity College Dublin bears no legal responsibility for the accuracy, legality or comprehensiveness of materials contained within the thesis, and that Trinity College Dublin accepts no liability for indirect, consequential, or incidental, damages or losses arising from use of the thesis for whatever reason. Information located in a thesis may be subject to specific use constraints, details of which may not be explicitly described. It is the responsibility of potential and actual users to be aware of such constraints and to abide by them. By making use of material from a digitised thesis, you accept these copyright and disclaimer provisions. Where it is brought to the attention of Trinity College Library that there may be a breach of copyright or other restraint, it is the policy to withdraw or take down access to a thesis while the issue is being resolved.

Access Agreement

By using a Digitised Thesis from Trinity College Library you are bound by the following Terms & Conditions. Please read them carefully.

I have read and I understand the following statement: All material supplied via a Digitised Thesis from Trinity College Library is protected by copyright and other intellectual property rights, and duplication or sale of all or part of any of a thesis is not permitted, except that material may be duplicated by you for your research use or for educational purposes in electronic or print form providing the copyright owners are acknowledged using the normal conventions. You must obtain permission for any other use. Electronic or print copies may not be offered, whether for sale or otherwise to anyone. This copy has been supplied on the understanding that it is copyright material and that no quotation from the thesis may be published without proper acknowledgement.

2007

TRINITY COLLEGE DUBLIN

THE USE OF COUNTER-MOMENTS

FOR

STEEL BEAM STRENGTHENING

Ph. D.

SUPERVISOR: DR. R. P. WEST

STUDENT: IAN EDWARD MAHER
STUDENT NUMBER: 98153421 2 CN

Declaration

I hereby declare that this thesis has not been submitted as an exercise for a degree at this or any other University and that it is entirely my own work. I understand and agree that the Library may lend or copy the thesis upon request.

Signed Ian Mabbs

Date 7/11/07

ACKNOWLEDGEMENTS

I thank Dr. West, my supervisor, for his contribution, direction and support throughout this research. I also thank my follow researchers and departmental staff for their support and advice. My thanks to my wife Bernie, and my family for their support.

Abstract

Many methods exist for the repair and strengthening of beams. With increasing traffic volumes and axle weights, the demand for performance of highway structures has increased. In new construction the demand optimised structural members is increasing. This research has examined a method of strengthening steel beams with a view to new construction rather than the repair of existing beams, however, the method researched could also be employed in retrospective repair.

A simply supported steel beam with a 6m simply supported span and a central concentrated load was used to used to explore a method of strengthening, which involves using external tendons to apply specific counter-moments (moment opposite to those induced by loading) at specific optimum locations along the length of the span to minimise the final bending moment diagram.

A steel beam was used to test two different tendon configurations. The first tendon configuration, which was contained within the overall depth of the beam, was not efficient and displayed slight improvement (that is 5%) in load capacity when compared to the same un-strengthened beam. The second tendon configuration tested increased the overall beam depth by 12% and was a more efficient tendon system. The load capacity of the beam with the second tendon configuration was 48% greater than the capacity of the un-strengthened beam.

CONTENTS

CHAPTER 1

INTRODUCTION

Many methods exist to strengthen structural members by retrofitting to facilitate increased loading or to repair deteriorated members. This research investigated a method of strengthening that could be used for structural upgrading or for employment in new construction, where there is an increasing demand for lighter, stronger and more efficient members. The principal objective of the research was to establish a method of strengthening a beam, of reduced depth, to carry the same loading as that which a deeper un-strengthened beam could carry, with the same span and support conditions. Providing a strengthened beam of less depth to do the work of a deeper beam would have significant cost implications, particularly now with multi-storey construction.

Many structures nowadays are constructed with a pre-fabricated facade fixed to a steel or concrete frame. Expensive finishes, such as polished natural stone, are often used with the facade pre-cast units and any design modification which reduces the building height will have a consequential benefit in reduced façade costs. Planning laws often impose height restrictions, particularly in urban areas, where living and business space is at a premium.

Previous research has been carried out, on which this current research is based, in an undergraduate project (Maher 1998). The project was primarily involved with proving the concept of using external tendons to apply "counter–moments", or moments opposite to those induced by loading, for beam improvement. The tendons were attached to levers welded to the underside of a model beam and stressed to apply concentrated moments at specific locations and of a specific magnitude such that the loaded bending moment diagram is optimised (minimised).

1.1 Objectives

The main objective of this research is to investigate the potential of using tensioned external tendons in steel beams to improve the efficiency of performance, specifically to use pre-applied moments and self-counter moments to enhance the capacity of the beam or to reduce the overall depth of the beam while maintaining the original (deeper) beam capacity. The beam depth reduction would serve to reduce construction cost in expensive facades. Alternatively, an additional story could be added without increasing the overall height of the building, provided a sufficient number of storeys were proposed for a given structure (or the order of 10 storeys), by reducing the overall height from floor to floor by the beam depth reduction. Another objective was to establish equations that would allow design charts to be developed for the strengthening system.

1.2 Methodology

Equations for the optimum counter-moment (applied moments via pre-stressed tendons opposite to loading) for various loads and beam supports conditions were established. FE analyses were carried out for both configurations described earlier and laboratory testing was carried out to verify both configurations.

To verify the proposed design in this research, a structural configuration was derived to achieve overall beam depth minimisation. Two tendon configurations were tested; the first had a tendon and lever configuration contained within the flanges of the beam (that is, with levers attached to the underside of the upper flange); the second had tendons attached directly to the underside of the bottom flange. The first tendon configuration had at least the same capacity as a beam over twice as deep (for the same span and support conditions) with a significant improvement in deflection. The second configuration had a greater capacity and less deflection than the earlier configuration and proved to be a more efficient system.

1.3 Layout of thesis

Chapter 2 examines the methods for the repair and strengthening of beams. Two main types of strengthening have been reviewed with this research. External plates bonded to concrete members and steel plates welded or bonded to a steel member constitute the first main type of repair reviewed. Plate bonding is used to upgrade the ultimate capacity of an existing member to accommodate loading in excess of original design loading or to repair structural members. Secondly, applying internal and external tendons to beams are also investigated. Internal tendons are discussed and this application is primarily involved with new construction (that is, tendons inserted into ducts, which are pre-cast into members). External tendons are examined both for tendons fitted retrospectively to upgrade the ultimate strength of members and external tendons applied to new construction. External tendons are becoming increasingly popular due to ease of access for long term maintenance and ease of fitting. .

The theory developed in the previous research by the author will also be presented in chapter 3. Equations for the magnitude and location of counter-moments applied to a simply supported beam with central concentrated load will be given. The equations will cover the cases for single or multiple pairs of counter-moments applied to a beam with simple supports. The theory was also expanded in to cover beams with counter-moments applied to fixed end beams with a central concentrated load. Multiple counter-moments applied to beams with a central concentrated load and asymmetrical loading and two span continuous beams with a central concentrated load on each span will also be covered. The resulting bending moment diagram in the un-strengthened two-span case has typically three peaks, one at each central concentrated load application and a peak over the mid support. One pair of counter moments were applied for each peak resulting in six counter moments being applied to the two-span continuous beam.

A parametric study will be discussed in chapter 3. Expressions will be developed for P_i, the initial tendon force, r_t, the rate of tendon force increase due to applied beam load and W, the maximum load that can be applied. The study will established the influence of, P_i,

and r_t , on the maximum load that can be applied. The study examined the implicit nature of the expressions and established the sensitivity of a variable contained with the expressions with regard to member load bearing capacity.

A finite element model for the test beam with both tendon configurations is discussed in chapter 4. Tetrahedral elements were found to model the solid flange and web plate elements closely with predicted results being within 1% error of those recorded in the test laboratory. The elements used to model the tendons had a provision to specify an initial strain, which was used to model the applied tendon forces.

Chapter 5 examines the predictions of linear FE analyses for both the earlier and the revised tendon configurations. The FE predictions and the derived equations (chapter 3) will be shown to compare closely in chapter 5.

Chapter 6 will discuss the predictions of non-linear FE analyses of the revised tendon configuration together with other methods of strengthening for similar beams. The ultimate load and mode of failure will be established for the various methods.

Chapter 7 will present the results of laboratory testing of both tendon configurations considered in the FE analyses. The findings from the laboratory testing of the beam with the revised horizontal tendon configuration will also be considered in chapter 7. The results of the testing compare closely to the predicted values from the finite element analyses (that is, no greater than 3% difference).

Chapter 8 covers the conclusions of the work on the test beam and recommendations.

CHAPTER 2

CURRENT METHODS FOR BEAM STRENGTHENING AND REPAIR

As growth in commercial and domestic traffic increases, so too does the demand on the infrastructure to convey the traffic. With increasing traffic volumes and axle loadings it is often necessary to upgrade existing beam members with bridge construction. Inferior traffic bridge strength is a major problem in the U.S. Bridges built in the 1950's during the construction of the U.S. interstate highway system are now approaching the end of their design life. A study carried out on the interstate system found that nearly 300,000 bridges were sub-standard (Ritter 1990). Many methods exist either to repair weakened members to withstand existing loads or to strengthen members to accommodate additional loading.

Similarly, in this respect, the demand for city and large town premium office space and residential space has imposed a demand on many existing buildings to accommodate loads that are greater than the loads for which the buildings were initially designed. On change of ownership, it is not uncommon for additional load-carrying capacity to be sought, giving rise to a need for strengthening of structural elements. There are two principal methods of structural strengthening and/or repair, namely, steel or CFRP (Carbon Fibre Reinforced Polymers) plates externally bonded to the surfaces of members for flexural and shear strengthening, or external tendons retrofitted to increase member capacity. These two main areas of repair and/or strengthening will be reviewed.

In general, the external plate method is associated with the repair of deteriorated members but may also be used to upgrade the load capacity of members. Internal tendons are, in almost all cases, associated with new construction rather than retrospective repair or strengthening but will be discussed briefly. The external tendon application is used to increase the capacity of members due to increased working loads, deficiencies in design or structural deterioration.

2.1 Plates Bonded to Structural Members

This method of repair involves the process of bonding plates of high tensile strength to locations on steel or concrete members where greater tensile or flexural resistance is required. This greater requirement for resistance may be due to, for example, deteriorated tensile reinforcement or greater applied loading. It may also be necessary to provide additional shear capacity for beams requiring flexural strengthening. The additional shear strength, provided via external plates bonded to the webs of beams, will also be discussed later in this chapter.

2.1.1 Steel plates fixed to steel members

Plate girders have been used for well over a century. The principle is to increase the second moment of area ("I" value) to accommodate the increasing bending moment along the span. This, however, was usually a method of construction rather than for retrofitted strengthening plates. Fixing steel plates to steel members nowadays almost always involves a method to either upgrade existing sound members, as is often the case for bridge construction, or to increase the fatigue strength of members exposed to the cyclic loading of traffic. Strengthening steel bridge members, which are often composite steel beam/concrete slab members, involves fixing cover plates to the lower face of the bottom flange, partially along the spans in areas of higher stresses (that is, in the mid-third of spans and over supports on the top flange in continuous beams). However, cover plates bolted or welded to the flanges of beams under cyclic loading have sometimes been found to fail prematurely. Research carried out (Miki et al. 1997) on the long-term flexural behaviour of cover plates under cyclic loading demonstrated that cracking typically appeared on welds at the ends of the cover plates and then propagate into the web at a location above the ends of the cover plate.

Research has also been carried out (Albrecht 1988) into the behaviour of steel beam strengthened with steel plates epoxy bonded to their tension faces. A comparative study was carried out on plates bonded to the tension flange of steel beams (with high strength

bolting at the plate ends to prevent de-bonding) as against welding the same plate to the tension flange with particular regard to the fatigue strength. Eighteen specimens of 101x356x43kg/m universal beam (UB) with and without plates attached were fabricated.

This research demonstrated that epoxy adhesives typically have an ultimate strain about 1/20 that of structural grade steel and, unlike steel, cannot deform plastically. The testing found that strengthening plates adhesively bonded to the tension flange of steel beams failed by de-bonding. If the strengthening plates were bolted at either end and adhesively bonded to the tension flange of a steel beam, the fatigue life could be increased by a factor of at least 20 compared to that of conventionally welded plates. The failure mechanism in this case was not due to plate end de-bonding but by crack propagation from the bolt-holes at the plate ends.

Bolting on steel plates is becoming less popular due to the difficulty involved in placing large steel plates onto the underside of steel beams, which can require many personnel and expensive lifting gear. The problem of corrosion exists with steel plate strengthening particularly where the steel is exposed to chlorides, principally as is in the case of highway structures (due to de-icing salts) in the US and UK.

2.1.2 Carbon Fibre Reinforced Polymer (CFRP) plates bonded to steel beams

The use of CFRP plates has become an increasingly popular method of strengthening beams. Highway bridges will, as traffic loading increases, require upgrading or strengthening. Tight budgets within local authorities will often require that the bridge upgrading be carried out as quickly as possible and with minimum disruption to traffic. Consequently, CFRP plates are commonly used as a method of strengthening the lower flange of steel/concrete beams used in the construction of highway bridges. Research carried out by the Federal Highway Administration (Hooks and Cooper, 2003) found that the need for speed of repair and minimum disruption to traffic have necessitated the development of non-traditional rehabilitation schemes. These authors found that the use of externally bonded CFRP plates was an ideal solution and gave minimum traffic

disruption. The method was also preferable for ease of fixing (that is, the light sheets could easily be placed on the beam soffit) and provided a quick method to improve flexural and fatigue strength of the bridge girders.

For example, Research carried on the rehabilitation of a bridge (Bridge 119) on behalf of the Delaware Department of Transport involved applying CFRP plates to the lower face of the bottom flange of steel girders along the length of the span (Chajes et al., 2002). The bridge was constructed of two approximately 650mm deep girders, which supported a concrete deck. The concrete decking was replaced with a new deck, which was made to act compositely with the strengthened beams. Non-destructive flexural tests were carried out on the original un-strengthened bridge, which were used as control tests for comparison with the strengthened test. The authors found that with the continued decline in the bridge infrastructure, the importance of advanced composites such as CFRP are increasingly being realised.

Research was carried out on a bridge strengthening project on behalf of the Iowa Department of Transportation with CFRP bonded plates (Phares et al., 2000). The bridge was a continuous three-span structure approximately 50m long in total with a 20m central span. The deck width was approximately 10m and it was supported by 6 deep beams, two outer beams 270mm wide by 840mm deep, two inner beams 270mm by 910mm deep and two other beams 270mm wide by 980mm deep (see figure 2.1). The bridge was originally a non-composite structure. A continuous unidirectional carbon fibre was employed for this strengthening project. The Ultra High Modulus (UHM) plates were selected for their non-corrosive characteristics, ease of application and high tensile strength properties. The tensile properties are given in table 2.1, which is reproduced from the above publication. The plates were bonded to the underside of the lower flange of the beams using a high strength epoxy resin to transfer high forces to the carbon fibre plates. The plates were located in the sagging moment regions of every beam in all three spans. The surfaces of the beams to which the plates were to be bonded were prepared by sanding and shot-blasting and, finally, with a primer was applied.

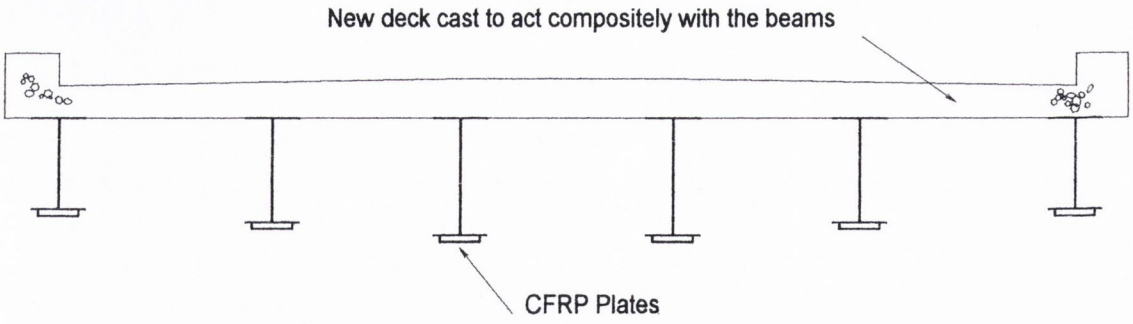

Cross-section of beam deck

Figure 2.1: A cross-section of the bridge decking with the CFRP plates bonded to the underside of the lower flange of the beams.

Ultimate tensile stress	Modulus of elasticity	Ultimate strain
1030MPa	137.7GPa	1.50%

Table 2.1: The properties of the CFRP used for the beam strengthening

When compared with an original un-strengthened control test, the bridge displayed an improvement in flexural performance with a reduction in working stresses. A 20 tonne truck was used to test the bridge and it was found that an improvement of 5-10% existed in the load carrying capacity of the bridge.

A railway bridge at North Harrow in London was assessed by London Underground LTD (Under-bridge assessment, 1984) and was found to be under the strength required to resist the loading of mainline trains, which the bridge carried in addition to underground trains. Originally, a method of welding steel cover plates was proposed. The final chosen method of strengthening was bonded CFRP plates attached to the underside of the lower flanges of the railway bridge. This method (Dodds, 2003) was chosen for the material's high strength (1030MPa) and low self-weight (1660kg/m^3), the ease of installation when

compared to the heavier steel cover plates and the ability to carry out the refurbishment with little or no interruption to the rail traffic.

The bridge is constructed from two main edge beam girders of 2.45m depth, which are simply supported. Cross-beams of approximately 690mm depth run from each of the main beams at 2.25m centres and are fixed just above the lower flange of the main outer beams. Secondry beams supported by the 690mm deep cross-beams and running parallel to the main outer edge beams are 250mm deep and fixed at 760mm centres. The 250mm deep beams are cast into the concrete beam decking and provide horizontal restraint to the structure. Figure 2.2 shows the two different sets of CFRP plates applied to the bridge beams

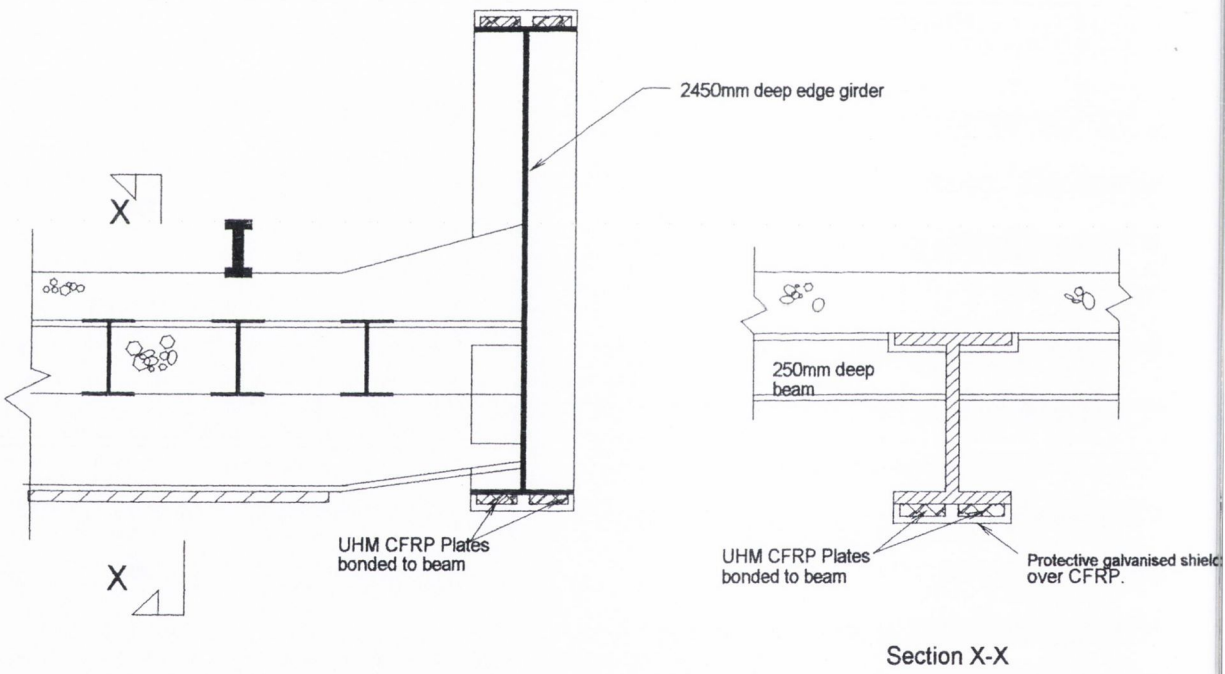

Figure 2.2: The UHM CFRP plates bonded to the bridge beams with the protective galvanised plates in place (Dodds 2003).

The problem of peeling associated with bonded CFRP plates was overcome by allowing the plates to run past the required length and to taper the end of the plate for the overrun length (3.5m for the main outer girders and 1.5m for the 690mm deep cross-beams). Given that the modulus of the CFRP is higher than that of the steel girders stress induced by flexure will give rise to stresses 1.7 times greater in the CFRP than the stresses in the beam. However, as is the case with most retrofitted plates, the dead load is already applied to the structure and it is only the additional live load stresses that need be considered for the above stress differential problem. The UHM CFRP has a characteristic tensile stress of 1030MPa and a characteristic compressive strength of one-third this value. The design stresses were all kept to within 40% of these tensile and compressive values. The clearance under the bridge, which is exposed to vehicular and pedestrian traffic, was reduced by 40mm with the strengthening process. This loss of head room was reclaimed by planing and resurfacing the road below. Galvanised metal sheet protection was provided for the CFRP along the underside of the main outer edge beams and the 690mm cross-beams to prevent damage against vehicle impact.

When members are strengthened with CFRP plates, the beneficial counter-moment is applied throughout the length of the plate either by pre-stressing and/or loading. The proposed method of strengthening in this thesis requires concentrated moments to be applied at specific locations (which was found to a more efficient method and is discussed in chapter 3) and is impossible to achieve with bonded plates due to their dispersive nature.

2.1.3 Steel Plates bonded to concrete members

This method of strengthening involves bonding plates to concrete members in localised areas to relieve stress. The method can be used to upgrade members to accommodate additional loading (or existing loading after fire damage), or to strengthen fatigued members to carry existing loading. The method of bonding steel plates to concrete members is preferred over fixing the steel plate with expanded bolts. When steel plates are bonded chemically, the plate/beam interface is a fully engaged mechanical bond. In

the case of bolting steel plates to concrete R.C. beams, the plate/beam interface is only partially engaged and, thus, the bonding method provides the greater increase in strength and stiffness to the member.

Research has been carried out (Zarnic et al., 1999) on the modes of failure of R.C. members with steel bonded plates. Four point bending test were carried out on RC beams with two different cross-sections. Figure 2.3 shows the four-point configuration together with the cross-sections of the beams tested. Section type A was a 200mm wide by 300mm deep RC beam with reinforcement of 0.56% of the total cross-sectional area of the section (more particularly, compressive reinforcement was 226mm^2 and tensile reinforcement was 339mm^2). Section type B was 800mm wide by 120mm deep with a total area of reinforcement of 0.4% (with compressive reinforcement of 256mm^2 and tension reinforcement of 384mm^2). Both beam types had the same span of 3.2m. Three beams of each group had steel plates bonded to their tension faces and a control specimen was tested for each beam type without plates attached. The steel plates were 4mm thick and 50mm and 100mm wide for section types A and B respectively. The plates were bonded to the surface of the beams with a 2mm layer of epoxy resin. The surfaces were prepared using sand-paper to provide a good key for the epoxy resin.

The testing showed that failure did not occur due to concrete crushing or steel plate rupture but, in all cases, was due to the loss of composite action due to de-bonding. Two distinct modes of failure due to de-bonding were identified as follows;

- Mode A de-bonding at some intermediate point between the applied load location and the steel plate end in a zone of cracked concrete.

- Mode B de-bonding at the plate end where the concrete was not cracked.

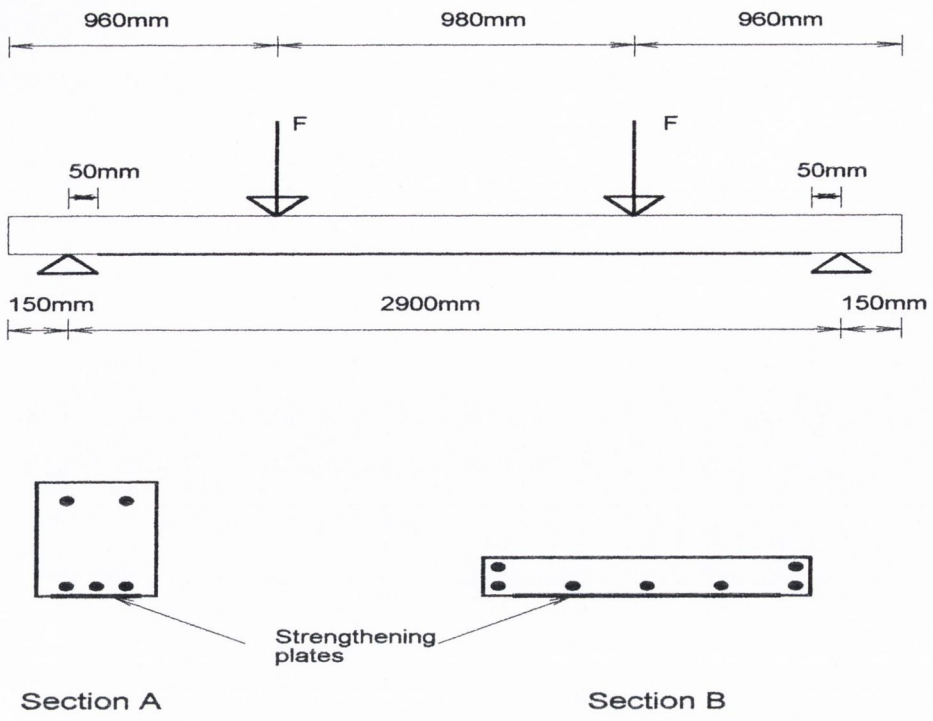

Figure 2.3: The four-point loading configuration and the psections of the two steel plated beams tested (Zarnic et al., 1999)

The researcher concluded that mode failure type A can be attributed to localized bond peak stresses that typically occur around cracks in tensile concrete areas with plates bonded to them. Mode failure type B occurs in the un-cracked zone of the concrete when the bond stress increases at the plate ends due to yielding and de-bonding of the steel plate from the mid-span outwards. The testing also demonstrated that RC beams strengthened with bonded steel plates have a ductile response, mainly due to plate and, subsequently, tension reinforcement, yielding. Improvements in ultimate load capacity with this application where of the order of between 25-35% to that of the control test beams.

A common problem with RC beams that are strengthened with bonded steel plates to increase flexural capacity is a deficiency in shear capacity to withstand the increased loading (that is, original design shear capacity is insufficient). Research carried out to investigate the shear strength of RC beams strengthened with bonded steel plates

demonstrated that the desirable ductile performance of a strengthened RC member can be achieved by ensuring that the ultimate shear force capacity of the strengthened member exceeds the shear force induced by the maximum flexural capacity loading (Collotti and Spadea, 2001).

The authors investigated a truss analogy concept to model the shear behaviour of the strengthened beams, which can be described as follows:

- The compression zone was idealised as a chord carrying a force C and the tensile zone was idealised as a chord carrying a force T. The distance between the line of action of the two forces was d, the lever arm (as in the case for RC beam design).
- The beam shear reinforcement is provided by the vertical links closely spaced at the supports.
- A perfectly plastic behaviour of the materials is assumed.
- The external bonded plate on the beam soffit is treated as conventional bar reinforcement, assuming a perfect bond between the concrete and steel plate interface.

A model was developed that could predict the ultimate shear strength of an RC concrete beam with bonded steel plates, thus allowing an investigation into the increase in flexural capacity.

The mode of failure of shear peeling of steel plates bonded to RC beams for flexural strengthening has been researched (Mohamed et al., 2001). Test beams were fabricated without shear links as it was required to have test beams with low shear strength. Earlier research had demonstrated that the shear links do not affect the shear peeling resistance of steel plated beams and also that the shear peeling failure was due to the critical diagonal shear crack close to the supports (Zhang, 1997). Tests were carried out with the beam shown in figure 2.4. Figure 2.5 shows the shear peeling mechanism failure.

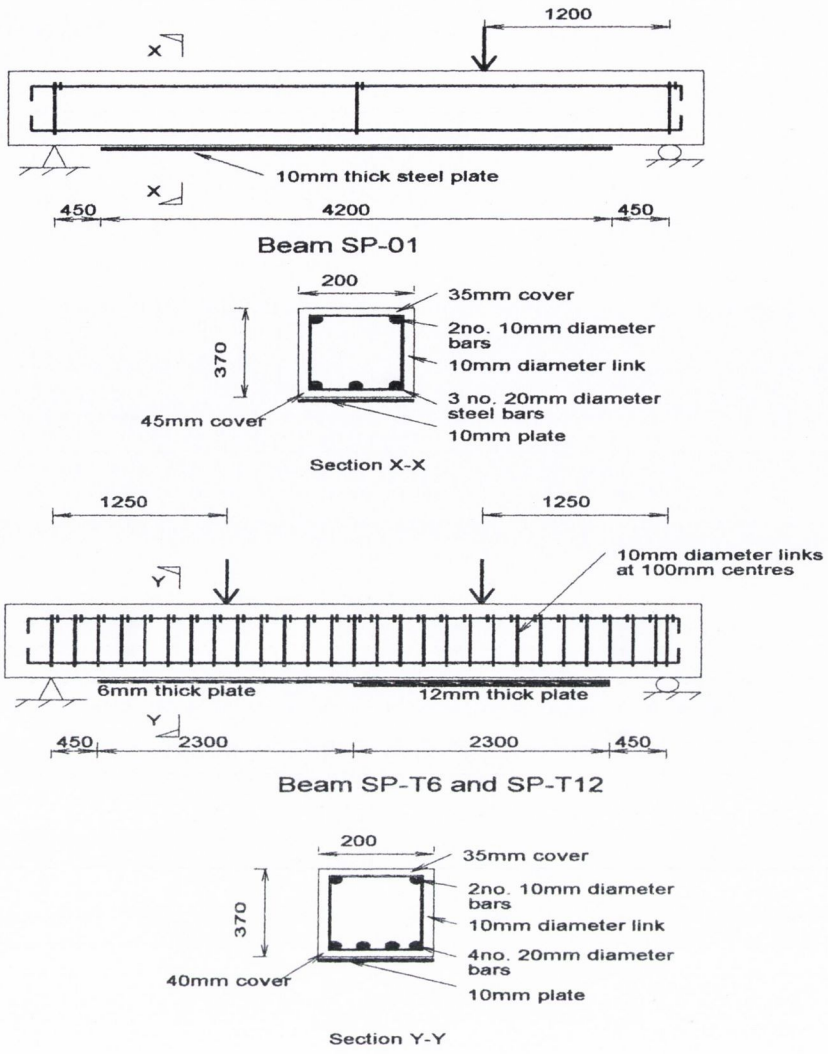

Figure 2.4: The two types of beams tested for shear peeling failure together with the beam sections. (Mohamed et al., 2001)

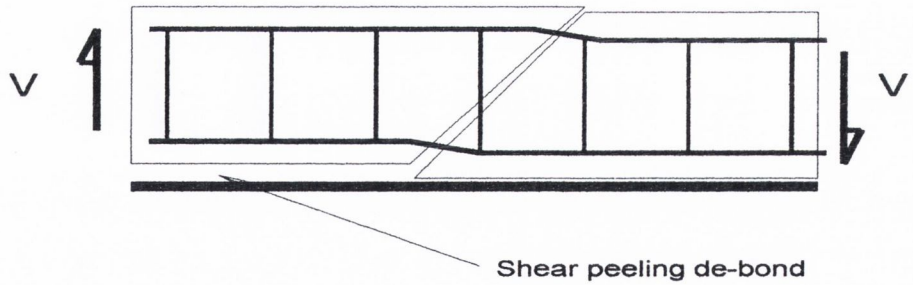

Figure 2.5: The mechanism of shear peeling of steel plates bonded to RC beams for flexural strengthening.

The theoretical shear strength of the un-plated beam was found to be 88.9kN. The shear strength of the plated beam was 63% greater at 140kN. The research demonstrated that plate end peeling due to shear is rapid and is caused by the formation of diagonal cracking close to the plate end and that shear links have a negligible effect in preventing end plate de-bonding due to shear.

Research has been carried out on beams with shear strengthening as well as flexural strengthening (Oehlers et al., 1998). The research investigated steel plates bonded to continuous beams for flexural strengthening. The research proposed a method of increasing the shear capacity of an existing RC beam by bonding steel plates to the webs and to the tension faces. This shear capacity increase would then yield an overall flexural capacity increase greater than in the case where steel plates only were bonded to the tension face of the beam.

Equation 2.1, derived from the research, calculates the maximum moment that would induce a flexure to the beam such that it would not allow plate de-bonding to occur.

$$M_{pure} = \frac{(EI)_{cp} f_b}{0.474 E_p t_{tfp}} \tag{2.1}$$

where,

M_{pure} The maximum moment

EI_{cp}= The flexural rigidity of the cracked section

f_b= The splitting tensile strength of the concrete

E_p= Young's modulus of the steel plate

t_{tfp}= The thickness of the steel plates on the tension face of the beam

0.474 is a coefficient that was derived empirically.

Figure 2.6 shows the configuration of the beams tested . All the beams were 180mm deep by 130mm wide. The plates bonded to the lower tension face of the beams were 5mm thick and the plates bonded to the webs of the beams were 4mm thick. The test beams had a constant steel bar reinforcement of two 16mm diameter high tensile bars for the tension reinforcement in the bottom of the section and two 10mm diameter high

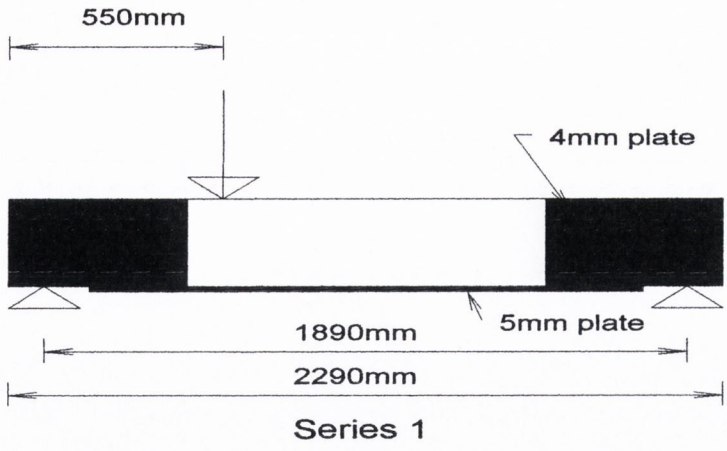

Figure 2.6: The configuration of beams tested with stee; shear and bending plates attached. (Oehlers et al 1998)

tensile bars for compressive reinforcement in the top of the section. The lengths of the shear plates bonded to the webs of the beam were varied in the tests. The Young's moduli for the steel plates were 203GPa and 210GPa respectively for the 4mm and 5mm thick plates. The epoxy resin had a tensile strength of 30MPa and a bond strength of $15N/mm^2$. The testing demonstrated that when the shear plates were increased in length from 90mm to 690mm, the shear capacity increased from 30.8kN to 60.6kN

The research demonstrated that plates bonded to the webs of beams increased the shear capacity, which improved their flexural capacity by preventing premature de-bonding of the flexural strengthening plates. The additional shear capacity that can be produced by the addition of the web shear plates is of the order of between 50-60% which gives rise to a flexural capacity increase of the order of (15-25%) and is a function of the plate length (that is, the bond length) and the plate thickness.

When compared to external tendons, bonded steel plates can significantly increase member self-weight (of the order of 40-60%) whereas a much lesser area of tendons can be used to withstand the same forces (due to higher working stresses); thus, overall self-weight is lower. Unlike the external tendon application examined with this thesis,

existing deflections cannot be restored when using bonded steel plates as pre-stressing is not viable owing to the lower yield stress when compared to tendons.

2.1.4 Carbon fibre reinforced polymer plates (CFRP) bonded to concrete members:

This method of strengthening is now more often used in place of steel plates, to upgrade concrete structural members or to improve their fatigue strength. During the late 1980's the method was researched and developed and in 1991 the first bridge in Switzerland was strengthened with CFRP plates (Meier et al., 1992).

Fibre reinforced polymers (FRP) are composite materials consisting of fibres and a polymer matrix. With civil engineering applications CFRP is mostly used, however, GFRP (Glass Fibre Reinforced Polymer) and AFRP (Aramid Fibre Reinforced Polymer) have been used to a lesser degree. The proportion of fibre and polymer together with the fibre orientation will determine the mechanical properties of the FRP. In general the more fibre present the better the constituent material will perform up to a maximum of 70% (by volume) as too much fibre present will not allow the fibre to be fully covered and bonded by the polymer. With regard to fibre orientation, the best results for tensile strength is to have the fibres aligned in the same direction as the applied tensile force. The material displays poorer properties in directions perpendicular to the fibre direction. The more common polymeric matrixes are epoxy, vinyl ester and polyester.

With most FRP, creep is a common event at higher stress and/or temperatures and research has shown that, provided the working stresses are kept within prescribed manufacturer's levels, creep will not be a significant factor (Busel, 2000). However, comparative research has shown that GFRP and AFRP display a significant decrease in tensile strength when subjected to long-term constant loading while CFRP displayed very little loss in tensile strength (Pisani 1998). In this regard, the CFRP has a great advantage over the other FRP in strengthening applications. The CFRP has very little reaction to the concrete alkaline environment. Previous studies have demonstrated that long-term exposure (more than 3 years) of FRP to concrete results in little ultimate capacity loss

(less than 4%) (Sen et al., 1998). The resistance to the alkaline environment is also based on the polymer matrix used. The authors found that epoxy and vinyl ester matrices performed favourably while the polyester matrix did not provide protection as the ultimate strength was significantly reduced by the alkaline environment (of the order of 25%).

An epoxy resin is applied to the prepared surface of the member upon which carbon fibre reinforced plastic plates are attached and cured. This method has the advantage of using lightweight materials and is often a preferred method of repair, particularly in restricted working spaces. Carbon fibre reinforced plastic plates (CFRP) have a high tensile strength (of the order of 800MPa) and remove the need for thick plates to be bonded on external surfaces. The mechanical properties and freedom from corrosion of carbon fibre reinforced plastic have resulted in its use for many applications.

For example, work has been published on the use of CFRP plates to strengthen RC beams in the refurbishment of the RC members of a swimming pool roof (Brosens et al., 2000). The swimming pool near Kalmthout, in Belgium was constructed in 1974. The roof construction consisted of pre-cast concrete "T" beams over which pre-cast concrete plates were placed and a 110mm thick cast in-situ concrete slab was then poured over the entire roof (see figure 2.7). An inspection of the concrete roof in 1996 showed that the concrete was severely damaged in several locations. The damage was extensive as the concrete roof was covered with a suspended false ceiling and had not come to the attention of the owners for many years. Concrete cover had spalled off and the steel reinforcement was severely corroded. Tests carried out indicated that chloride ingress and concrete carbonation had breached an insufficient cover and induced steel corrosion.

The authors stated that a good understanding of the force distribution is required when designing external plate bonding strengthening retrofits. It is important to fully understand the existing stress distributions in a member before designing an external plate bonding strengthening application. End anchorage must be considered when designing bonded plates as the plate end is a discontinuity where high shear stress

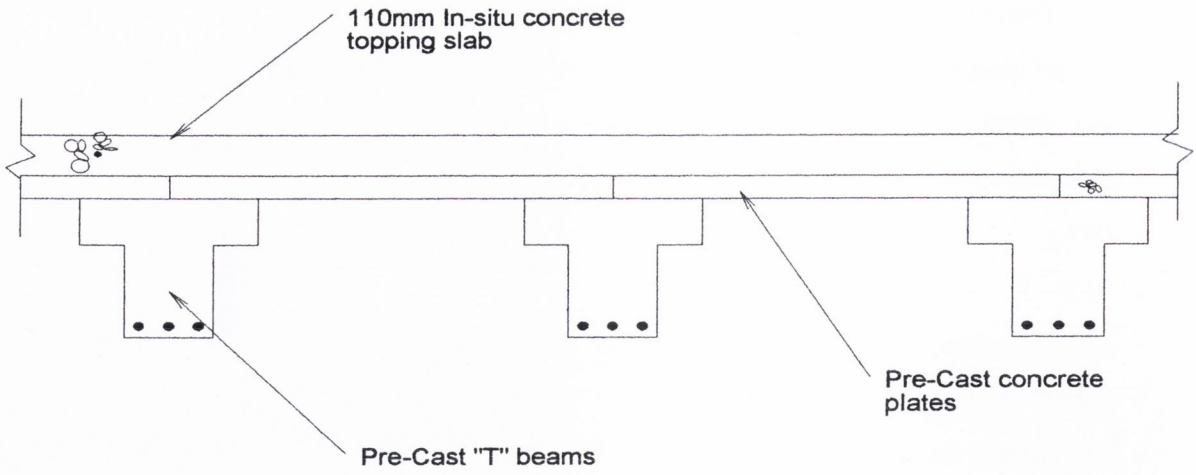

Figure 2.7: The general arrangement of the swimming pool roof. (Brosens et al., 2000)

concentrations can develop, which can give rise to plate end peeling. If provision for adequate anchorage length is not possible, it is suggested that mechanical anchorage should be provided, such as bolting.

Saadatmanesh and Malek (1998) carried out research to develop design guidelines for reinforced concrete beams strengthened with carbon fibre plates. The method employed was to first sandblast the tension face of the beam to be strengthened (in this case the lower face of the beam) to provide a good bond at the plate-concrete interface and then to fix the carbon fibre plate with epoxy resin. The carbon fibre plate improved the strength and stiffness of the RC beams. The strain in the concrete and in the plate at the interface was assumed to be equal and the strain throughout the section was assumed to be linear. as shown in figure 2.8.

With the beams in this research, enough cross-sectional area was provided by the carbon fibre plates to ensure a balanced design, whereby, simultaneous failure of the compression block and the tension reinforcement would occur.

This research found that high local stresses occurred at the "cut off" points at the plate ends close to the supports which needed to be considered in the overall capacity design.

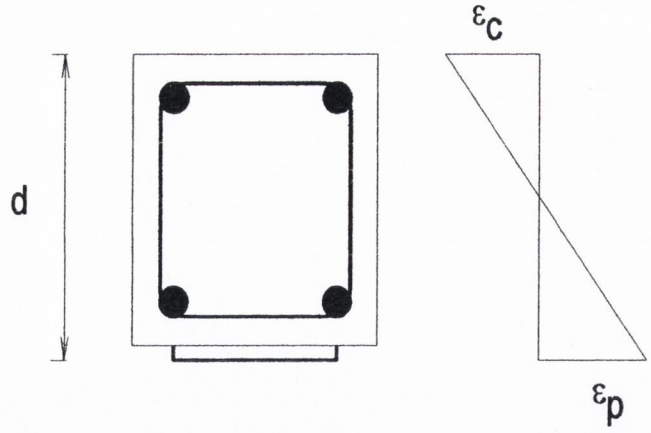

Figure 2.8: The assumed linear strain of the section with the carbon fibre plate attached. (Saadatmanesh et al., 1998)

This problem can be avoided by using large enough dimensions for the bonded plate. The researcher showed that rupture of the plate and concrete crushing were the main modes of failure that needed to be considered in the ultimate strength design calculations. Local failure of the concrete at the plate ends and plate de-bonding due to shear should also be considered. The research demonstrated that the method can improve beam capacity in beams that need to be upgraded to allow for increased loads and for beams with insufficient tension reinforcement due to design errors, omission of reinforcement due to construction error or due to corrosion. The beams tested with the external CFRP flexural strengthening plates displayed a brittle response at failure with a sudden rupture and/or de-bonding of the CFRP plates. It is notable, therefore, that, unlike steel plates which have a ductile failure, the CFRP plates have an undesirable brittle failure.

The problem of possible shear strength deficiency must be also considered for RC beams that have flexural strengthening CFRP plates. Research into the behaviour of RC beams strengthened with both flexural and shear CFRP has been carried out (Li et al., 2001). A beam was tested with flexural and shear strengthening and loading was applied via a four-point bending system shown in figure 2.9. The beams were all 1350mm long by 200mm deep by 130mm wide and reinforced with four 8mm diameter high yield bars (2

top, 2 bottom) and had 6mm diameter links at 150mm centres. The soffit and web plates were attached using a resin.

In figure 2.9, dimension *a* between the two concentrated load is 300mm with the two loads applied symmetrically about the centre of the beams. The beam failed in shear in the typical regions near the supports with a total load, F, of 81kN. The mid-span deflection at failure was 3.1mm. The beam had an improvement in load capacity of the order of 10-20% compared to the un-strengthened beam. Two significant observations can be made with the tests results, as follows:

- RC beams with the same internal steel reinforcement and concrete strength and the same external CFRP plate flexural strengthening will display increasing flexural capacity with increasing external shear CFRP plate reinforcement.

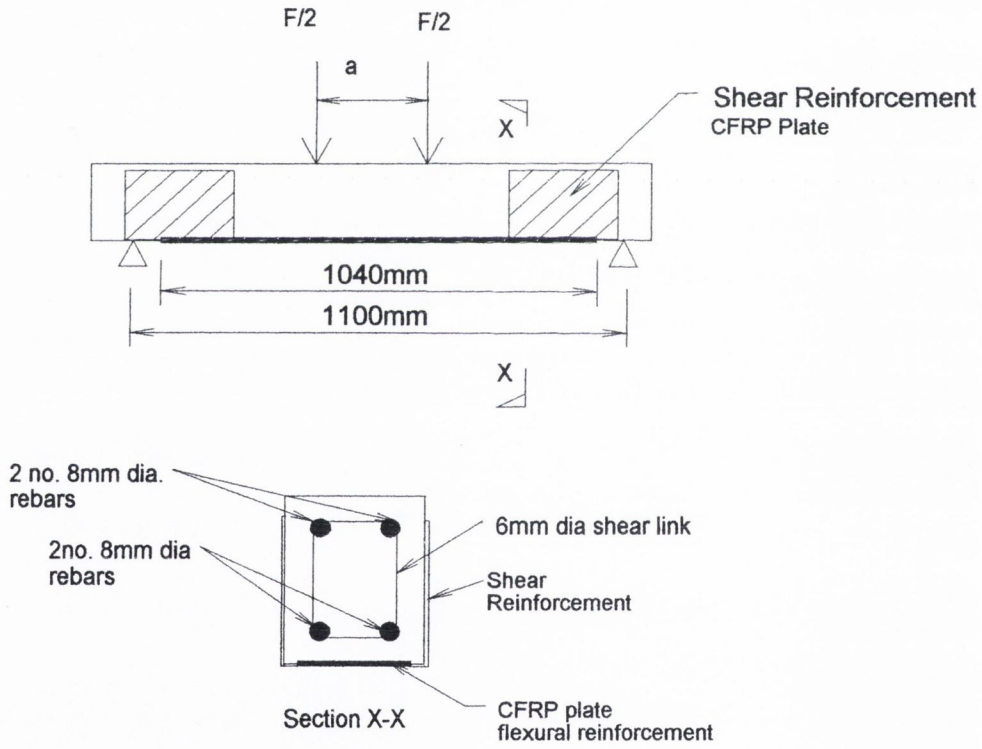

Figure 2.9: The four-point loading system together with a typical test beam section. 25mm minimum cover was provided for all reinforcement. (Li et al., 2001).

- RC beams with the same internal reinforcement and external flexural strengthening will have less mid-span deflection with increasing external shear CFRP plate reinforcement.

However, the testing demonstrated that it is not necessary to cover the entire side faces of the RC beam with shear plating to achieve the maximum flexural strength. A similar beam was tested which had shear plating applied to the beam ends and over the zones of maximum shear force. The maximum loading and deflection were the same for this beam as for the beam with full web plating. The research concluded that, when considering an RC beam for externally bonded CFRP plating for strengthening, it is necessary to consider both flexural and shear strengthening.

Gangarao and Vijay (1998) investigated the bending behaviour of concrete beams with carbon fibre fabric wrapped around and bonded to three faces of the beam (that is, the soffit and two vertical sides). The objectives of the research were to;

- Increase the flexural strength of the beams
- Increase the member stiffness for pre and post yielding stages
- Evaluate failure modes based on wrapping configuration
- Compare theoretical predications with experimental data

The 2.74m span RC beam shown in figure 2.10 was used with all the testing. Four-point loading was applied to the beam spaced symmetrically about the centre of the beam with a distance of 0.61m between each load. Control tests were carried out on beams without carbon fibre wrapping to compare with those with carbon fibre wrapping. The carbon sheeting had an elastic modulus of between 240-260GPa and had a minimum tensile failure stress of 2823MPa. The concrete for the beams had a 37MPa characteristic compressive strength and the Young's modulus for the concrete was 35GPa. The yield strength for the internally bonded steel reinforcement was 460MPa.

The testing demonstrated that, when compared with the control reinforced concrete beam tests, which had a typical ultimate load of 120.2kN, the load increased to a value of 170.1kN, yielding a 41% increase in capacity. The mode of failure with all the carbon fibre wrapped beams was crushing of the concrete between the points of application of the loads. The deflection of the carbon fibre wrapped beams was also reduced. The control beam gave a maximum mid-span deflection of 22mm under a loading of 120kN and the carbon fibre wrapped beams yielded typical defections of 11mm with the same loading, representing a 50% reduction.

With this application, however, wrapping CFRP about all the exposed faces may not be practical with regard to rettrofitting as members may have existing services, fixed or close to their webs.

Norris, et al. (1997) carried out research with RC beams wrapped on both vertical side faces and the lower face of the beam with regard to shear and flexural strengthening. Beams of two lengths were employed in this research, the longer length (2440mm) being used as flexural specimens (type A) and the shorter beams (1220mm) being used as shear

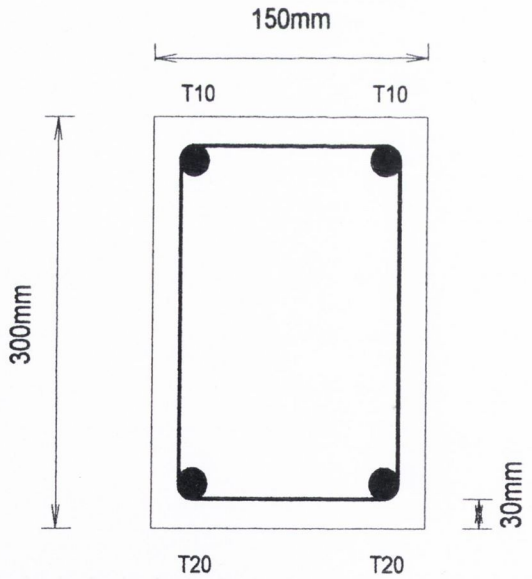

Figure 2.10: Section used with all tests with and without carbon fibre wrapping. (Gangarao et al., 1998).

specimens (type B). Type A beams had four 10mm diameter high tensile reinforcing bars (2 top and 2 bottom) in the section with 6mm diameter links at 150mm spacing throughout the length of the beam. Type B beams had two 16mm diameter high tensile steel reinforcing bars in the bottom of the section and two 10mm diameter high tensile bars in the top with 6mm diameter links throughout the length of the beam. The concrete had an average cube compressive stress of 36.5MPa.

Test results for the flexural specimen type A demonstrated that a load of 138kN caused the tension steel to yield as compared with a yield load of 40kN in the control specimen. However, unlike steel, carbon fibre reinforced plastic plates demonstrate a totally elastic behaviour until failure. This resulted in sudden failure in concrete beams mostly due to de-bonding on the tension faces.

The type B shear specimens had carbon fibre bonded to the full height of the web to simulate the action of shear links. The shear specimens did not fail in shear but failed due to the yielding of the tension reinforcement. An ultimate load of 145kN was applied to the beam without shear failure as compared to the control shear specimen, which failed in shear at 100kN.

The research concluded that carbon fibre sheet wrapping bonded to the webs and tension faces of existing RC beams can significantly increase their strength and stiffness. The magnitude of the strength and the mode of failure are related to the orientation of the fibres with respect to the beam longitudinal axis. When fibres were placed perpendicular to tension cracks in the beam at mid-span or shear cracks close to the supports, a large increase in stiffness and strength was observed and a sudden brittle failure occurred in both cases due to high stress concentrations at the ends of the carbon fibre sheets causing de-bonding.

Research has also been carried out on the problem of CFRP plate de-bonding causing premature flexural failure (Spadea et al., 1998). The function of this research was to explore the possibility of using externally bonded anchor plates at the ends of the CFRP

flexural strengthening plates to increase the beam flexural capacity by preventing premature failure.

All the beams in this research had the same internal steel reinforcement, which was four 16mm diameter high yield bars (2 top, 2 bottom,) and 4mm diameter shear links at 150mm centres. The concrete grade and section size was the same for all specimens as was the loading arrangement, which was a four-point loading system. Figure 2.12 shows the four beams tested, together with the typical test beam cross-section.

The research showed that bonding CFRP plates without consideration for end anchorage results in a sudden and premature failure. The CFRP without such anchorage was unable to make full use of the composite action of CFRP plate with the beam.

With beam A3.2 and A3.3 in figure 2.12, the provision of end anchorage and transverse confinement to the CFRP flexural strengthening plate allowed 98.6% of the ultimate capacity of the CFRP flexural strengthening plate to be employed. The beams with the end plated flexural strengthening carried loading 70% greater that the loading of the un-strengthened beam. The ductility of the beam with the flexural strengthening and without the end anchorage was less than the beams with the end plate anchorage. The evidence of the research demonstrated that using external plate bonding to strengthen RC beams is essentially a structural engineering process and should be governed by structural design as well as by the mechanical bonding properties of the resin.

Another possible mid-span failure mechanism of CFRP flexural strengthening plates has been investigated (Sebastien, 2001). This research focuses on a failure mechanism whereby large shear forces are transmitted from the CFRP plates through the bonding adhesive to the cover concrete of the internal beam reinforcement. The test beams had crack-inducers located at their mid-span as shown in figure 2.13. The crack-inducers were placed at mid-span to standardise the initial flexural crack as the exact location of the initial flexural crack is not entirely predictable. The author selected one of a typical batch of beams to illustrate the test results (Beam B1).

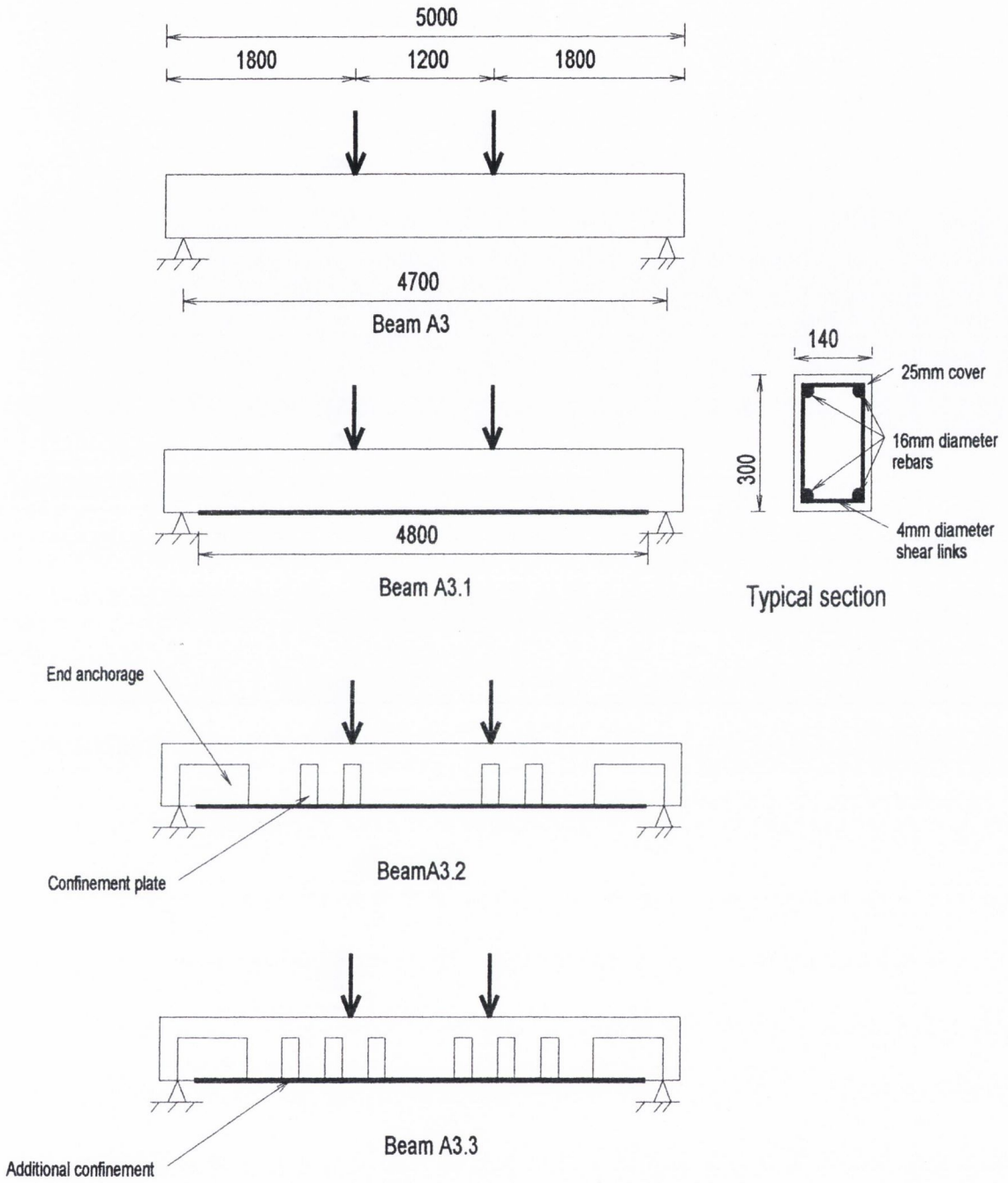

Figure 2.12: The beams tested with end anchorage provided in beams A3.2 and A3.3 together with the typical beam section and internal reinforcement. (Spadea et al., 1998)

When the beam B1 was gradually loaded to 25kN (at each loading point) the initial flexural crack formed. The loading was increased to 75kN, at which point the main tensile steel reinforcement yielded and CFRP flexural strengthening plates began to de-bond at mid-span. The author observed that the failure arises from plate de-bonding that starts at the toe of mid-span flexural cracking, as shown in figure 2.13.

Two main phases in the failure were noticed after mid-span flexural crack initiation.

- In the first phase, termed the initiation phase, inclined cracks form near the toes of the flexural cracks. As bending continues, the inclined cracks become wider and cause the CFRP plates to move downward locally. The CFRP plate applied a "dowel" action on the adhesive and cover concrete to one side of the inclined crack. This action continues along the plate/cover concrete interface and leads to horizontal crack propagation, as shown in figure 2.13.

The second phase, termed the de-bonding phase, initially displays steady and gradual horizontal crack propagation with each increment of loading. Eventually, the horizontal crack suddenly runs to the ends of the CFRP plate, resulting in complete "unzipping" on the plate from the beam soffit. The energy released

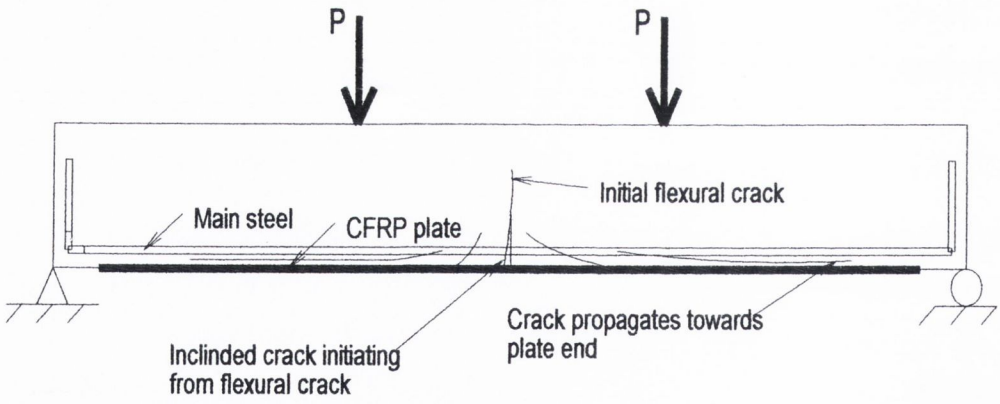

Figure 2.13: The typical failure mode for mid-span de-bonding arising from flexural cracking. (Sebastien, 2001)

- from the plate unzipping can be sufficient to tear portions of cover concrete from the beam soffit.

A publication by Arduini and Nanni (1997) describes such behaviour at the RC beam mid-span and stated "de-bonding started at one of the flexural cracks in the constant moment region (under 4 point loading) and propagated towards the CFRP sheet end until total delamination occurred". A more recent publication by Rahimi, and Hutchinson (2001) concurred and stated " Failure occurred within the constant moment zone. In contrast to the typical failure patterns reported for steel beams, plate end peeling was not a primary failure mechanism for CFRP plated RC beams".

Sebastian (2001) states that CFRP plate de-bonding from end peel has been extensively researched, whereas little work has been carried out on mid-span de-bonding, which propagates from flexural cracking. The main conclusions from the research were:

- Mid-span de-bond initiates at flexural cracks in the central portion of the beam and propagates horizontally near the concrete adhesive layer.

- The concrete fracture is driven by high shear stresses transmitted to the concrete from the plate and adhesive.

- Soon after the initial mid-span de-bond, the process is self-propagating.

- Mid-span de-bond failure mode is more likely to occur if large shear span loads are present (giving rise to large mid-span moments) and if the plates are curtailed close to the supports where the bond shear stresses are lower.

Applying externally bonded plates to beams for strengthening will improve their performance in the order of 10-35% depending on the material used. CFRP will have improvement percentages at the higher end of the range. The deflections are reduced in the order of 20-30%. In contrast, steel plates have percentage reductions in deflection at

the higher end of the range owing not only to the interaction between the beam and plate, but also to the beam stiffness of the plate itself, particularly where thick plates (25-50mm) are employed.

2.1.5 Strengthening with pre-stressed CFRP

Two key advantages of employing pre-stressed bonded CFRP plates are a resultant higher reinforcing steel yielding load in concrete beams and a better use of the strengthening material. Other advantages are reductions in crack size and stress relief in the beam's steel reinforcement.

Previous research has demonstrated that increases in yielding loads of 50% can be achieved with four-point loaded beams strengthened with pre-stressed CFRP, when compared to similar un-strengthened beams. When compared to similar beams strengthened with conventional non pre-stressed CFRP bonding improvements of 25% can be achieved (Wight et al., 1995 and Nordin et al., 2001).

Figure 2.14 shows a comparison of load versus mid-span deflection for the three types of beams tested: type A are un-strengthened beams, type B are similar beams strengthened with non-pre-stressed CFRP and type C are similar beams strengthened with pre-stressed CFRP. The chart plotted is based on results obtained from previous research (Nordin et al., 2001) and concur with results from other research (El-Hacha et al., 2001 and Wight et al., 1995). It shows three typical stages of deflection with regard to load increase for each type of beam. The end of stage one (between 10- 20kN) is where the concrete cracks, at the end of stage two (between 60-80kN) is where the steel yields and at the end of the third stage is loading to ultimate strength. It can be seen that a reduction in mid-span deflection of the order of 25-35% exists in the mid-span deflection when compared to the non pre-stressed CFRP plated beam and of the order of 50% when compared to the un-strengthened beam.

The strain in the concrete/steel reinforcement is often the limiting condition when applying non pre-stressed CFRP plates for strengthening. This will lead to the CFRP material not being utilised to the full potential and, ultimately, results in higher fabrication cost to the client.

When applying non pre-stressed CFRP plates, in most cases, dead and service loading exist and are not always possible to remove. Pre-stressing can indirectly reverse the stresses and deflections due to these loadings and will allow a greater utilisation of the CFRP strengthening material. In this case, a higher initial cracking load and yield load can be achieved, as can be seen with case "c" in figure 2.14. However, the ductility of beams with pre-stresses CFRP plates are reduced as the initial strain on pre-stress will result in the ultimate strain being reached sooner.

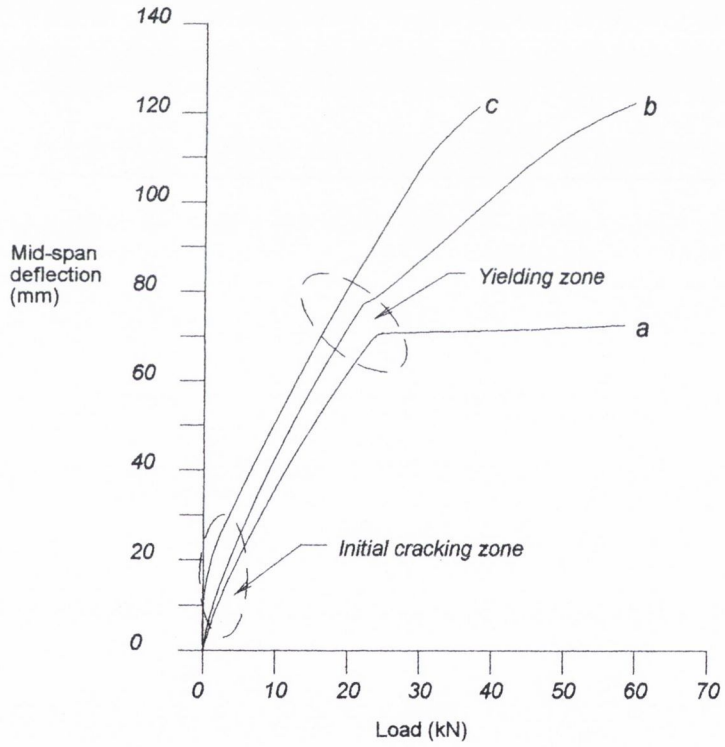

Figure 2.14: Plot of load versus mid-span deflection of (a) un-strengthened beams, (b) beams strengthened with non pre-stressed bonded CFRP plates and (c) beams strengthened with pre-stressed CFRP plates (Nordin, et al., 2001).

The problem of end peeling arises also with pre-stresses CFRP plates and research has been carried out on the potential use of mechanical anchorage to prevent this problem (El-Hacha et al., 2003). Research into the mode of failure of pultruded CFRP plates found that significantly greater loading could be applied to the strengthened beam after the initial end peeling had occurred and that this provided a visual warning of imminent collapse (Garden et al., 1998).

Previous research has found that failure is most likely to occur on the CFRP/concrete interface or within the bottom layers of concrete close to it (Garden et al., 1998). Member surface preparation is more important when applying pre-stressed CFRP plates due to higher shear stresses present when compared to non pre-stressed plates. The shear stresses on the CFRP resin/beam soffit interface with pre-stressed plates can be so high as to cause failure of the internal concrete reinforcement whereas, in the case of non-pre-stressed plates, failure due to end peeling or de-bond will more readily occur (Quantrill et al., 1998). For the reasons discussed, mechanical end anchorage will allow the pre-stressed CFRP plates to be fully utilised.

Methods used in the laboratory to pre-stress CFRP plates are difficult to apply in a practical application on site. Provision must be made for both the pre-stressing method and an adequate anchoring system. Small cylinder hydraulic jacks are often used to pre-stress CFRP and this method was developed in Switzerland for research that investigated beams strengthened with pre-stressed CFRP strips (Andra et al. 1999). The method uses steel end-plates bolted to the member that provide a reaction for the jacking.

Plate end anchorage to prevent peeling or interface shear de-bond has been employed in research carried out on pre-stresses CFRP plates (Garden et al., 1998). The anchorage system employed was a steel plate that was bonded to each end of the CFRP strip. The steel end plates had holes drilled in then which allowed bolts to pass through and into the concrete beam's soffit. These bolts were then anchored with epoxy resin.

It must be borne in mind that in order for any CFRP plate strengthening method to be successful , and especially with pre-stressed CFRP plates, the surface of the concrete must be carefully prepared and inspected for quality (that is, voids, laitance layers etc.). In some instances concrete cover can be in too poor a condition to allow pre-stressing with laminates (Taljsten, 2002).

A main advantage of pre-stressing is the ability to reverse dead load deflection and thus increase serviceability loading. For example, Hythe Bridge in Oxford was strengthened with pre-stressed CFRP strips based on a feasibility study by Mouchel Consulting to increase the bridge capacity (Darby et al., 1999). The bridge consisted of cast iron beams with a concrete deck. The strips were bonded to the beam soffits and pre-tensioned to 18 tonnes each. The pre-stressing was designed to totally relieve the tensile stresses in the lower flange of the beams under a full capacity loading of 40 tonnes. The pre-stress reversed the stresses and deflections induced by dead loading such that additional capacity was available for live loading.

The advantages and disadvantages of pre-stressing CFRP plate techniques have been outlined in a technical report (CEB-FIP (*fib*), 2006) and are as follows:

Advantages:

- Provides stiffer flexural and ultimate responses to loading .
- Delays crack formation in the shear span with eventual cracking smaller and well distributed (which impacts on bond development).
- Closes existing cracks in concrete structures.
- Improves serviceability and durability of existing structures.
- Provided the concrete section remains un-cracked, will improve shear resistance.
- Smaller area of CFRP plating is required with pre-stressed application when compared to strips with no initial stress.
- If adequate anchorage lengths are provided, premature end peel is avoided thus increasing overall capacity of members.

- With regard to concrete beams, a greater compression zone results owing to the neutral axis being lowered with the presence of pre-stress, thus improving structural efficiency.
- It can significantly increase the load at which reinforcing steel yields when compared to non stressed member.

Disadvantages:

- A greater number of operations and equipment are required resulting in greater expense.
- More time required for pre-stressing methods. Pre-stressing and placing equipment must remain in place until adhesive has fully cured.
- The pre-stress is distributed over the length, not concentrated at the ends

Partially pre-stressed concrete beams with CFRP plates

Beams with CFRP plates bonded to portions of their clear span (generally the mid-third portion) have been employed as a retrofitted strengthening method. This approach is relatively more cost effective than plating the entire beam's soffit with CFRP. Laboratory and analytical research has shown that the use of pre-stressed CFRP plates represents a significant contribution to the advancement of the FRP strengthening technique (Triantafillou et al., 1992 and Deuring, 1993). Recently methods have been developed for pre-stressing CFRP plates that have been used on site (Luke et al., 1998).

With pre-stressed CFRP plates the mode of failure differs from that of plates with no initial pre-stressing. Typically, plates attached to mid-third portions of a span (that is, with higher flexural stress) and with no initial pre-stress will de-bond at the plate ends provided the strain is not limited (Chan et al., 2001). With pre-stressed CFRP plates attached to partial portions of the span failure is more likely to occur by plate rupture due to initial plate strain and the problem of plate end de-bond allows relatively greater capacities in beam strength to be achieved (Nguyen et al., 2000). However, comparative tests between beams that had CFRP bonded along the entire soffit and beams with

partially bonded plates showed that beam with full span strengthening achieved higher ultimate strength loads (of the order of 20-30% greater than partially strengthened beams) (Chan et al., 2001).

Owing to the low modulus of elasticity of CFRP (of the order of 12GPa) the reduction in the deflection of beams plated throughout their length must be limited. Futhermore, beams that are partially plated with pre-stressed CFRP plates have been found to have a greater flexural deformability (Abdelrahmen et al., 1999). The use of partial plates for pre-stressing deteriorated RC beams due to corroded steel reinforcement improved the flexural strength (of the order of 25%) and flexural defomability (of the order of 15-20%).

Design guidelines have been published to provide methods of analysis for beams retrofitted with CFRP plates, in which a section proposes an approach for pre-stressed partially plated beams, as shown in figure 2.15 (Oehlers et al., 2001). As mentioned earlier, beams partially plated with pre-stressed CFRP plates will fail at mid-span due to flexural stresses in the bonded concrete/plate interface, which gives rise to plate de-bonding that rapidly propagates outwards to the plate ends.

Owing to this it is suggested (Oehlers et al., 2001) that the "hinge approach" should be adopted. The authors find that with this approach, the shear de-bonding criteria is not the limiting criteria; excessive flexural cracking over a small hinge region at mid-span that gives rise to relatively higher bending stresses in the medium that results in initial mid-span de-bonding. As with pre-tensioned tendons, deflections are reduced with CFRP pre-stressing, of the order of 15-20%, due to initial pre-camber and flexural stiffening (Nguyen et al., 2000).

Partial pre-stressing of CFRP on steel members

Sebastian (2005) proposes a method of analysis for strengthening steel members with fully or partially pre-stressed CFRP bonded plates. He points out that some

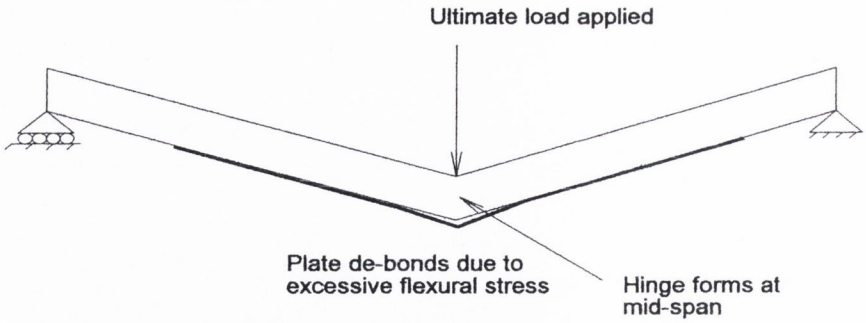

Figure 2.15: "Hinge method" of failure assumed for pre-stressed CFRP plate (Oehlers et al., 2001).

considerations that apply to strengthened concrete structures do not apply when designing strengthened steel members.

De-bonding plate failure due to material flexural cracking and end peel plate failure due to shear cracking are not considered in the case of steel strengthened members. However, adhesive and plate material failure (rather than parent material failure) are more likely to occur with CFRP strengthened steel members. Figure 2.16 shows the fully plastic section considered.

The following assumptions are made with the proposed method of analysis:

- The steel is assumed to be elastic –perfectly plastic
- The CFRP plate is assumed to linear elastic to failure.
- The adhesive is assumed to be linear with a shear stress distribution that peaks at mid-span and decreases moving towards each CFRP plate end.

With the section assumed to be fully plastic, the following equation was developed:

$$M_{ult} = \sigma_y \left\{ A_f (d_w + t_f) + \frac{(6\alpha(\alpha-1)+3-2\alpha^2))b_w d_w^2}{6} + \frac{E_p A_p}{E_s} \left(\frac{2(\alpha d_w + T)(\alpha d_w + T_1) t_p (\alpha d_w + T_2)}{2\alpha d_w} \right) \right\} \quad (2.2)$$

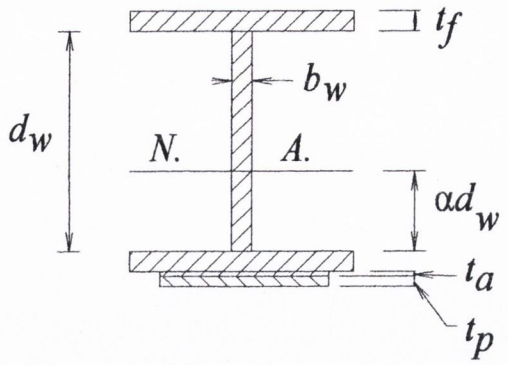

Figure 2.16: Plastic section with CFRP plate considered by Sebastian (2005).

where,

M_{ult}= The ultimate moment capacity of the strengthened section

σ_y= The yield stress of the steel beam

A_f= The cross-sectional area of the beam flange (6610mm^2)

d_w= The depth of the web between the upper and lower flanges (251mm)

b_w= The width of the beam web

t_f = The thickness of the flanges (25.3mm)

E_p = The elastic modulus of the CFRP plate (229GPa)

A_p= The cross sectional area of the CFRP plate (768mm^2)

t_a= The thickness of the adhesive layer (1mm)

t_p= The thickness of the CFRP plate (3.2mm)

$T = t_a + t_f + t_p/2$

$T_1 = t_a + t_f$

$T_2 = t_a + t_f + 2t_p/3$

αd_w= The dimension from the upper surface of the lower flange to the neutral axis

The factor α is calculated using equation 2.3, which is a quadratic equation that results from equating the horizontal tensile and compressive section forces.

$$2E_s b_w d_w^2 \alpha^2 + d_w(A_p E_p - E_s b_w d_w)\alpha + A_p E_p T = 0 \qquad (2.3)$$

Sebastion (2005) concluded that the suggested rigid bond method of analysis predicts a largely linear shear stress distribution between the plate/flange interface during the elastic response under loading. During the advanced elasto-plastic phase the shear stress distribution is largely non-linear within the mid-span yield zone where the peak shear stresses result. The analysis was compared with results from a non-linear FE "bond slip" analysis that predicted results of the plate/flange interfacial bond stresses that were similar in distribution but had lower values (that is, 18% lower for peak yield zone stresses for a simply supported beam with a central concentrated load.). The use of a reduction factor was suggested for more accurate shear bond stress predictions and further investigation would be required to establish such factors for different load and beam support types.

Steel beams strengthened with pre-stressed CFRP plates have been investigated (Schnerch et al. 2005) with a view to establishing their response under ultimate loading. High modulus (457GPa) pre-stressed CFRP strips were bonded to the tension (lower) flanges of steel/concrete composite beams. Four point loading was applied to 6400mm span simply supported composite beams. A pre-stressing force produced an initial strain of 0.06% in the CFRP plate prior to bonding and curing of the adhesive. The work revealed that the load-deflection response was essentially bi-linear (that is, elastic and plastic linear) to ultimate loading and that most of the strength increase occurred at the stage after the steel had yielded but before CFRP plate rupture. The findings concurred with similar research carried out (Sen et al., 2001 and Tavakkolizadeh et al., 2003). Ultimate strength increases of the order of 18-20% were observed with no plate de-bonding.

Interfacial galvanic corrosion is an important consideration for both pre-stressed and passively engaged CFRP plates bonded to steel members. The Galvanic action resulting from CFRP in contact with steel has the potential to accelerate the corrosion of the steel and also the CFRP plate itself (Miriyala et al., 1992). The provision of a suitable bond layer that has the necessary properties (that is, not an electrolytic solution) can prevent Galvanic action taking place provided no electrical connection exists between the two

materials (Francis, 2000). The type of adhesive selected can impact on the design life of a retrofit and neat resin is less permeable than a matrix resin, thus preventing moisture intake at the plate/beam interfaces (Choqueuse et al., 1997). The use of barrier layers have been shown to be an effective method preventing the moisture ingress necessary for Galvanic action (Brown, 1974 and Tavakkolizadeh, et al., 2001). It has also been shown that, coupled with the problem of galvanic action, moisture ingress at the beam/plate interface can cause plastification of the adhesive matrix (McBagonluri et al., 2000).

The end peel and de-bonding that occurs due to strengthened concrete member shear and flexural cracking respectively under ultimate loading is not a consideration with steel strengthened members and adhesive and/or CFRP plate rupture is the primary failure mechanism (Sebastion, 2005).

However, the problem of applying concentrated moments at specific locations cannot be solved with pre- stressed CFRP bonded plates. The beneficial moment increases from the plate ends to a maximum at the plate centre. If a prescribed moment is applied at the plate end, then too much is applied at the plate centre, or conversely, if the prescribed moment is applied at mid-span too little is applied at the plate ends.

CFRP plates can be applied to strengthen in situ members relatively quickly and with little disruption. The method of strengthening can improve member capacity with very little increase in self-weight (of the order of 15-25%) and reduce deflection (of the order of 10-15%) (Sebastion, 2005).

2.2 Structural Members Strengthened with Tendons

The two types of tendon application used to strengthen structural members are internal and external tendon configurations. Internal tendons generally are installed at the construction stage and external tendons are more often fitted retrospectively. However, external tendon applications are fast becoming the preferred option to internal tendons, particularly in box girder bridge spans. A publication on the comparison of the use of

internal tendons to external tendons found that external tendons have attracted much attention in the past, while internal tendons have come into much criticism (Hewson, 1993).

2.2.1 Internal tendons

Internal tendons are located within the cross-section of the member and can be either pre or post tensioned. In concrete, post tensioned members are inserted into ducts cast within the member along its length. As with all tendon applications the problem of tension loss due to creep exists, particularly with concrete. The problem of friction loss due to duct curvature also exists with internal tendons.

Tendon maintenance, when internal, can be costly. The ability to monitor and replace tendons that are grouted within ducts is severely problematic. Research carried out into the long-term maintenance of grouted post-tensioned tendons, examined the area of corrosion testing (Hamilton et al., 2000). The injection of cement grout within ducts can become "air-locked", giving rise to voids. These voids can, in time, bring about the onset of corrosion to the tendons, particularly on or near expansion/construction joints. If, however, proper grouting methods and materials are used, the member should perform to its full life expectancy. The cement grout provides a high alkaline protective barrier to the tendons and bonds the tendon to the duct to allow higher tendon stresses to develop.

Large-scale field tests have demonstrated that cracking of grout in post-tensioned cable ducts will occur under service load conditions (Hamilton, 1995) and should be monitored regularly. Internal tendons have the advantage of greater protection from corrosion than external tendons or cable stays. Internal tendons, however, will usually have less eccentricity than those of external tendons in that internal tendons must lie within the cross-section of the member with a minimum cover while external tendons can be placed below the member cross-section and, thus, enhance eccentricity.

A research publication by Canadian research consultants, outlines a protocol for the evaluation of structures with internal tendons (Rogowsky et al., 2002). The document reports that the major factors for influencing strand failure are the amount of moisture the building is exposed to, contaminates within the tendon sheathing and susceptibility of the tendon to develop stress corrosion cracking. The report suggests the following procedure for investigation:

The authors concluded that post-tensioned structures are unlike ordinary reinforced concrete structures and the assessment of post-tensioned structures requires particular expertise. The assessment of tendon metallurgy is a relatively new area and judgement must be used when assessing the tendon condition. It can be seen that long term monitoring and maintenance of internal tendons can be problematic and costly. Engineers are now looking at alternatives to internal tendons for post-stressing applications with particular regard to access, long term monitoring and maintenance. Beams strengthened with internal tendons typically have improvements of between 15-25% in capacity when compared to the same beams with no tendons applied. The percentage improvements for beams with internal tendons are, in general, lower than beams with external tendons applied, as external tendons will have greater eccentricities.

2.2.2 External tendons

External tendon applications were initially retrofitted to structures for strengthening. The external tendons were often fixed to the underside of bridge decking beams to upgrade them for new traffic loadings. External tendon applications, however, are becoming more popular in new construction methods and are attracting much attention. (Hewson, 1993). External steel tendons were first used in the 1950's and initially some problems were encountered with corrosion before the introduction of protective sheaths and cathodic protective methods. When adopted as a strengthening method, external tendons have the advantage of adding little weight to the original structure with easy access and maintenance and with little disruption to the user (Nordin, 2005).

Other materials have been researched for tendon use and originally glass FRP was used. However, owing to the comparatively higher modulus of elasticity, aramid and carbon FRP are more commonly used. Research was carried out into the behaviour of concrete beams externally strengthened with FRP and it was found that load-displacement responses, in the short term, were almost the same as in similar beams externally strengthened with steel tendons (Mutsuyoshi, 1991). FRP displays low, if any, ductility under high loading and it has been demonstrated that, owing to this, a greater ultimate load can be achieved with lower energy absorption when compared to steel tendons (Stoll et al., 2000). However, in respect of plastic design, it is necessary to predict the collapse load and mechanism and, were FRP tendons to be used, this can be problematic, in that sudden rupture is more likely to occur at ultimate loading. Table 2.2 shows the characteristics of the FRP materials and steel used for tendons (Pisani et al., 1998)

Extensive research in Canada has been carried out into the use of FRP tendons on concrete members (McKay et al., 1993 and Fam et al., 1997). One of the main advantages with FRP tendons is that of self-weight. FRP tendons have almost the same tensile strength as steel and are approximately five times lighter.

A de-merit of CFP tendons is that of end anchorage; owing to the anisotropy of the material, forces perpendicular to the longitudinal axis will more readily crush the polymer. The conical barrel and wedge mechanism used for tendon end anchorage relies on the radial compressive strength of the material for fixing. It is manufactured using a pultruded (that is, drawn through a die) method with epoxy impregnated carbon fibres. Both the potted anchor block and barrel and wedge anchorage systems can be employed with this tendon. If the barrel and wedge anchorage system is used, a dry lubricant must be applied to assist in wedge setting. The wedge mechanism is shown in figure 2.17.

When compared to steel, CFP tendons are more problematic with regard to end anchorage and, when large composite CFP cables are employed, the barrel and wedge

Typical properties	Steel Euronorm (Fe7S1860)	GFRP	AFRP	CFRP
Fibre vol. (%)	n.a.	65	50	65
Density (g/cm^3)	7.85	2.15	1.25	1.6
Tensile strength (MPa)	1250	1350	1400	1270
Tensile modulus (GPa)	195	50	62	147
Ultimate elongation (%)	>3.5	3	2.4	1.3
Thermal expansion coefficient (axial 10^{-6}/°C)	12	5.2	1.8	0.68
Thermal expansion coefficient (radial 10-6/oC)	12	35(approx.)	35(approx.)	20(approx.)
Strength decrease after 100 years (%)	0(approx.)	30	>30	0(approx.)
Relaxation 20°C(%)	3	4	>30	3

Table 2.2: Characteristics of steel and FRP tendons (Pisani, 1998)

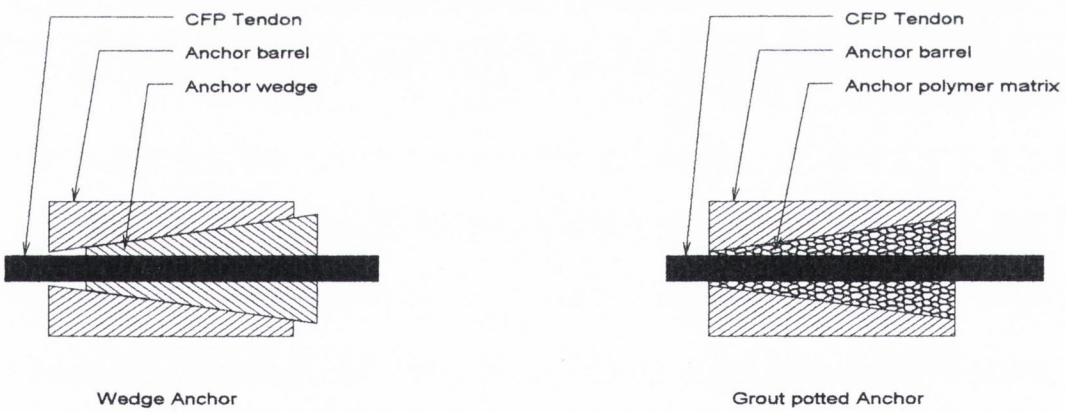

Figure 2.17: Typical CFP tendon end anchorage details (Benmokrane et al. 2000).

mechanism cannot be used. The potted grout anchor method allows 90% of the CFP tendon ultimate strength to be developed before end anchorage failure. Table 2.3 shows the properties and manufacture data of the more popular CFP tendons used in construction (Benmokrane et al., 2000).

Tendon	Nominal diameter	Cross-section (mm^2)	Mean tensile strength (MPa)	Elastic modulus (GPa)	Ultimate strain (%)	Density (g/cm^3)	Poissions ratio
Arapree-8	7.5	44.2	1506	62.5	2.4	1.25	0.38
Technora	8	50.2	2140	54	3.7	1.3	0.35
Leadline	7.9	46.1	2550	150	1.3	1.67	n.a.
CFCC	7.5	30.4	2120	137.3	1.57	2.1	n.a.

Table 2.3: Properties of CFP tendons used in construction (Benmokrane et al., 2000).

As well as local radial crushing, a common problem with the barrel and wedge method of anchorage is slippage of the CFP tendon through the wedge which does not "bite" into the material as it would with a steel tendon. Some investigation has been carried out into this problem (Nanni et al., 1996) which showed that the tendons are still effective after local end anchorage crushing has taken place. A possible solution was forwarded (Al-Mayah et al., 2001) where the wedge surfaces were gritted to increase the grip and a noticeable improvement was achieved. Non metallic barrel and wedge mechanism have also been investigated and, while some slippage occurred, it was found to be a reasonable alternative to the stainless steel barrel and wedge (Harada et al., 1995).

Research has been carried out on the maximum recommended pre and post-stressed FRP tendons (Dolan et al., 2001). The authors state that stressing beyond the limits shown

here in Table 2.4 will significantly shorten the service of the FRP tendons (f_{pu} = ultimate stress in pre-stressing tendon).

The relaxation in FRP tendons have three components (R_1, R_2, and R_3) which are by virtue of the manufacturing methods which are additive.

1. Upon initial stressing a portion of the load is carried by the polymer matrix and, after some 24-96 hours, matrix relaxation occurs. The modular ratio of the polymer matrix

Type of fibre	Pre-tensioned	Post-tensioned
Carbon	$0.65 f_{pu}$	$0.65 f_{pu}$
Aramid	$0.60 f_{pu}$	$0.50 f_{pu}$
Glass	*Not recommended*	$0.45 f_{pu}$

Table 2.4: Recommended jacking stresses for FRP tendons (Dolan et al., 2001).

and fibre (n_r) and the proportion by volume of polymer resin (v_r) are the two factors considered in this component of FRP tendon relaxation (R_1), where
$R_1 = n_r v_r$.

2. Not all fibres in FRP tendons are aligned longitudinally after the pultrusion manufacturing process and the relaxation resulting from fibre straightening (R_2) is of the order of 2%.
3. The final component considered is the losses typically associated with steel tendon pre-stressing (that is, member axial compressive shortening and friction losses), R_3.

Steel tendons

Steel tendons have been used for several decades to strengthen structures for both new and retrofitted tendons applications. Three processes are employed to produce the high tensile and ductile stands used in pre or post tensioning, as follows:

1.Cold drawn or deformed carbon steel (tempered prefered)

2. High carbon hot rolled alloy steel

3. Hot rolled and heat treated carbon steel

These methods produce a type of steel that is ideal for pre or post stressing as it remains in an elastic range for relatively high stresses (of the order of 1200-1600MPa) and displays good ductility once the elastic limit is reached. The high tensile steel also has good bonding qualities to concrete with low relaxation over time and high resistance to fatigue and corrosion. The most common method of production is the cold drawn application. Circular wires are produced of smaller diameters (of the order of 4-8mm) and are wrapped helically around a central wire such that the tendon is produced with the same diameter as a larger solid bar but with greater flexibility and better quality control.

The yield stress of pre-stressing steel is not as well defined as in the case of conventional steel reinforcement. Depending on the manufacturing process of the tendons and carbon content of the steel, the yield point is defined as the point at which the stress-strain curve deviates from the linear trend (that is, usually close to the point were the strain is 0.01%). The elastic modulus of pre-stressing steel, again, will depend on the manufacturing process and is of the order of 195-205GPa.

With regard to relaxation of high tensile steel tendons, if the initial stress, f_{pi} , is less than $0.55f_{py}$ (where f_{py} is the tendon yield stress), then the resulting relaxation will be negligible (Collins et al., 1991). If the properties of the material are known, relaxation with time can be accurately predicted.

Temperature will have an effect on the rate of relaxation. The higher the ambient temperature the quicker will be the loss due to relaxation over a given time. It has been demonstrated that an increase from 20°C to 40°C will result in an increase of 50% in relaxation over 100 hours (Collins et al., 1991). However, with regard to external tendons, losses due to creep and relaxation can be monitored and restored more readily than with internal tendons.

Increase in temperatures of the order of 400°C will reduce the stiffness and strength of strands to the order of 50% of their original (Collins et al., 1991) It is for this reason that adequate fire protective coatings are provided, together with enough tendons such that their working stresses are well below their yield stresses.

If external tendons are employed outdoors, protected sheaths and/or anti-corrosive materials must be used to protect against corrosion. Tendons composed of smaller strands are susceptible to corrosion due to the small cross sectional area and relatively high stresses (that is, a small reduction in cross-sectional area will result in a significant increase in working stress).

Research was carried out into the behaviour of concrete members originally designed with or strengthened by external post-tensioned tendons (Harajli et al., 1999). The behaviour of externally pre-stressed members is, in concept, similar to the behaviour of internally pre-stressed members. A major difference arises due to the fact that, for beams strengthened with internal tendons subjected to external loading, the position of the tendons relative to the beam neutral axis remain the same. When beams are strengthened with external tendons and subjected to external loading, the external tendons are free to move relative to the neutral axis of the beam and between anchor points. With increasing structural deformation, second-order effects become more prevalent. Harajli et al. investigated a method of analysis for second order effects using simply supported beams with mid-span deviators, shown in figure 2.18 for example. The test beam configuration illustrated in figure 2.18 was also used in earlier research to investigate the behaviour of beams strengthened with external tendons (Khairallah et al., 1997).

Harajli et al. (1997) developed an equation (equation 2.4) to predict the upward pre-camber in an existing beam strengthened with external tendons as shown in figure 2.18.

$$\delta_o = \frac{K_p A_{pe} f_{pe} e_m}{E_c I_c} \tag{2.4}$$

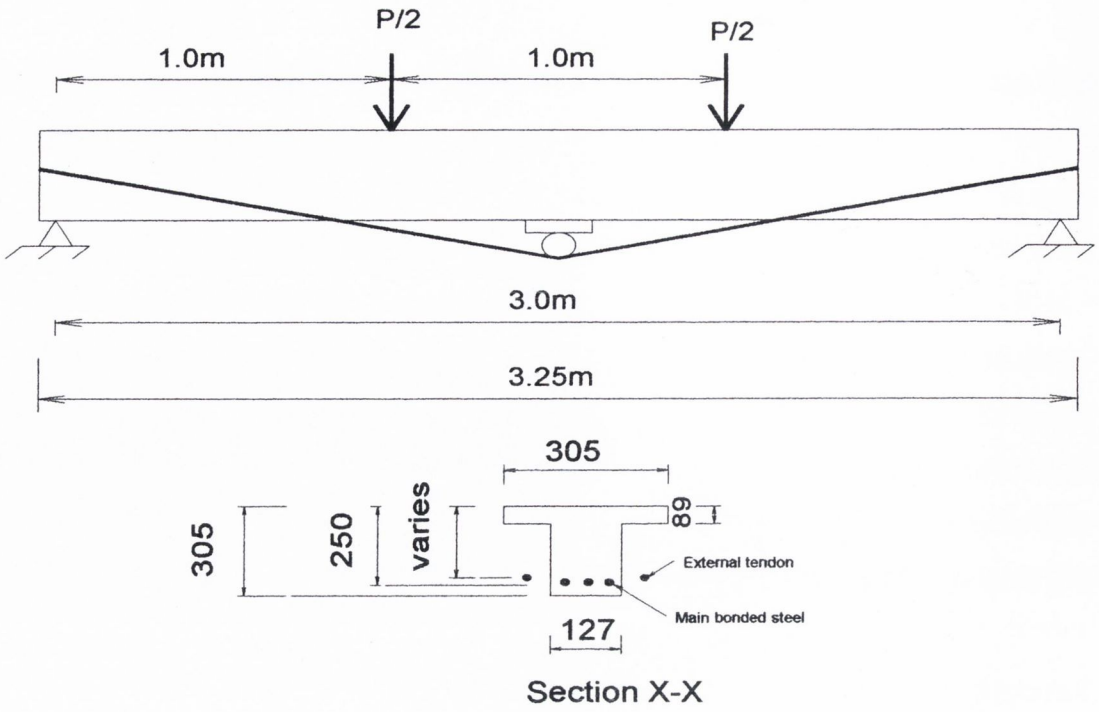

Figure 2.18: Typical RC beam with external tendons and deviators (Harajli, et al., 1999).

where,

E_c= Young's modulus of concrete.

I_c= Section moment of inertia.

A_{pe}= Area of external tendons

f_{pe}= Initial pre-stress in external tendons

K_p= Moment multiplier whose value depends on the moment diagram produced by pre-stressing, which can be expressed as follows:

$$K_p = \left[1 + \frac{4}{3}\left(\frac{e_s}{e_m} - 1\right)\left(\frac{L - L_d}{2L}\right)^2\right]\frac{L^2}{8} \tag{2.5}$$

where,

e_s= The eccentricity of the tendon at the supports

e_m= The eccentricity of the tendon at the mid-span

L= Clear span

L_d= The distance of the deviator from the support

The research by Khairallah et al. (1997) was used to validate the mathematical model proposed by Haraji et al. (1999), as in equations 2.4 and 2.5. The research was carried out using test beams to the specifications as shown in figure 2.18. A total of 12 were tested, divided into four main series, each with different areas of internal bonded steel reinforcement and external tendon diameters. The test beam types are given in Table 2.5.

Earlier research had demonstrated that the load-deflection response and ultimate flexural strength of continuous beams strengthened with external tendons differed from beams strengthened with internal un-bonded tendons (Tan et al., 1997) and the results of the experimental work were used to validate equations 2.4 and 2.5.

The beams used for testing comprised the familiar simply supported span and four-point loading system. The typical beam section (with tendons) is shown in figure 2.19. Six 3m beams were tested with T16 internal steel reinforcement and six 3m beams with T12 internal reinforcement. All beams had two 15.7mm external strands with the tendon configuration shown in figure 2.19.

The research found that the predicted load-deflection responses for the beams were within 4% of the test results for both cases examined. When external tendons are applied to new concrete members, the main difference between internal and external tendons is the change in eccentricity with deflection for external tendon applications (second-order effects), if deviators are not used.

Series Number	Number and size of bars	Number and size of tendons
1	2 x T12	2 x 7mm dia.
2	3 x T12	2 x 5mm dia.
3	2 x T16	2 x 7mm dia.
4	3 x T16	2 x 7mm dia.

Table 2.5: Test beam types used in testing regime. (Haraji et al.,1997)

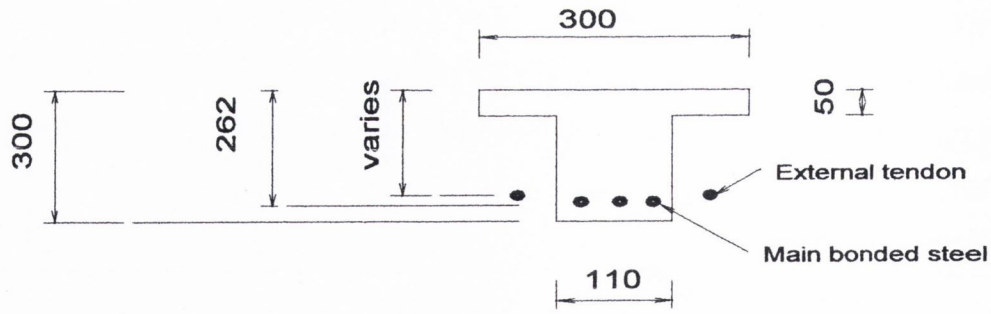

Figure 2.19: The typical beam section in a testing regime used to verify the mathematical model (Tan et al. 1997).

The research showed that the beams had an elastic load-deflection response, but with a lower rate of deflection than would be the case for similar un-strengthened beams, for the initial pre-plastic deformation stage. The plastic deformation stage for the tests showed that, for central concentrated loads, the system produced less significant second-order effects because the loading produces greater plastic deformation and less tendon mid-span eccentricity at failure.

The research concluded that external pre-stressing is a very effective technique for strengthening concrete flexural members. Improvements in capacity of the order of 25-30% were achieved when compared to the ultimate loads with the control specimens. Provision of a moderate amount of external pre-stressing will lead to significant deflection recovery, lower service load deflection, and a substantial increase in ultimate flexural capacity of the member.

Work has been carried out on the relative efficiency of external tendons as compared with traditional internal methods (Picard et al., 1995). The research compared an external tendon application on a continuous beam with an internal parabolic tendon profile more commonly used with post-tensioning application.

The research examined the advantages and disadvantages of external prestressing. The work found that the merits of external pre-stressing were:

- Concreting of new structures is improved as there are no internal or fewer internal (combined with external) tendons.
- Cross – section dimensions of concrete members can be reduced due to the partial or full elimination of internal tendons and, thus, ducting.
- Profiles of external tendons are easier to check during and after installation.
- Grouting is improved because of a better visual control of the operation and, therefore, a better long-term protection of the prestressing steel is achieved. Inspection is easier during the life of the structure.
- External tendons can be replaced if the corrosion protection allows the release of the prestressing force. (that is, tendons with lubricated sheathed strands).
- Friction losses are reduced, as external tendons are connected to the structure only at anchorage and deviation points.

The study also examined the de-merits of external prestressing which were found to be as follows:

- Tendons located outside the box section would have greater exposure to weather conditions and have a shorter working life.
- External tendons are more accessable than internal tendons and as such are more prone to sabotage or fire.
- External tendons are subject to vibration and their free length, therefore, should be limited.
- Deviation and anchorage zones required for external tendons should be designed to accommodate large longitudinal, transverse and shear forces and must be carefully designed and detailed.
- Anchor point failure in the case of internal tendons has limited consequences as the tendon force is normally transferred throughout the full length of the tendon by bond. In the case of external tendons, anchorage failure is critical as the tendon is rendered redundant. It is for this reason that anchor points for external tendons should be carefully protected against corrosion.

- The actual eccentricities of external tendons are generally smaller compared to internal tendons.

It should be borne in mind that with respect to the last point, the authors were referring to box girder bridge spans, where the internal tendon would be positioned in a duct in the upper or lower slab and the webs of the box section, unlike the external tendon, which would be positioned below the upper slab or above the lower slab of the section.

The authors considered a statically indeterminate beam that had external "localized" tendons or tendons that do not run along the full length of the beam that were fixed to the beam at anchor points externally. The beam with localized tendons applied is shown in figure 2.20, together with the resulting bending moment diagram and the component bending moment diagrams. This tendon configuration demonstrated that it is possible to apply beneficial bending moment to sections, in this case over the central support, in a statically indeterminate beam without tendons at that section of the beam.

In the final resulting bending moment diagram shown, in figure 2.20, expressions for M_l and M_r are given by equations 2.6 and 2.7 respectively and the final bending moment at the central support, M_f, is given by equation 2.8.

$$M_l = Pe\left(1-1.5\frac{L_1^3}{L^3}\right) \tag{2.6}$$

$$M_r = \frac{1.5PeL_1^3}{L^3} \tag{2.7}$$

$$M_f = \frac{-1.5PeL_1^2}{L^2} \tag{2.8}$$

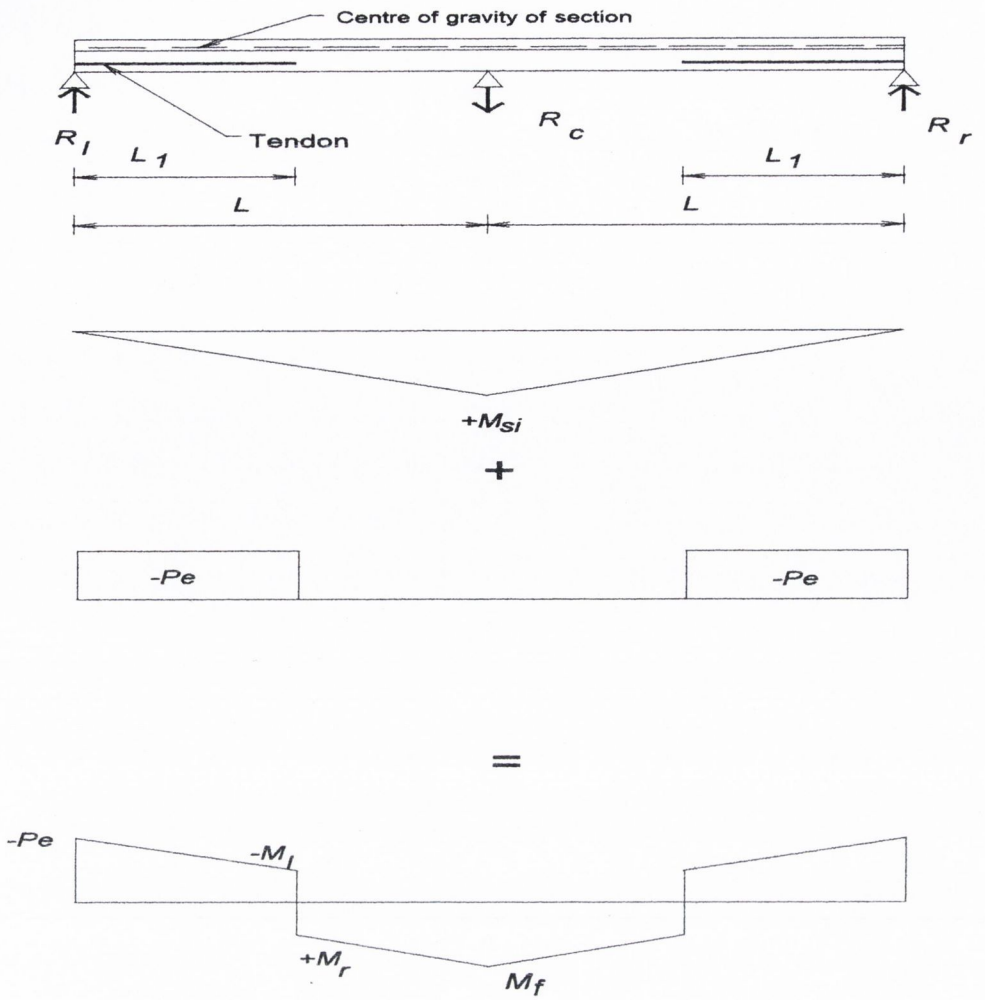

Figure 2.20: Localised tendons applied to a continuous beam, with the resulting bending moment diagrams.

It can be seen from the bending moment diagram in figure 2.20 that a beneficial moment arises over the central support even with the tendons extending only for a short portion over the two adjacent spans.

The authors also found that applying a combination of continuous linear tendons together with localised tendons at the interior supports could produce a more efficient tendon profile overall than with the local tendons only (that is, a 14% improvement in ultimate capacity). The linear tendons were more difficult to optimise than conventional internal parabolic tendons and further research was required in this regard. The research also

concluded that the local external linear tendon profile was less efficient than the internal parabolic tendon profile, in that, per unit of total tendon force applied, an internal parabolic tendon profile could apply more beneficial moment to the beam (of the order of 8%).

The authors carried out further work on the analysis of continuous beams pre-stressed with inclined localised tendons (Picard et al., 2000). The end span of a continuous beam was considered first, with an inclined tendon as shown in figure 2.21. The tendon runs from two points expressed at distances $\beta_1 L$ and $\beta_2 L$ from the exterior support. The moment over the internal support M_p was calculated using the method of virtual work and is given by equation 2.9.

$$M_p = \left[\frac{1.5\beta_1\beta_2(\beta_1 e_i + \beta_2 e_j) - \beta_1^3(e_i + 0.5e_j) - \beta_2^3(0.5e_i + e_j)}{\beta_2 - \beta_1}\right] P_i \qquad (2.9)$$

where;

e_1= The eccentricity of point 1

e_2= The eccentricity of point 2

P_i= The pre-stressing force in any given local tendon.

If the ratio e_i/e_j was expressed as a dimensionless parameter, K, equation 2.9 becomes:

$$\frac{M_p}{P_i e_j} = \left[\frac{1.5\beta_1\beta_2(\beta_1 K + \beta_2) - \beta_1^3(K + 0.5) - \beta_2^3(0.5K + 1)}{\beta_2 - \beta_1}\right] \qquad (2.10)$$

This allows a design chart to be plotted, where the left side of the equation was plotted on the "Y" axis and the right side of the equation was plotted on the "X" axis, as shown in figure 2.22. The plot shows the relationship for different K values. For example, a value for K =1, which implies that $e_i = e_j$ and the tendon is horizontal and below the section neutral axis, as shown in figure 2.23. Where the plot shows a value for K =0, this implies that $e_i = 0$ and that e_j has a value below the section neutral axis.

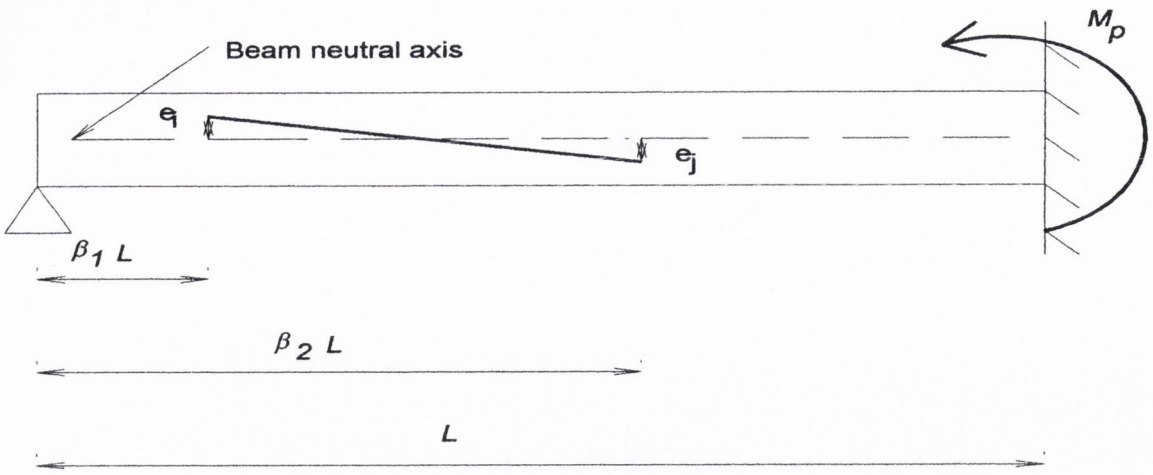

Figure 2.21: The end span of a continuous beam with a local external tendon with the left end above the beam neutral axis and the right end below (Picard et al., 2000).

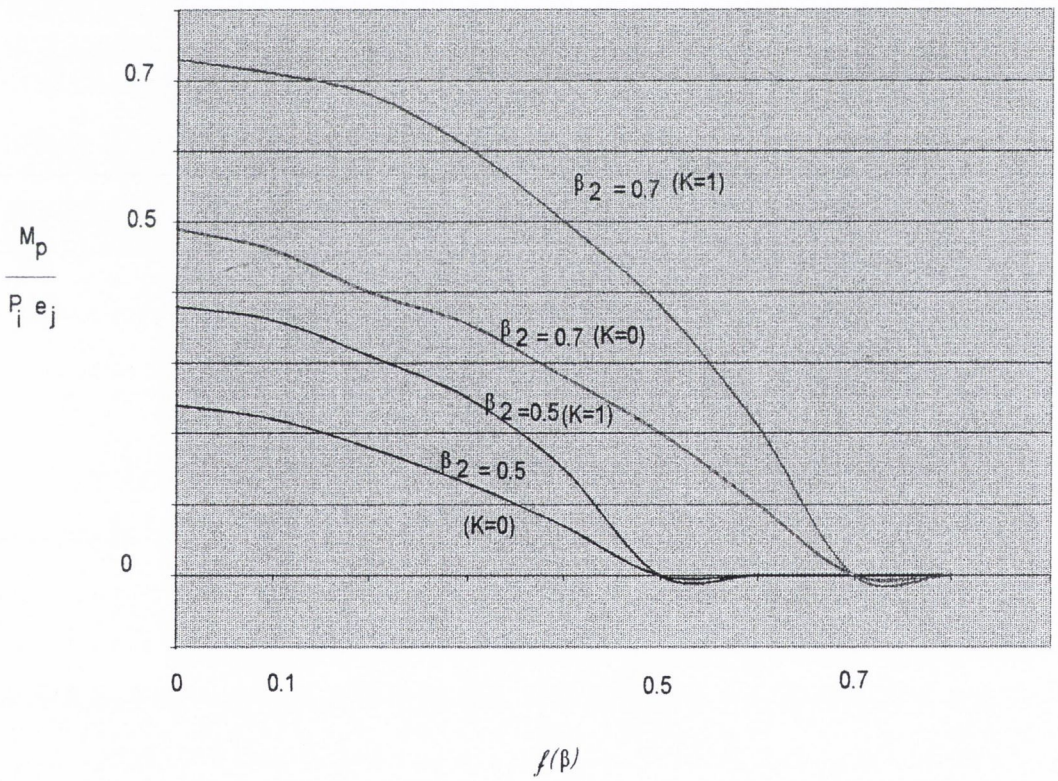

Figure 2.22: A plot of varied tendon length and eccentricity in the end span of a continuous beam (Picard et al., 2000).

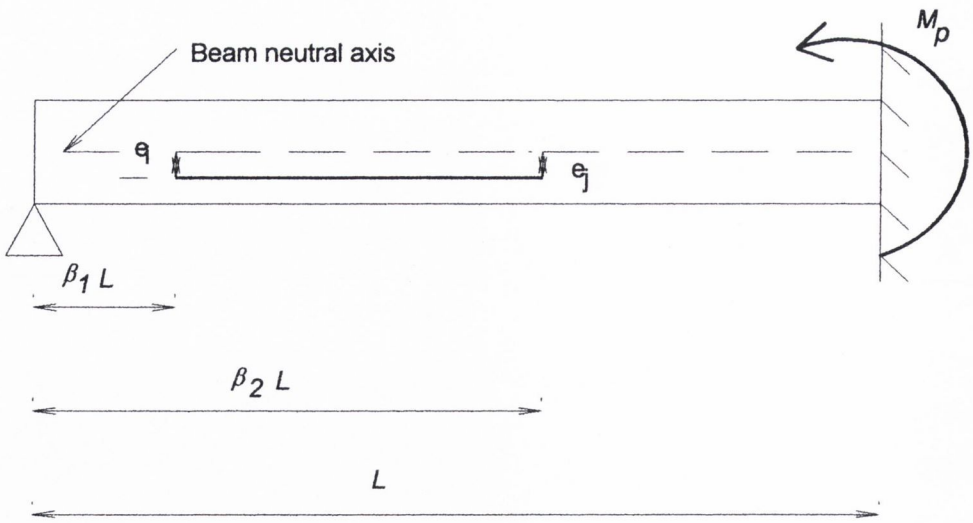

Figure 2.23: Horizontal tendon configuration (Picard et al., 2000).

The research found that in order to obtain a positive fixed end moment (that is, over the internal support), e_j must have a positive eccentricity (that is, below the beam neutral axis). To maximise this positive fixed end moment, the maximum available space under the beam section neutral axis must be utilised for e_j.

A localised tendon over the interior support was also considered in the research and is shown in figure 2.24. Similar equations were developed for this configuration as for the previous configurations and a similar design chart plotted. However, a combination of both tendon configurations shown in figures 2.23 and 2.24 gave the best results in terms of beneficial applied moment.

The research concluded that the effect of varying the geometric parameters of the tendon profiles had an effect on the fixed-end moments that were applied. However, it is not sufficient to only consider the fixed-end moments; the resulting pre-stressing moments throughout the entire structure should also be considered. With localised tendons, different pre-stressing forces may be used to obtain the most favourable effects.

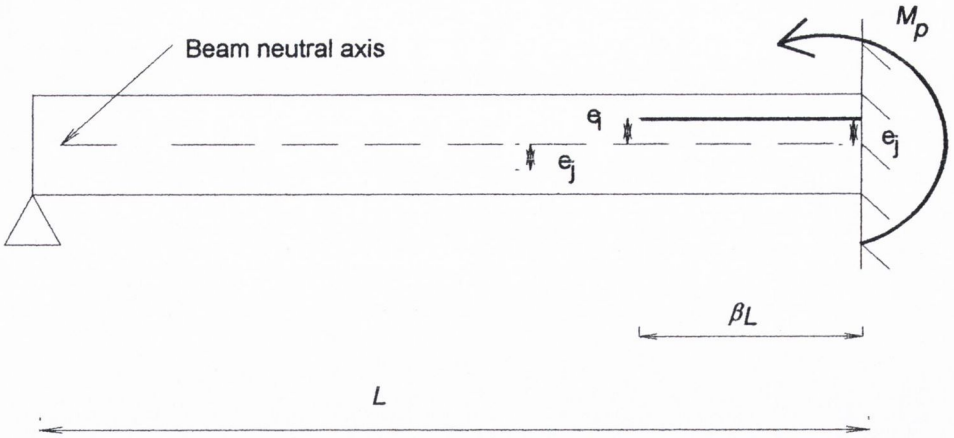

Figure 2.24: Horizontal tendon over the interior support (Picard et al., 2000).

With this local tendon application, the bending moment is being reduced due to the presence of a central support (which attracts moment). With regard to continuous beams, the locations and forces of external tendons are considered for each individual case such that the moments due to loading are reduced. No account is taken of the interaction between tendon force and load application and tendon forces are assumed to be constant. However, there are specific optimum locations and tendon forces with respect to the type of loading and supports for single and continuous beams. These locations and tendon forces can be expressed in terms of loading and span. Such tendon configurations are considered in this thesis and are discussed in chapter 3.

External post-stressing in segmental bridge box girder design is one of the major developments in bridge construction in recent years. The principle of segmental bridge construction is to hold together segments of the deck by external tendons within the box girder. A publication (Rombach, 2002) on segmental concrete box girder bridge construction found that, unlike classical monolithic bridge construction, little disruption takes place to traffic flow. Cost savings are possible, as the segments are pre-cast in workshop conditions. Figure 2.25 shows a typical segmental box girder span in which the span will have three types of segments, as follows:

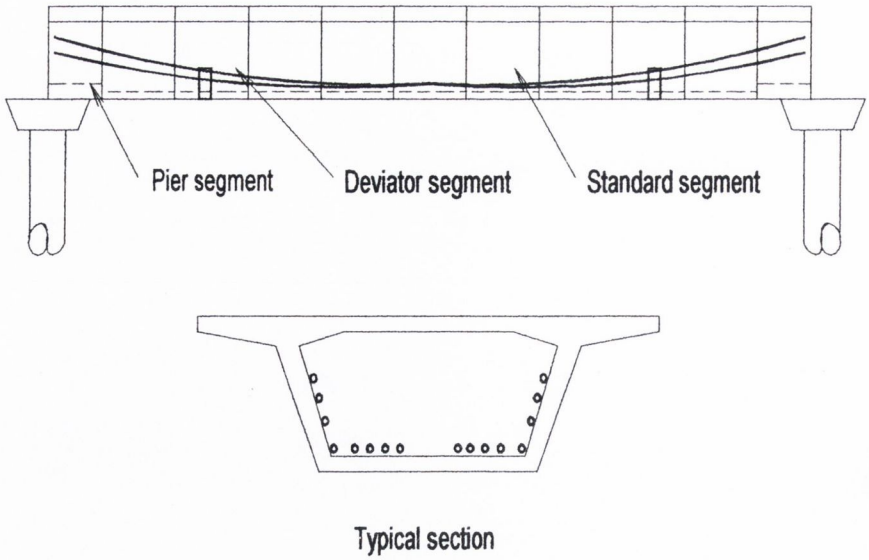

Figure 2.25: The different types of box girder segment required for external pre-stressing (Rombach, 2002).

- Pier segments, which will require thick webs and base slab to withstand the high stresses induced by tendon anchorage.
- Deviator segments, which form the required tendon profile along the length of the span.
- Standard segments, which will have thinner webs than the other segments.

The author discussed the advantages and disadvantages of using external pre-stressing in segmental box girder construction, which may be summarised as follows:

Advantages:

- Damaged tendons can easily be replaced.
- Less dead load with the structure as thinner webs are possible without tendons incorporated.
- Less friction loss with external tendons.
- Tendon forces can be adjusted after construction.
- Greater permissible pre-stress forces are allowed with external pre-stressing.

- Inspection is facilitated and long-term maintenance is easier with external tendons.

Disadvantages:

- Additional internal bonded steel reinforcement is required within the segments
- Additional costs are incurred due to tendon deviators and large anchor block details to withstand the higher stresses associated with external tendons at end anchorage
- Only straight tendon configurations or configurations with straight portions can be used with external tendons (that is, no parabolic configurations are possible, as in the case of internal tendons).

Access to external tendons is an important factor when designing external tendon highway structures either for structural retrofitting or for applying external tendons to new construction. A design manual publication for roads and bridges in the UK road authorities (DMRB, 2001) states that, "post-tensioned structures using external or un-bonded tendons shall be detailed such that inspection of all individual tendons and their eventual replacement is possible without restricting traffic on the highway".

For example, work has been carried out on the conversion of an internally post-tensioned bridge box section construction to an external post-tensioned installation. A specialist sub-contractor published a report on the upgrading of the Kinston Bridge, Glasgow (Balvac Ltd., 2001). The Kingston Bridge carries the M8 traffic over the river Clyde and is reputed to be one of the busiest motorways in Europe. The bridge is constructed with pre-cast box girder concrete segments, which originally had internal tendons in the webs and floor of the box segments. The box girder segments were jacked up off the original piers and supported by temporary buttresses. The original piers were demolished and new piers were constructed.

Balvic Ltd, on behalf of Balfour Beatty Ltd., carried out the installation of 230 tonnes of external post-tension strands. The new strands required the installation of new deviator

blocks and anchor blocks. The anchor blocks were fabricated with steel sections that were fastened to the original structure with high tensile fixings. The deviators were fabricated from circular steel sections that were anchored to the structure. The tendons ranged in length from 170m to 200m. The specification called for the facility to de-stress and replace an individual tendon while the remaining tendons remained fully tensioned (DMRB, 2001). With the external tendons in place, 88MN of tendon force was applied to the bridge decks, prior to being lowered onto the new bridge piers. The bridge remained open to the M8 traffic, for the most part, and during construction the bridge was constantly monitored to ensure safety. This preferred method of strengthening removed the future problems associated with internal tendons such as long-term monitoring and replacement.

An international post–stressing company issued a publication as a guide to engineers designing an external post-tension application (Aebehard, 1993). The guide considered the components of external post-tensioning and discussed the design considerations for each. The anchors used for external tendons were the same as those used for internally bonded tendons. However, more recently, as discussed earlier, a greater demand for external tendon replacement has driven the development of anchors specifically designed for external tendons. These end anchors allow tendons to be stressed, de-stressed and then removed if necessary. The deviators used for external post-tensioning applications are steel tube sections (bent to a minimum radius, never less than 2.5m) through which the tendon passes. A specified minimum radius ensures that no damage occurs to the tendon when tensioning and that the protective coating is not breached. The steel deviator tubes are cast into concrete for new applications or secured with bolted fabricated steel sections in a retrofit. The publication outlines the importance of protection of tendons from corrosion and gives guidance on a number of possible methods of corrosion protection.

Research has been carried out in the area of external tendon monitoring by Japanese research consultants (Sumitro et al., 2003). For example, the Kamikazue viaduct in Tokyo is a box girder pre-cast segmental construction with external tendons contained

within the box section. The viaduct is 630m long in total with 17 spans each of 34.2m with 14 pre-cast segments. The decking is 16m wide. The pier segments are 4.5m wide and have clearance to provide full time monitoring apparatus. The tendon deviator segments were located 10.9m from the centre of each pier. The height of the box girder construction was 2.6m.

Applying strain gauges to the tendons was not possible as the tendons had an epoxy coating. Electro-magnetic sensory technology was adopted for this application. The monitoring device measures the change in electro-magnetic properties of the tendons. The stress and temperature are factors that will effect the electro-magnetic properties of a tendon. Knowing the ambient temperature, the device can measure the stress present in a tendon. The stress monitors were also used on a full-scale test to verify the safety of the anchor blocks and to measure the friction loss at the tendon deviators. A stress monitor was placed at either side of the deviator block with the tendons tensioned to the working stresses. The difference in stress, and thus the force, could be calculated, which was the loss in force due to friction. A full-scale test allowed the jacking force losses, and long-term creep coefficient to be calculated.

External tendons will generally improve the capacity of beams at a higher percentage than internal tendons owing to the greater availability of tendon eccentricity (that is, of the order of 20-30%). The external tendon configurations reported in this research (Picard et al., 2000) are used to apply beneficial moments that serve to reduce the moments due to loading. Earlier research by this author had considered the use of tendons to reduce peak bending moments on loaded beams but with a more specific method of applying beneficial moments of specific magnitude at specific locations so as to not only reduce the peak bending moments but to minimise them.

A major problem with steel-concrete composite beam strengthened with external tendons is that of cracking in the upper concrete which causes problems with the durability and maintenance of the concrete (Brozzetti, 2000). However, in the case where a

compressive tendon force is applied in the hogging moment zone, an increase in yield and ultimate load results, together with a decrease in cracking (Li et al, 1995).

Research was carried out on steel-concrete composite bridge beams with a view to crack prevention in the upper concrete decking (Ryu et al., 2004). The tendons were located on the webs of the steel box girder over the supports and as close to the decking as was practically possible (see Figure 2.26). Loading some 40% (1000kN) greater than the un-strengthened load that would cause excessive cracking (600kN) in the decking was measured without excessive cracking resulting.

With internal tendons long term monitoring and maintenance are problematic as is quality control during installation. When external tendons are employed the long term monitoring and maintenance can be carried out much more efficiently where tendons can be readily replaced if necessary. If one considers (as discussed in the next section) concentrated moments to strengthen beams, internal tendons are not viable as moment is applied along the length of the tendon to the beam. External tendons, however, will allow concentrated moments at specific optimum locations.

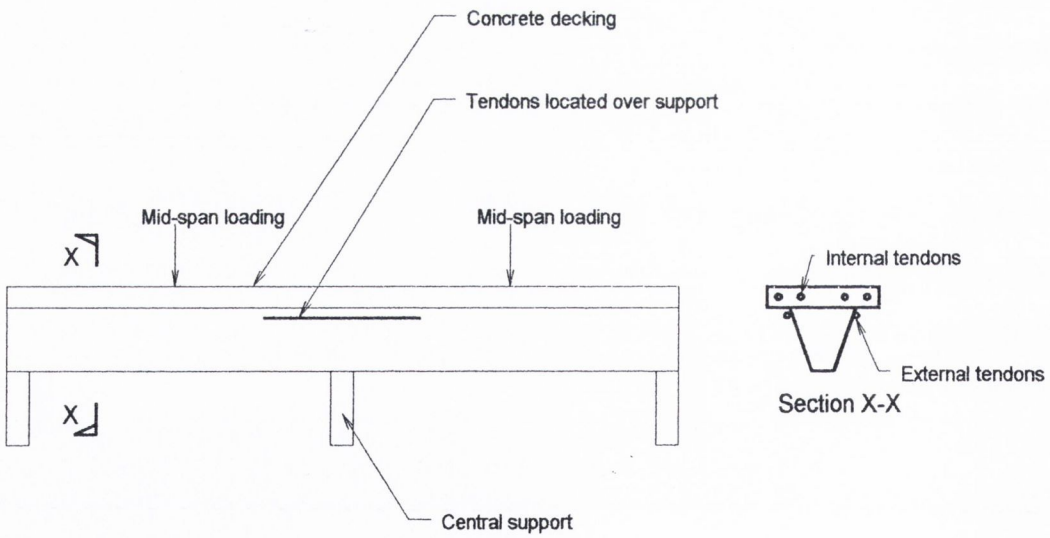

Figure 2.26: Arrangement of tendons over supports (Ryu et al., 2004)

2.3 Previous work on the use of tendons to apply counter-moments in steel beams

A final year undergraduate project, carried out by the author, investigated the use of external tendons in steel beams to apply specific moments at specific locations so as to minimise, the bending moment diagram (Maher, 1998). This was undertaken prior to the partial tendon in concrete work by Picard (2000) reported in section 2.2.

The work involved initially examining the case of a simply supported beam of span L, with a central concentrated load, *W*. This loading resulted in the typical triangular bending moment diagram yielding a maximum moment at mid-span (M_{max})of WL/4. If counter-moments (that is, moments opposite to those induced by loading) are applied to the beam, this will reduce M_{max} at mid-span. If these counter-moments are applied at one-third the distance from the supports to the point load (where in this case, the loading is symmetrical) and if the magnitude of the counter moments is two-thirds the un-strengthened maximum bending moment, this will result in the optimum bending diagram. The peak moment, M_{max}, is now one third the original maximum moment (that is, WL/12 - see figure 2.27). The term "pair of counter moments" refers to two counter moments applied to a beam, one each side of a concentrated load and of equal and opposite magnitude, induced via a tendon or tendons.

It should be noted that, while the bending stresses are reduced to one-third their original value, additional axial compressive stress will be present in the beam due to the tendon application. However, there normally is a net improvement, which is dependant on tendon eccentricity. The greater the tendon eccentricity, the lesser is the axial force that is required to apply the optimum $2/3M_{max}$ counter moment and, thus, the greater the overall improvement.

2.3.1 Analysis

Initially a number of different load cases were analysed; simply supported beams with a central concentrated load, simply supported beams with an asymmetrical concentrated

load and fixed end beams with a central concentrated load.

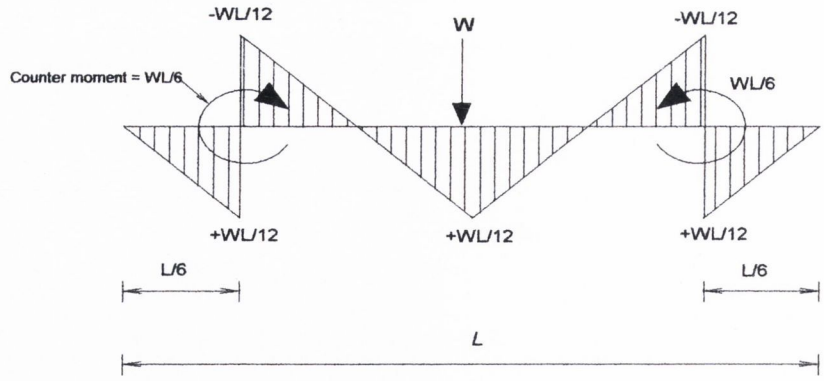

Figure 2.27: The optimised bending moment diagram for a simply supported beam with a central concentrated load (Maher, 1998).

In the case of a simply supported beam with a central concentrated load, the areas of the beam with lower flexural stresses (that is, the sections closer to the supports) were considered with a view to attracting stresses towards these sections and away from the areas of higher stress at and closer to the mid-span.

With many steel members, the areas of maximum bending and/or axial stresses only are considered in design when sizing. In all other areas, the member could be considered to be over-designed. Members with varying cross-sections are not financially viable with current manufacturing processes. The method of applying counter-moments at areas of lower stress "engages" the beam to attract higher stresses to such areas and reduce the stresses at mid-span. A number of different locations were considered and, by superposition, it was found that the optimum location was one-third the distance from the supports to the point load. Moving the location of the counter-moment to the left or to the right of this point will result in a higher maximum moment in the final bending moment diagram. Changing the magnitude of the counter-moment by a lesser or greater amount will also result in a higher maximum moment in the final bending moment. Thus, in this case, the minimum maximum moment arises by application of this pair of counter moments of this magnitude at this location.

For the case of a simply supported span with a central concentrated load and m pairs of counter moments applied, it can be shown (Maher 1998) that the optimum locations of application of the counter-moments are:

$$l_m = \frac{L(2n-1)}{(4m+2)} \tag{2.11}$$

where

l_m = The location of the counter moments from the supports towards the mid-span for the n^{th} pair of counter moments

L = The clear span

m = The number of pairs of counter moments applied

n = The n^{th} pair of counter applied from 1 to m

The magnitude of these counter moments can be expressed as (see Appendix A):

$$M_{co} = \frac{M_{\max}}{2m+1} \tag{2.12}$$

where;

M_{co} = Applied counter moments at each location

M_{max} = Maximum moment in the unstrengthened beam.

Note also that the maximum moment in the final bending moment diagram is half that of the applied counter moment (that is, $M_{co}/2$).

The final maximum moment on the beam, in the case of a single pair of counter moments on a simply supported beam, is reduced by 66% from that of the original un-strengthened beam. However, of course, an axial force must be applied via tendons to generate the counter-moments to the beam. Therefore, while the bending stress reduction is 66%, the compressive axial stress which is present due to the tendon forces, reduces the overall improvement of 66% in load carrying capacity. The overall improvement will depend on the magnitude of the axial stress, which itself is dependant on the tendon eccentricity.

2.3.2 Testing

A model was fabricated to test the proposed theory of the benefit of applying counter moments. The section size at this stage was not critical in that a practical constraint of construction (that is, the overall beam depth) was not a primary consideration. It was decided, therefore, to use a 4 m long R.S.J. (102 x 64 x 9.65Kg/m) together with 76 x 38 x 6.7 Kg/m channels which were used as "down stands" or levers to apply the counter moments. The pre-stress forces were applied via 16mm diameter threaded bars, used instead of tendons, that were tensioned up by tightening nuts at one end. Two pairs of counter moments were applied to the test beam (see figure 2.28). This required two pairs of levers to be attached to the beam - two inner and two outer levers, the outer levers being longer to allow the outer lever tendon to pass the inner lever tendon without interference. Both tendons were centred on the vertical axis to prevent unfavourable secondary moments about the minor (y-y) axis. The optimum configuration of the test beam was calculated using equations 2.11 and 2.12.

Monitoring apparatus

Half bridge strain gauges were fitted to the beam on the top flange upper face and the lower flange bottom face on either side of the location of the application of the counter moments to monitor the bending and axial stresses at each location. The portions of the beam between the inner and outer levers and the portion between the inner levers had strain gauges fixed at the neutral axis to monitor the axial strain and, thus, axial forces. Knowing the axial forces at the above locations allowed the forces in each tendon to be calculated using equilibrium. As a secondary check, strain gauges were fixed to each tendon to retrieve direct readings.

A hydraulic jack was used to apply a 4kN load and a load cell was inserted between the jack and the beam, monitoring the load application.

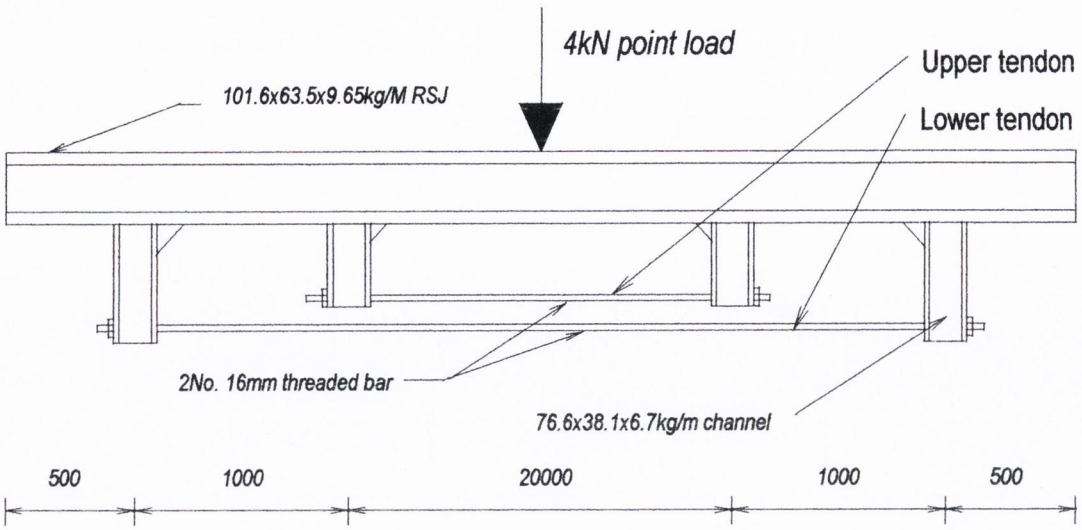

Figure 2.28: The configuration of the test beam used in earlier research (Maher, 1998).

Testing regime and results

Three types of tests were employed:

1. Neutral test – No "tendons" fixed to the beam
2. Passive test –Bolts hand tightened and "passively engaged"
3. Active test – "Tendons" tensioned to required pre-load tensile forces

Neutral test

This test was used as a control test and involved two types of test, the first being a straightforward point load test to check the unstrengthened and unstiffened flexural behaviour of the beam (by un-stiffened it is meant no levers or stiffeners were attached to the beam). With the 4kN central concentrated point load applied, the maximum stress recorded was 48.9MPa with a deflection of 10.4mm at mid-span.

The next neutral test involved testing the beam with levers and stiffeners attached to investigate whether these additions had any significant impact on the flexural behaviour of the beam. The results in this case matched closely with the previous test, giving

results of 48.6MPa for the maximum stress and a maximum deflection of 10.2mm. The latter test demonstrated that no significant alteration to the flexural behaviour of the beam had occurred.

Passive test

When a central concentrated load was applied with the tendons passively in place, a subsequent tension arises in the tendons. The magnitude of this tension depends on the eccentricity of the tendons from the beam neutral axis. The function of this test was to better understand the interaction between the tendons and the beam. No pre-tension force was applied to the tendons so that the amount of force induced in the tendons could be measured independently upon application of the central concentrated point load. The nuts on the thread-bar were hand-tightened such that they were just engaged prior to load application.

The results of this test showed that, after application of the concentrated central load, the final forces in the tendon were too high which, in turn, applied too much counter moment. It was decided, at this stage, to carry out an analysis on an existing computer model of the test beam to establish the component of additional force in the inner tendon when a unit tensile force was induced in the outer tendon. Similarly, the component of additional force induced in the outer tendon when a unit tensile force was applied to the inner tendon was established. Using superposition and assuming linearity in both of the above tendon load cases, an equation was derived such that a pre-tension force could be prescribed for each tendon to give, after the application of the central concentrated load, a final tensile force that would apply the correct counter moment for the optimum bending moment diagram. The equations were as follows.

$$N_T = 0.835P_T + 0.112P_B \tag{2.13}$$

$$N_B = 0.863P_B + 0.037P_T \tag{2.14}$$

where;

N_T = The final required force in the upper tendon to give the optimum applied counter moment

N_B = The final required force in the lower tendon to give the optimum applied counter moment

P_T = The initial pre-tension force in the upper tendon

P_B = The initial pre-tension force in the lower tendon

The equations were used to calculate the required initial pre-tension force in each tendon to give the final optimum bending moment diagram (that is, a five peaked diagram with a maximum moment of 0.5kNm).

Active test and results

This tests series was split into two types of testing; first a specific tensile force in the tendons was applied and then the central concentrated load was varied; the second test type involved applying varying initial pre-tension forces in the tendons and applying the same concentrated central load.

Type 1- Constant pre-tension force in tendons

This test was carried out to investigate the relationship between the concentrated load and the tensile forces in the tendons. It was found that the load application/tendon force interaction was linear and a concentrated load increment of 5kN yielded a tensile force increment of 4.2kN and 5.1kN in the inner outer tendons respectively. The difference in tensile force increase between the upper and lower tendons was attributed to the difference in tendon eccentricity from the neutral axis of the beam, where the upper and lower tendon eccentricities were 275mm and 325mm respectively. It was confirmed from a number of trial computer analyses that the greater the eccentricity, the greater the tensile force increase with respect to a concentrated central load increase (that is, the slope of the plot of point load vs. tendon force increased with increasing tendon eccentricity). The testing allowed a graph (figure 2.29) to be plotted showing the linear relationship between tendon load increase and concentrated load application.

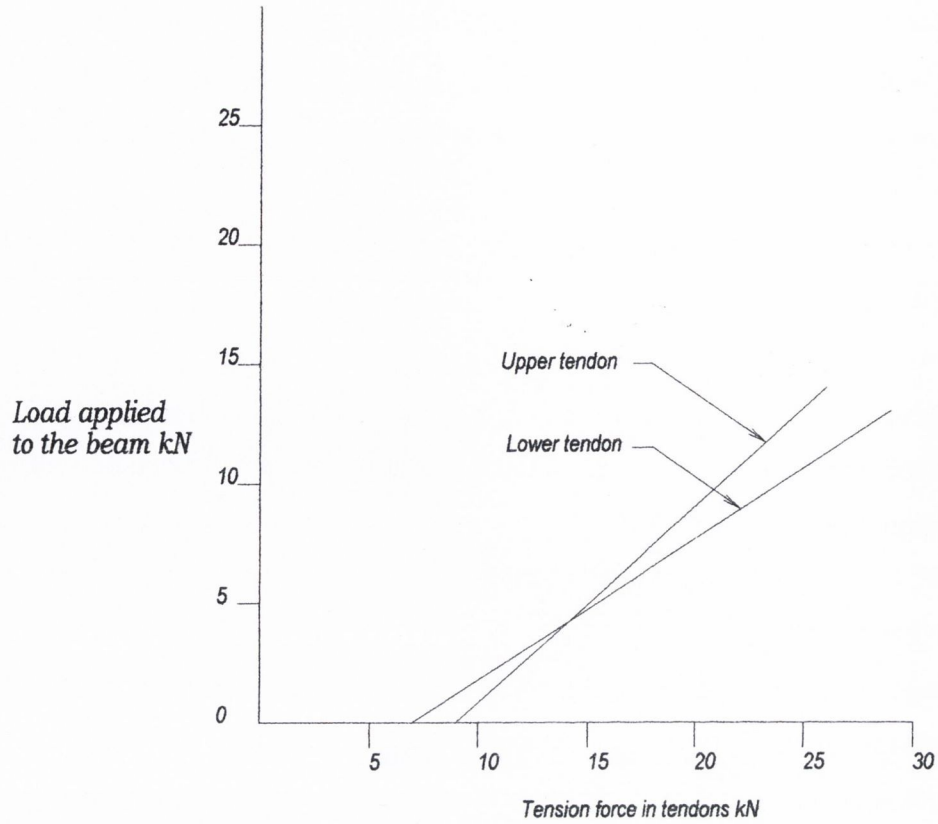

Figure 2.29: Linear relationship between load increase and tendon force increase for upper and lower tendons for a given pre-stressed load in each tendon.

Type 2 - Constant concentrated load applied

This type of test was carried out to investigate the behaviour of counter-moment application, via the tendon force, with varying initial pre-tension forces but for a concentrated load of the same magnitude applied (4kN). It was found that the rate of increase of counter-moment applied, with respect to an increase of central concentrated load, again, was linear.

The testing also showed that irrespective of the amount of initial pre-tensioning in the tendons, the rate of change of counter-moment, with respect to an increase in the central concentrated load, was constant (that is, the slope of the plot was the same at any "shift" along the horizontal pre-tension tendon force axis).

A final test was carried out with the exact amount of pre-tension force required to deliver the optimum bending moment diagram. The required final applied counter moments were 1kNm applied at the levers. It was found that applying a 4kN central concentrated load to the beam induced a 4.057kN force in the upper tendon and a 5.018kN force in the lower tendon. Subtracting these forces from the required 7.272kN and the 6.15kN force (calculated from equations 2.13 and 2.14) in the upper and lower tendons respectively left the required pre-tension forces of 3.125kN and 1.132kN. With these initial tensile forces in the tendons, the application of the 4kN central concentrated load gave the optimum five-peaked bending moment diagram, which is shown in figure 2.30. The delivery of the stresses associated with this moment distribution was confirmed by the strain gauges.

The testing also found that, while the deflection increase was linear with load (figure 2.31), the rate of deflection was less than the case of the un-strengthened beam. A 4kN central concentrated load yielded a mid-span deflection of 5.8mm in the un-strengthened beam compared to 2.6mm in the strengthened case. This represented a 45% reduction in deflection.

In this configuration, the tendon eccentricities were large compared to the beam depth. When a load is applied, this results in significant tendon force increase, which applies (that is, very little pre-tension is required) relatively large counter-moments.

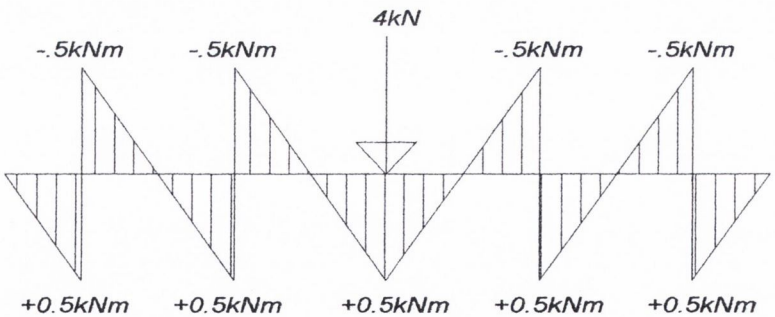

Figure 2.30: The optimum bending moment diagram with the two pairs of counter-moments applied.

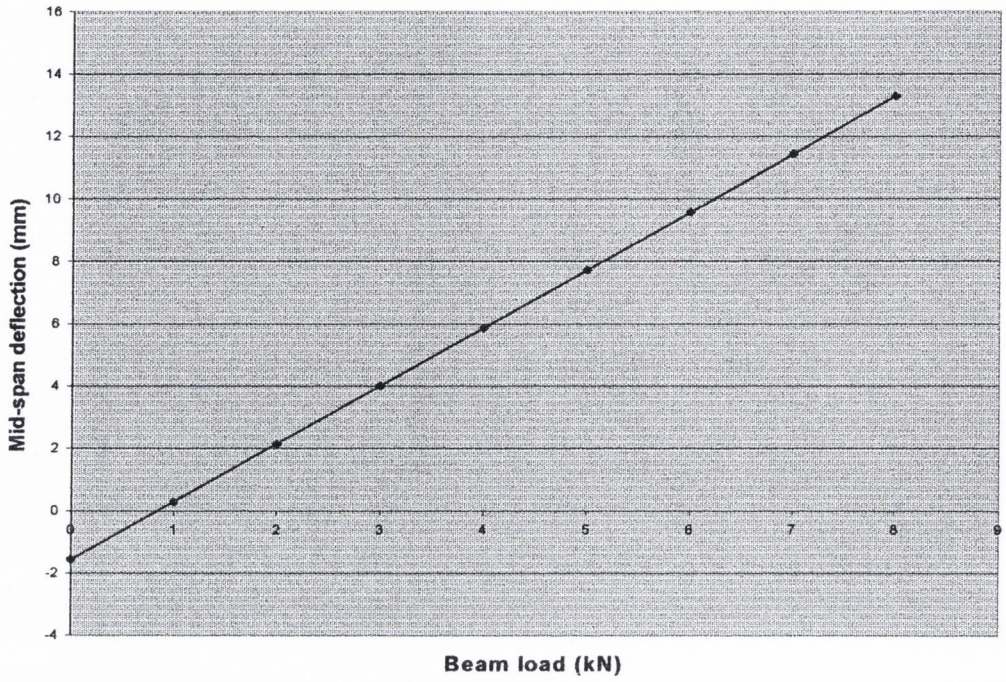

Figure 2.31: Deflection versus beam with a central concentrated load for constant pre-stressed load.

2.4 Lateral torsional buckling of steel sections.

Over 60 years ago the Steel Structures Research Committee (U.K.) established that linear-elastic design is unlikely to predict an accurate representation of the structural response of members (Kemp, 2003). In the 1960's, limits on serviceability and ultimate loading were the basis for a new approach to design that was based on inelastic behaviour.

2.4.1 Ductile approach to design

Most design codes are now based on ultimate and serviceability limits states with regard to the steel ductility, which allows the structure to deform significantly beyond the elastic

limit, while maintaining an ultimate resistance above or just at the design loading. The main benefits of the ductile design are as follows (Kemp, 2003):

- Greater efficiency of flexural strength and stiffness.
- Allowance for greater error in design assumptions with regard to load paths or structural responses.
- Greater margin of safety with regard to unexpected or rare loads.
- Greater ductility is often achievable at little extra cost.

A limit-state criterion for a structure to be sufficiently ductile is as follows (Kemp, 2003):

$$\theta_a \gamma_a = \theta_r \gamma_r \tag{2.15}$$

where:

θ_a = the available rotation in the structure.

γ_a = the load factor

θ_r = the rotation of the member at full plastic moment resistance.

γ_r = the load factor.

The structure must be geometrically free to rotate under loading such that full plastic moment resistance can be achieved (that is, sufficient deflection can occur).

2.4.2 Lateral torsional buckling load

For member selection with this research, it was necessary to consider torsional buckling strength as well as flexural strength about the major axis. When establishing the ultimate flexural loads for steel members, it is necessary to consider lateral torsional buckling about the minor axis of the section. Design codes allow the maximum allowable load to be calculated (BS5950: 2000) based on lateral torsional buckling deformation of the beam. This load will more often be the ultimate load of the beam and will be lower than the local section capacity load. It has been shown (Hancock et al., 1997) that beams with very thin webs will distort laterally in a manner analogous to compressive column minor axis buckling rather than lateral torsional buckling.

Research has been carried out on the ultimate strength of I sections based on inelastic lateral torsional buckling (Trahair et al., 2004). The work developed a method of designing steel members against out-of-plane failure by using a reduced elastic section modulus about the minor axis. The following expression was used to calculate the ultimate beam strength, M_b:

$$M_b = \gamma_{IM} M_{yz} \tag{2.16}$$

where:

M_{yz} = the elastic buckling moment of the section of a simply supported beam and is given by (Trahair et al., 2004):

$$M_{yz} = \sqrt{\frac{\pi^2 EI_y}{L^2}\left(GJ + \frac{\pi^2 EI_w}{L^2}\right)} \tag{2.17}$$

where:

E = the elastic modulus

G = the shear modulus

L = the span

I_y = the major axis moment of inertia

I_w = the minor axis moment of inertia

J = the section torsional constant

The reduction factor, γ_{IM}, is given by:

$$\gamma_{IM} = 0.9 - \frac{1}{1.2}\left(\frac{M}{M_{px}}\right)^2 \tag{2.18}$$

where:

M = the applied moment about the major axis.

M_{px} = the plastic moment capacity of the section.

For simply supported beam with restraints at mid-span that prevent lateral and rotational displacement, the ultimate flexural torsional buckling moment can be expressed as follows (Valentino et al., 1998):

$$M_{yz} = \sqrt{\frac{4\pi^2 EI_y}{L^2}\left(GJ + \frac{4\pi^2 EI_w}{L^2}\right)} \qquad (2.19)$$

The authors (Trahair et al., 1993) reported that the predicted lateral torsional buckling moments for simply supported beams with uniform moments applied were higher than the predictions resulting from the design codes (of the order of 5%). However, when considering simply supported members with bi-axial bending, the proposed approach yielded capacities less than the design codes (of the order of 5-10%) (AS4100, 1990).

If lateral restraint is provided between the supports of a beam (preferably at mid-span) this will increase the ultimate loading by effectively reducing the lateral buckling length under consideration. The designer may take advantage of the presence of a brace provided there is sufficient information to predict the resulting increase in ultimate strength and provided that the brace is strong enough to withstand any actions induced by out-of-plane buckling (Yura, 1993 and Valentino, et al. 1997). When calculating the ultimate lateral torsional buckling load, the design codes (for example, BS5950) take into account the effect of yielding and imperfections, such as residual stresses, and initial crookedness and twist (Trahair, et al. 1993).

In chapter 3 a proposed method of strengthening will be discussed where axial compressive force and moment are applied to a steel "I" section. The beam-column approach (Steel Designers' Manual, 2005) for the capacity design checks was adopted for this application using an established design code (BS5950:2000).

2.5 Optimisation analysis for frames

An M.Sc. dissertation carried out by Mc Bride (2001) investigated the possibility of applying counter moments to portal frames to reduce the bending moments induced by loading. The method is analogous to that of a continuous beams as discussed above with the exception that with portal frame analysis, the members were allowed to develop their

full plastic moment capacity and were not confined to elastic moments. The method employed in Mc Bride's work was the upper bound or unsafe theorem.

Having established the conventional upper bound optimum solution for a given structure, Mc Bride then considered minimising the optimum solution with the introduction of counter moments so as further to reduce the section sizes. A way of expressing the application of the counter moments in terms of the plastic moment capacity, m_*, was required. With the introduction of counter moments, it was necessary to apply a combination of the applied counter moments and the concentrated loads acting simultaneously such that, at each critical section under consideration throughout the structure, the effect of both the constant counter-moments and the variable concentrated loads were expressed. What resulted, for a pinned portal frame with a central concentrated load, was a 17 peaked bending moment diagram with three pairs of counter moment, one for each of the critical regions in the portal frame. How practical such a solution might be remains to be seen.

2.6 Conclusions

A number of strengthening applications have been reviewed under two main headings; plates bonded to beams and tendons used to strengthen beams. The external plate bonding methods of strengthening are predominantly used for structural up-grading in retrofit. Of the two main types of tendon application, (that is, internal and external) the external tendon application is more associated with structural retrofitting. The external tendon applications reviewed were primarily concerned with improving member capacity and not have particular regard to the tendon location longitudinally (that is, mostly applied along the length of the beam, as with conventional post-stressing).

When external tendons are used to strengthen beams a relatively small amount of work and disruption is caused when compared to plate bonding methods. Some problems have been discussed with regard to the use of CFP tendons for member strengthening.

However, if the proper material is selected for a particular application, results can be achieved that are comparable with steel.

Pre-stressed CFRP bonded plates have been shown to be a viable option for member strengthening, However, the problem of end anchorage associated with this, and many other FRP applications, requires mechanical end anchorage details which accrue more cost.

With this current research, a system of beam strengthening was investigated where an external tendon application could be used for both existing steel beam strengthening and also with regard to prefabricated beams used in new construction. However, as the concept of using counter-moments to optimise maximum bending moments has not been tested in practice, it is timely to research more deeply the potential of this method and, in so doing, the practical constraint of keeping the beam tendons within the beam depth will be explored.

CHAPTER 3

ANALYSIS OF A BEAM STRENGTHENED WITH EXTERNAL TENDONS TO APPLY COUNTER-MOMENTS

Chapter 2 included a review of the theory developed in previous research of the use of counter-moments in simply supported beams, symmetrically loaded with concentrated loads. The theory in this current research encompasses both simply supported and fixed end beams loaded with concentrated and uniformly distributed forces and two span continuous beams with two concentrated loads located symmetrically and asymmetrically, one on each span.

3.1 Theory

In many structural applications, the design is primarily based on the maximum moment and a member size is selected based on that one moment. In regions of the beam other than that where the maximum moment arises, the member could be considered to be over-designed. This research investigates a method of more fully utilizing the section capacity along the length of the member by reducing peak bending moments using a pair of counter-moments placed strategically on the beam. One way in which this can be achieved in practice is by attaching a pair of plates to the side under the upper flange on both sides of the web close to both ends of the beam. Allowing the plates to extend down as far as possible towards the upper surface of the lower flange gives the maximum possible tendon eccentricity (measured from the beam section neutral axis) for a tendon which can then be attached to these plates via, for example, thick-wall tubing. Stressing up the tendons on both sides of the beam then induces a counter-moment on the beam at the location at which the plates are attached.

In this way, for example, in a simply supported beam with a central concentrated load, the method involves applying to the beam, at specific locations, pairs of equal and opposite couples or moments in a sense opposite to those induced by loading. These

counter-moments would be symmetrically placed about the centre line and of a specific magnitude so as to optimise the beam capacity, that is, the maximum moment on the beam would be minimised. The net result of applying these specific counter-moments at these specific locations is to re-distribute the maximum moments along the length of the beam to such an extent that they can no longer be reduced further for this number of counter-moments. The resultant bending moment diagram will have a typical "saw tooth" shape (see Figure 3.1). It must be borne in mind that while bending stresses themselves can be reduced considerably (see section 3.2.1), there is a corresponding increase in the axial compressive force along the length of the beam between the locations of application of the counter-moments. This axial force is applied by the tendons and restricts the extent of improvement in beam capacity. The axial force required to deliver a particular counter moment will vary with tendon eccentricity and it is for this reason that overall beam improvement is directly related to the tendon eccentricity.

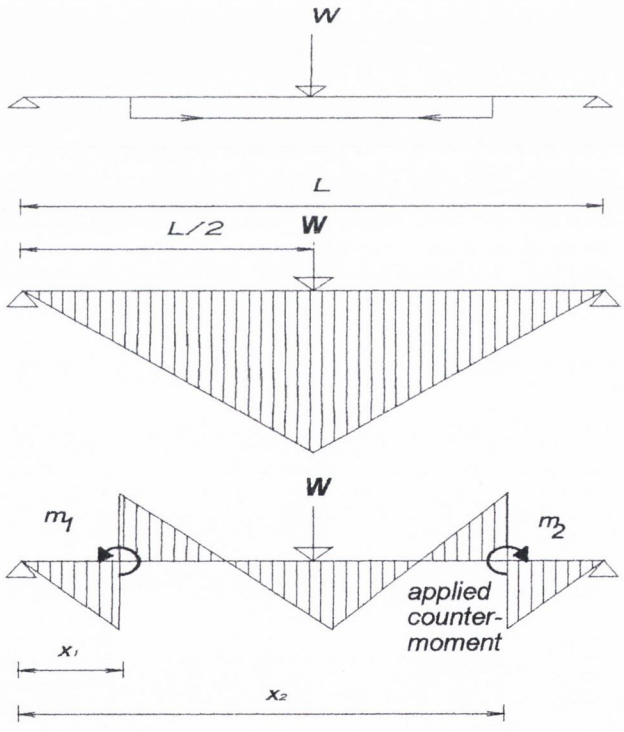

Figure 3.1: Tendon attached to the beam together with bending moment diagrams for the un-strengthened beam and the optimised bending moment diagram for the strengthened beam

3.2 Counter-moments applied to a single span beam

In the following section, different load cases will be considered for a single span beam with simple supports or with fixed ends. The basic objective is the same in each case, that is, to minimise the maximum bending moment on the original bending moment by applying counter-moments to the beam. The development of the equations for each of the cases discussed in this section is given in full in Appendix A.

3.2.1 Single pair of counter-moments on a simply supported beam

Consider more closely the case of a central concentrated load, W, on a simply supported beam of span L. The resulting bending moment diagram is a typical symmetrical triangle with a maximum moment of WL/4 ($=M_{max}$) at mid-span (see figure 3.1). If a pair of counter-moments, m_1 and m_2, are applied to a simply supported span at distances x_1 and x_2 respectively from the left support, either side of the load , the resulting bending moment diagram has a typical five peaked shape (with positive and negative peaks) where the maximum peak is denoted by $|m_{max}|$ (see figure 3.2). It is easy to show that to achieve the optimum condition, all five peaks must be equal and have the value WL/12 (that is, $M_{max}/3$). The magnitude of the counter-moments which needs to be applied to achieved to ahieve this optimum, in this case, must be two-thirds the original maximum moment of the unstrenghtend case.

To observe the specific advantages accruing for this, consider a case of a simply supported beam spanning 6m with a second moment of area, I, of 22530×10^4 mm^4, a Young's elastic modulus of 208GPa and a central concentrated load of 100kN. With an imposed limiting stress of 185MPa, the un-strengthened case hand calculation will show that the beam will have a maximum mid-span moment of 150kNm and a maximum mid-span deflection of 9.6mm. If one pair of counter-moments of 100kNm is applied at 1m from each support and, again, a 100kN central concentrated load is applied, the resulting maximum bending moment will be 50kNm and the mid-span deflection will be 5.4mm.

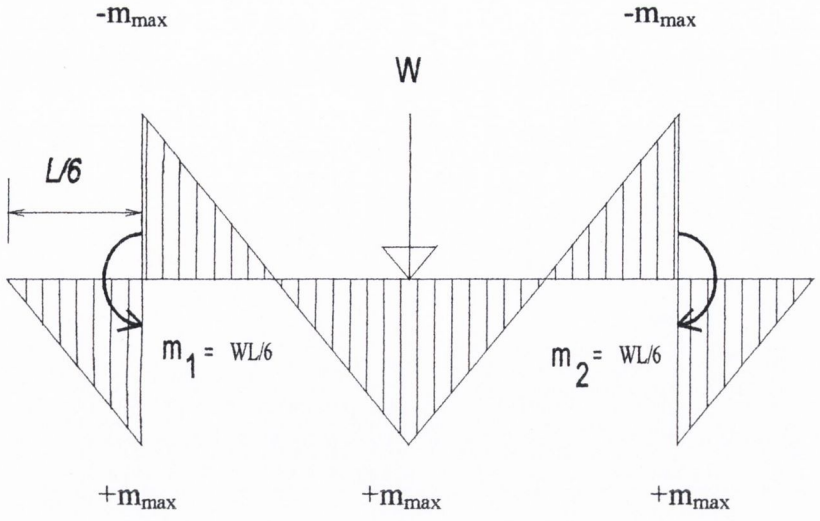

Figure 3.2: Optimised bending moment diagram showing five equal peaks of one-third M_{max}

This represents a 67% reduction in maximum bending moment and a 49% reduction in deflection.

In the case of a simply supported beam with a uniformly distributed load of intensity ω (kN/m) acting along the full length of the span, a similar principle applies. Here, again, to achieve the optimum bending moment diagram, where two equal and opposite counter-moments, m_1, are applied, it can be shown that the counter-moments must be equal to $2M_{max}/3$, or $\omega L^2/12$. By letting x_1 equal the distance from the left support to the point where the value on the original bending moment diagram is $\omega L^2/24$ (that is, $M_{max}/3$), it can be shown that $x_1=L(1/2-1/\sqrt{6})$. Here, again, $|m_{max}| = M_{max}/3$ at optimum m_1 and x_1 (see Appendix A).

3.2.2 Central concentrated load with multiple counter-moments

If one pair of counter-moments is applied, the maximum moment can be reduced by a factor of three. If multiple pairs of counter-moments are applied to a simply supported

beam with a central concentrated load, as there is more beneficial counter-moment, there is a greater resulting reduction in the maximum bending moment.

From the optimum bending moment diagram (see figure 3.3), it can be deduced that, in general, $m_1 = m_2 = m_i \ldots = m_n$, where i = 1 to n (n is the total number of pairs of counter-moments, m_i). It can be shown that (Maher 1998):

$$|m_{max}| = \frac{|M_{max}|}{2n+1} \tag{3.1}$$

where $|M_{max}|$ is the maximum moment on the original bending moment diagram and $|m_{max}|$ is the resulting maximum moment on the optimised bending moment diagram. Note also that the moment just to the right of the applied counter-moment $|m_i^+|$ is equal in magnitude to the moment just to the left, $|m_i^-|$, and that $|m_{max}| = m_i/2$.

The optimum location, x_i^*, of the ith counter-moment pair, m_i, on the left hand half of the span is given by the expression

$$x_i^* = \frac{L}{2}\left[\frac{2i-1}{2n+1}\right] \tag{3.2}$$

The corresponding location, $x_i^{*'}$, of the equal and opposite moment, m_i, on the other half of the span is, by symmetry,

$$x_i^{*'} = L - x_i^* \tag{3.3}$$

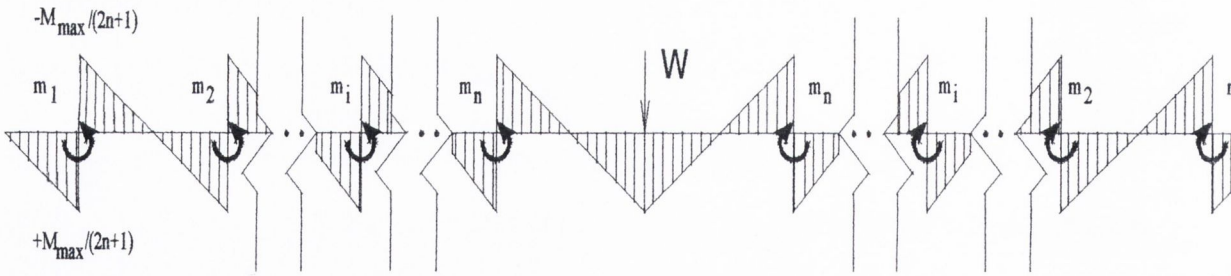

Figure 3.3: The application of "n" pairs of counter moments

For example, with three pairs of counter-moments (that is, n=3) applied to a simply supported beam with a concentrated central load, from Eq. 3.1, $|m_{max}| = M_{max}/7 = WL/28$, and $m_1=m_2= 2|m_{max}| = WL/14$. From Eq. 3.2, $x_1^* = L/14$, and similarly $x_2^* = 3L/14$ and $x_3^* = 5L/14$. The optimised bending moment diagram is given in Fig. 3.4, with $|m_{max}| = M_{max}/7$.

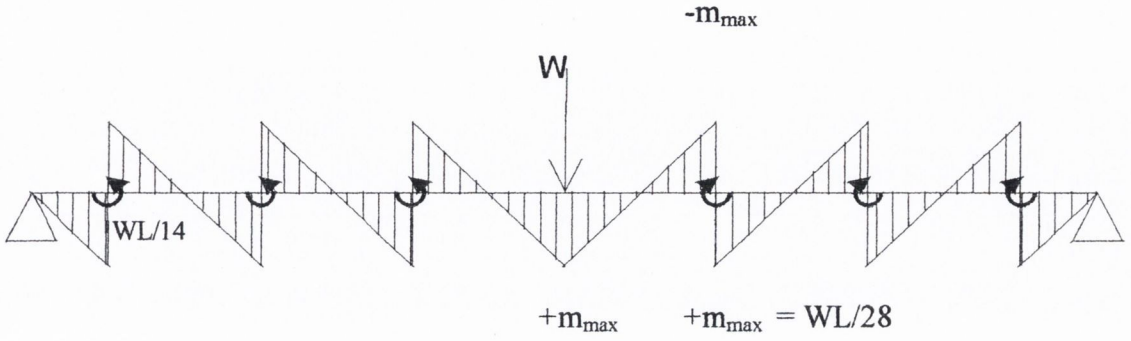

Figure 3.4: Optimised bending moment diagram with three pairs of counter moments applied. All peaks are of magnitude of $+/-M_{max}/7$

3.2.3 Non-symmetrical concentrated load

Consider the case of a non-symmetrical concentrated load on a simply supported beam. This loading yields a typical non-symmetrical triangular bending moment diagram with $M_{max} = Wab/L$, where "a" and "b" are the distance from the left and right supports to the point load respectively (see figure 3.5). In the case of just one counter-moment pair, $m_1 = 2M_{max}/3 = 2Wab/3L$. This case differs from that of the symmetrical case in that the locations of application of the m_1 pair are not placed symmetrically about the concentrated load, although the counter-moments themselves are equal in value.

The counter-moments are applied at the locations where the value of the moment on the original bending moment diagram is $M_{max}/3$. Therefore, the locations of the counter-moment pair are $x_1=a/3$ and $x_2=L-b/3$ from the left support.

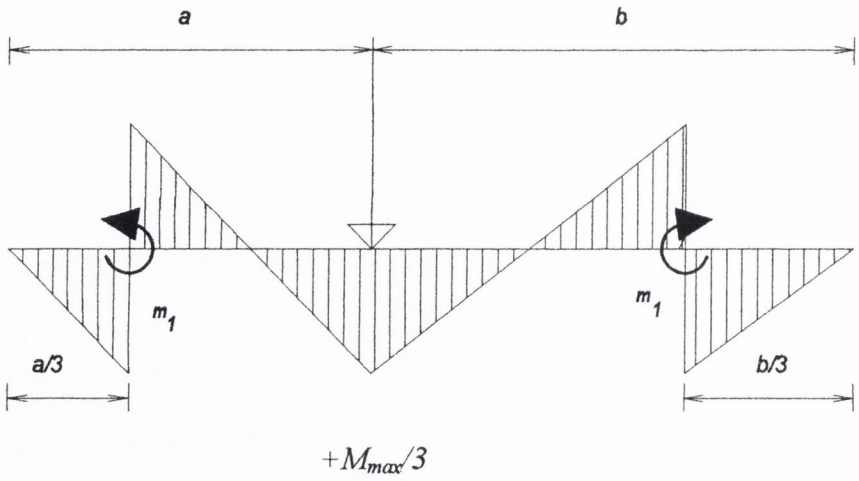

Figure 3.5: Bending moment diagram for non-symmetrical concentrated load showing five equal peaks

In the case of multiple pairs of applied counter-moments, the analysis is similar to that of the symmetrically loaded simply supported beam. The expression for the magnitude of $|m_{max}|$ is the same as that for the symmetrically loaded beam with multiple pairs of counter-moments, namely

$$|m_{max}| = \frac{M_{max}}{2n+1} \tag{3.4}$$

The location of the optimum position, x_i^*, for the ith counter-moment, m_i, on the left hand side of the concentrated load becomes:

$$x_i^* = \frac{a(2i-1)}{(2n+1)} \tag{3.5}$$

Similarly, for the right hand side of the concentrated load, measured from the left support, the location of the optimum position $x_i^{*'}$, for the ith counter moment is given by Eq 3.6.

$$x_i^{*'} = L - \frac{b(2i-1)}{(2n+1)} \tag{3.6}$$

For example, if two pairs of counter-moments are applied (n=2), with, say, L=15m, a=5m, b=10m and W=250kN, then M_{max}=833.34 kN.m. Letting $m_1=m_2 = 2M_{max}/3$ =333.36 kN.m, then $|m_{max}|$=166.67kN.m, $x_1^* = 1m$, $x_2^* = 3m$, $x_3^* = 9m$ and $x_4^* = 13m$, giving the optimum bending moment diagram as in Fig. 3.6. This represents a reduction in maximum moment of 80%. With an "I" value of ,say, $50500x10^4$ and a Young's modulus of 208kN/mm^2, the maximum un-strengthened mid-span deflection would be 16.3mm. With the counter moments applied, the maximum mid-span deflection would be 8.8mm approximately and represents a 46% reduction compared to the unstrengthened case.

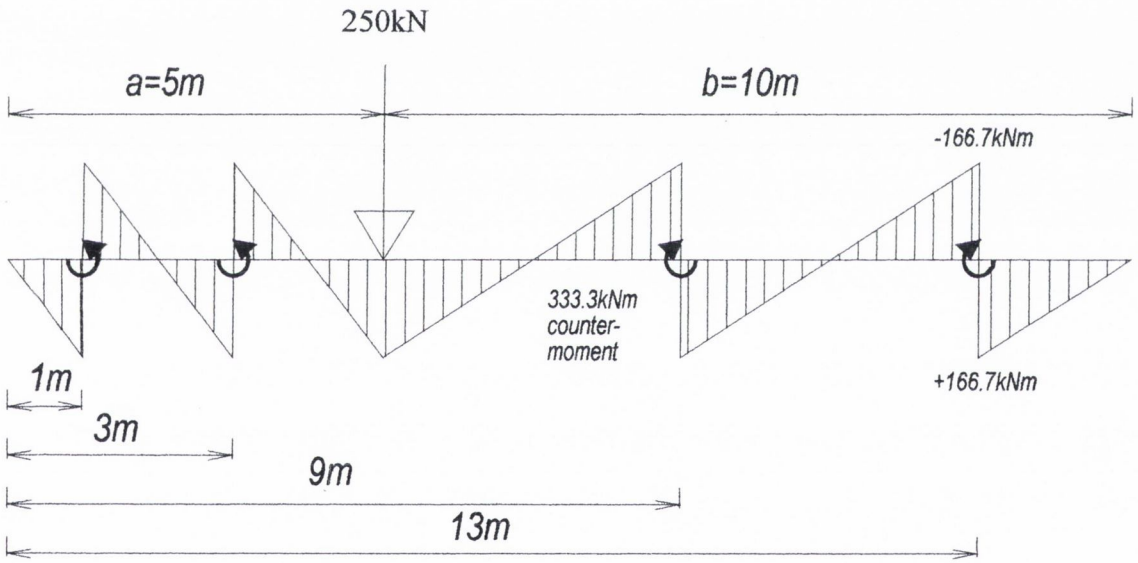

Figure 3.6: The final bending moment diagram of the beam with the asymmetrical loading and two pairs of optimum counter moments applied.

3.2.4 Fixed-end beam with a central concentrated load

In the case of a fully fixed-end beam with a central concentrated load, the best that can be achieved, with one pair of counter-moments applied (n=1), is to reduce M_{max} by a factor of 2, where M_{max} is WL/8. If, in this case only, m_{max} is applied at L/4 and 3L/4 from the left support, as a pair of counter-moments, the resulting bending moment diagram will be a typical 7 peaked shape with all peaks equal to WL/16. The reduction is less than in the case of the equivalent simply supported beam due to the beneficial moments that pre-exist at the supports which already serve to reduce the moment at midspan compared to the simply supported case (see figure 3.7).

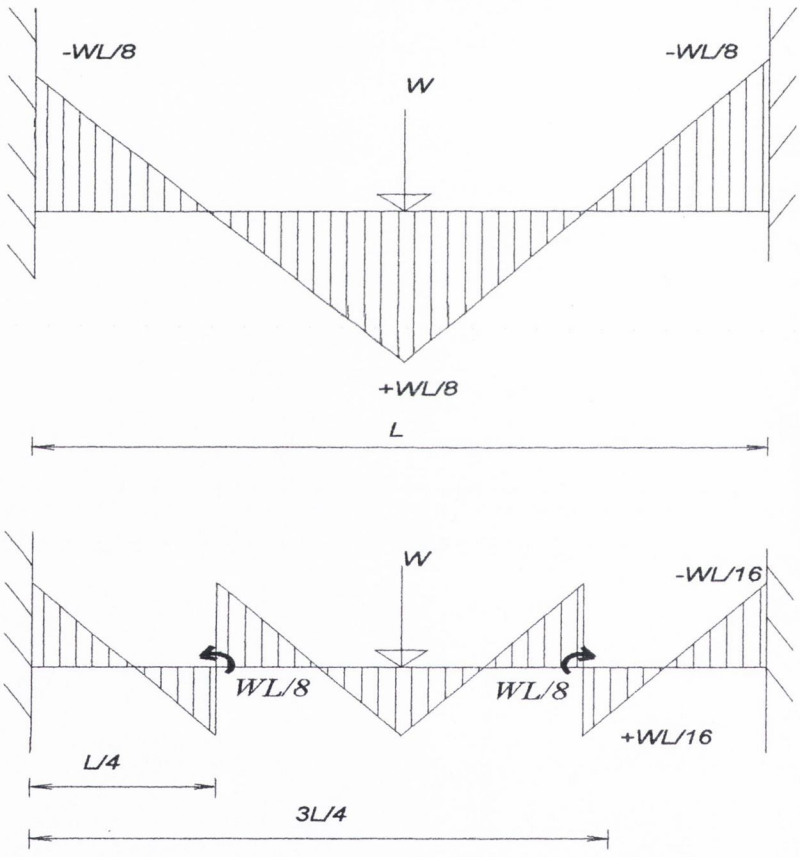

Figure 3.7: Optimised bending moment diagram of a fixed end beam with a central concentrated load and one pair of counter moments applied.

Considering the case for multiple pairs of counter-moments applied to a beam with fully fixed ends and a central concentrated load, it can similarly be shown that $m_1=m_2=m_i=m_n$ and that maximum moment is given by:

$$|m_{\max}| = \frac{M_{\max}}{n+1} \tag{3.7}$$

The point of application of each counter-moment to the left of the central concentrated load is given by the expression

$$x_i^* = \frac{iL}{2(n+1)} \tag{3.8}$$

For example, if one applies two pairs of counter-moments (n = 2) to a fixed-end beam with a central concentrated load, W=200kN with say, L = 14.0m, for which M_{max}=350kN.m, then m_i = ±233.4kN.m (i = 1 to 2) and $|m_{max}|$=116.67kN.m (note also that there are 11 peaks in the bending moment diagram), with optimum locations, x_i^*, as shown in Figure 3.8. This represents a maximum moment reduction of 66%, somewhat less than the simply supported counterpart (that is, 100kNm, and represents a reduction of 85.7%).

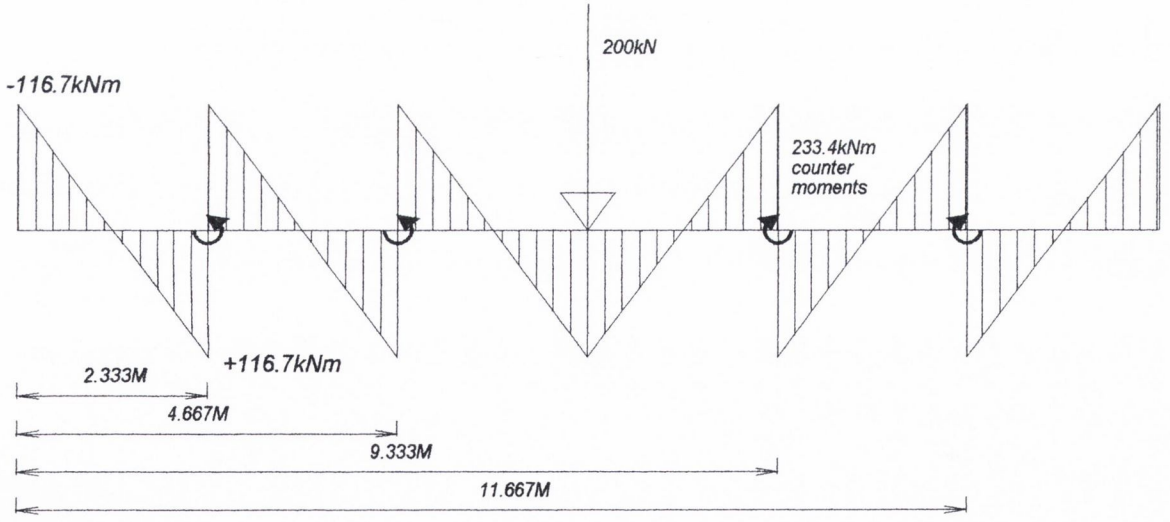

Figure 3.8: A fixed end beam with a central concentrated load and two pairs of counter moments applied.

3.3 Counter-moments applied to two-span continuous beams

Consider now the case of a two span continuous beam with a concentrated load on each span and a knife-edge support at the ends. This type of loading will yield a typical three peaked bending moment diagram with the possibility of M_{max} being in one of three locations; either under one of the concentrated loads or over the central support. Introducing an additional counter-moment pair of reverse sign about the central support, in addition to the counter-moment pairs in each span, will reduce the peak support hogging moment, allowing an optimum to be achieved.

3.3.1 Two-span continuous beam with an equal central concentrated load on each span and with the two spans of equal length

In the case of a symmetrical two span continuous beam with an equal central concentrated load on each span, one pair of counter-moments is applied for each of the three peaks, with the direction of the counter-moment pair for the central support being reversed. Let the maximum sagging moments to the left and right of the central support, which will be equal in this case, be denoted by M_l and M_r. Let the maximum moment over the central support be denoted by M_c. Each of these peaks on the original bending moment diagram will have one associated pair of counter-moments (left and right) m_{ll} and m_{lr}, m_{cl} and m_{cr}, m_{rl} and m_{rr} (see figure 3.9).

The resulting bending moment diagram has a fifteen-peaked shape. The locations of application of these counter-moments are x_1 to x_6 respectively as shown. The location and magnitude of the counter-moments were calculated using software that was developed by the author specifically for this purpose and will be discussed later in this chapter. The solution to this problem has a maximum resulting moment of approximately 3.4 times less than that of M_{max}.

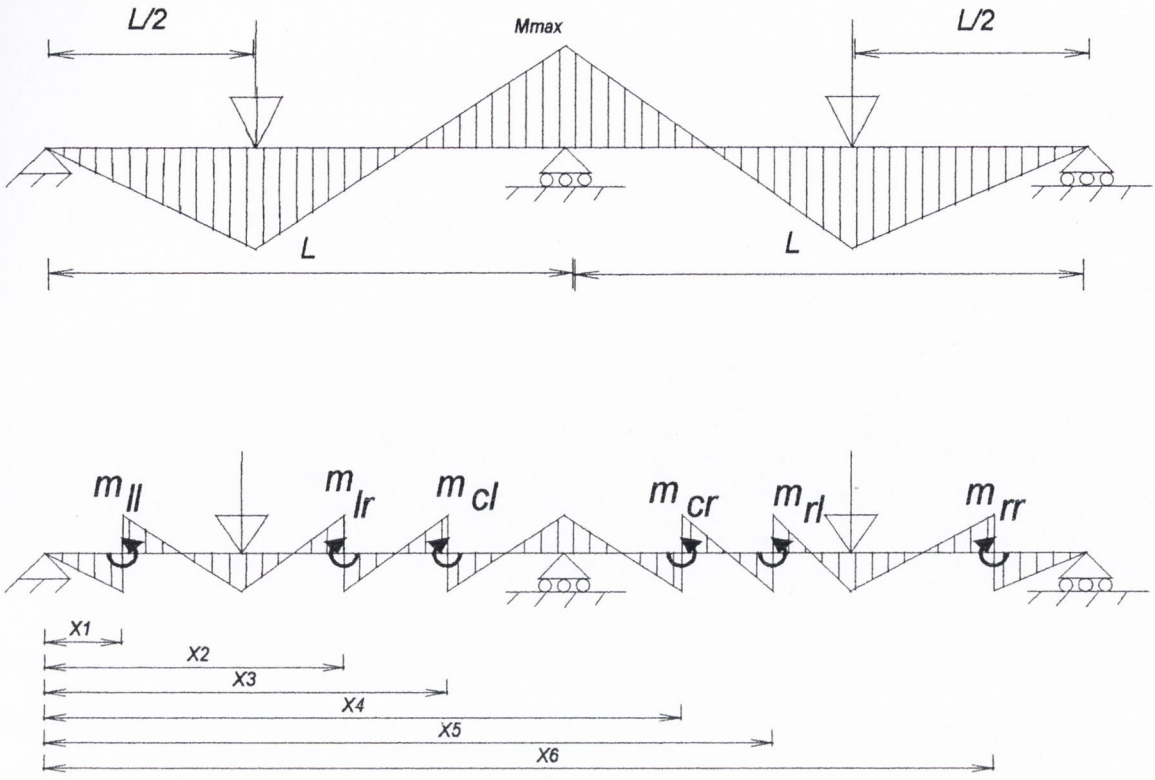

Figure 3.9: The bending moment diagram for a two span continuous beam with central concentrated loads on each span and the bending moment diagram with counter moments applied.

3.3.2 Two- span continuous beam with non-central concentrated loads on unequal spans

Consider the case of a two span continuous beam in which the spans are of different lengths (L_1 and L_2) and the concentrated loads, W_1 and W_2, are applied at any location in either span at A_1 and A_2 from their left hand support, as shown in figure 3.10. The original typical three peaked bending moment diagram may have a maximum moment, M_{max}, in any one of three locations depending on the geometry and the loading.

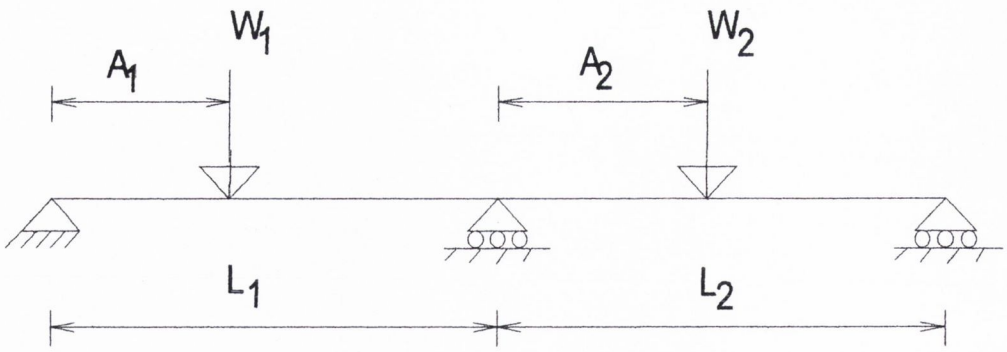

Figure 3.10: A two span continuous beam with asymmetrical concentrated load on each span.

To analyse this more general problem, equations were first developed for the application of only one counter-moment, m_1, located at a distance, a, from the left hand support on the left hand span, with the applied concentrated loads removed from each span (see figure 3.11). It can be shown that the resulting moment over the central support, m_r, is given by (Maher, 1998)

$$m_r = \left[\frac{m_1 L_1}{2(L_1 + L_2)}\right]\left[\left[\frac{3a^2}{L_1^2}\right] - 1\right] \tag{3.9}$$

If, as before, m_1^- and m_1^+ are denoted as the value of the moment just to the left and right, respectively, of the point of application of m_1. It can also be shown that (Maher, 1998)

$$m_1^- = \left[\frac{a m_1 L_1}{2L_2(L_1 + L_2)}\right]\left[\left[\frac{3a^2}{L_1^2}\right] - 1\right] \tag{3.10}$$

from which m_1^+ is calculated, thus:

$$\left|m_1^+\right| = \left|m_1\right| - \left|m_1^-\right| \tag{3.11}$$

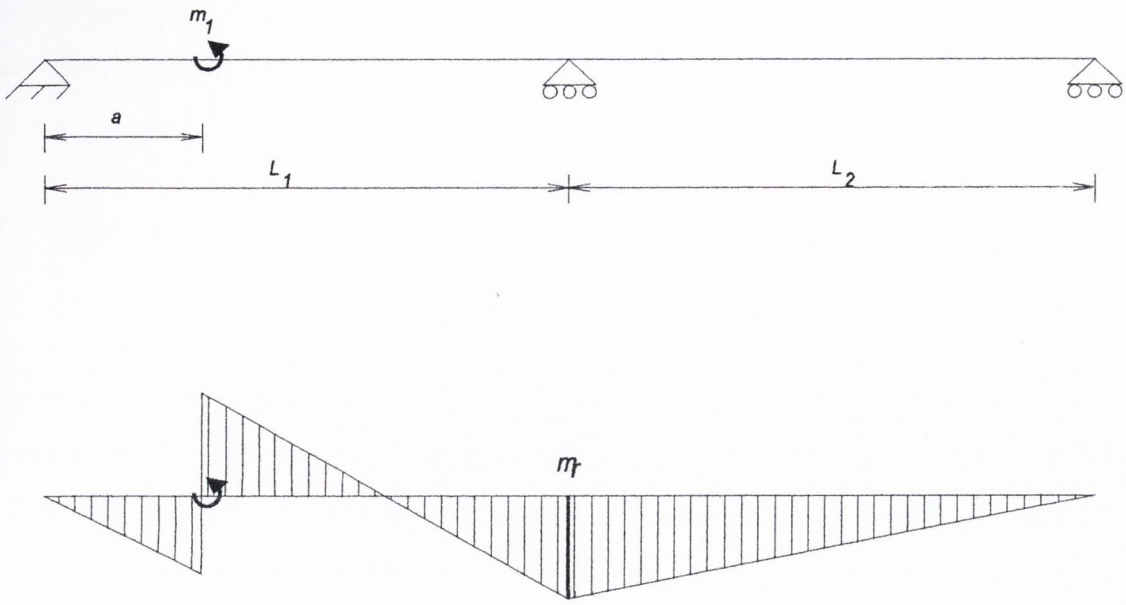

Figure 3.11: The bending moment diagram for a two span continuous beam with a single concentrated moment applied to one span and the resulting bending moment diagram.

Using superposition, when all six counter-moments were applied to the spans with concentrated loads, the resulting bending moment diagram is a fifteen-peaked shape (similar to Fig. 3.9). Fifteen equations were derived to establish the fifteen bending moments that arose along the length of the continuous beam (that is, the moments just to the left and right of the application of the six counter moments, giving twelve, and the three resulting moments at the location of the three original peaks). The equations were expressed in terms of m_1-m_6, x_1-x_6, A_1 and A_2, L_1 and L_2 and W_1 and W_2 (see Appendix B).

The location and magnitude of the six counter moments to yield the optimum bending moment diagram, with a load in each span of the beam, proved to be very tedious to calculate by hand and, hence, software was written to solve the equations numerically (see Appendix C). The software uses an iterative process loosely based on a Newton-Raphson hybrid method with a weighted correction factor (Kreyszig, 1993). The weighted correction factor will change with each iteration such that the greater the difference from the current $|m_{max}|$ for any given variable (namely, x_1-x_6 and m_1-m_6) in the

ith step, the greater will be the correction to that variable in the i+1 th step. The bending moment diagram is adjusted in this way such that as many as possible of the peaks will have the same value, $|m_{max}|$, and the remaining peaks will have values as close as possible to but no greater than $|m_{max}|$. With one pair of counter-moments applied to each peak on the original bending moment diagram, typically the reduction factor is in the range $3.2 < |M_{max}| / |m_{max}| < 3.45$.

By way of example, let L_1= 11m, L_2 = 10m, P_1 = 160kN, P_2 = 190kN, a_1= 5m, and a_2 = 4m (a_2 is measured from the left support of the right span as in figure 3.10), then the resulting original bending moment diagram will have values of 281.8 kNm, –339.9 kNm and 252.1 kNm at the left point load, central support, and right point load respectively. If moments m_1 to m_6 are applied at locations x_1 to x_6 (see figure 3.12), the resulting bending moment diagram will be as shown in figure 3.12.

The locations and magnitude of the counter moments are as follows
x_1=1.667m, x_2=6.941m, x_3=8.884m, x_4=12.990m, x_5=18.243m, x_6=19.528m, m_1 to m_6=198.34kNm, with a maximum resulting net moment of 98.47kNm. This represents a reduction in peak moment of 70.9%.

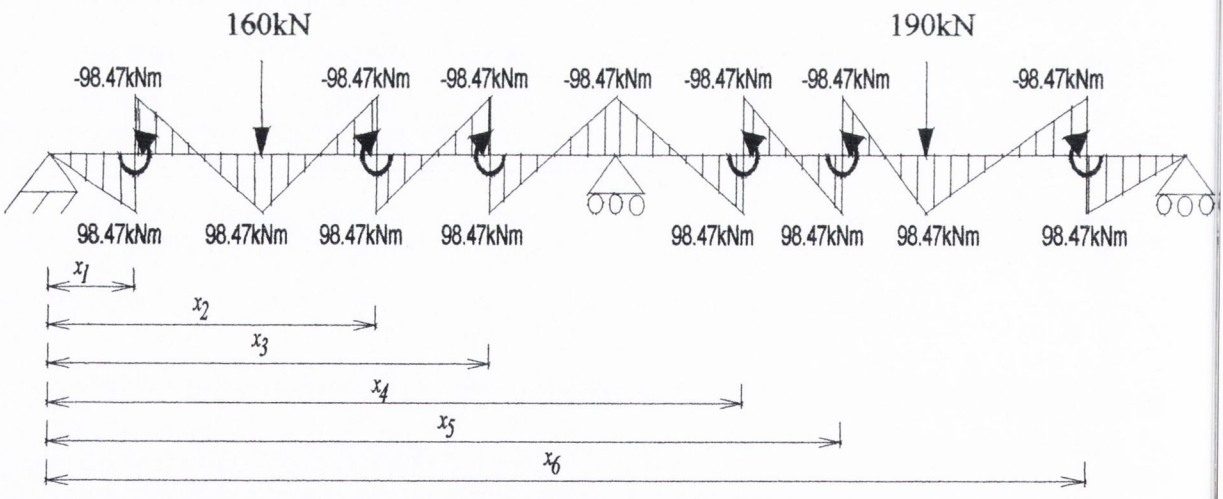

Figure 3.12: The final bending moment diagram with the counter moments applied to the two span asymmetrically loaded beam example.

3.4 Criteria for beam improvement

When a counter-moment is required at a specific location in a beam, this can be induced by attaching tendons to both sides of the beam web and tensioning them up. This could be achieved by pre-stressing the tendons prior to the application of the load. However, it should be noted that when loading is applied to a beam with tendons attached, a passive tendon force is also induced in the tendons which, in turn, will provide additional beneficial counter-moment.

The tendon will perform with increasing efficiency as its eccentricity from the section neutral axis increases. When the tendons are located nearer to the beam's neutral axis, an initial pre-tension force is required to reach the required optimum counter-moment on loading. The optimum bending moments are achieved with a combination of P_i (the initial pre-tension force) and a further tendon force component due to load application Wr_t, where r_t is the rate of passive tendon force increase due to load application.

However, note that whenever tendon forces are present, an axial force results in the beam. This imposes an additional axial compressive stress to complement the bending stresses due to loading and counter moment.

With no centrally concentrated load applied, when an initial tendon force is applied the critical portion of the beam for stress is at the lower flange between the point of application of the counter moments (that is, between the levers). There, the critical stress is the compressive axial stress due to the initial tendon force combined with the compressive bending stress induced via the counter moment. In the upper flange, the same axial compressive stress exists in combination with the tensile bending stress arising from the induced counter-moment. If the overall stress is to be kept to within a limiting stress of, say, $+/-\sigma_l$, the limiting criteria before loading will be that the lower flange stress, between the levers, must not exceed this value. For the unloaded beam under the maximum pre-stress equal to this capacity, σ_l, at the lower flange, this flange will now have an effective capacity of $+2\sigma_l$ on application of the concentrated load. This

is because the lower flange can now be stressed from its pre-loaded state of $-\sigma_l$ to $+\sigma_l$, because applying the central concentrated load will induce positive tensile stress in the lower flange.

Consider now the upper flange of the portion of the beam between the points of application of the counter moments. The limiting criteria for applying as much counter moment as possible, prior to loading, is the resulting compressive stress at this stage in the lower flange. With the lower flange stressed to a maximum prior to loading (and given that the lower flange will, in this case, always be stressed to $-\sigma_l$,) the resulting stress in the upper flange will depend on the tendon eccentricity. If the tendon eccentricity is large enough to provide, in the upper flange, more positive tensile bending stress due to the counter moment, than negative compressive stress due to the axial force induced by the tendons, then the resulting stress will be a positive tensile stress. When the resulting stress in the upper flange is a (positive) tensile stress prior to loading (see figure 3.13), there will be an improved capacity of the beam on loading. In terms of stress, the improved capacity will be the original assumed stress limit of $-\sigma_l$, (that is, the allowable compressive capacity in the top flange) plus that amount of resulting tensile stress arising from pre-tension. If the tendon eccentricity is so low as to provide, in the upper flange, less (positive) tensile bending stress due to the counter-moments, than the (negative) compressive axial stress due to the axial force induced by the tendons, then the resulting stress will be a negative compressive stress. In this case, prior to loading, the beam will only have a loading capacity of the original un-strengthened capacity compressive stress of $-\sigma_l$, less that absolute amount of resulting compressive stress (that is, the beam will have a lower than original un-strengthened capacity). This is because loading will induce compressive stress in the upper flange and when a net compressive stress exists due to pre-tensioning, some portion of bending capacity has to be employed prior to loading. In this case, a reduction in overall beam capacity will always result, irrespective of how much counter-moment is applied.

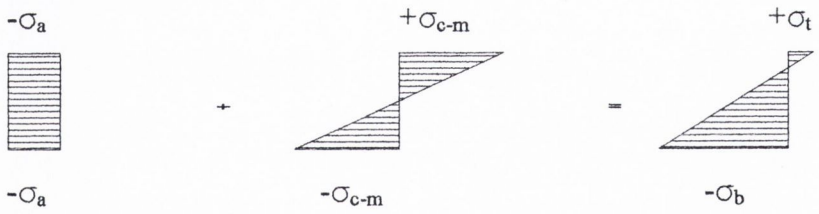

$|\sigma_{cm}| - |\sigma_a| > 0$ *implies beam improvement (sufficient tendon eccentricity)*

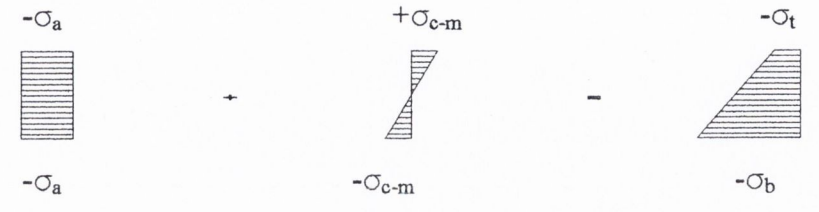

$|\sigma_{cm}| - |\sigma_a| < 0$ *implies lower than original capacity(insufficient tendon eccentricity)*

Figure 3.13: Stress component diagrams for tendon eccentricities adequate and inadequate for beam improvement respectively, where:

σ_a = the axial compressive stress due to the tendon force (=P/A)

$\sigma_{c\text{-}m}$ = the bending compressive stress in the lower/upper flange due to the counter moment (=Pe/Z)

σ_t = the resulting stress in the upper flange of the pre-loaded beam between the application points of the counter moments

σ_b = the resulting stress in the lower flange of the pre-loaded beam between the application points of the counter moments

It can be seen, therefore, that the limiting criteria for overall beam improvement of a simply supported beam with a centrally concentrated load is that, prior to loading and with the counter-moments applied by initially stressing the tendons, the resulting upper flange stress must be a tensile stress. The degree to which the beam may be improved will depend on the magnitude of the resulting tensile stress in the upper flange after the application of the counter moments and prior to the application of the centrally concentrated load. The greater the tendon eccentricity, the greater the resulting tensile stress, and, thus the greater will be the overall improvement of the beam capacity. Also, a greater resulting tensile stress, implies greater self-counter moment capacity owing to the greater tendon eccentricity as described in section 2.3.2 (passive test). The stress diagrams in figure 3.14 illustrate the

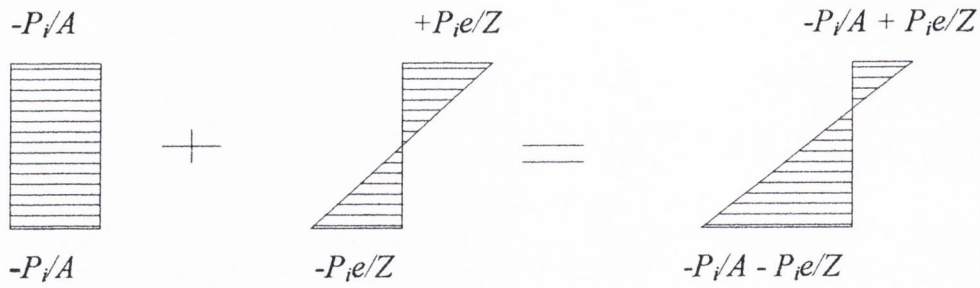

Figure 3.14: The stress component diagrams for the beam with an initial pre-tension force applied and no central concentrated load where:

P_i = the maximum initial total tendon force

e = the tendon eccentricity from the N. A. of the beam section

Z = the section modulus

A = the cross-sectional area of the section

relationship between the component stress diagrams at the pre-loaded stage (mid section stresses) which are critical at the lower flange.

3.4.1 Limit on initial tendon force

The limiting criteria for the maximum amount of initial tendon force, P_i, that can be applied is the compressive stress in the lower flange between the locations of application of the counter moments, which must not exceed σ_l. A minimum value for the tendon eccentricity (e) can be established with the above criteria and is derived as follows:

If

$$\left|-\sigma_a - \sigma_{c-m}\right| \leq \sigma_l \tag{3.12}$$

Then,

$$\frac{P_i}{A} \frac{P_i e}{Z} \leq \sigma_l \tag{3.13}$$

which gives an expression for the maximum allowable P_i, the initial tendon force prior to loading, as

$$P_i \leq \frac{\sigma_l}{\left(\frac{1}{A}+\frac{e}{Z}\right)} \tag{3.14}$$

As explained earlier, for overall beam improvement, the top flange stress must be tensile under the initial total tendon force. That is,

$$\left|\frac{P_i e}{Z}\right| - \left|\frac{P_i}{A}\right| > 0 \tag{3.15}$$

which gives:

$$e > \frac{Z}{A} \tag{3.16}$$

This shows that the application of loading will apply further tendon force and, thus, additional counter-moment, and, provided the tendon eccentricity (*e)* is greater than *Z/A*, this additional counter-moment will provide net stress benefit. The beam can be considered to be partially self-regulating in that, while a pre-loading tendon force may be applied, further tendon force is induced as loading occurs. The pre-loaded tendon forces are necessary if the self-counter moment is less than that required for the optimum counter moment.

3.4.2 Limit on applied load, *W*, for a given initial tendon force, P_i

If the tendon eccentricity *e* is greater than *Z/A*, the upper flange will always reach the limiting stress before the lower flange at the end of loading stage and this becomes the limiting criteria for stress as the load *W* is applied. This applies for all cases of steel sections with tendon levers at optimum locations and with external tendons attached to them. With the maximum initial tendon force, P_i , applied to the pre-loaded beam, an expression for the maximum central concentrated load *W* that can be subsequently applied can be developed as follows:

If r_t is the rate at which tendon force is induced as the central concentrated load increases, then the final post-loaded tendon force, P_f, will be:

$$P_f = P_i + Wr_t \tag{3.17}$$

Equation 3.17 applies to tendon eccentricities greater than Z/A for tendon configurations that are above or below the lower beam flange. The value of r_t depends on external factors, namely the tendons, beam and lever arm stiffness and the rigid body rotation of the lever arm as the beam rotates. The term r_t be expressed as follows (see Appendix D for proof).

$$r_t = \frac{\dfrac{eL^2}{9EI}}{\dfrac{2L}{3E_tA_t} + \dfrac{2L}{3EA} + 2\left\{e\sin\left(\dfrac{eL}{3EI}\right) + \dfrac{L_l^3}{3E_lI_l}\right\}} \tag{3.18}$$

where:

E_t= the tendon elastic modulus

A_t= the cross sectional area of the tendons

E_l= the elastic modulus of the tendon lever steel

I_l= the section moment of area of the tendon levers

L_l= the effective lever length (from the beam's soffit to where the tendon is attached to the lever)

Equation 3.18 was derived using the force method of analysis to analyse a "released" beam structure (which was indeterminate to one degree of freedom) with an imaginary cut in the tendon. The displacement of the released structure horizontally at the cut tendons is divided into four components that resist the displacement in the real structure: The term $2L/3E_t A_t$ is the axial stiffness of the tendons; The axial stiffness of the beam (over the length of the tendons only) is $2L/3E A$; The rotation of the beam at the points of counter-moment application is expressed by the term $esin(eL/3E I)$; The component $L_l^3 / 3E_l I_l$ represents the cantilever deflection of the tendon lever. This term may be omitted when the lever length is so small as to have no significant effect on the overall horizontal displacement of the tendons.

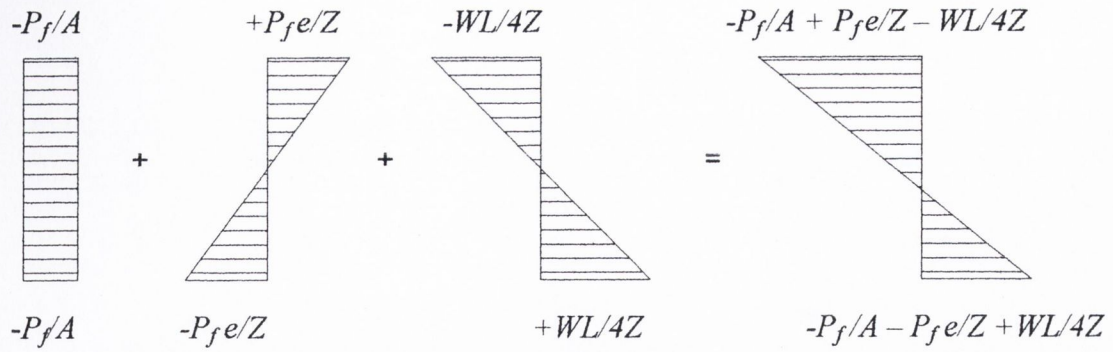

Figure 3.15: The post-loaded stress component diagrams for a beam with tendons.

The post-loaded stress diagrams are shown in figure 3.15 and include the bending stress diagram arising from the applied central concentrated load, W. Assuming for all cases, that e is greater than Z/A, then, as discussed earlier, the limiting criteria for the beam loading will be the compressive stress in the upper flange.

The maximum permissible applied load W is, therefore, defined by the limiting stress in the upper flange, thus:

$$-\frac{P_f}{A}+\frac{P_f e}{Z}-\frac{WL}{4Z}\geq -\sigma_l \tag{3.19}$$

And substituting equation 3.17 yields,

$$\left(P_i+Wr_t\right)\left(\frac{e}{Z}-\frac{1}{A}\right)-\frac{WL}{4Z}\geq -\sigma_l$$

Rearranging the above equation and using equation 3.14 for P_i gives equation 3.20, the maximum central concentrated W that can be applied to the beam.

$$W_{max}\leq \frac{\sigma_l\left\{1+\left(\dfrac{1-\dfrac{Z}{eA}}{1+\dfrac{Z}{eA}}\right)\right\}}{\left(\dfrac{L}{4Z}+\dfrac{r_t}{A}-\dfrac{r_t e}{Z}\right)} \tag{3.20}$$

3.5 Deflection

An equation can be derived that expresses the final mid-span deflection of the strengthened beam for any given initial tendon force and any subsequent applied central concentrated load.

The component of upward (negative) deflection, δ_i, under the initial tendon force, P_i, can be expressed as follows (see Appendix D):

$$\delta_i = -\frac{eP_iL^2}{9EI} \tag{3.21}$$

where EI is the beam stiffness.

The component of additional imposed upward deflection, δ_{rt}, from passive engagement of the tendons due to the application of a central concentrated load, W, can be expressed as (see Appendix E):

$$\delta_{rt} = -\frac{eWr_tL^2}{9EI} \tag{3.22}$$

The component of downward (positive) deflection, δ_w, due to the applied central concentrated load, W, can be expressed using the conventional expression for a central concentrated load on a simply supported beam (Steel Designers' Manual, 2005)

$$\delta_w = \frac{WL^3}{48EI} \tag{3.23}$$

The expression for the final deflection can then be expressed as follows:

$$\Delta = \delta_i + \delta_{rt} + \delta_w$$

which gives,

$$\Delta = \frac{WL^3}{48EI} - e(P_i + Wr_t)\frac{L^2}{9EI} \tag{3.24}$$

3.6 Parametric study

A parametric study was carried out to investigate the interaction between the variables contained within Equation 3.20. The study considered the effect of each variable separately while keeping the remaining variables constant. All standard UC, UB and RSJ sections were examined in the parametric study. The purpose of the study was to develop charts which would allow a designer to establish the best choice of strengthened steel section, in the case of a new application and, in the case of a retrofit, the best tendon location and force so as to achieve the optimum result for a particular site restriction (that is, minimum member depth, loading, span, etc.). Analyses were carried out that varied the span, tendon eccentricity, central concentrated load, initial pre-tension, P_i and the member section properties, I, Z, and A. The latter were dependant variables, in that a change in one section variable would result in a change in all.

3.6.1 Relationship of initial tendon force to tendon eccentricity

The study firstly examined the behaviour of UBs with initial pre-tension tendon force to establish r_t for the various beams. The beams had the same imposed limiting stress, σ_l, and span. The beams had varying lever lengths (with adequate stiffness for every length) at the optimum counter moment locations. Figure 3.16 shows plots of P_i versus e for various sections. The plots demonstrate that as e increases less initial tendon force P_i is required to induce a limiting stress. In general, the plot with all sections follow a non-linear trend line (as expected) of the approximate form ax^b.

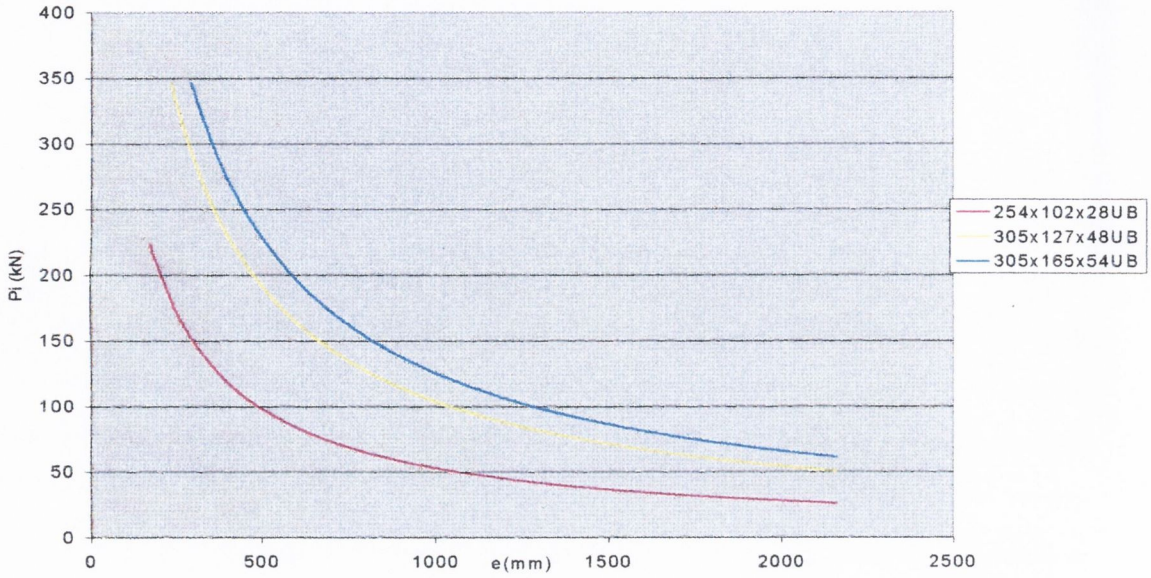

Figure 3.16: Plot of maximum P_i (equation 3.14) versus e for various sections.

3.6.2 Tendon force increase rate, r_t, with respect to differing section sizes

The rate of tendon force increase was examined with different section sizes which had the tendon eccentricity shown in figure 3.17. A plot of the relationship between the r_t and section size (expressed as I/A) is shown in figure 3.18. It can be seen from the plot that members with lower flexural stiffness yield higher values of r_t. The ratio of I/A is an expression of the flexural stiffness and axial stiffness which both impact on the ratio r_t. In general, slender beams with relatively lower cross-sectional areas will have higher r_t values for a given tendon eccentricity and the local buckling capacity will govern the maximum tendon force.

The plot demonstrated that over the range I/A values of 300-1600cm^2 the change in r_t is relatively low (0.1-0.6). When considering the I/A range from 20-300cm^2 the change in r_t is far greater (0.6- 9.3). This allows greater passive tendon forces to be developed due to the lower flexural stiffness and greater axial resistance.

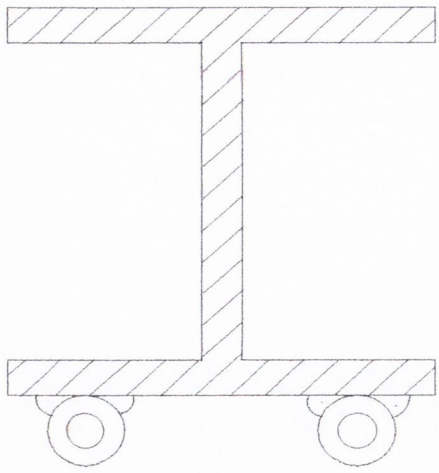

Figure 3.17: Typical tendon configuration for beams.

It can also be seen in figure 3.18 that clusters of points occur along the trend-line. Each cluster of points represents sections with approximately the same tendon eccentricity. In figure 3.19 a cluster of points were re-plotted on a larger scale which represented sections whose tendon eccentricity was approximately the same. It can be seen that the points can be fitted very closely to a linear plot.

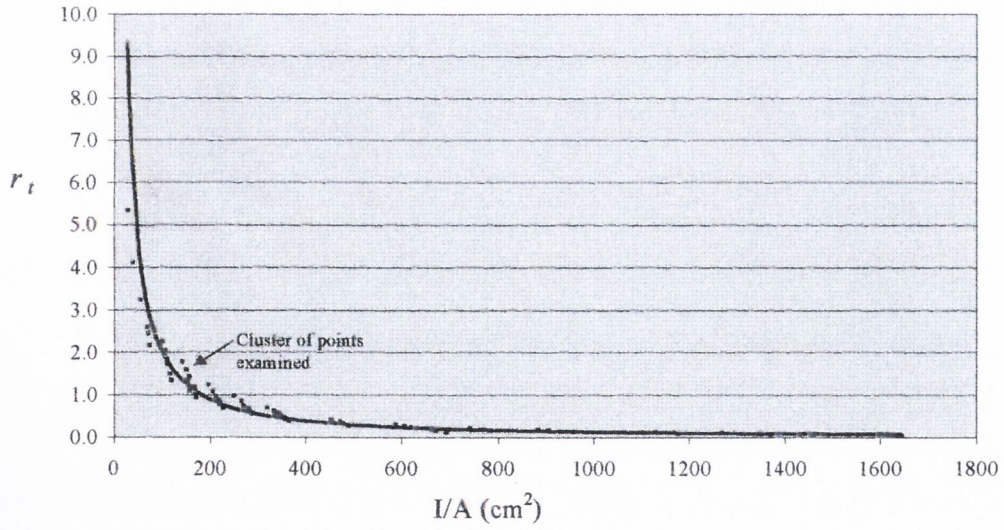

Figure 3.18: Plot of equation 3.18 for r_t (kN/kN) versus I/A values for universal beams

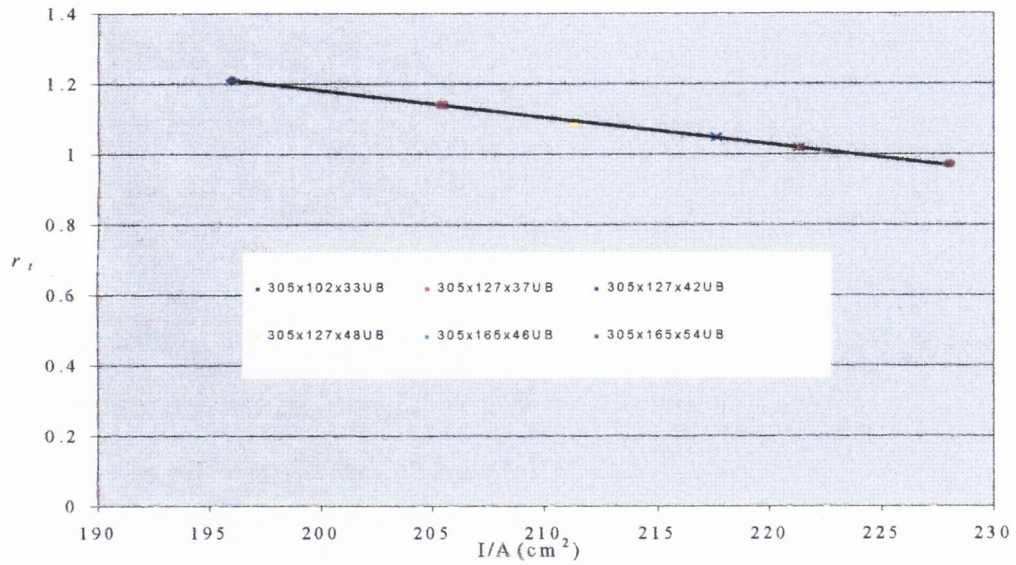

Figure 3.19: Plot of varying I/A values with members with approximately the same tendon eccentricity. (186+/-5mm)

Figure 3.19 illustrates that as the ratio of I/A increases for sections with approximately the same tendon eccentricity, r_t decreases approximately linearly.

Tendon eccentricity yielding the optimum r_t value

The value of the optimum tendon eccentricity (that is, the tendon eccentricity that gives the greatest r_t value) was investigated for various sections. It was found that the optimum tendon eccentricity occurred just when the self counter-moment generates hogging moment at the tendon levers (see figure 3.20). The ratio r_t increases with increasing tendon eccentricity when sagging moment (and, thus, downward deflection) is present under final loading but when the eccentricity is so great that hogging moment (and, thus, pre-camber) results under final loading (via self-counter moment), r_t decreases. This is because the passively engaged tendons rely on downward flexural deflection of the beam to induce tendon force. When the tendon eccentricity is greater than the optimum, the rate at which passively engaged tendon force is induced is less than the rate at which tendon force is lost due to beam hogging. Figure 3.21 shows the relationship between r_t and tendon eccentricity, e. Further increase in load capacity will occur with tendon eccentricities greater than the optimum value, however, the increase in capacity will be at

a reducing rate per unit increase of eccentricity. This will result in increasingly lesser member capacity benefit with overall member depth increase. This is clearly evident in figure 3.21, where a peak r_t value can be observed.

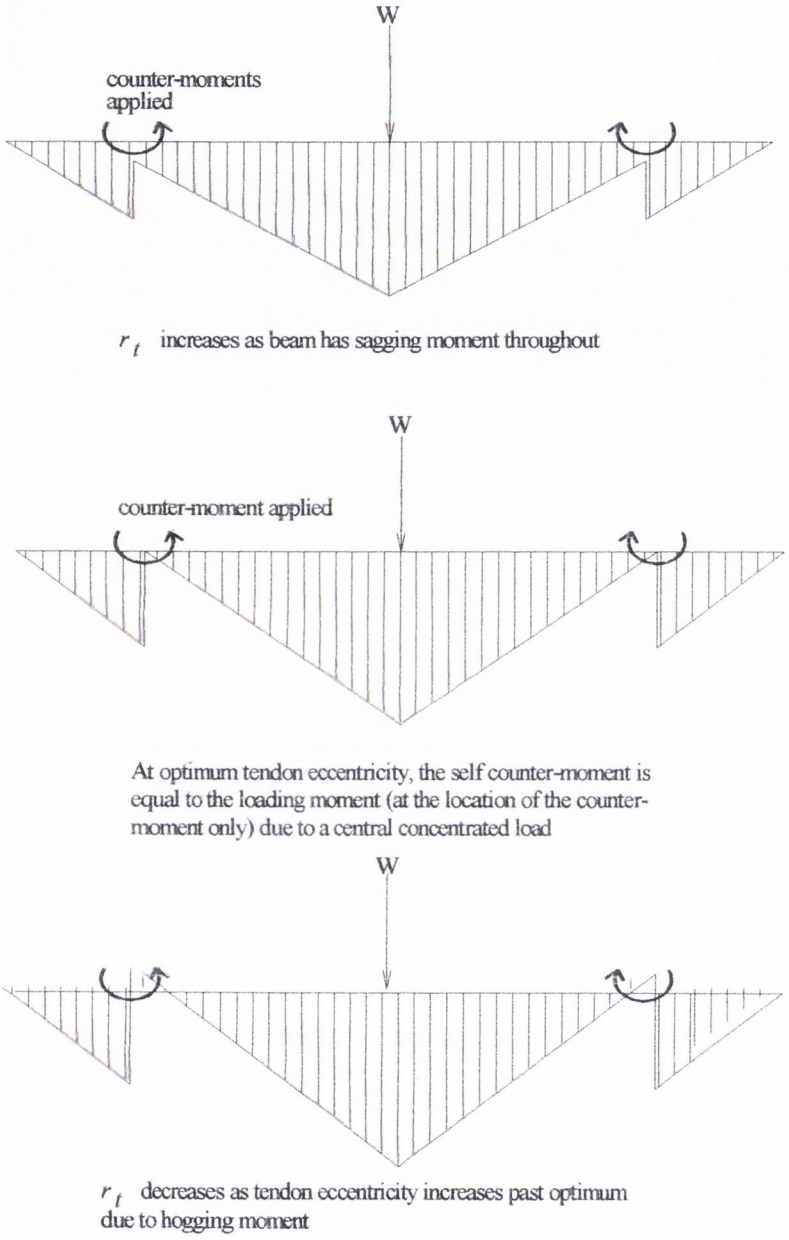

Figure 3.20: Three stages of increasing tendon eccentricity (from top to bottom), before the optimum, at the optimum and eccentricities greater than the optimum.

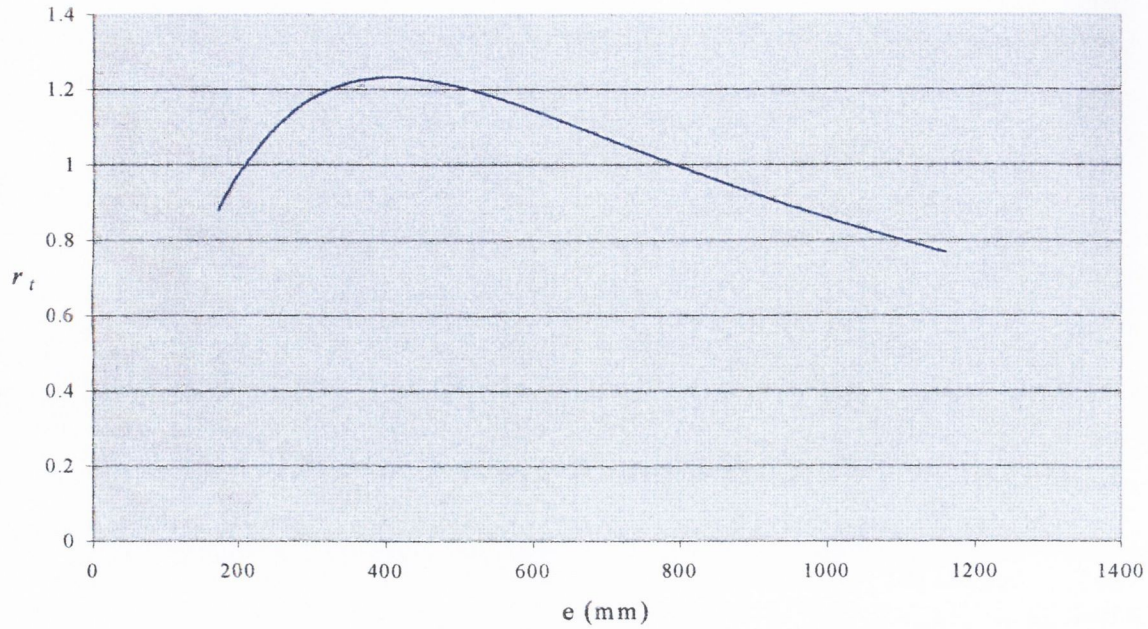

Figure 3.21: The relationship between tendon force increase with respect to tendon eccentricity for a 254x254x132 UC.

A number of sections were examined to establish the location of the optimum tendon eccentricity. A sufficient lever bending stiffness was provided to remove significant cantilever deformation of the lever. The parametric analysis showed that the greater the flexural stiffness of the beam, the greater would be the optimum tendon eccentricity. The analysis also showed that the greater the cross-sectional area of the member the greater would be the optimum tendon eccentricity. In a practical setting where a specific self-counter moment is required and where overall member depth, and thus the tendon eccentricity, is restricted, it may be possible to achieve the required self counter-moment by providing additional tendons. In addition to applying a greater number of tendons, lighter members with lower flexural stiffness will have optimum tendon eccentricities that are closer to the section neutral axis.

Figure 3.22 shows the relationship between curves of r_t versus e for various sections. The plots demonstrate that as the section size increases and, thus, the section stiffness increases, the resulting peak in the r_t rate is lower than with the smaller flexible beams.

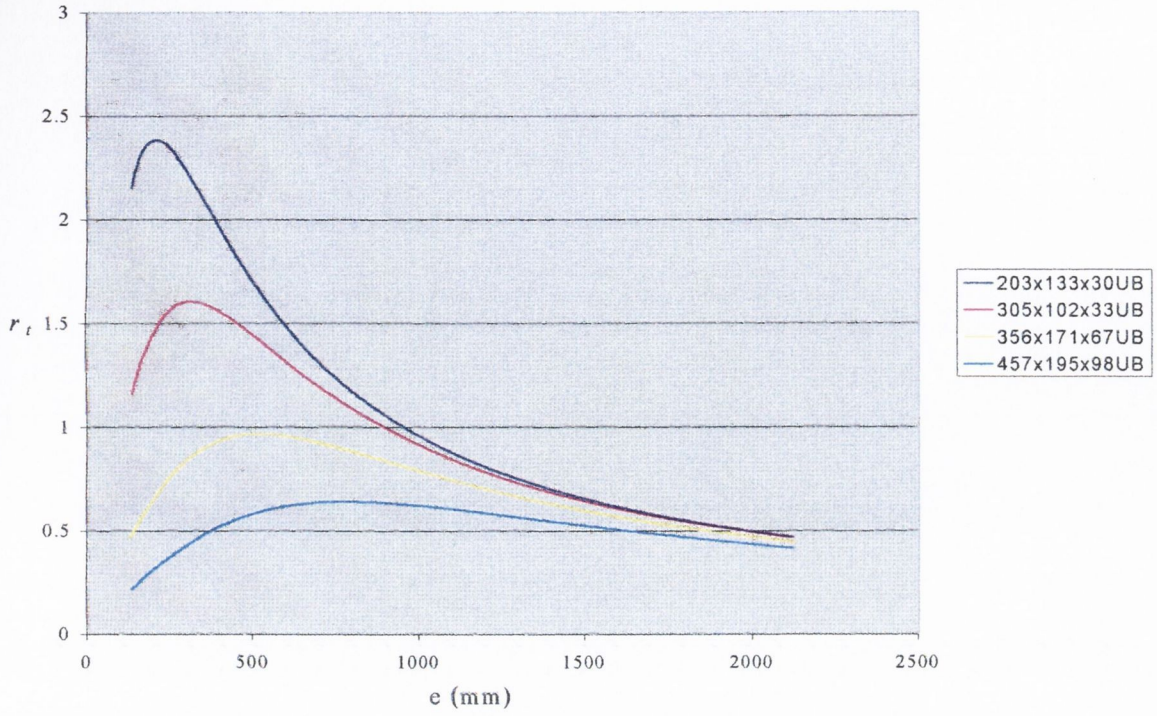

Figure 3.22: Plots of r_t versus e for various sections.

Tendon cross-sectional area

A plot of the increase in r_t with respect to cross-sectional tendon area increase yielded a predominantly linear plot and showed that twice the tendon area would approximately double the r_t value on the same beam with all other parameters constant (see figure 3.23). The trend line equation in this plot is a very good fit for the points plotted

It was also found that, with all other parameters being constant and with the same member, a higher cross-sectional area of tendons resulted in a lower optimum tendon eccentricity, that is, the optimum tendon eccentricity was closer to the beam's neutral axis. Figure 3.24 shows the resulting optimum tendon eccentricity for various cross-sectional areas of tendon provided for the same beam. It can be seen that as the area of tendon increases the optimum value for r_t occurs at a lower tendon eccentricity and has a greater rate of tendon force increase when the same magnitude of central concentrated load is applied. As discussed earlier, the provision of a greater number of tendons can provide efficient counter moment where headroom restricts greater tendon eccentricity.

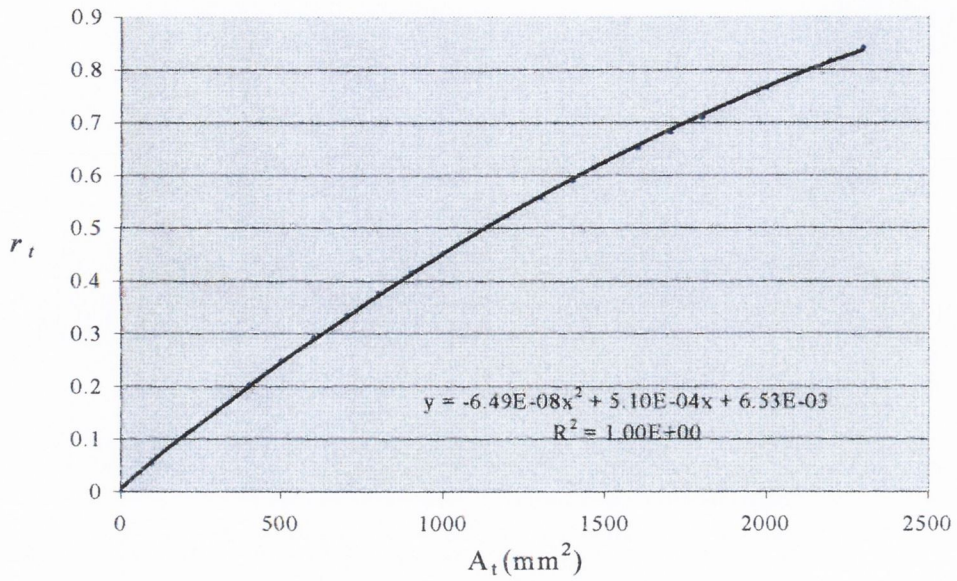

Figure 3.23: Increasing r_t with respect to increasing cross-sectional tendon area with constant eccentricity.

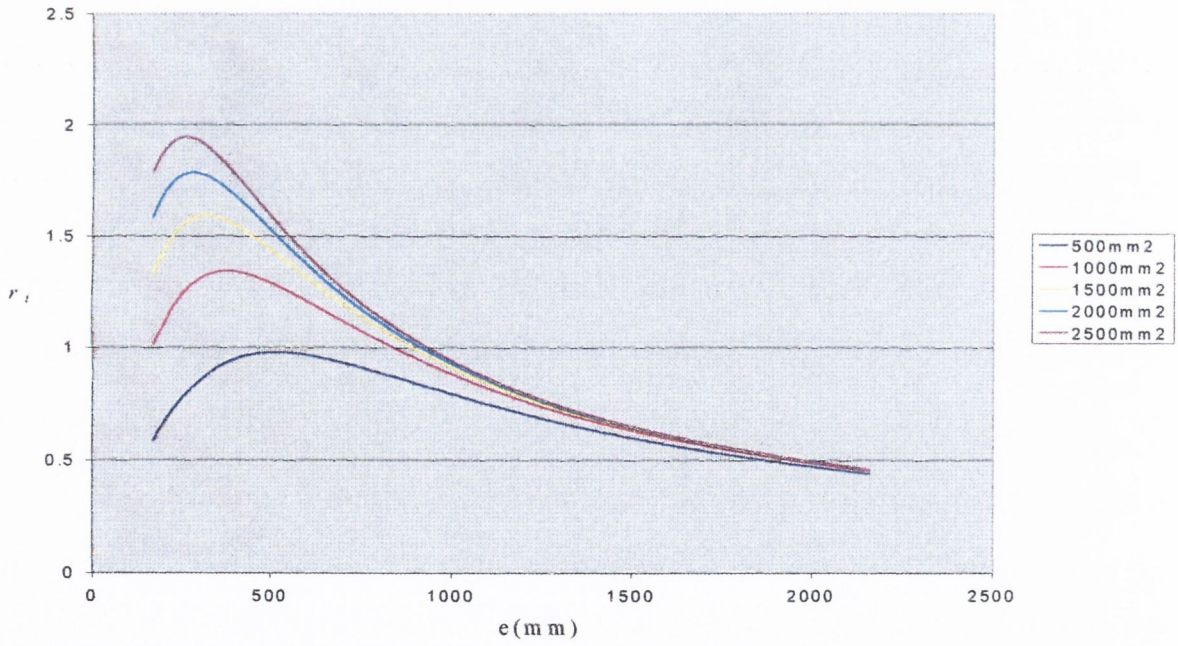

Figure 3.24: The ratio r_t plotted against tendon eccentricity for various cross-sectional areas of tendon.

Tendon lever flexural stiffness

The tendon configuration employed for this portion of the parametric study is shown in figure 3.25. Again, with all other parameters being constant and with the tendon eccentricity at the optimum (520mm) for the 252x254x132UC previously used, varying the lever flexural stiffness yielded a non linear response in the r_t rate as shown in figure 3.26 (that is, expressing the lever stiffness as a factor, α, of member stiffness E_bI_b). The plot demonstrates that for a given tendon cross-sectional area ($850mm^2$) and member (as for the previous case) the tendon lever flexibility will impact on the resulting r_t rate. With relatively flexible levers the r_t rate is somewhat lower (by approximately 16.5%) than with levers as stiff or stiffer than the member. It was also found that as the lever stiffness was greatly increased ($2x10^{20}$ cm^4) the r_t rate converged to a limiting value (that is, 1.0025kN/kN in this case). It can be seen that adequate lever stiffness should be provided in order to achieve the maximum r_t rate.

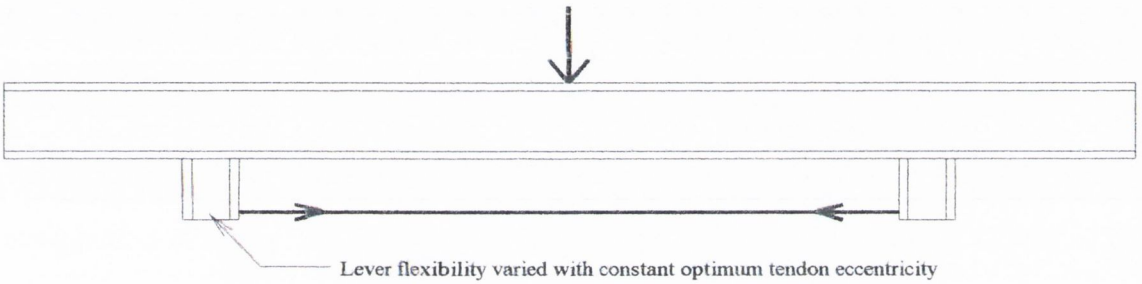

Figure 3.25: Tendon configuration used for lever flexibility analysis.

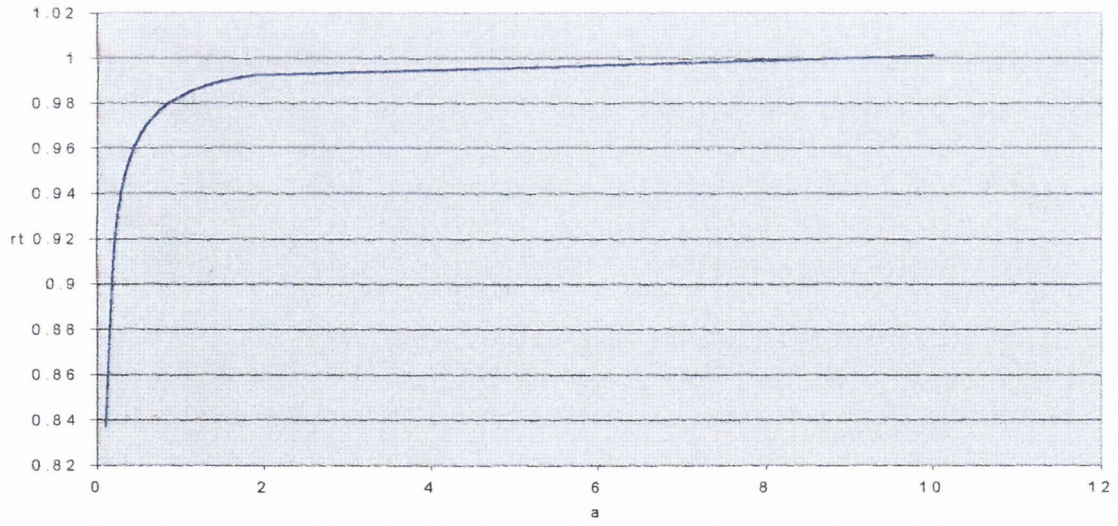

Figure 3.26: The ratio r_t plotted against varying lever flexural stiffness expressed as a factor (α) of member flexural stiffness.

It can be seen from figure 3.26 that over 90% of the potential r_t rate can be achieved when the lever section is least as stiff as the beam section.

3.6.3 Central concentrated loading.

Central concentrated load and initial pre-tension force

The amount of initial pre-tension force applied will govern the amount of central concentrated load that can be applied. Figure 3.27 shows plots of increasing initial pre-tension forces applied and their corresponding maximum possible (for the tendon configuration and eccentricity shown in figure 3.17) central concentrated loads for both a 254x254x132 UC and a 533x210x122 UB. The plots confirm the linear relationship between P_i and the corresponding maximum central concentrated load indicated in equation 3.20. The maximum P_i for the UC was 1125kN with a tendon eccentricity of 170mm and 1670kN for the UB with a tendon eccentricity 290mm. If the maximum amount of initial pre-tension force is applied (for any given limiting stress for a particular member with a constant tendon eccentricity) this will allow the maximum central concentrated load to be applied. If a value lower than the maximum possible pre-loaded P_i is applied the resulting maximum possible load will be lower. This will apply in all cases where less than 100% of self counter-moment is provided with the strengthened beam (that is, where initial pre-stress must be applied for optimum counter-moment).

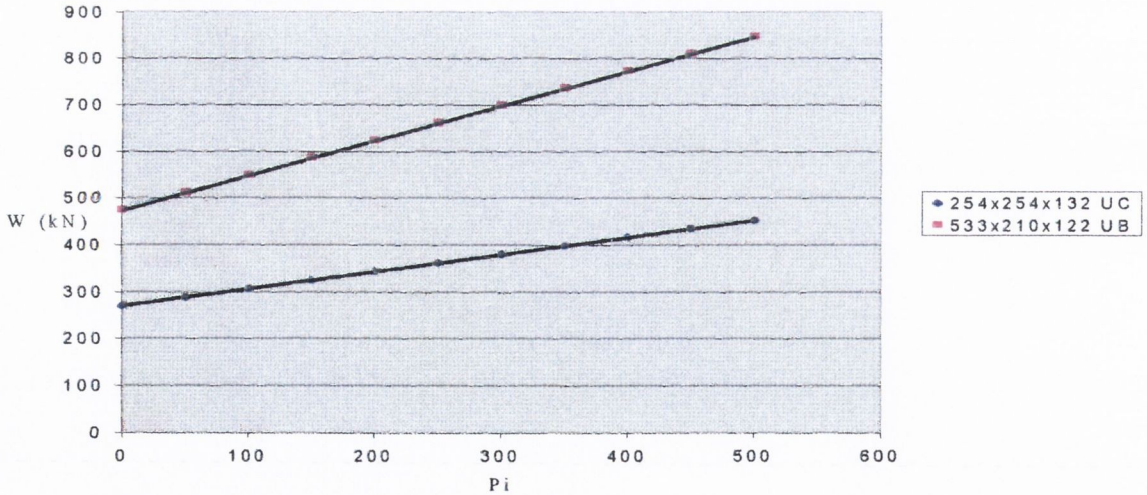

Figure 3.27: Maximum central concentrated load with increasing initial tendon force under limiting stress σ_l and constant tendon eccentricity.

Central concentrated load and member flexural stiffness

Figure 3.28 shows a plot of the percentage improvement in the maximum permissible load (expressed as a percentage over the un-strengthened load) for various sections. As discussed earlier, r_t increases as the ratio I/A decreases. This allows members whose I/A ratio is relatively low to achieve greater percentage improvement when the strengthened load is compared to the un-strengthened load for a given limiting stress.

The upper trend-line represents the percentage improvement compared to the un-strengthened load when the maximum initial pre-tension tendon force is applied and the lower line represents the improvements when no pre-tension force is applied (for an imposed limiting stress). It can be seen in figure 3.28 that beams with relatively lower I/A values can achieve load carrying improvements of the order of 30-50% and as the I/A ratio increases, the improvement in performance decreases. This compares to 0-20% if no initial pre-stress is applied. The percentage improvements are for the tendon configuration shown in figure 3.17 and would be greater if the tendon eccentricities were closer to the optimum eccentricity. The plots demonstrate that the difference in load improvement between when no P_i is applied and when it is, is of the order of 20-30% for each section plotted.

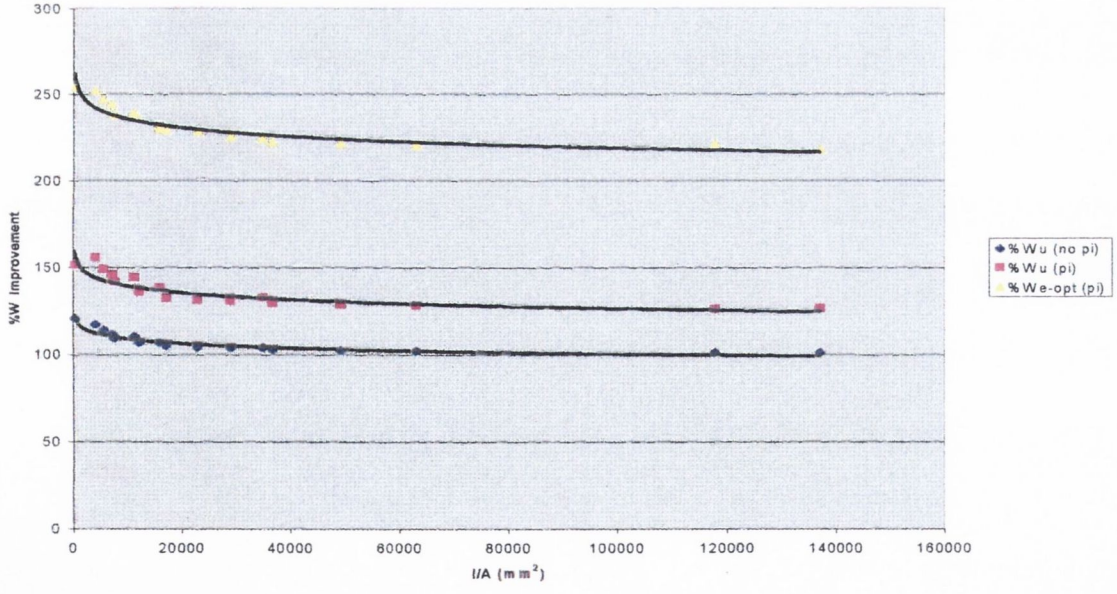

Figure 3.28: Percentage improvement (for the tendon configuration shown in figure 3.17) in load versus I/A with and without initial pre-tension force.

Figure 3.28 shows also the percentage improvement with the eccentricity at the optimum. It can be seen that the improvements are of the order of 220-245% with the tendon eccentricity at the optimum. In this case, less P_i is required to apply the maximum required counter-moments and, therefore, allows greater improved load carrying capacity due to less axial capacity being required for tendon force.

Lever length

Figure 3.29 shows a chart with a plot of central concentrated load, W(flex) (that is, the maximum load W that can be applied) versus increasing lever length (that is, not applying the configuration and eccentricity shown in figure 3.17) with a lever stiffness equal to the beam's flexural stiffness (heretofore referred to as flexible levers (with I=22530cm^4)) and with no initial pre-stress, P_i. The chart also shows a plot of a similar beam under a central concentrated load, W(stiff), with levers of very high stiffness (I=2x10^{20}cm^4). That is, at any given lever length, a further increase in lever stiffness will result in a negligible change in r_t . The plot shows that increasing tendon eccentricity is always beneficial to W_{max} , provided the lever has sufficient flexural stiffness.

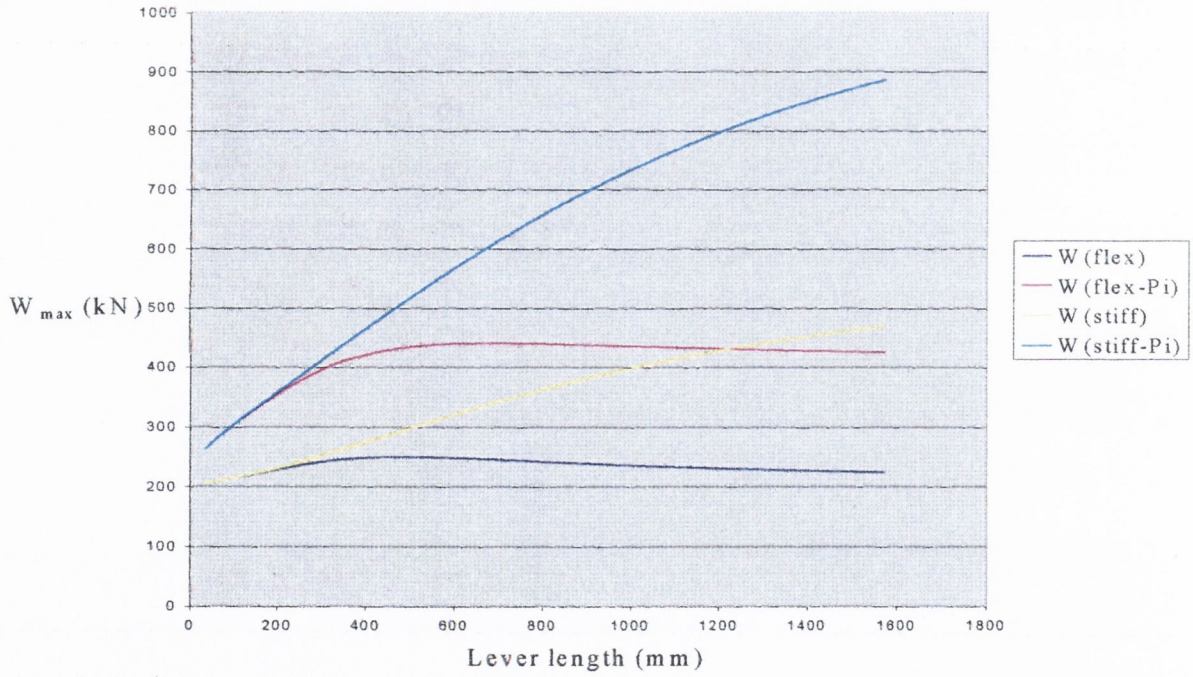

Figure 3.29: Plot of load for similar beams with increasing lever length for both flexible and stiff levers.

Considering the plots (with no initial pre-stress) for both flexible and stiff levers, it can be seen that with relatively short lever lengths (of the order of 150mm or less) very little difference can be observed in load carrying capacity. This can be attributed to the negligible difference in flexural stiffness between the stiff and flexible tendon levers over the shorter lengths which both yield approximately the same r_t rate. Figure 3.29 demonstrates that as the lever length is increased the load bearing capacity continues to increase with the stiff levers . This is due to the greater difference in the r_t rate between the stiff and flexible tendon levers and concurs with figure 3.26.

Furthermore, with the flexible levers, it can be observed from figure 3.29 that at the optimum lever length (for r_t) the rate of load improvement decreases as expected. With the flexible levers, as the levers are increased past the optimum value, which is lower than for the stiff levers, the load capacity is reduced. This is due to loss in self counter-moment as the flexible levers have insufficient stiffness to allow additional tension to be applied to the tendons under bending.

Figure 3.29 also shows a plot of W(flex-P_i) versus lever length with the full initial pre-stress, P_i , applied for the flexible tendon levers and a plot of W(stiff-P_i) versus lever length with initial pre-stress applied for the stiff tendon levers.

For the case where P_i is applied with flexible tendon levers (W(flex-P_I)) greater load capacity is achieved (as expected) compared to the case with flexible levers and no P_i is applied. The plot is similar in shape with, again, a loss in capacity past the optimum lever length.

The case where P_i is applied with stiff tendon levers (W(stiff-P_i)) demonstrates that as the lever length increases load capacity increases. The optimum lever length (that is, with optimum eccentricity such that the greatest r_t rate is achieved) will provide the greatest self counter-moment under loading. However, clearly, when initial pre-stress is applied, increasing the lever length past the optimum will, ultimately, increase member capacity.

The extent to which the levers can be extended down may be governed by in-situ conditions.

Span length

Figure 3.30 shows a plot of a factored central concentrated load (W_s) versus span increase for a strengthened 254x254x132UC with the tendon configuration shown in figure 3.17. The figure also shows a plot for an un-strengthened beam with ultimate limit state load (W_u) with increasing span and a plot of an un-strengthened beam with serviceability limit state load (W_{sls}) with increasing span. Serviceability requirements dictate the maximum load for the un-strengthened case. For the strengthened case the ultimate limit state load dictates with mid-span deflection always less than minimum serviceability deflection and is discussed in the next section.

It can be seen in figure 3.30 that as the span increases, for both cases, the difference between the strengthened and un-strengthened beam also increases.

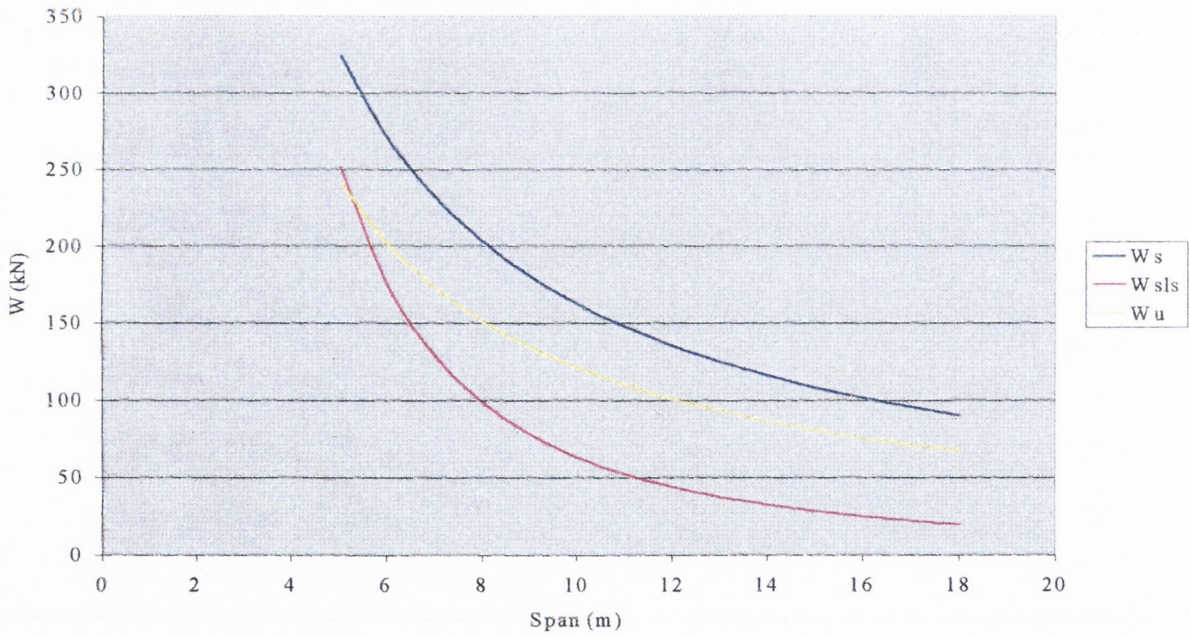

Figure 3.30: Central concentrated load versus span for strengthened and un-strengthened beam.

When the beam has a span of 5m the strengthened beam has 29.% greater load capactiy than for the un-strengthened case but when the beam spans 18m, the strengthened load is 66% greater, while remaining within the serviceability requirements (span/360). This is due to an increase in r_t as the span increases (see figure 3.31), which provides greater self counter-moment and reduces the mid-span deflection.

The increasing load improvement with span can also be attributed to the initial pre-stress giving rise to pre-camber and, thus, allows further load to be applied without exceeding serviceability requirements. Figure 3.32 shows the mid-span deflection (pre-camber shown as positive) of strengthened beams (δ_s) with full pre-stress, the mid-span deflection of un-strengthened beams with ultimate state loading (δ_u) and the mid-span deflection of beams with serviceability deflection (δ_{sls}). It can be seen from figure 3.32 that for the strengthened beams ultimate limit state requirements will always govern maximum

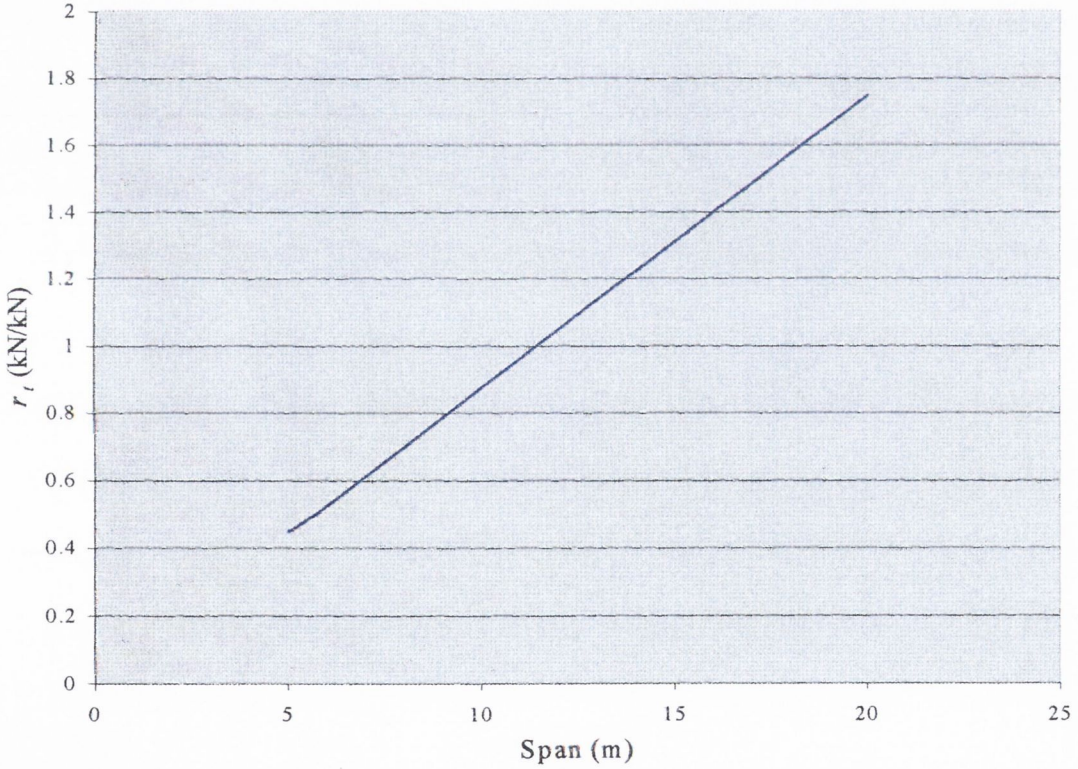

Figure 3.31: Relationship between span increase and r_t .

loading. It can also be seen that for spans in excess of 8.4m (for the beam considered here) the beam remains in camber which, as explained earlier, will provide a greater r_t rate than when the beam has sagging moment at mid-span. For the un-strengthened beams the maximum load will be limited by serviceability requirements and, as demonstrated in figure 3.30, will be lower.

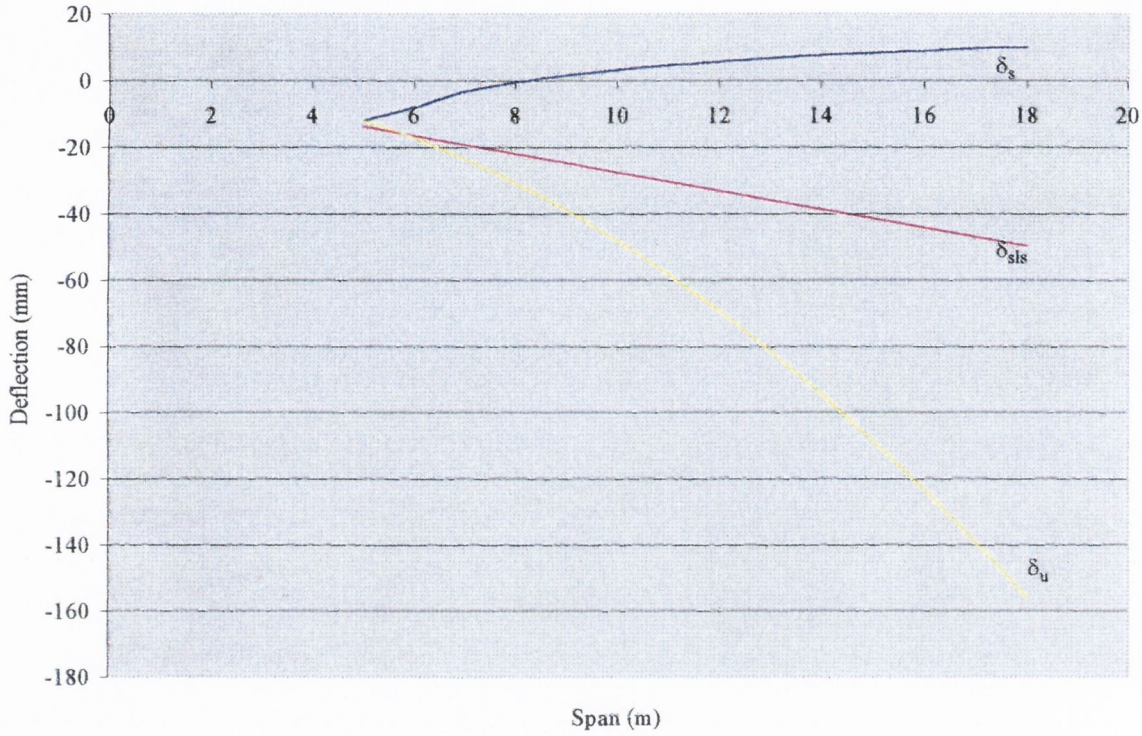

Figure 3.32: Mid-span deflection versus span length for strengthened beams, un-strengthened ultimate limit state beams and un-strengthened serviceability limit state beams.

3.6.4 Deflection

The serviceability limit state will often limit section capacity where deflection is limited to span/360. The method of strengthening with tendons attached to the underside of the lower flange of section can not only improve flexural strength but can also reduce deflection and, thus, increase limit state loading.

Figure 3.33 shows the mid-span deflection of an initially unloaded 254x254x132 UC with a maximum initial tendon force (for an imposed limiting stress). The UC had a 6m span with a tendon force of 1400kN and a tendon eccentricity of 170mm which yielded a pre-camber of 16.34mm (positive upward deflection). Subsequent central concentrated loading produces a downward linear deflection as can be seen in the plot.

It can be seen from figure 3.33 that, in addition to the initial pre-camber (which reduces the total deflection), the rate of deflection is smaller than with the un-strengthened beam. The lower rate is due to additional counter moment being induced with loading. In general, significant mid-span reduction is achieved with the strengthening application considered and can significantly improve loading to members with serviceability limiting criteria.

Figure 3.34 shows a plot of the mid-span deflection of the beam with an increasing tendon eccentricity (assuming stiff tendon lever stiffness provided) with a constant central concentrated load applied and with the maximum initial pre-tension force applied. It can be seen in this plot that the deflection is non-linear with respect to increasing eccentricity. As the tendon eccentricity increases the mid-span deflection decreases.

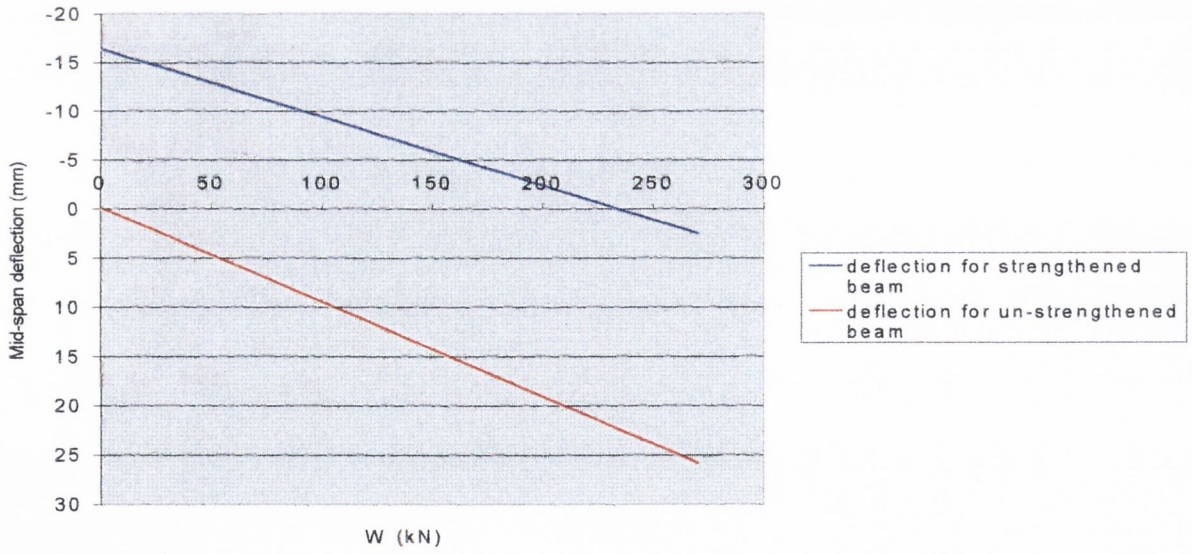

Figure 3.33: Deflection of un-strengthened and strengthened beam with a 16.34mm initial pre-camber versus increased loading.

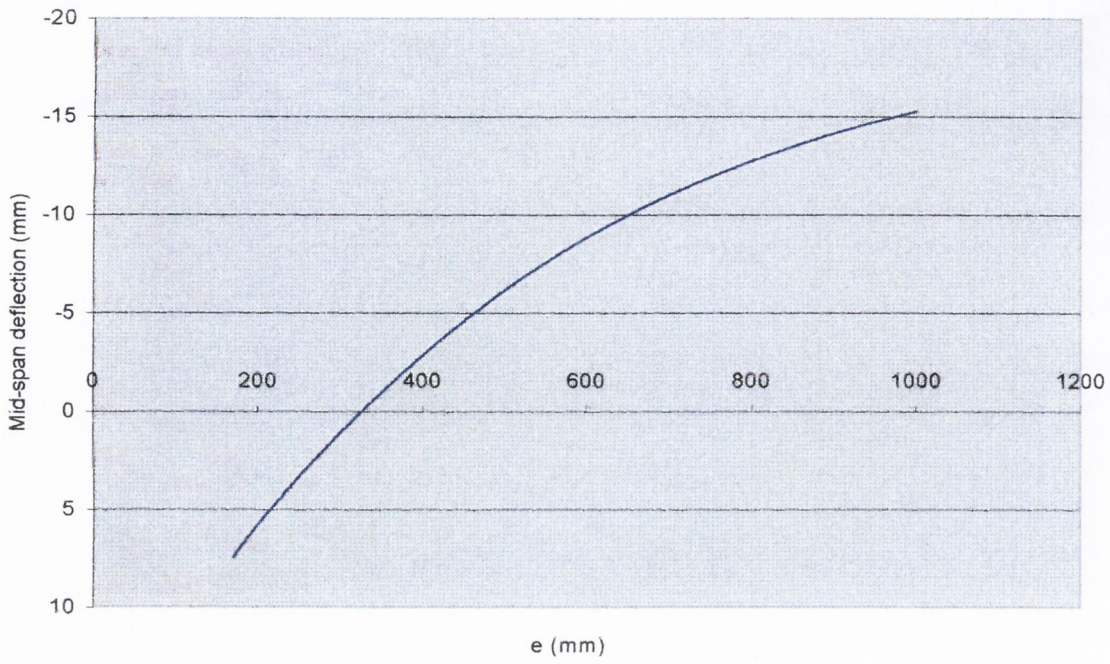

Figure 3.34: Deflection versus increasing tendon eccentricity with a constant central concentrated load with maximum initial P_I and constant central concentrated load.

This is due a greater counter moment and, thus, greater pre-camber, and a greater self-counter moment capacity upon load application, with increasing tendon eccentricity. It can be seen from the plot that with eccentricities in excess of 320mm (for the section considered) the beam remains in pre-camber under a constant loading of 260kN.

3.7 Conclusions

The theory for optimising (minimising) the bending moment on beams with a variety of loading and support conditions and under the action of a number of counter-moments has been examined in this chapter. The theory allows the location and magnitude of counter moments to be calculated.

Equations were developed to calculate the maximum initial pre-loaded tendon force, P_i, the rate of tendon force increase with respect to a central concentrated load application, r_t, and the maximum load that can be applied, W, for any given imposed limiting stress.

An expression for calculating the deflection has also been developed which allows the reduction in deflection due to counter-moment application (from both initial and self-counter moment) to be calculated.

A parametric study showed relationships between the key parameters including I/A, e, A_t, and L. It was also shown that the eccentricity giving rise to the optimum r_t occurs just at the point where the bending in the beam moves from hogging to sagging. The greater the eccentricity from the optimum value , the lesser will be r_t, that is, any further increase in overall member depth will result in less efficient benefit with regard to self counter moment. However, provided sufficient lever flexural stiffness exists, increasing the lever length and, thus, the tendon eccentricity, to a value greater than the optimum will result in significant member capacity(that is, of the order of 40-60% depending on lever length).

The study also demonstrated that when the number of tendons applied is limited due to having a light member (that is, relatively small cross-sectional area), increasing tendon eccentricity will reduce the required initial tendon force (thus, reducing the required number of tendons). An increase in tendon eccentricity will also result in self counter-moment due increase and a greater r_t rate up to an optimum value as shown figure 3.21.

The cross-sectional area of the tendons has a significant contribution to the r_t rate. With all other parameters constant, the rate of change of r_t with respect to tendon area is approximately linear as shown in figure 3.23 (that is, provided twice the tendon cross-sectional area will approximately double the r_t rate). A higher r_t rate will provide greater self counter-moment and, thus, increase member capacity. It can be seen from figure 3.24 that the greater the tendon area, the closer optimum tendon eccentricity, will be to the beam's neutral axis. This is particularly relevant where overall member depth is constrained and providing longer levers is not possible to provide the required counter-moment for a particular case. The provision of an adequate cross sectional area of tendons could provide a sufficient r_t so as to provide the required counter moment.

The downward deflection of members with a constant eccentricity under an increasing central concentrated load is linear as is upward deflection under pre-camber but at a slower rate. Increasing tendon eccentricity will reduce final mid-span deflection by the provision of greater pre-camber and greater self counter-moment which "slows" the rate of downward deflection. If the serviceability limit state is the limiting criteria for design, greater loading can be achieved as the tendon eccentricity is increased due to this reduction in deflection under a given load. However, more often with counter-moment applied to strengthened beams, the limiting criteria is the ultimate limit state with mid-span deflection far less than the serviceability limits under loading well in excess of the maximum serviceability loading.

CHAPTER 4

FINITE ELEMENT MODEL SELECTION OF A BEAM WITH COUNTER-MOMENTS APPLIED BY TENDONS

4.1 Introduction

The objective of the previous research carried out (Maher, 1998), as described in section 2.3, had primarily been to prove that it was possible, in principle, to apply specific counter moments at optimum locations along the span of a simply supported beam, so as to achieve a final optimum bending moment. The final optimum bending moment diagram will be the resulting bending moment diagram after the initial required pre-tension force in the tendons (inducing the initial counter moments) and the concentrated central load (which increased further the counter moments through increased tension in the tendons) has been applied to the beam. To achieve a minimum value, this optimum bending moment diagram must have all peaks equal (that is, in the case of one pair of counter moments applied, five equal peaks of positive and negative bending moment). The practical constraints of construction were not a primary consideration with the earlier research.

With the current research, however, the limitations imposed by design criteria were considered (that is, the overall depth must be kept to a minimum) while still trying to achieve the optimum final bending moment diagram. It was decided to test a full-scale steel beam and, in the design, to minimise overall depth. Welding long down-standing levers to the underside of the lower flange, as in the case with the previous testing, is not considered to be practical in that this will increase the overall depth of the member considerably.

For simplicity, a case of a simply supported beam with a span of 6m and a central concentrated load of 200kN was considered. The design was based on a limiting stress (185MPa) that would ensure the beam would remain within the elastic range and was not

stressed to the ultimate loading. This choice of parameter enabled a safe laboratory testing program, as described in the next chapter.

Hand calculations demonstrated that, with this span and loading, a 686x254x125 UB was required (see appendix F.1). This beam had a depth of 615mm, which was used as a benchmark comparison in terms of the percentage improvement in member depth reduction for the strengthened beams considered.

As in the original configuration, it was decided to investigate the possibility of welding levers to the underside of the upper flange and on both sides of the web at the optimum locations along the span (For weld design see appendix G). Tendons could then be attached to these levers to apply the optimum counter moment for the given loading (see figure 4.1). With this tendon configuration, higher tendon forces were required to apply counter-moments than with the previous tendon configuration due to the low eccentricity. However, the configuration had the advantage that the tendons and levers were contained wholly within the overall depth of the beam.

It was predicted that, with counter-moments applied, a significant increase in member capacity would result. It was expected that if the tendon lever was welded to the upper flange and extended down to within 15mm of the lower flange, it would provide the maximum possible tendon eccentricity and, thus, reduce the tendon forces required to apply a given counter moment.

It will be shown that FE analyses demonstrated that stiffening plates were required to engage the upper and lower flanges to transmit the counter moments into the beam. It was found that the tendon lever fixed to the upper flange generated high shear and bending stresses in the flange, when the tendon forces (600kN per tendon, as required to apply the necessary 200kNm counter moment) were applied to the lever. The beam-tendon interaction of this tendon and lever configuration and the stiffening plates used to engage the upper and lower flange will be discussed later in this chapter.

4.2 Beam and tendon configuration

A number of trial finite element analyses were carried out using the "Encad" software package entitled "ENFELA". The function of these analyses was to investigate the most suitable UC for the testing. All testing carried out with the test beam should be such that the maximum stress arising should not exceed +/- 185MPa (that is, safely within its elastic stress range). This would ensure that the beam could be repeatedly re-tested without having any plastic deformation and also ensured that the beam was safe against ultimate failure under a high tensile force in the tendons, which would be dangerous.

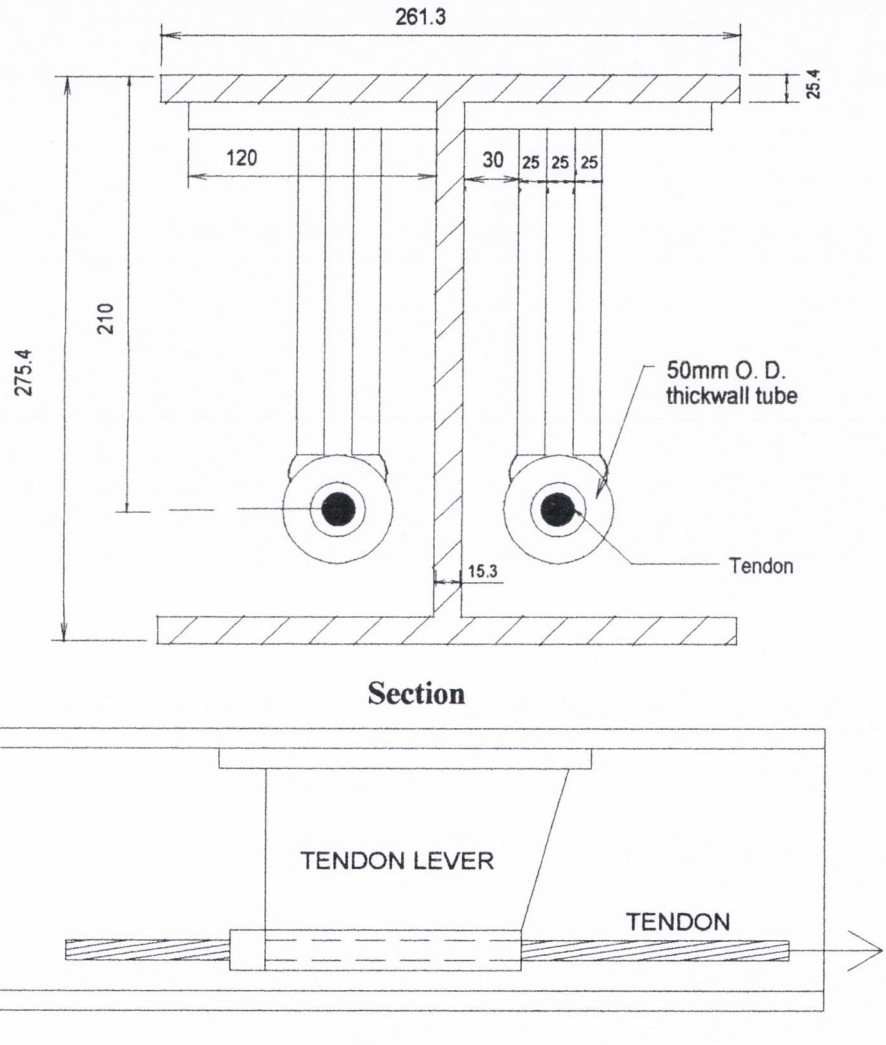

Figure 4.1: The tendon lever detail employed for the strengthened beam

Using "ENFELA 2-D" finite element analyses were carried out on a number of trial beams with tendons running horizontally from lever to lever (both tendons modelled as a 2-D pinned end member). The levers are located at the optimum location along the span, which are, in this case of one pair of counter moments applied on a 6m span, 1.0m from the left and right supports (as calculated from the theory in the previous chapter), that is, one-third the distance from the supports to the application of the central concentrated load (see figure 4.2).

Local analyses of the lever-beam interaction were carried out to investigate where the lever should be located on the beam to apply the counter moment at the correct location. The local flexural and shear strength of the upper flange plate, where the levers were attached, were also investigated with regard to the possible need for stiffeners, which will be discussed later in this chapter. The assumption with regard to the location of the levers was, at this stage of the analysis, considered sufficient for the selection of a suitable UC member for further detailed analysis.

With the type of tendon and lever beam strengthening application shown in figure 4.2, the lever length, with its consequent tendon eccentricity, will govern the magnitude of tendon force required to apply a prescribed counter moment for a given loading on the beam.

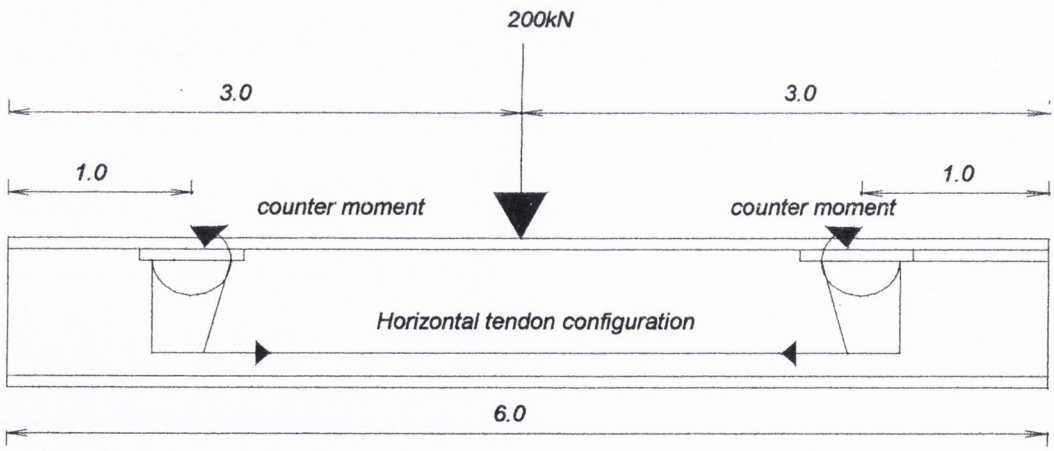

Figure 4.2: Tendon and lever configuration considered for the test beam analyses (Vertical scale exaggerated).

When overall member depth in not a primary consideration, the tendon lever can be longer (that is, below the beam, as in Maher 1998), which results in a lower tendon force required to apply a particular counter moment. This lower tendon force results in a lower portion of the beam capacity being engaged to withstand the axial force induced by the tendon forces and a greater portion of the beam capacity being available to withstand the bending moments induced by loading. Hence, it is desirable to maximise tendon eccentricity. With particular regard to the beam and tendon configuration in figure 4.2, the tendons and levers are located wholly within the overall depth of the beam as a fundamental design requirement and, as such, the overall depth to which the tendon lever can extend is highly constrained.

A number of beams were analysed with the FE software and it was found that a substantial proportion of the stress capacity (40-50%) was taken by the axial force induced by the tendons. The universal beams analysed behaved more like slender columns and, with respect to the un-strengthened beam, did not give a large beam depth reduction (that is, of the order of 15-20%). The loads for the lighter beams strengthened with the tendon configuration in figure 4.1 were more likely to be limited by minor axis buckling (as in the case of slender columns) or premature lateral torsional buckling due to the substantial section capacity reduction owing to the high compressive axial forces. Thus, a universal column (254x254x132 kg/m UC) was selected, as it was considered that a more compact member would be more suitable for the combined axial and bending stresses induced by the tendons, due to the relatively high minor axis capacity when compared to beams of the same depth.

The beam was modelled in the 2-D FE analysis as three plates that were rigidly fixed together, the upper and lower flange plates and the web plate. The plates had in-plane bending and deflection with no out-of plane effects. The upper and lower flange plates were modelled with 25.4mm thick plate elements and the web plate was modelled with 15.3mm thick plate elements. Each element initially selected was approximately 60mmx50mm (that is, 275.4/6 and 6000/120) in size so as to keep the aspect ratio of the elements within a range that would yield accurate results. The stiffening plates fixed to

the upper flange where the tendon levers are attached to the beam and the stiffening plates attached to the outer edges of the upper and lower flanges at the same location, were modelled with 25mm thick plate elements. The ENCAD finite element sub routine programme entitled ENFELA, uses a method of back substitution to solve the elastic stiffness equations for the quadrilateral elements. The programme firstly checks the nodal numbering, and re-numbers the nodes, where necessary, to ensure a minimum size stiffness matrix by keeping adjacent node numbers to a minimum difference.

4.3 Mesh verification

A preliminary trial analysis was carried out on the simply supported UC beam with no tendons or levers attached under a 200kN central concentrated load. The results of this analysis were used in a comparison with hand calculations on the same beam and loading. The mid-span deflection. The FE analysis gave a mid-span deflection of 19.6mm and mid-span bending stresses of +/- 185.9MPa on the upper and lower flanges respectively (negative stress is tensile in the software sign convention). Navier's equation (equation 4.1) for simple bending theory was used to calculate the beam stresses for comparison with the FE predictions (Steel Designers' Manual, 2005):

$$\frac{M}{I} = \frac{\sigma}{y} \tag{4.1}$$

where M = the moment at the section under consideration, I= the second moment of area of the beam section, σ = the bending stress at the section and y = the distance from the neutral axis to the beam fibre under consideration.

The maximum deflection, δ, of a simply supported beam under a central concentrated load is approximately (Steel Designers' Manual, 2005):

$$\delta = \frac{WL^3}{48EI} \tag{4.2}$$

where W is the central load, L *is* the clear span, E is the material elastic modulus and I is the section second moment of area.

The mid-span section stresses were calculated as +/- 184.5MPa in the outermost fibres of the upper and lower flanges. Equation 4.2 predicted a mid-span deflection of 19.1mm. These were within 0.75% and 2.55% of the FE results for the stress and deflection respectively.

A further beam was modelled with a finer mesh size (namely, 45x50mm quadrilateral elements). This beam, with the same loading and conditions as the previous analysis, yielded negligible differences in results compared to the previous coarser mesh (within 0.5% for stress and 0.7% for deflection. Given that the results of this analysis compared well to those of the hand calculation predictions, it was considered that a further refinement in the mesh was not necessary.

In the next analysis, the tendons were added and modelled as single tensile members with a given cross-sectional area and Young's modulus. The tendons were not constructed with separate beam elements, as in the case of some other FE software packages. This particular FE package had the advantage of allowing the incorporation of a pinned and/or rigid frame within a meshed model. Both tendons were modelled as a single 2-D beam element pinned to specific nodes on the meshed beam model.

Some difficulty was encountered, however, with the application of the pre-stressing forces to the tendons. A provision within the FE package allowed prescribed members to be pre-stressed. This provision was, however, with particular regard to pre-stressed concrete members and an overall tendon force and profile is required. The assumption was that an adequate number of tendons would be provided to accommodate the prescribed force. This force is applied to the concrete member, via tendons contained within, and will always be compressive. When a pre-stress force was applied to the tendons and analysed here, the results showed that the tendons behaved as members that offered resistance to the pre-stress forces (that is, treating the tendon itself as a concrete pre-stressed member) and not simply as tensile members, thus not allowing the tendon forces to be applied properly to the steel beam. This was overcome by applying an alternative device involving the application of a local positive axial displacement, (that is,

stretching the tendons and then pinning them to the levers), and using their axial stiffness (PL/EA) to predict an appropriate initial approximate extension. However, if the total tendon force is applied to the beam, as a compressive force, the steel beam would consequently shorten (by a smaller amount than the initial tendon displacement), thereby reducing the tendon pre-stressing force. An approximate linear equation was used to predict the pre-loaded total tendon force, and is as follows:

$$\delta_t = \delta_b \frac{A_b}{A_t} \tag{4.3}$$

where,

A_t= Total cross-sectional area of tendons

A_b= The cross-sectional area of the beam

δ_t= The displacement of the tendons

δ_b= The axial shortening of the beam

This equation assumes a linear relationship between the two displacements. Some non-linearity exists due to the levers themselves deflecting like cantilevers when the tendon forces are applied, as well as some rotation due to beam bending. It was considered, for the purposes of the first estimation, that the above non-linear factors were not a considerable portion of the total final beam-tendon displacement and that, with just a few iterations of the above expression (Ghali et al., 1997) a good first approximation could be derived. This approximation could save many trial analyses to find the final exact required tendon extension. Further refined applied displacements were then applied to the tendons until the final required force resulted in the two tendons. Further trial analyses were carried out on the tendon/beam interaction and will be discussed later in the chapter.

4.4 Analysis of tendon configurations

FE analyses of the universal column were carried out with different types of tendon configurations, which were as follows (see figure 4.3):

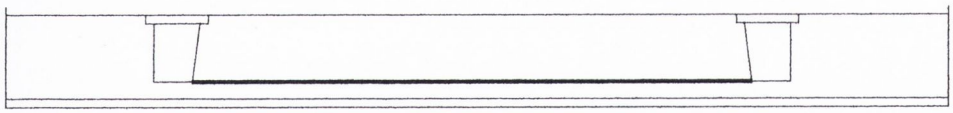

Horizontal tendon configuration

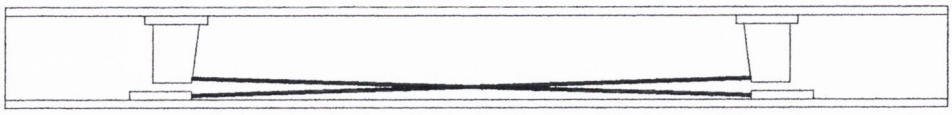

Downward cross configuration

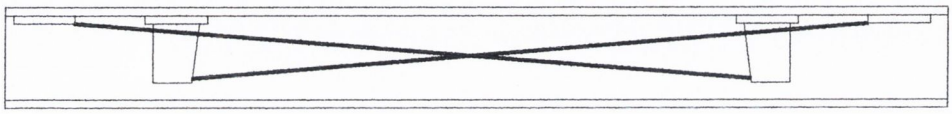

Upward cross configuration

(configuration thus on both sides of web for all cases)

Figure 4.3: The three tendon configurations analysed and compared for overall beam improvement.

- Horizontal tendon configuration
- Downward cross configuration
- Upward cross configuration

For the tendon configuration comparison, the 2-D ENFELA software was used. Analyses were carried out on the simulated test beam model with the three tendon configurations that is, the horizontal, downward-cross and the upward-cross tendon configuration.

4.4.1 Analysis of beam with a horizontal tendon configuration with no central concentrated load applied

This configuration was used for a comparison with the other tendon configurations. The constraint, again, was to limit the maximum stress to within 185MPa and apply as much

counter moment as possible in order to establish the most efficient tendon configuration (that is, the configuration that will apply the maximum amount of counter moment to the beam per unit of tendon force). This would have the effect of maximising counter moment application while minimising tendon force.

The FE analysis of the horizontal tendon configuration with no central concentrated load applied predicted that the greatest total tendon force (and, thus, maximum axial force) that could be applied to the beam was 1494kN. This force was found to apply, via the down-stand levers, counter moments of 153kNm, delivering a maximum compressive stress of –183.8MPa (with a top flange stress of 4.8MPa). These counter-moments were less than those required for the intended test loading conditions (that is, 200kN central concentrated load on a 6m span, requiring 200kNm counter moments for optimum conditions). The mid-span section stresses were +4.8MPa in the upper flange and –183.8MPa in the lower flange, which was the maximum stress observed. The axial force was back calculated as 1494kN and the resulting counter-moment as 153kNm using the above stresses. The maximum resulting deflection with this FE analysis was -0.6mm (that is, an upward deflection of 0.6mm at mid-span).

4.4.2 Analysis of beam with a downward cross tendon configuration with no central concentrated load applied.

The beam was also analysed with the downward cross configuration of tendons (figure 4.3). Each tendon was fixed to a lever at either side of the centrally concentrated load with the other end of the tendon fixed to the lower flange at a location beneath the opposite lever. This configuration had a total of four tendons, two on either side of the web. The maximum stress was, again, restricted to +/-185MPa.

The maximum stresses occur in the same location (mid-span) as in the previous horizontal tendon configuration and were –7.9MPa and –184.1MPa in the upper and lower flange respectively under an axial force of 1625kN and a counter-moment of

143kNm. The maximum deflection was -0.5mm at mid-span (that is, an upward deflection of 0.5mm).

The analysis demonstrated that, for practically the same maximum stress in the beam, with the downward cross configuration, it required a greater (8.7% increase) tendon force to apply approximately the same magnitude of counter moment. A further FE analysis of the same model but with a lower tendon force (equal to that of the horizontal configuration) demonstrated that, for a total tendon force of 1494kN, the maximum counter moment that could be applied was 129kNm as compared with 153kNm with the horizontal tendon counter moment. It was concluded that this tendon configuration was not as efficient as the previous horizontal tendon configuration discussed, in that, it has a lower amount of counter moment applied per unit of total tendon force applied to the beam. However, given that, in this configuration, four tendons are used as compared with two tendons in the previous tendon configuration, twice the overall tendon force can be applied for similar diameter strands, with a subsequent penalty in cost.

4.4.3 Analysis of beam with an upward cross configuration with no central concentrated load applied

The third configuration considered was an upward cross tendon configuration (figure 4.7). Each tendon had an end fixed to a lever while the other end of the tendon was fixed to the upper flange at a location over the support furthest away from the lever. This configuration also had a total of four tendons, two on either side of the web. The maximum predicted deflection from the analysis was –0.3mm at the mid-span with a maximum stress of –122.2MPa and -184.6MPa in the upper and lower flange respectively. The end anchorage for the tendons in this configuration were located above the beam neutral axis as can be seen in figure 4.3. This results in moment opposed to beneficial counter-moment being applied and, thus, yielding a lower beneficial counter-moment.

The analysis demonstrated that for this tendon configuration applied to the beam, with a total tensile tendon force of 2580kN, while keeping the maximum stress to within

185MPa, the maximum counter moment that could be applied was 51kNm. This counter-moment, as compared to that of the horizontal tendon configuration, was approximately 67% lower. The deflected shape displays predominantly axial compressive shortening owing to the high axial force and comparatively low applied counter-moment.

A further FE analysis of this configuration confirmed that for a tendon force of 1494kN (that is, the force applied to yield the imposed limiting stress with the first configuration), the maximum amount of counter moment that could be applied to the beam was 29kNm, and was substantially less than the original horizontal tendon case.

4.4.4 Selection of tendon configuration

Of the three types of tendon configurations analysed, the horizontal tendon configuration produced the most efficient results. By "efficient" it is meant that the highest magnitude of counter moment applied per unit of compressive axial force is applied to the beam via the tendons. The total compressive force in the beam being induced is irrespective of the number of tendons that are used (that is, two or four). The horizontal tendon configuration gave a counter moment of magnitude of 0.102kNm per unit of compressive force in the beam whereas the downward and upward cross configuration, gave counter moments of 0.079Nm and 0.019kNm per unit force respectively. Hence, the former configuration was chosen for further investigation with the test beam.

4.5 Local lever and flange analysis

Typically with external tendons applied to beams, high concentrations of stress occur at the tendon anchor points and it is for this reason that local analyses were carried out, at the portions of the beam with the levers attached, to establish the magnitude and locations of the maximum stresses.

4.5.1 Analysis without additional flange stiffening

The local stresses at the point of application of the counter moments were now considered. The tendon loading, applied by the levers welded to the upper flange, gave

rise to a large shear force and bending moment imposed on one flange only. It was necessary to firstly investigate whether the upper flange could withstand such a loading and, secondly, whether the lower flange should be engaged, with the use of stiffeners, in the resistance of this loading.

All previous FE analyses, with the exception of the local analysis of the lever, had been carried out in two dimensions using ENFELA. Owing to the vertical symmetry of the model, it was considered that two- dimensional analysis would suffice for the initial sizing of the member and tendon configuration. To confirm the results of the 2-D analyses, and for completeness, three-dimensional analyses were carried out on the beam. To this end, the popular ANSYS FE analysis structural software package was used.

A FE model of a portion of the beam (that is, an analysis on half the beam) was constructed, using ANSYS, where the lever and plates were attached to the beam. An axial load of, say 800kN, was applied to both levers where the tendon would be attached, as a representation of the tendon tensile forces. The half beam was restrained in five degrees of freedom at the nodes on the continuity boundary being which was free to displace vertically only. The other end had only vertical displacements restraints at the simple support at the bottom flange. The modelled beam was free to move axially at the simple support so as to facilitate the development of axial force between the points of application of the tendon levers only (as is the case with the complete beam).

An analysis with no additional stiffening was firstly carried out. By additional stiffening it is meant stiffening that would constrain the upper and lower flanges to act together to resist axial and bending stresses applied via the tendons. The results of the unstiffened local lever/ beam FE analysis (that is, without the additional flange stiffening) yielded a maximum stress of +288.7MPa (compressive) in the upper flange where the web meets the upper flange. Figure 4.3 shows a view of the stress contours. The maximum stress exceeded the steel yield stress (265MPa) and demonstrated that additional stiffening would be necessary.

It can be seen from figure 4.4 that the upper flange undergoes a substantial rotational distortion while trying to impart a counter-moment to the beam. The principal nodal stresses just to the left of the levers in the upper and lower flanges were +43.9MPa and –44.1MPa respectively. The stresses are as expected for bending with no axial force present. The resulting stresses just to the right of the levers in the upper and lower flanges were both compressive and were 1.1MPa and 191.3MPa respectively. The analysis demonstrated that axial force and bending moment are present at this section. The moment just to the right of the levers was calculated as 156.8kNm and the axial force as 1600kN (as expected due the forces applied to the levers). The change in the sign of stress from left to right in the upper and lower flange confirmed the presence of counter-moment. The stress component diagram of the section to the right of the tendon levers is shown in figure 4.5. It can be seen that the axial component of stress is just lower in magnitude than the beneficial counter-moment (+/-1.1MPa). This can be attributed to a low tendon eccentricity which requires a very high tendon force to deliver a modest counter moment.

The maximum horizontal lever deflection was 5.85mm, with a mid-span beneficial pre-camber of 13.3mm and was within 0.5% of the calculated mid-span deflection yielded by equation 3.24. However, it can be seen from the deflected shape of the un-stiffened portion of the beam, that the upper flange undergoes a much greater distortion than the lower flange at the location of the tendon levers. A method of stiffening the beam locally was employed (and discussed in the next section) such that the upper and lower flange could act together to dissipate the high concentration. The effective transmission of counter-moment into the beam also relies on the upper and lower flange acting together. Hence it was concluded that stiffening plates were required.

4.5.2 Analysis with additional stiffening

Fixing plates to the outer vertical edges of the upper and lower flanges on both sides of the beam at the location of the levers will engage the upper and lower flanges to act

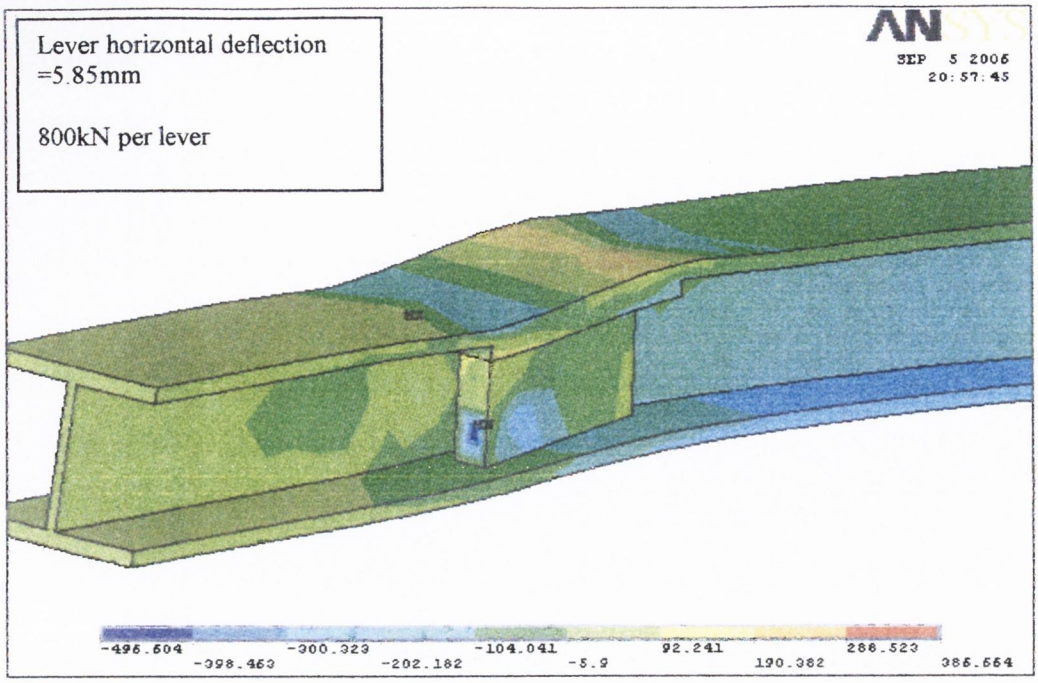

Figure 4.4: Local stress contours of tendon and lever configuration

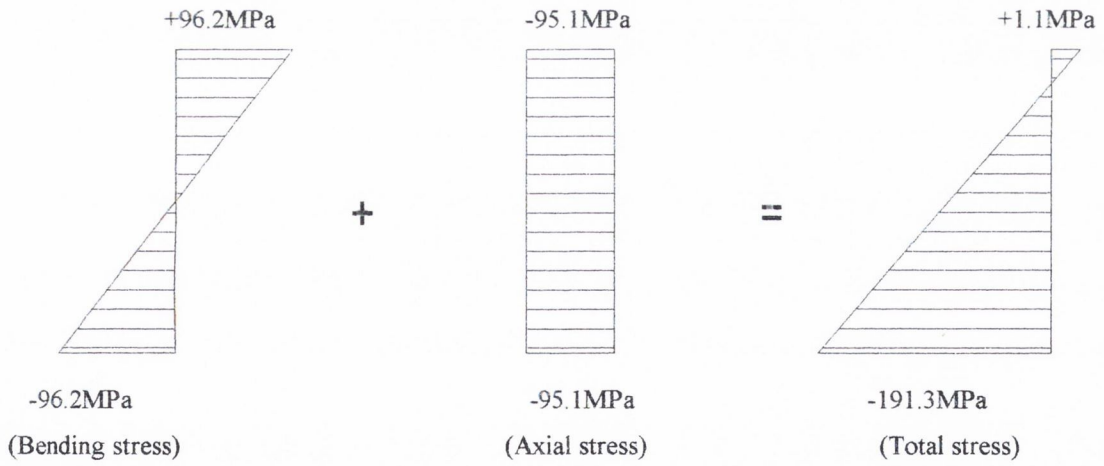

Figure 4.5: The stress component diagram just to the right of the levers in the un-stiffened beam.

together to resist the combined axial and bending stresses imposed by the tendons. A further analysis was carried out using the same half beam and with the outer flange plates attached at the lever location. Figure 4.6 shows a view of the local stress contours at the tendon levers with the upper and lower flange outer edge stiffeners in place. The results in this case demonstrated that, with the same 800kN horizontal load per tendon, the maximum resulting stress was -158.3MPa in the upper flange. The stress component diagrams to the left and right of the location of the tendon levers yielded almost the same bending moments and axial forces as in the case without stiffeners. The local analysis with the stiffeners attached demonstrated that the lower flange could be engaged to reduce the maximum overall local stress that resulted from applying the axial force and counter moments.

Figure 4.7 shows the deflected shape of the portion of the beam with the outer edge upper and lower flange stiffeners in place together with the upper flange stiffeners. The deflection at the free end of the tendon lever was 2.1mm, which was considerably less than in the un-stiffened case (5.85mm). In the stiffened case, the vertical deflection at the right support (where there is no vertical restraint) was 13.3mm as in the previous analysis. One can conclude that no significant change global behaviour results from the additional stiffeners, although at the point of application of the counter-moments are significantly reduced.

4.6 3-D Modelling of beam using ANSYS

3-D analyses of the horizontal tendon configuration with local stiffeners were carried out using the ANSYS finite element software. The resulting predictions will be discussed in chapter 5. The beam model was constructed using three 6m long plates, two plates 25.4 mm thick and one 15.3mm thick, the two thicker plates being the upper and lower flange and the thinner plate being the web. The plates were "glued" together, assuming full structural continuity of the plates along the interface of the plate joints (figure 4.8). The levers were then modelled using rectangular and prismatic solid blocks. "Bar" elements were

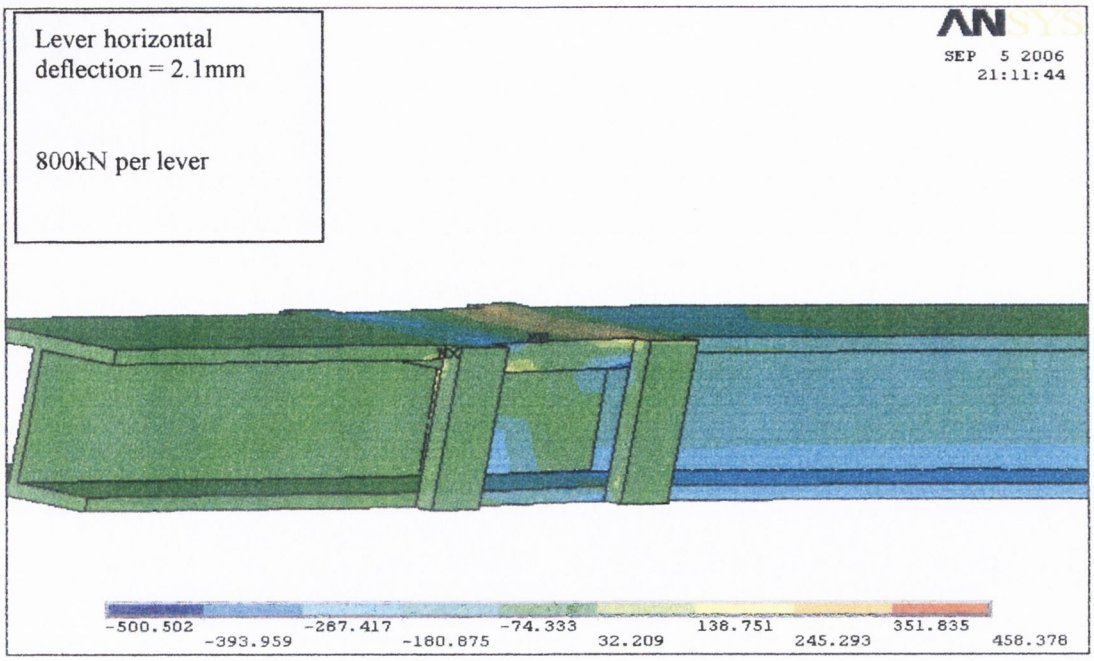

Figure 4.6: Half analysis with local lever stiffening plates attached.

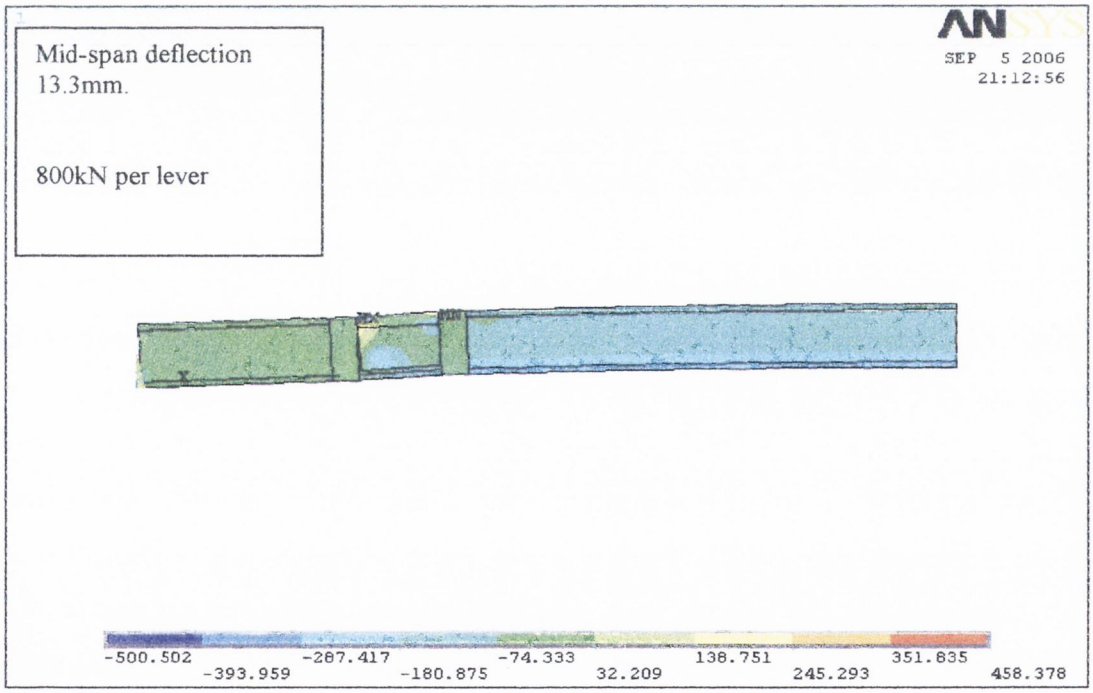

Figure 4.7. Deflected shape of half analysis of beam with stiffeners.

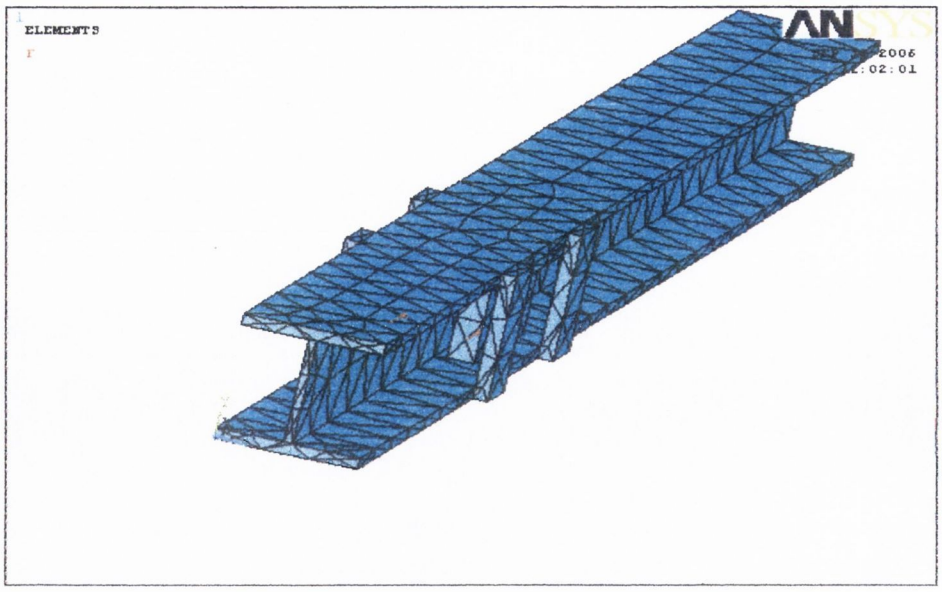

Figure 4.8 Model of beam with solid elements

used to model the tendons. Bar elements are used in preference to "Beam" elements where the force in the member being modeled is axial only, while beam elements are preferred where bending, shear, and axial forces are present within the member. These bar elements allowed a prescribed strain, and thus stress, to be applied such that the required initial pre-stress force could be applied to the beam.

The selection of the elements proved to be troublesome owing to the geometry of the section (that is, relatively thin plates with respect to their length). Solid block or "brick" elements were firstly used to mesh the model and it was found that the program would abort owing to the large aspect ratio of the elements, which lay outside the required criteria for analysis. The program prompted a suggestion that 13 node tetrahedral elements would better model the thin solid plates of the model. These tetrahedral elements consisted of a node at the end of each edge and a node at the mid-point along each edge (see figure 4.9). The program allowed an automatic mesh generation facility to be employed such that the mesh was very fine at supports and at points of load

application and coarser at intermediate points. The mesh could be subsequently refined and results could be compared with each refinement until the change in the result was

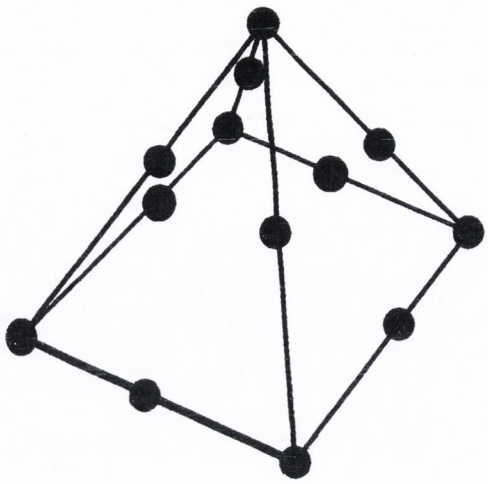

Nodes at endpoints and mid-points

Figure 4.9: The tetrahedral element used to model the 3-D beam

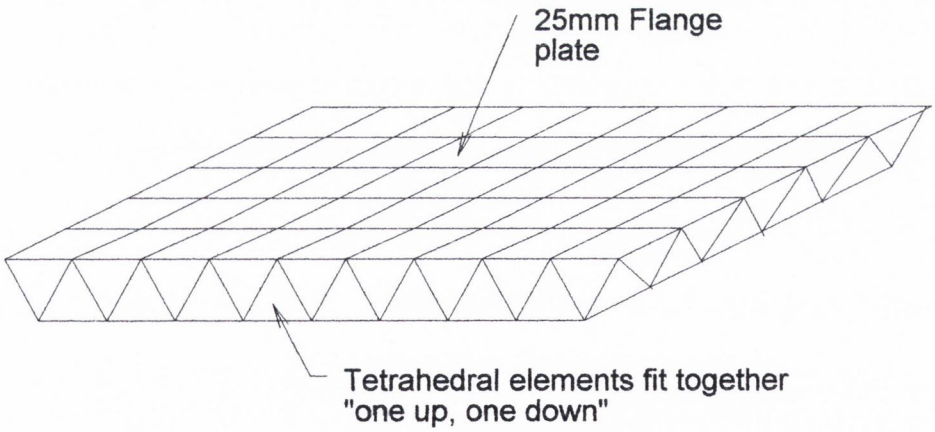

Figure 4.10: Configuration of solid elements

within a prescribed tolerance, which in this case was chosen as 1%. Figure 4.10 shows the pattern of how the elements would fit together in the meshed solid plates.

The model was fixed at one end for the three translational displacements in the X, Y, and Z planes and at the other end in the X (vertical) and Z (lateral) planes only. The software required that both beam ends be laterally restrained. The beam was free to rotate at both ends (that is, no rotational stiffness was provided) so as to simulate simple supports.

The iterative Newton-Raphson technique for the solution of geometric non-linearity in structures (that is, the extent of deflection will effect the magnitude of axial force in the tendons and beam) was applied to this problem (Ghali and Neville, 1997). A provision for the solution of such problems was present in the ANSYS package and provided a suitable method of analysis for the modelled test beam.

4.7 Design calculations to BS5950

In addition to the deflection and local flexural and axial stress checks undertaken in the FE analysis, it was also necessary to undertake standard design calculations to BS5950 (British Standards Institute, 2000). The un-strengthened beam was considered together with two different tendon configurations, the first being the horizontal tendon configuration already described. A subsequent configuration, with tendons passed through thick-wall tubes attached to the underside of the lower flange (the latter configuration will be discussed in a later chapter) was also checked.

The overall capacity, lateral torsional buckling load together with local web shear and local buckling capacities were investigated for the original 686x254x125 UB and for the 254x254x132 UC selected for strengthening (see appendices F1 and F2). Table 4.1 shows the results of the capacity checks.

It can be seen from table 4.1 that the lateral torsional buckling load of the un-strengthened UC is greater (245kN) than for the case of the strengthened beam with

			Web bearing (kN)		Web stiffness (kN)	
	LTB Load (kN)	Shear Capacity (kN)	End	Mid-span	End	Mid-span
686x254x125UB	202.7	1746	406	698	218	325
254x254x132UC (un-strengthened)	245	1120	657	1119	581	1714
254x254x132UC (strengthened within flanges)	215	"	"	"	"	"
254x254x132UC (strengthened below lower flange)	284	"	"	"	"	"

tendons between the flanges (215.8kN). The strengthened beam with tendons below the lower flange, however, proved to be a viable option with a predicted ultimate load of 284kN. However, for the more slender sections (such as a 686x254x125UB), the lateral buckling may govern the design. In such cases, the tendon method for strengthening may not be appropriate, at the very least, the buckling capacity would need to be checked for adequacy.

The design checks were all sufficient to withstand the 200kN maximum central concentrated load to be applied in the planned laboratory testing with both tendon configurations.

4.8 Conclusions

The method of applying the counter-moments was investigated with particular regard to the local stresses induced by the tendon forces at the point of application of the counter-moments. Three types of tendon configuration were considered: the upward-cross, the downward-cross and the horizontal tendon configuration. Of the three types of configuration considered, the horizontal tendon configuration applied the greatest ratio of applied counter-moment per unit tendon force (that is, 0.102kNm/kN). The tendons with this configuration were fixed to the underside of the upper flange through levers, which induced high shear and bending stresses in the upper flange. It was found that fixing plates to the underside of the upper flange together with external stiffeners to the outside edges of the upper and lower flanges engaged both the upper and lower flanges to transmit the counter-moment into the beam quickly and, thus, dissipate the high

concentration of stresses in the upper flange. A suitable 3-D finite element model has been developed to allow full non-linear analysis of a beam subject to counter-moments through the use of tendons.

CHAPTER 5

FINITE ELEMENT LINEAR ANALYSIS OF A BEAM WITH COUNTER-MOMENTS

5.1 3-D Analysis of the beam with the horizontal tendon configuration

The 3-D model described in section 4.7 was used for three types of linear analyses using the horizontal tendon configuration.

1 Un-strengthened beam analysis
2 Passive tendon analysis
3 Active tendon analysis

5.2 Un-strengthened beam analysis

The model in this 3-D analysis had no tendons, tendon levers or lever stiffeners attached. The purpose of this analysis was to compare the results of the beam with no levers or stiffeners attached to those of the stiffened beam to examine the effect, if any, of such levers and stiffeners. A function also of this analysis was to verify the modelled beam against hand calculations for mid-span deflection and mid-span section bending stresses.

A 200kN central concentrated load was applied to the model beam. The results of this analysis yielded a mid-span deflection of 19.4mm and mid-span section bending stresses of +/-184.8MPa. The peak bending moment was subsequently deduced as 301kNm and is within 0.3% of the expected value. Hand calculations had predicted a maximum bending stress at mid-span of 184.5MPa and a mid-span deflection of 19.1mm (see appendix H). The results of this 3-D FE analysis also confirmed the prediction of the earlier 2-D analysis (see chapter 4) carried out for the un-strengthened test beam which yielded mid-span section stresses of 183.6MPa and a mid-span deflection of 19.4mm.

Neutral beam analysis with lever stiffeners attached

The levers and lever stiffeners were then attached to the model beam. The levers were fixed to the plates attached to the underside of the upper flange at the optimum location from each support. The lever stiffeners consisted of plates running from the top flange to the lower flange, fixed to the outer edges of the flanges, on both sides of the beam (see figure 5.1). Design calculations were carried out for plate sizing of the tendon lever and stiffening plates (see Appendix G).

The results of this analysis, with the same load, yielded a mid-span deflection of 18.8mm and a mid-span section bending stresses of +/-185MPa. The results demonstrated that it was acceptable to assume that the levers and lever stiffeners had no significant impact on the overall flexural behaviour of the beam.

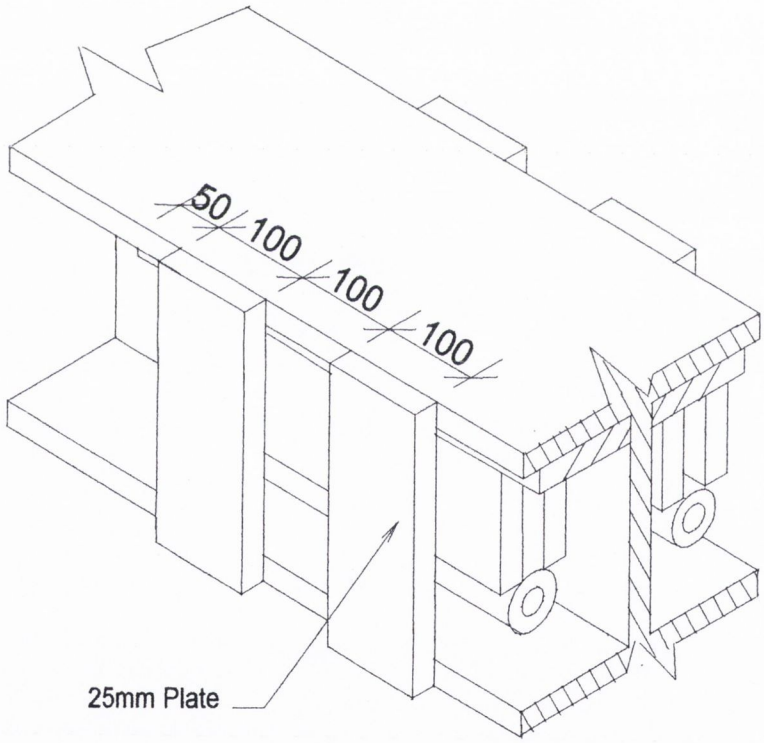

Figure 5.1: Part-view of the beam with 100mmx25mm stiffeners welded to the outside edges of the upper and lower flanges

5.3 Passive analyses

The function of these analyses was to establish the relationship between the central concentrated load application and consequent tendon force increase. The analyses involved applying a central concentrated load to the beam with the tendons in place but without any pre-stress applied to the tendons and observing the increase in tendon force when the load was applied. From this, a ratio of tendon force increase compared to applied load increase was derived. The ratio was thought to be directly proportional and two tests were carried out with different loads to examine if this was so. The analyses were as follows,

- Passive analysis with a 100kN central concentrated load
- Passive analysis with a 200kN central concentrated load.

5.3.1 Passive analysis with a 100kN central concentrated load

This analysis involved applying, to the modelled test beam described above, a 100kN central concentrated load. The tendons were fixed to the levers but had no initial pre-stress prior to loading (passively engaged). The analysis yielded a tendon force of 11.0kN when a central concentrated load of 100kN was applied. This result agreed closely with the predicted tendon force increase to load increase ratio of 0.105kN/kN, as described earlier in the 2-D analysis.

The mid-span section stresses were –92.2MPa (compressive) in the upper flange and +91.0MPa (tensile) in the lower flange. Figure 5.2 shows the mid-span section stresses together with the component section stresses. These stresses are not symmetrical as there is an induced axial compressive force of 11kN present in the beam, which is equal and opposite to the tendon forces. It can be seen also in figure 5.2 that a small counter moment is applied due to this induced force of 11kN. The self counter-moment in previous work carried out (Maher, 1998) was much greater than in this case due to the lever arms extending significantly below the beam, yielding a much larger eccentricity.

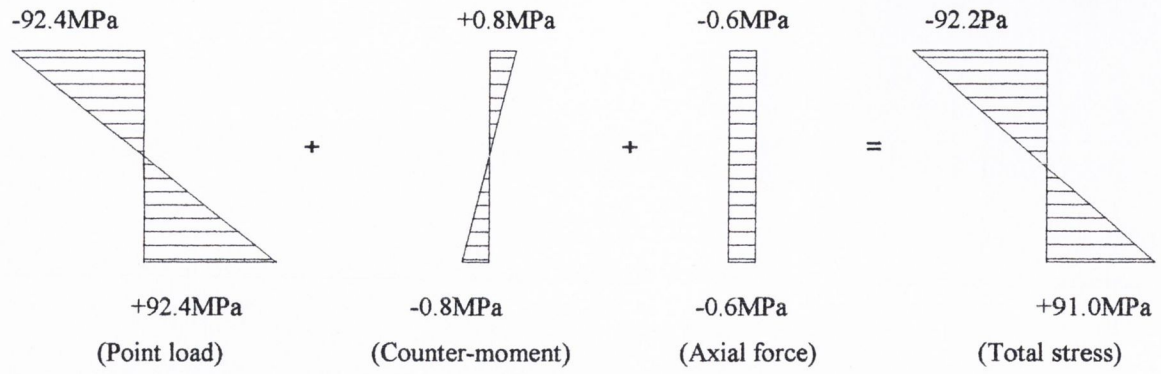

Figure 5.2: The mid-span section stress component diagrams with the tendons passively engaged and with a100kN central concentrated load applied.

5.3.2 Passive analysis with a 200kN central concentrated load

The primary function of this test was to establish the linearity of the relationship between central concentrated load application and tendon force increase for the tendon configuration under consideration despite using the non-linear analysis facility in the software. With the tendons passively engaged on the computer beam model, the FE analysis showed that an overall tensile force of 22.0kN was induced with a 200kN centrally concentrated load. The stress diagrams below show the axial force stress component, the bending stress component and the final combined stress diagram (see figure 5.3).

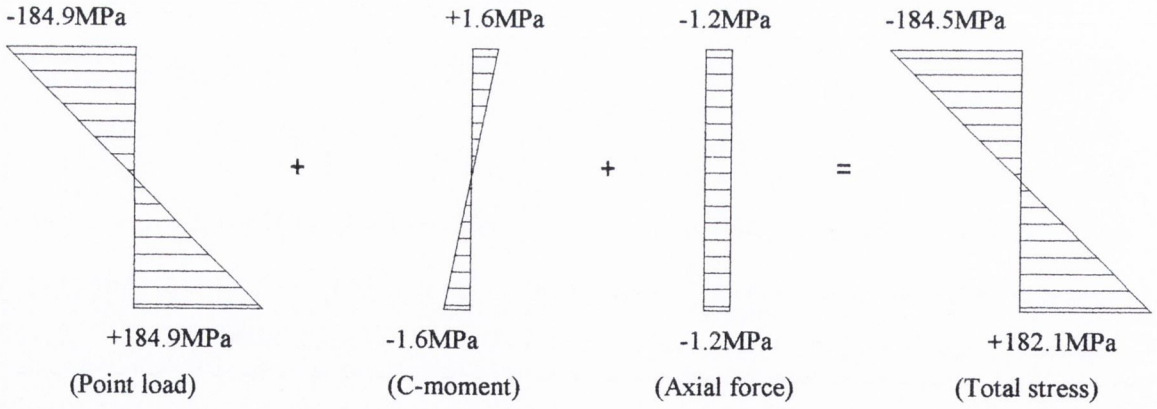

Figure 5.3: The beam mid-section stresses with a 200kN central concentrated load applied and with the tendons passively engaged.

The results of the 100kN and 200kN passive tests were plotted on a chart shown in figure 5.4. The chart confirmed the linearity of the relationship of tendon force with respect to central concentrated load over the range of load applied. However, the stiffness of the tendon lever itself will impact on the tendon force to load relationship. In general, the longer the lever is, the greater the flexibility of the lever and the more non-linear the tendon force/beam load relationship. The levers, in this case, are relatively stiff and behave more like stiff corbels than cantilevers and have negligible horizontal deflection in flexure. It is for this reason that the tendon force to beam load relationship in figure 5.4 is linear.

The mid-span deflection was 9.35mm under a load of 100kN. This deflection was slightly less than the case for the un-strengthened beam (that is, 9.4mm for a 100kN load). This slightly lesser deflection was expected due to a small tendon force being present which induces a small counter-moment. The final mid-span deflection under a load of 200kN was 18.6mm, again slightly less than in the un-strengthened case (19.4mm).

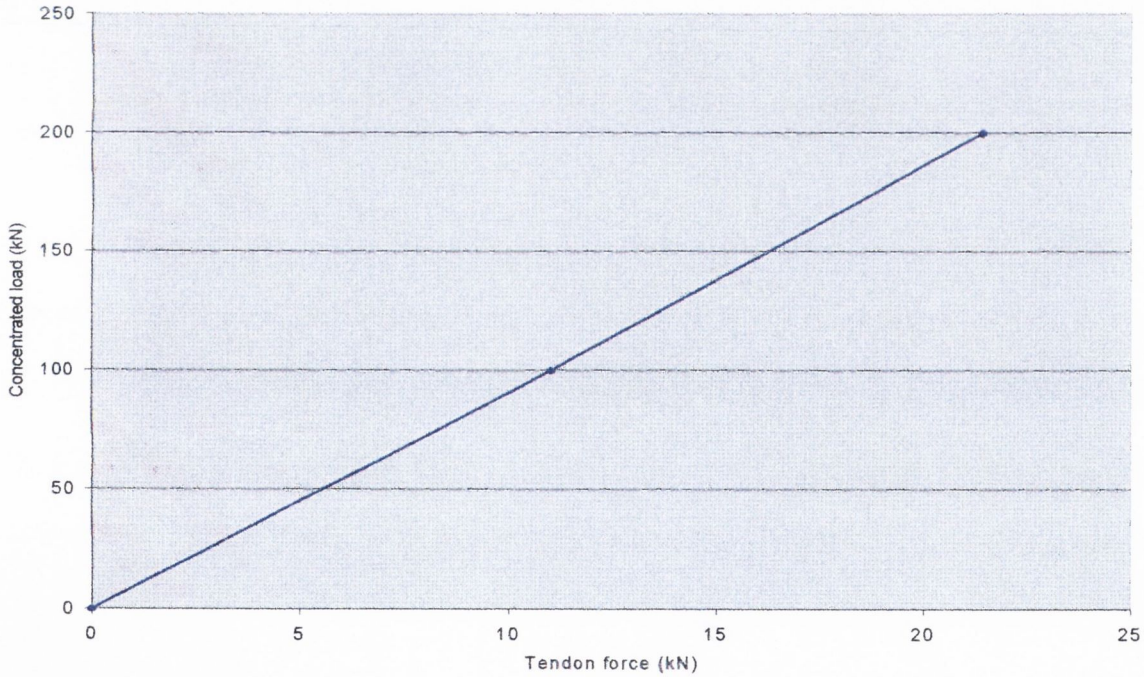

Figure 5.4: Plot between tendon force increase and central concentrated load application under a 200kN load with tendons passively engaged.

The equation for r_t (3.18) predicted a rate of 0.109kN/kN, thus, yielding a predicted tendon force increase of 21.8kN with a 200kN central concentrated load applied and was within 1% difference of the FE predicted tendon force increase.

5.4 Active analyses

It had been decided to use two 15.7mm core diameter "super-strand" tendons on the laboratory test beam (that is, one each side of the web). The characteristic breaking strength of these tendons is 265kN. It is common practice to keep the working tendon forces to within 80% of the characteristic breaking strength for a given tendon, (Allen, 1986) which in this case is 192kN. It was decided, for safety reasons, to apply no more than 180kN per tendon on the laboratory test beam. The active analyses were thus carried out with tendons fully tensioned to 360kN (that is, 2x180). These analyses were used as a comparison with the passive analyses with particular regard to the tendon force increase with respect to central concentrated load increase. The beam model in the previous analyses was also used in this analysis. The cases to be considered are;

- Active tendon with no central concentrated load applied
- Active tendon with a 100kN central concentrated load applied
- Active tendon with a 200kN central concentrated load applied

5.4.1 Active analysis with no central concentrated load applied

This analysis involved applying a 360kN total tendon force to the beam and observing the resulting applied counter moment. The measured value of the resulting counter moment was used to calculate the actual tendon eccentricity.

The maximum beam stresses were at the mid-span section and were +0.6MPa (tensile) in the upper flange and –43.2MPa (compressive) in the lower flange. The total mid-span section stresses are shown in figure 5.5 together with the component section stresses. The maximum deflection was -2.08mm at the mid-span section.

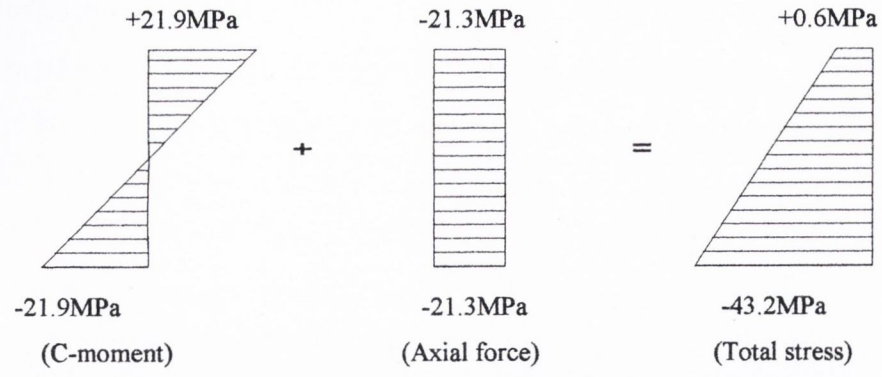

Figure 5.5: Mid-span section stresses with 360kN tendon force applied and no loading

The resulting applied counter moment, as indicated by the reported stress, was 35.8kNm and the resulting axial force in the beam was calculated to be 360kN as expected. This allowed the tendon eccentricity of 0.098m to be calculated. It can be deduced from the figure that this tendon and lever configuration is not efficient, in that, a relatively large tendon force of 360kN yields a low counter-moment of 35.8kNm This arises specifically from the requirement that the tendon stays within the flange of the beam, which in this case is a shallow UC (276.3mm deep). Z/A for this arrangement is 96.0mm, just below the actual eccentricity.

5.4.2 Active analysis with a 100kN central concentrated load

This analysis involved applying a 100kN central concentrated load to the modelled test beam. The initial tendon force was first established with a preliminary FE analysis with no central concentrated load and with the initial required pre-strain in the tendon bar elements. The initial total tendon force was 350kN (i.e. 175kN in each tendon) and was over 97% of the final required tendon force. This high proportion of initial pre-loaded tendon force was necessary owing to the poor self-counter moment performance of the tendon configuration (that is, an expected tendon force increase of 10.2kN on application of the 100kN load).

It was found from the analysis that the final applied counter moment was 36kNm after the application of the 100kN central concentrated load. The results of this analysis

compared well with the results of the passive analysis, in that the calculated tendon force increase was 10.4kN. The results of this active analysis also indicated that the relationship between the tendon force increase due to a central concentrated applied load remained linear irrespective of the initial pre-loaded tendon force, provided the beam and tendon stresses were within the elastic range, for the given beam geometry.

The maximum resulting stresses were at the mid-span section and were –92.1MPa (compressive) in the upper flange and +49.3MPa (tensile) in the lower flange. The mid-span section stresses are shown in figure 5.6 together with the component stresses. Figure 5.7 shows the resulting bending moment diagram corresponding to this analysis together with the optimum bending moment diagram for a 100kN central concentrated load applied to the beam. The maximum moment in this analysis was 114kNm at the mid-span, which represents a 23.3% reduction in the un-strengthened beam bending moment. The optimum bending moment diagram for this loading would have a maximum bending moment of 50kNm, as shown in the said figure, which is a 66% reduction in moment, compared to the un-strengthened case. In order to achieve the optimum bending moment diagram it would be necessary to apply 100kNm counter moments. The laboratory conditions limited the amount of counter moment that could be applied to 36kNm. This limitation is imposed because of the available tendon size (and, thus, capacity), as well as the inherent tendon eccentricity.

The results of this analysis indicated that while the bending moment is reduced, the resulting maximum stress is just below the maximum stress in the un-strengthened case (0.6MPa). This is due to the tendon force producing a relatively small counter moment, which resulted in a counter-moment stress component (beneficial component) being greater than the axial component (un-beneficial component) by only 0.6MPa. The resulting tendon force increase was within 0.2% difference of that predicted using equation 3.18 for r_t.

The maximum deflection was 7.6mm at the mid-span of the beam. Hand calculations had predicted a mid-span deflection of 9.7mm with 100kN central concentrated load applied

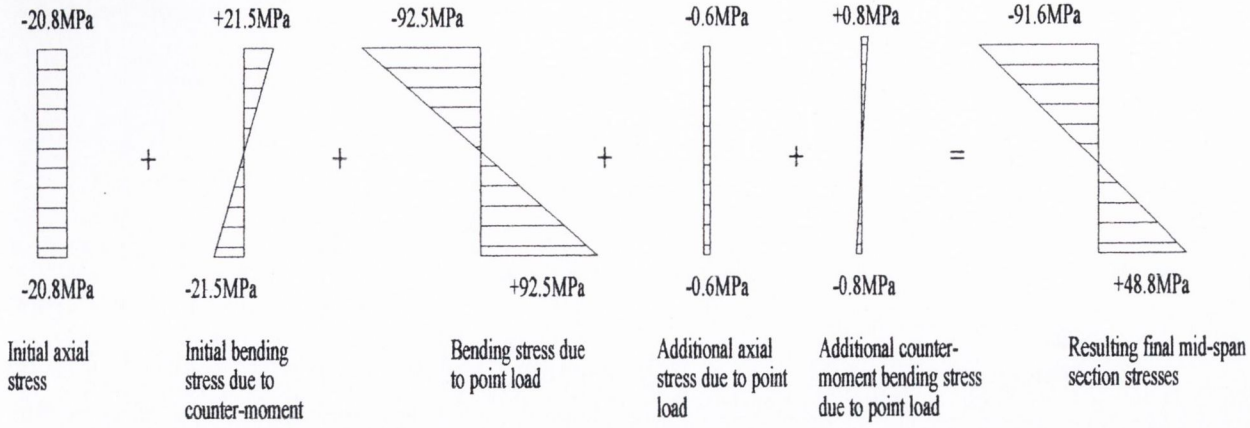

Figure 5.6: The mid-span section stresses with a 100kN central concentrated load and the tendons actively engaged

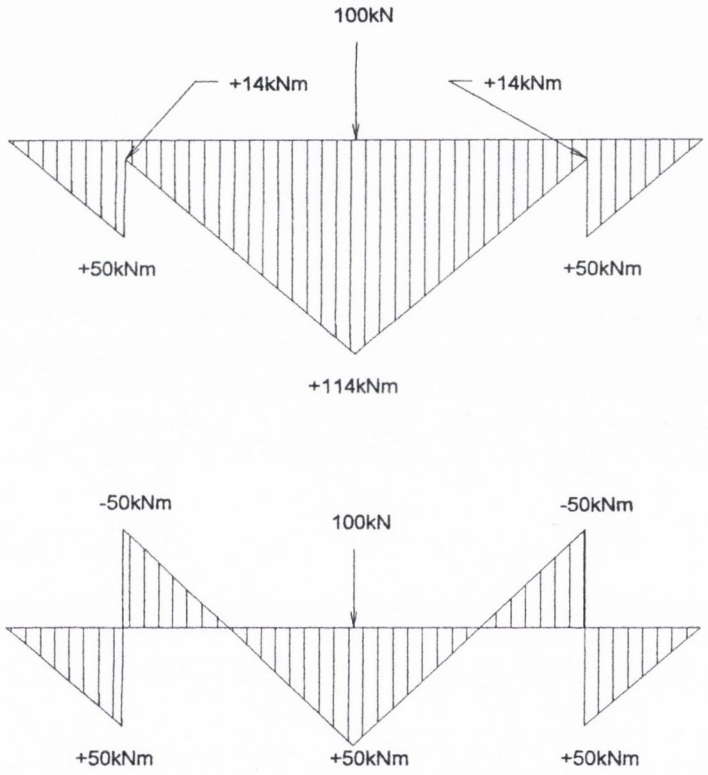

Figure 5.7: The bending moment diagram for a 100kN central concentrated load with 36kNm counter moments applied, together with the optimum bending moment diagram for the same loading.

to the un-strengthened beam. The reduction in this case was relatively poor and yielded a 21.6% reduction compared to the un-strengthened case.

5.4.3 Active analysis with a 200kN load applied

The analysis in this case had the same fixed tendon force as in the previous case with a 200kN central concentrated load applied. Based on the predictions of the passive test with a 200kN load applied, a pre-loaded tendon force of 338kN was required (that is, 360kN-22kN), which was 93.8% of the required post-loaded tendon force. Again, in this case a high proportion of the final tendon force had to be applied prior to loading, however it was slightly less than in the previous case as more self-counter moment was being employed due to the greater loading. Pre-loaded analyses established the initial strain required for the tendons.

The results of this analysis compared well to the predictions with the passive analysis. A post-loaded axial beam force of 360.1kN arose which represented an increase of 22.1kN and also indicated that the tendon force increase with respect to load application was linear up to this loading. Again, as in the previous analysis, this analysis indicated that a linear relationship was present irrespective of the loading, provided the loading induced stresses in the beam and tendons were within the elastic range.

The maximum resulting stresses were at mid-span and were –184.7Mpa (compressive) in the upper flange and +141.9MPa (tensile) in the lower flange (figure 5.8). Figure 5.9 shows the resulting bending moment diagram together with the optimum bending moment diagram for this case. The maximum moment in this analysis was 264.8kNm at the mid-span, which represents an 11.8% reduction in the un-strengthened beam bending moment. The optimum bending moment diagram for this loading would have a maximum bending moment of 100kNm, as shown in figure 5.9, which is a 66% reduction in bending moment compared to the un-strengthened case. In order to achieve the optimum bending moment diagram it would be necessary to apply 200kNm counter moments. The limitations outlined in the previous case with regard to tendon capacity and limited eccentricity also apply in this case.

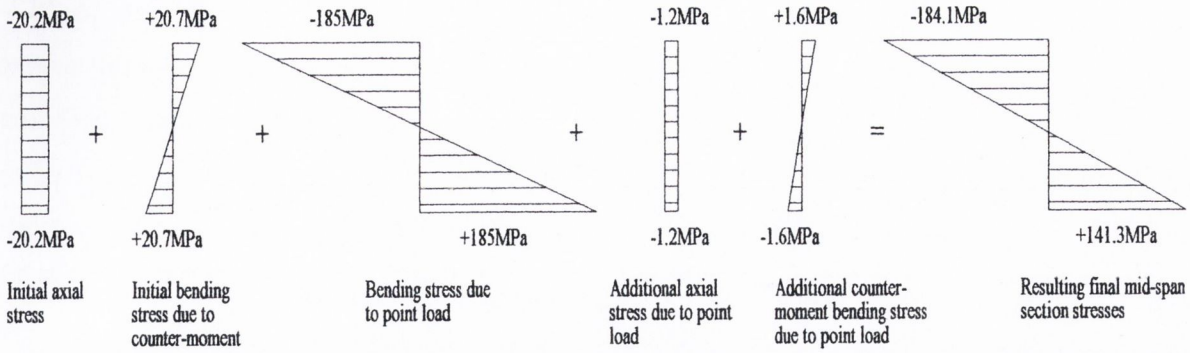

Figure 5.8: The Mid-span section stresses with a 200kN central concentrated load and tendons actively engaged.

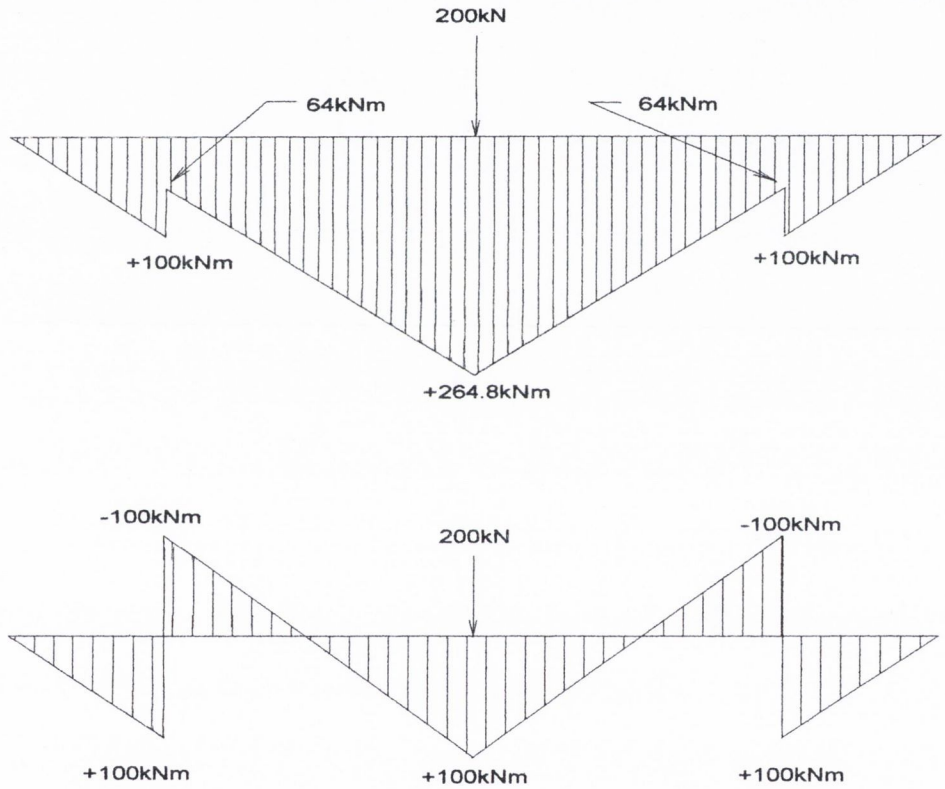

Figure 5.9: Bending moment diagram for 200kN central concentrated load with 35.2kNm counter moments applied together with the optimum bending moment diagram for the same loading.

The predictions of this analysis indicated that, again very little improvement could be achieved as the axial component stress was slightly lower than the beneficial counter moment stress component (that is, a benefit of 0.9MPa). The slightly greater difference in improvement, when compared to the previous case, is due to the greater load which allows greater self counter-moment to be induced. Again, as in the previous analysis, the predicted tendon force increase due to load application compared favourably with the calculated value using equation 3.18 (within 0.1%).

The maximum deflection was 18.6mm at the mid-span of the beam. FE Analyses of the un-strengthened beam predicted a mid-span deflection of 19.4 mm. The pre-loaded beam had a maximum mid-span pre-camber of 2.1mm.

5.5 Full capacity analysis of beam

The previous analyses have assumed a limitation in tendon size for practical reasons. Now consider the analyses where no such restriction exists.

Owing to symmetry of the tendon configuration and having investigated local stresses at the counter-moment locations, a single 2-D analysis was considered sufficient to predict the response of the beam under maximum loading. The resulting load would be compared to that of the original un-strengthened beam to examine the efficiency of the beam if counter moments were to be introduced. It must be borne in mind that the objective is to achieve at least the same load capacity (that is, 200kN) as that of the original beam with a minimum overall depth. Using equations 3.14 and 3.20 derived in consideration of the criteria for beam improvement to calculate P_i and W, respectively, the initial force and peak load that can subsequently be applied were found to be 1525kN and 203.5kN respectively.

A FE analysis was carried out with this pre-load tendon force and central concentrated load and resulting maximum mid-span stresses are shown in figure 5.10 together with the

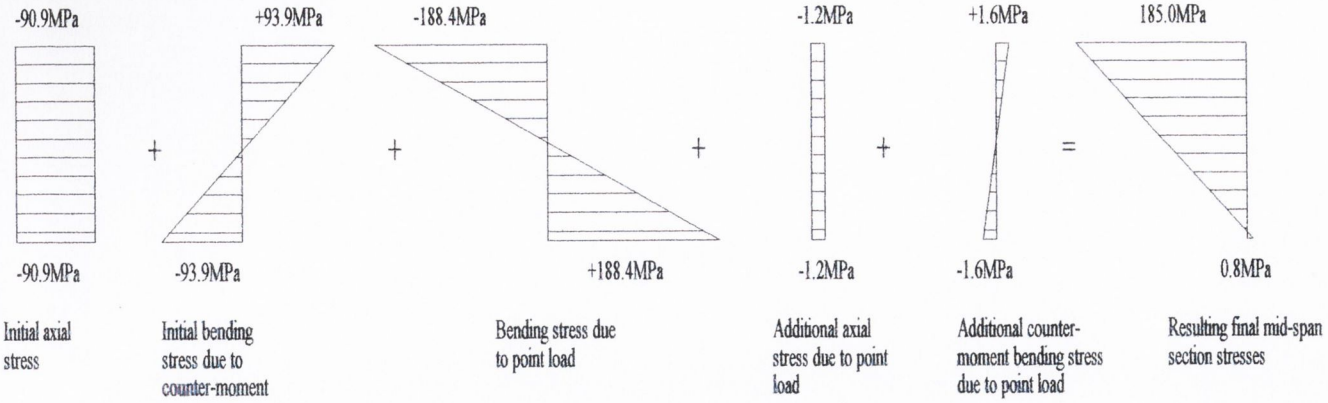

Figure 5.10: Figure shows the mid-span section stresses with maximum central concentrated load applied and the tendons actively engaged.

component stresses. The maximum resulting bending moment was at the mid-span section and was +145.3kNm (sagging). This moment represented a 49.7% reduction when compared to the un-strengthened case.

The maximum deflection was 13.8mm downward at the mid-span and represents a 26% reduction in deflection compared to that of the un-strengthened beam with the same central concentrated load (which was 19.1mm, in excess of a limiting criteria of span/360, that is, 16.4mm).

The analysis showed that the deflection was now within the required limit of span/360. Figure 5.11 shows the beam stress contours with a 203.5kN central concentrated load applied and a final counter moment of 154.7kNm applied under an axial beam force of 1547kN. It can be seen that there is a concentration of compressive stress in the upper flange of the mid-span section which is due to the axial tendon force and maximum compressive bending stress due to loading.

The improvement in the load capacity with the strengthened beam, with respect to central concentrated load capacity, was low (1.75%) because, as discussed earlier in this chapter, the tendon configuration did not produce as high a magnitude of counter-moment as was originally planned. However, the maximum serviceability limit state load of 173.9kNm

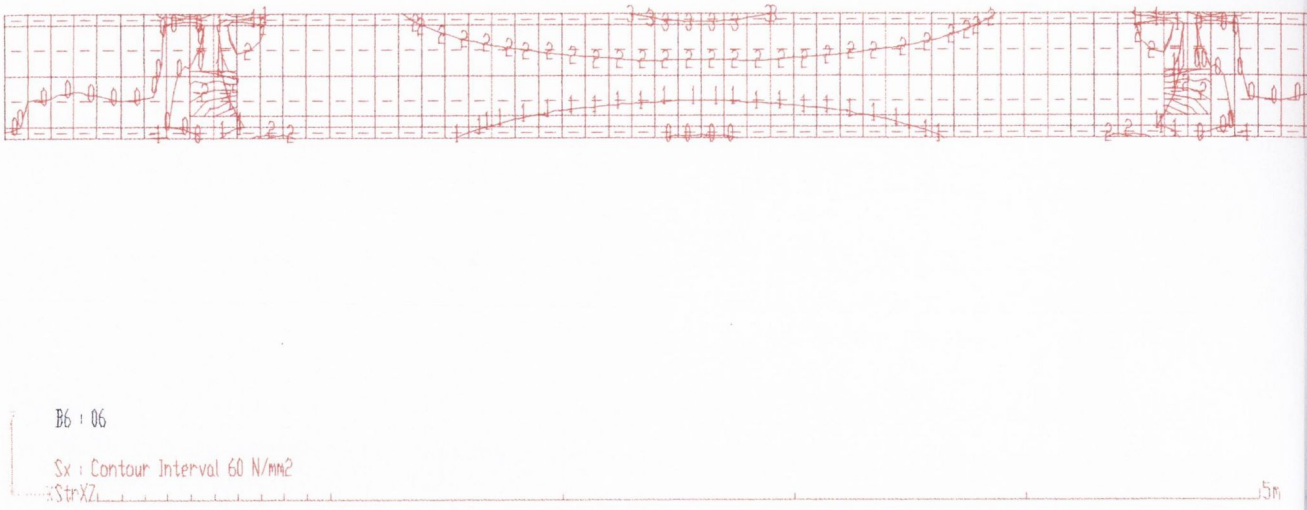

Figure 5.11: The stress contours of the modelled test beam with maximum loading for the tendon configuration between the upper and lower flange.

is somewhat lower than the strengthened beam load of 203.5kN which, in this regard, represents a 14.4% increase in capacity.

With the calculated P_i and W applied to the beam the resulting tendon force increase compared favourably with the value predicted using equation 3.18, and, as in the previous cases, was within a 1% difference.

5.6 Analyses of effective tendon eccentricity

The results of these analyses demonstrated that the effective tendon eccentricity was 98.0mm. The neutral axis of the section at the point of application of the counter moment shifts up from 138.1mm to 164.3mm (measuring from the bottom face of the lower flange) due to the addition of stiffening plates attached to the upper flange as shown earlier in figure 5.1. Given that the centre of each tendon is located 65.4mm (25.4mm lower flange thickness plus 15mm clearance plus half the 50mm diameter thick wall tube) from the lower face of the bottom flange, the difference between the two dimensions is very close to the predicted effective tendon eccentricity (that is, 98.9mm against 98.0mm predicted).

Further trial FE analyses were carried out to examine whether there was a benefit of extending tendon levers from the underside of the upper flange to as low as possible to the upper face of the lower flange to maximise eccentricity, or, whether this tendon lever configuration resulted in a net eccentricity that was the distance from the centre of the tendon to the beam's section neutral axis irrespective of how the tendon is attached to the beam. Two tendon configurations were considered, the first being the tendon configuration as in the previous analysis and the second was a similar beam with tendons attached directly to the web at the same eccentricity as the first. The results of the analyses are discussed in the following two sections.

5.6.1 Tendon eccentricity analysis of existing horizontal tendon configuration

The first tendon configuration analysed for was a tendon lever and horizontal tendon configuration, as in the previous analyses, with a 1200kN tendon force applied to the un-loaded beam. The analysis yielded mid-span section stresses of –144.0MPa (compressive) and 1.2MPa (tensile) in the lower and upper flanges respectively. Figure 5.12 shows the mid-span component section stresses together with the final section stresses. The maximum stress at the location of the tendon levers was –143.3MPa and occurred in the upper flange. The maximum web stress at the tendon lever location was 110.4MPa. Figure 5.13 shows the resulting stress contours together with the deflected shape of the beam. The maximum pre-camber was 2.7mm and occurred at the mid-span.

The resulting applied counter moment was calculated from the section stresses as 117.6kNm as expected (that is, 1200kN tendon force by 0.098m tendon eccentricity).

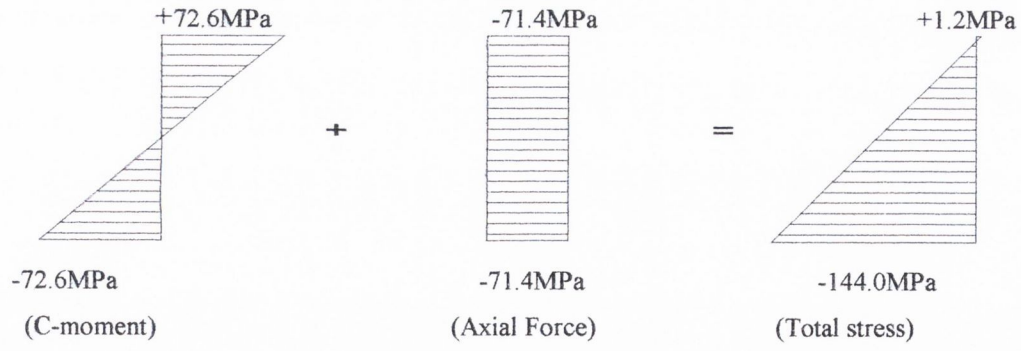

Figure 5.12: Mid-span section stresses with 1200kN tendon force and no loading

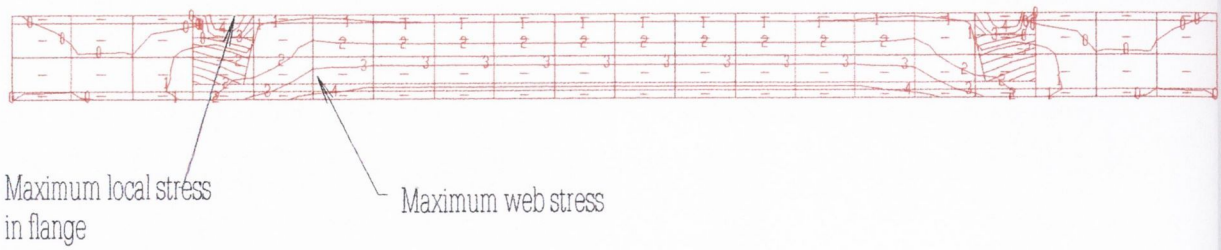

Stress contours = 40N/mm^2

Stress contours

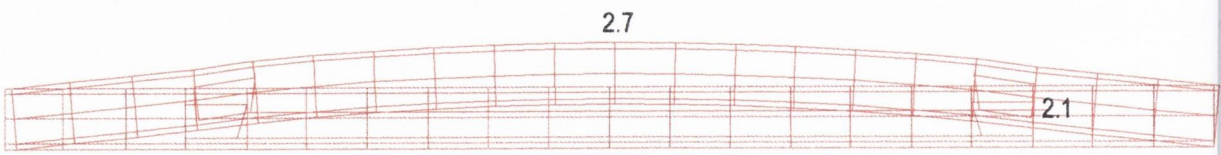

Deflected shape

Figure 5.13: Stress contours and deflected shape of the beam with a 1200kN tendon force and no loading.

5.6.2 Tendon eccentricity analysis of beam with tendons attached directly to the web

A similar beam was analysed with tendons directly attached to the web such that their eccentricity was 98mm with a tendon force of 1200kN and no loading. An initial analysis yielded a maximum local web stress, where the tendons were attached to the web, of 277.2MPa which exceeds the maximum web stress in the previous analysis and also exceeds the local maximum stresses for the tendon and lever configuration with and without local stiffening. Figure 5.14 shows the location of the maximum web stress.

The mid-span pre-camber also compared closely to the previous case and was 2.65mm. The beam stress contours together with the deflected shape are shown in figure 5.15 and

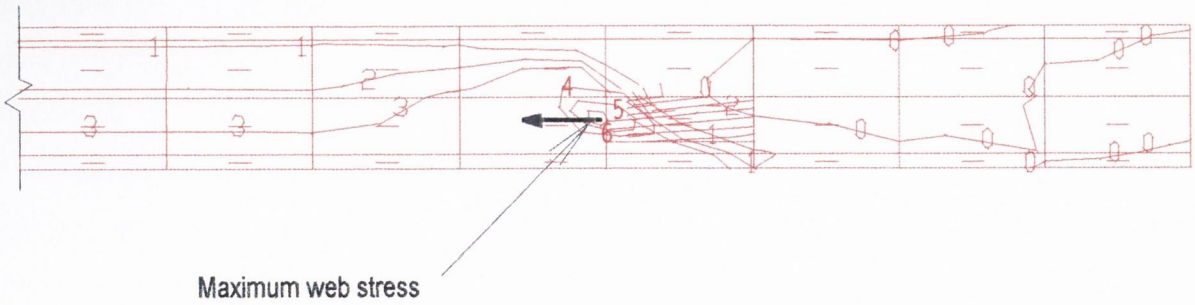

Figure 5.14: Local web stress with tendons attached directly to the beam web and no stiffening plates.

compared closely with figure 5.13 for the first arrangement. The principal difference is the distribution of the stresses at the location where the tendons are attached to the beam.

These mid-span stresses confirmed that the tendon and lever configuration had the same net effect as attaching the levers directly to the web with the same eccentricity. A tendon force of 1200kN yielded almost the same counter moment and pre-camber for both cases considered. The analyses predicted that the benefit of employing tendon levers is to directly impart moment to the flanges and, therefore, the web will not have to withstand excessively high local stresses to deliver moment to the flanges.

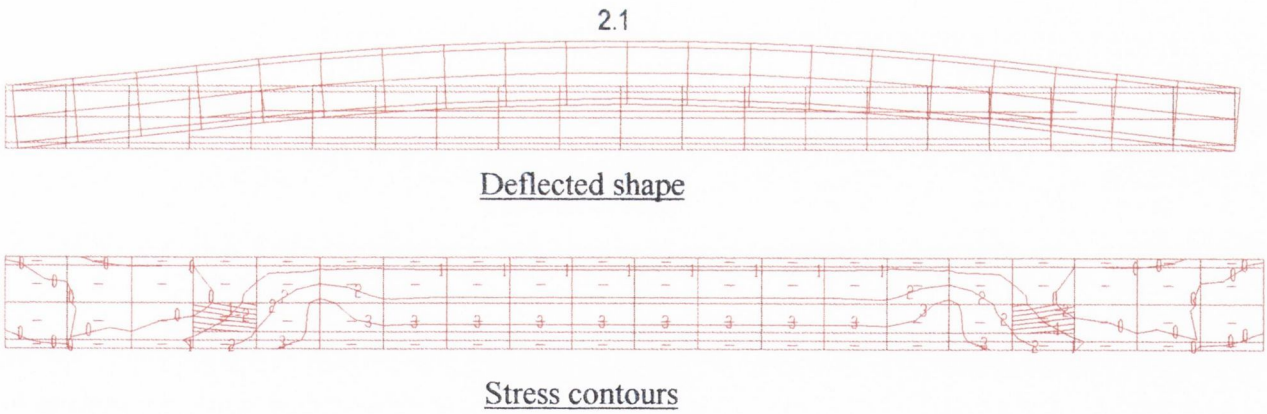

Figure 5.15: Stress contours and deflected shape of beam with tendons directly attached to the beam web.

In both cases, it should be noted that, owing to the low tendon eccentricity, the additional axial force that must be applied and, thus, the additional axial stresses, to reduce the maximum moment (via the counter moments) engages a large proportion of the beams' stress capacity. This effective reduction in stress capacity regulates the benefit of reduction in bending stress due to counter moment. It is for this reason that a 49.7% reduction in maximum bending moment will only provide a small increase in load capacity (1.75%) and, also, prevents the optimum counter moments of 200kNm and, thus, the optimum bending moment from being achieved. The next section examines a revised tendon configuration designed to overcome the deficiency.

5.7 Analysis of the beam with a lower horizontal tendon configuration

It was found with the horizontal tendon configuration previously analysed, that there was little improvement in the central concentrated load that the un-strengthened beam could carry compared to that of the strengthened beam. The tendons, located just above the upper face of the lower flange, required over 95% of the tendon force needed for the development of the final counter moments to be applied as initial pre-loaded tendon force. The remaining 5% of the tendon force was induced by the central concentrated load application (that is, in self-counter moment). As discussed in chapter 4, the tendon eccentricity of 98mm was just above the value required to give beam improvement (that is, Z/A=96.2mm). This accounts for the low improvement in capacity of the beam analysed to date.

A new tendon configuration was considered, while still bearing in mind the constraint of keeping the overall beam depth to a minimum. The new configuration was adopted, where thick-wall tendon tubes were attached to the underside of the lower flange of the beam. The tubes were located at the optimum locations for counter moment application with respect to the longitudinal axis of the beam (1m in from each support - see figure 5.16 and figure 5.17). Placing the tendon thick-wall tubes on the underside of the lower flange meant that:

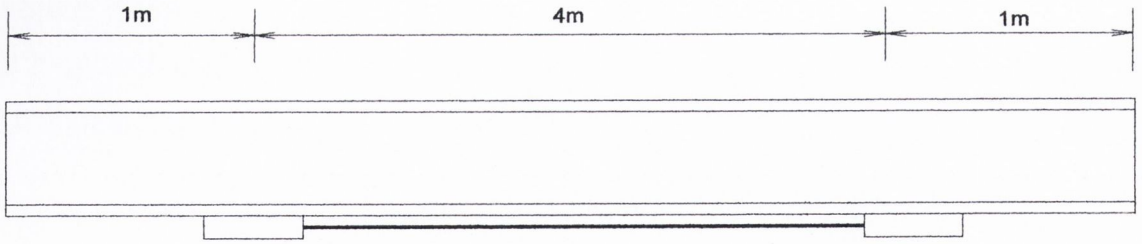

Figure 5.16: The revised tendon configuration with the thick-wall tubes and tendons placed on the lower face of the lower flange.

- The loss of tendon eccentricity, in the previous configuration, due to the allowance of clearance between the thick-wall tube attached to the tendon lever and upper face of the lower flange (that is, 15mm), could be gained with the new tendon configuration, as no such clearance was necessary.

- Placing the tendons on the lower face of the lower flange gained an additional 25.4mm, the lower flange thickness.

- The tendons centred on the 60mm diameter thick wall tube, adding a further 30mm to the tendon eccentricity.

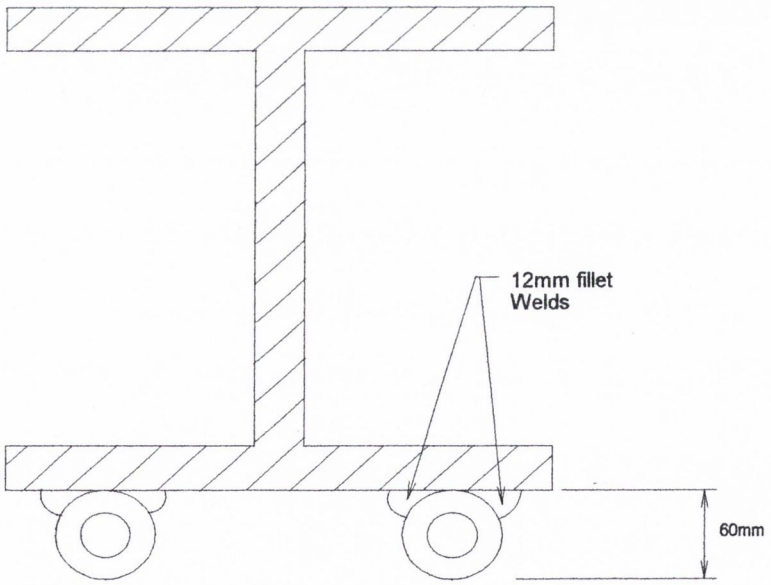

Figure 5.17: Cross-sectional view of the tendon thick-wall tubes welded to the underside of the lower flange.

With this new tendon configuration, a theoretical tendon eccentricity of 170mm could be achieved, resulting in an overall beam depth of 335mm (that is, the section depth plus the thick-wall tendon tube diameter of 60mm). With the previous tendon configuration, a tendon eccentricity of 98mm resulted from an overall beam depth of 276mm. For an increase of member depth of 60mm an increase of tendon eccentricity of 72mm could be achieved. The previous tendon configuration had a member depth to tendon eccentricity ratio of 2.79 and the new tendon configuration had a ratio of 1.91. The lower the ratio, the more efficient the member.

5.8 Local analysis of thick-wall tubes placed on the underside of the beam lower flange

A 3-D FE analysis was carried out using ANSYS, where the thick-wall tubes are located on the underside of the lower flange, to examine the mechanism of stress distribution when high tensile forces are present in the tendons. The half beam analysis was modelled as in the previous local analysis without local stiffeners. The thick-wall tubes were modelled as 300mm long solid rectangular blocks with an equivalent cross sectional area as the thick-wall tubes, attached to the relevant portion of the beam, with horizontal point loads applied to simulate the tensile tendon forces. The plot in figure 5.18 shows the stress contours of the local beam with, say, 800kN horizontal force (as previously) applied to each of the thick-wall tubes. The resulting maximum local stress in this case was 148.5.MPa in the lower flange at the location of the levers.

It can be seen from figure 5.18 that no excessive distortion results at the location of the counter moments and that no additional stiffener plates are required with the lower horizontal tendon configuration. The mid-span (right support) deflection with the half model was 23.1mm and was close (less than 0.2%) to the value predicted by equation 3.24. Figure 5.19 shows the deflection of the half beam.

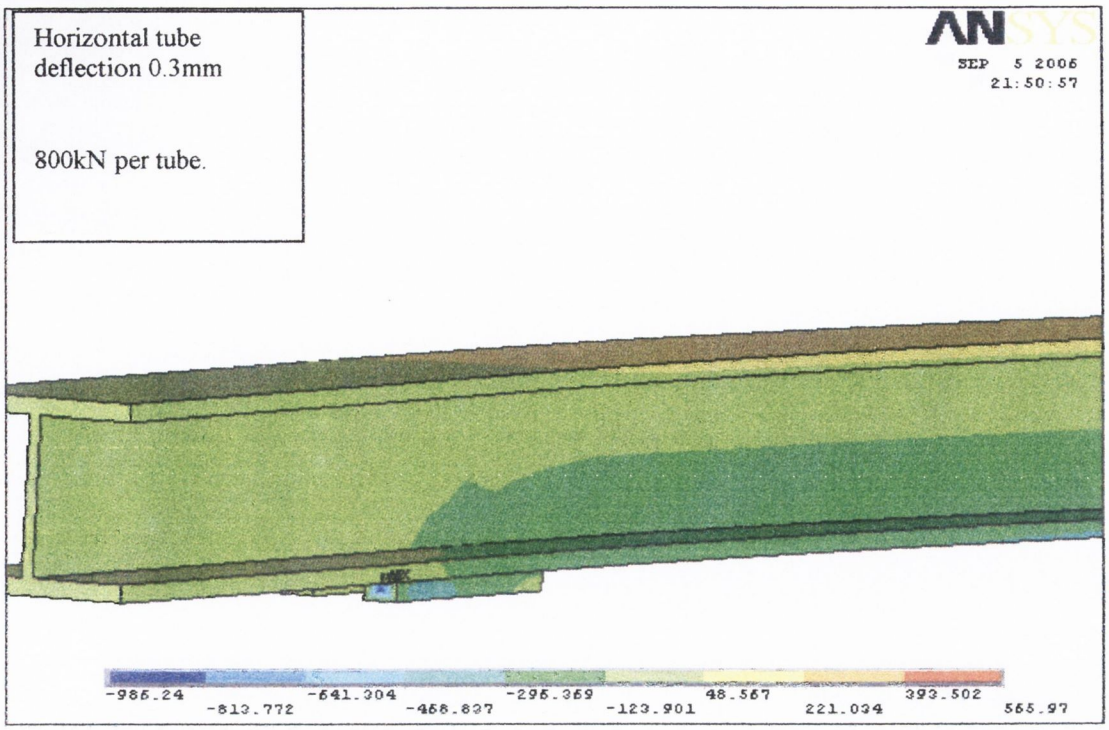

Figure 5.18: Stress contours of half analysis of beam with tendons to underside of lower flange.

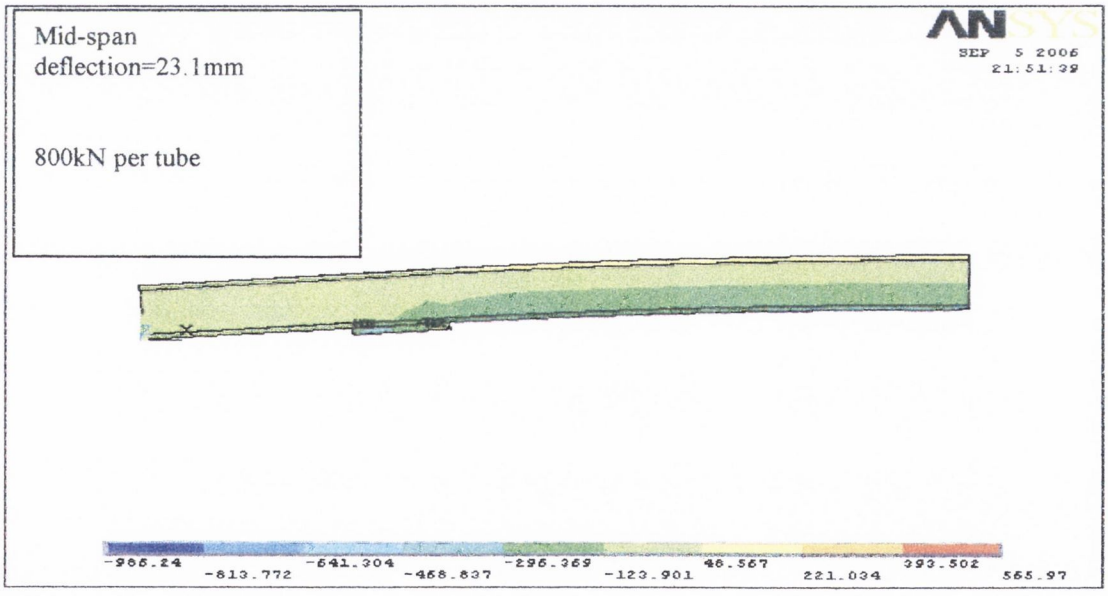

Figure 5.19: Deflected shape of half beam analysis of lower tendon configuration.

The analysis established that, unlike the previous configuration, the new lower tendon configuration required no additional plate stiffening. Figure 5.20 shows the component actions of bending moment and shear force of the earlier tendon lever applied to the upper flange, compared with the action of the current tendon configuration under consideration, which applies a direct shear stress only to the lower flange.

The lower flange can distribute all of the applied force into the beam without the assistance of the upper flange, unlike the previous tendon configuration. This is due mainly to the method of application of the force with the lower tendon configuration. The force is applied by horizontal shearing action along the tube lower flange interface. This transmits mainly direct axial stresses into the lower flange.

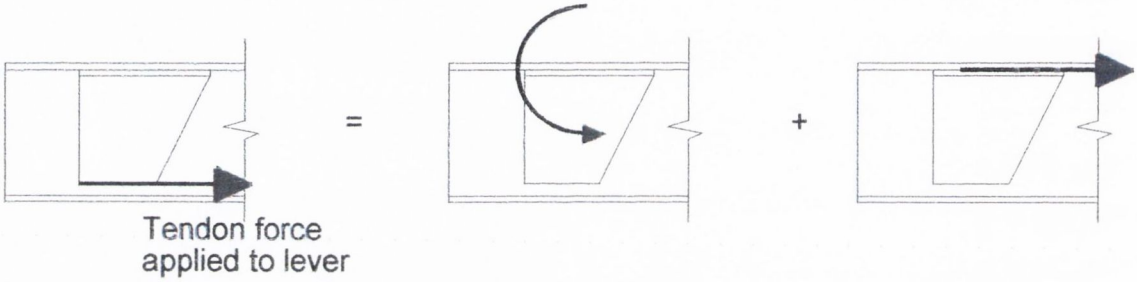

Earlier tendon configuration

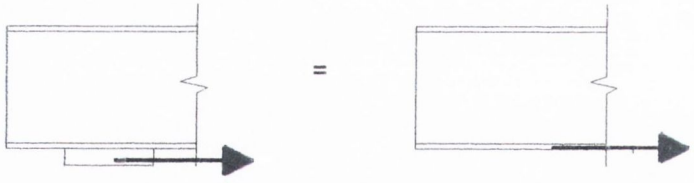

Current tendon configuration under consideration

Figure 5.20: The component actions of the two tendon configurations cons

5.9 Analysis of the lower tendon configuration

With the local analysis of the tendon counter moment application carried out, the test beam with the new tendon configuration was now ready for a global analysis. The 3-D beam was analysed using the ANSYS finite element software package which was also used with the earlier tendon configuration. The beam was modelled with the same tetrahedral elements used earlier. The tendons had the same bar elements that had a provision for the application of an initial strain. This allowed, for the case of active analysis, with pre-tension forces applied to the tendons.

Analyses were carried out on the beam with the new tendon configuration, the results for which were used in a comparison with those of the previous FE analyses. The loading applied in the lower tendon configuration was the same as that of the earlier horizontal tendon configuration. The results of the previous analyses had demonstrated that the relationship between central concentrated load increment and tendon force increase due to that loading was linear. This meant that, provided the beam stresses were kept within the elastic range and the geometry remained linear, tendon force increases could be predicted with reasonable accuracy without resorting to non-linear analysis. With the lower tendon configuration it was necessary to investigate if this also was the case. The analyses carried out on the modelled test beam were as follows:

- Neutral analysis
- Passive analysis
- General active analysis
- Optimum active analysis

5.10 Neutral analysis

This analysis was carried out to investigate whether the introduction of the thick-wall tubes (without tendons) to the underside of the lower flange would have any effect on the overall flexural behaviour of the beam. It was considered likely that the thick-wall tubes would have little, if any, effect based on the results of the earlier neutral beam FE

analysis. A 100kN central concentrated load was applied to the modelled beam and the resulting maximum mid-span section stresses were -92.4MPa (compressive) in the upper flange and +92.4MPa (tensile) in the lower flange. The results of the analysis yielded a maximum deflection of 9.35mm, recorded at the mid-span. As the resulting deflection without the tubes attached was 9.4mm, the difference in deflection was within 1% and was considered negligible.

5.11 Passive analysis

The passive analyses (that is, with tendons passively engaged) served two main functions; firstly, to be used as a comparison with the future laboratory testing and, secondly, to better understand the relationship between tendon force and applied central concentrated load and between tendon force and tendon eccentricity. The passive analyses undertaken were as follows:

- Passive analysis with a 100kN central concentrated load
- Passive analysis with a 200kN central concentrated load
- Tendon eccentricity trial analyses

The purpose of applying two concentrated loads to the beam with the passive analysis was to achieve three points (that is, two results and the origin) on a plot of load versus tendon force increase so that it would be possible to confirm whether or not plot was strictly linear.

Passive analysis with a 100kN central concentrated load

This FE analysis using ENFELA was carried out to model the future laboratory test. A 100kN central concentrated load was applied to the beam with the tendons passively engaged.

The stress component diagrams of the mid-span section of the beam are shown in figure 5.20. In this case, there is zero stress at a distance of 130.1mm from the lower face of the lower flange (that is, 8.1mm below the neutral axis of the UC beam). The maximum stress was –90.3MPa (compressive) in the upper flange and +83.7MPa (tensile) in the lower flange. The resulting maximum deflection was 8.7mm downwards at mid-span. A 100kN central concentrated load in the neutral analysis produces a mid-span deflection of 9.4mm. This indicated that the 54kN (total) tendon force, which arises in this analysis, would produce an upward pre-camber of 0.68mm. The final deflection represents an 8.5% reduction in deflection.

Figure 5.21 shows the plot of the stress contours on the modelled. The sections just to the left and right of the left and right counter-moment locations respectively, have zero stress contours at the mid-height of the beam section. It can also be seen that the portion of the beam between the points of application of the counter-moments has almost symmetrical stress contours with the zero stress contour slightly below the mid-height of the beam section. This downward shift in the stress contours can be attributed to the presence of the axial force in the beam, applied by the tendons, which confirms the presence of the counter-moments. The resulting r_t rate from this analysis was the same as for the calculated value using equation 3.18 and was 0.525kN/kN.

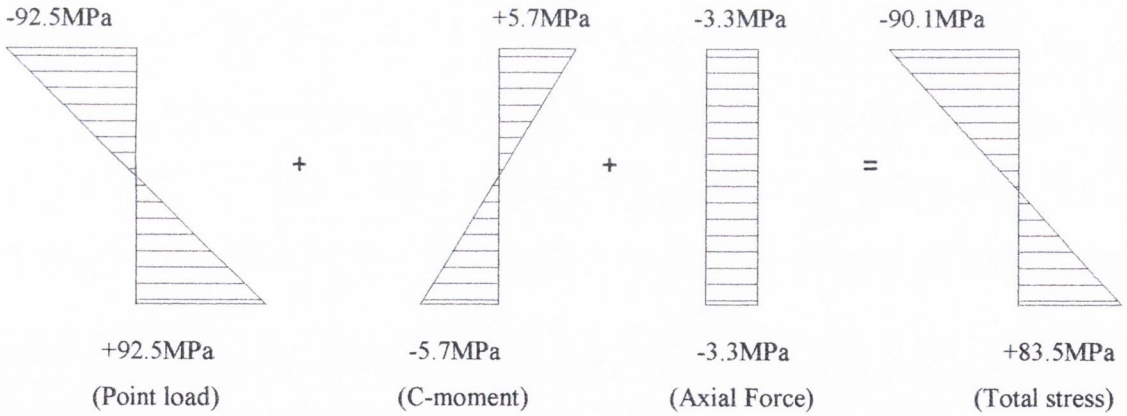

Figure 5.20: The stress component diagrams at the mid span section with a 100kN central concentrated load and the tendons passively engaged.

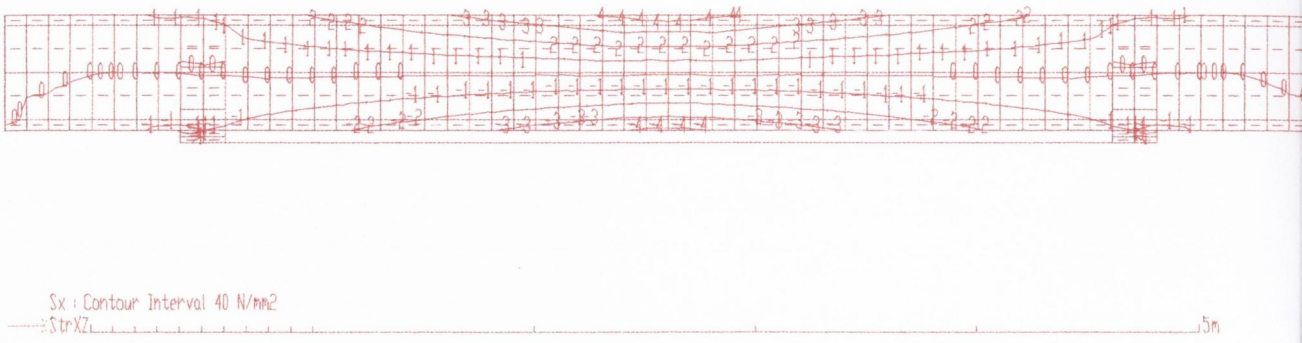

Figure 5.21: The stress contours of the revised beam with a 100kN central concentrated load applied and tendons passively engaged.

Passive analysis with a 200kN central concentrated load

This analysis was carried out to establish the relationship between the central concentrated load and the increase in tendon force. A central concentrated load of 200kN was applied to the modelled beam in which the tendons were fixed to the levers on the underside of the lower flange and were passively engaged. The analysis showed that a force of 108kN developed in the tendon. This result gave the same tendon force increase to unit concentrated load as in the previous analysis, as expected. This ratio is over five times greater than in the previous tendon configuration. The more self-counter moment that can be applied, the greater will be the beam's self regulating capacity and, thus, the greater the overall load bearing capacity.

The total stress diagram at mid-span is shown, together with the component stress diagrams, in figure 5.22. It may be noted that an axial tendon force of 108kN applied a counter moment of 17.9kNm, which resulted in a bending stress of +/- 10.6MPa at the mid-span section and, indeed, throughout the length of beam between the points of application of the counter moments. The corresponding eccentricity is 168mm which compares favourably with the predicted value from geometry of 170mm.

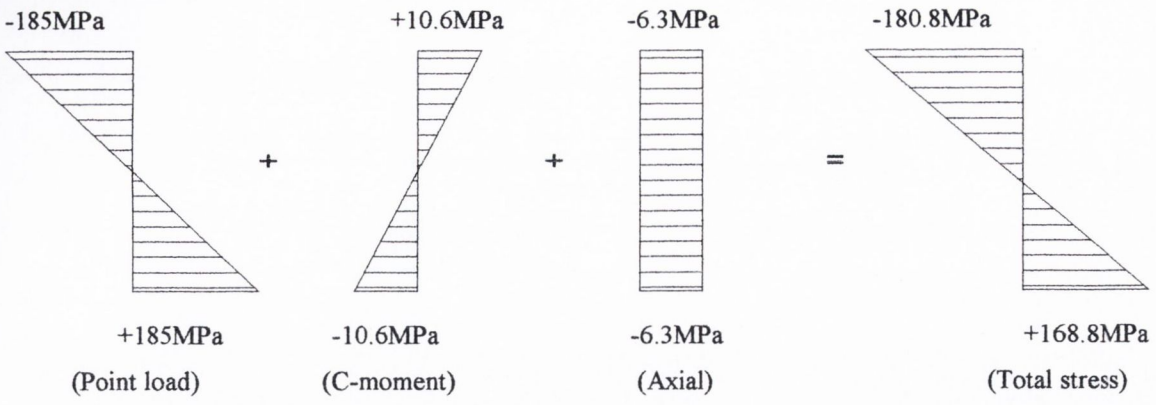

Figure 5.22: Mid-span section stresses of the beam with tendons passively engaged and with a 200kN central concentrated load applied.

The maximum resulting deflection in this analysis was 17.6mm downwards at the mid-span. FE analysis had predicted a deflection of 18.8mm with the un-strengthened beam. This implies that a total tendon force of 108kN would, in the pre-loaded beam, produced an upward camber of 1.2mm. The resulting overall post-loaded beam deflection of 17.6mm was a reduction of 9.8% compared to that of the un-strengthened beam and was due to the presence of the self-counter -moment. The previous configuration had a tendon eccentricity of 98mm, which would produce a pre-camber of 0.24mm with a tendon force of 108kN (that is, the relationship between tendon force and pre-camber is linear for a given eccentricity). Thus, a 70% increase in tendon eccentricity produced almost a 500% increase in pre-camber.

Tendon eccentricity trial analyses

The results of the analysis in the passive test of the beam with the lower tendon configuration yielded a total tendon force increase of 108kN under a 200kN applied load. A series of trial analyses were carried out to better understand how the tendon force changes with respect to a change in tendon eccentricity (see figure 5.23). Using the modelled beam set up for the passive analysis, the thick-wall tubes were removed and replaced with stiff levers extending down from the lower face of the lower flange. The levers were at the optimum locations along the beam for counter moment application

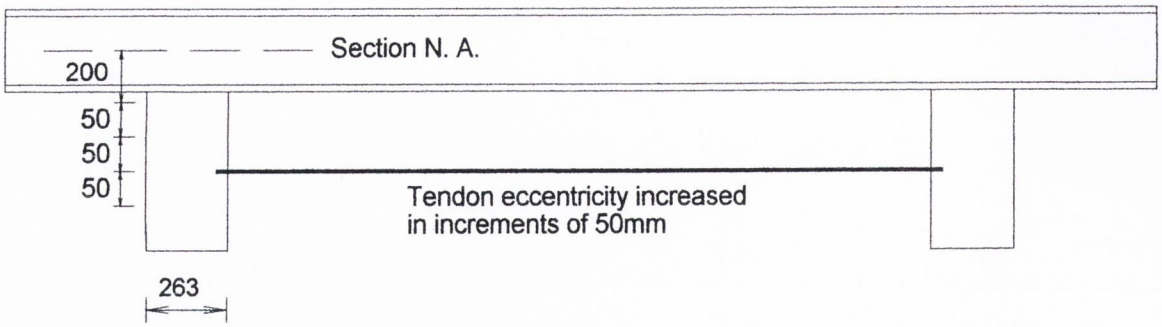

Figure 5.23: Beam and longer tendon levers positions modelled for the tendon eccentricity trial analysis.

(that is, 1m from each support). These longer levers were modelled with a rectangular section and an equivalent section moment of inertia to that of the test beam (that is, 150mm wide by 263mm, deep, giving $I=225.40 \times 10^6 mm^4$). A node or "keypoint" was located on each lever at a distance of 62mm from the soffit of the bottom flange to give a distance of 200mm from the beam section neutral axis. Subsequent keypoints were then also located at 50mm intervals below this first keypoint, on each lever, so that the tendon could be fixed horizontally with varying eccentricity from 0.2m to 1.2m from the beam section neutral axis.

The behaviour in this trial analysis differs from that for the tendon configuration with the thick-wall tubes attached directly to the bottom flange. As the tendon eccentricity increases, a greater counter-moment is applied directly to the beam via the tendon lever (for a given tendon force), as well as the shear force applied to the lower flange. With the bottom flange thick-wall tube tendon configuration, the beneficial section stresses result solely from the shear force applied to the lower flange, via the thick-wall tubes.

The plot in figure 5.24 indicates that the relationship between tendon eccentricity and induced tendon force due to the application of a central concentrated load is not linear. The plot shows that an optimum value of approximately 171.3kN induced tendon force exists at a tendon eccentricity of 0.51m, when a 200kN central concentrated load is applied to the beam with the tendons passively engaged. This optimum exists because as the eccentricity increases, the flexibility of the lever interacts with the developing tendon force.

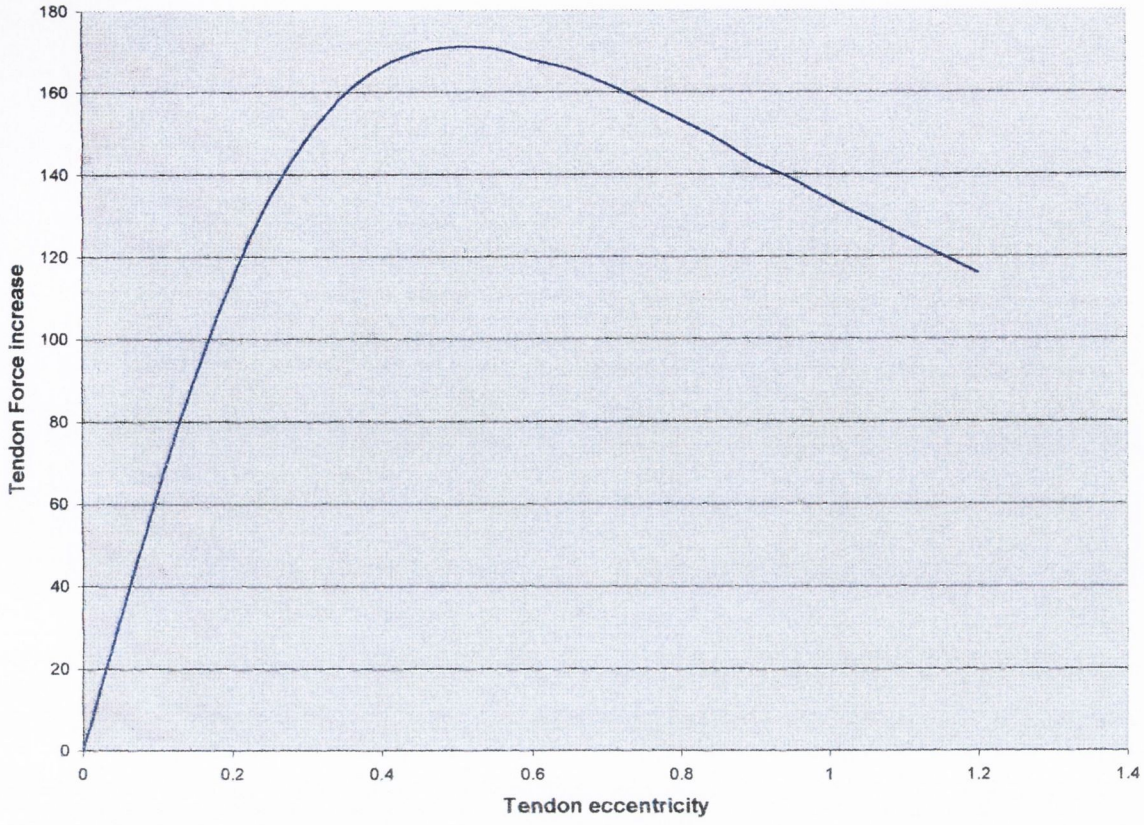

Figure 5.24: The relationship between tendon force increase and tendon eccentricity upon loading in the passive case.

The optimum tendon eccentricity of 0.51m was examined to investigate how the flexibility of the lever itself had an effect on the passive induced tendon force. The section moment of inertia of the down-stand levers was varied, while the length of the levers was kept at the optimum length of 0.51m. A plot of induced tendon force increase due to the application of a 200kN central concentrated load and increasing tendon lever "I" value is presented in figure 5.25. The tendons throughout these analyses were passively engaged and at a constant eccentricity of 0.51m. The plot demonstrates that when the levers are more flexible, the induced tendon force is lower, while a higher lever down-stand I value yields a higher tendon force increase for the same tendon eccentricity.

The results of these analyses helped to better understand the behaviour of the beam in the plot in figure 5.24. As the tendon eccentricity increases, the passive tendon force

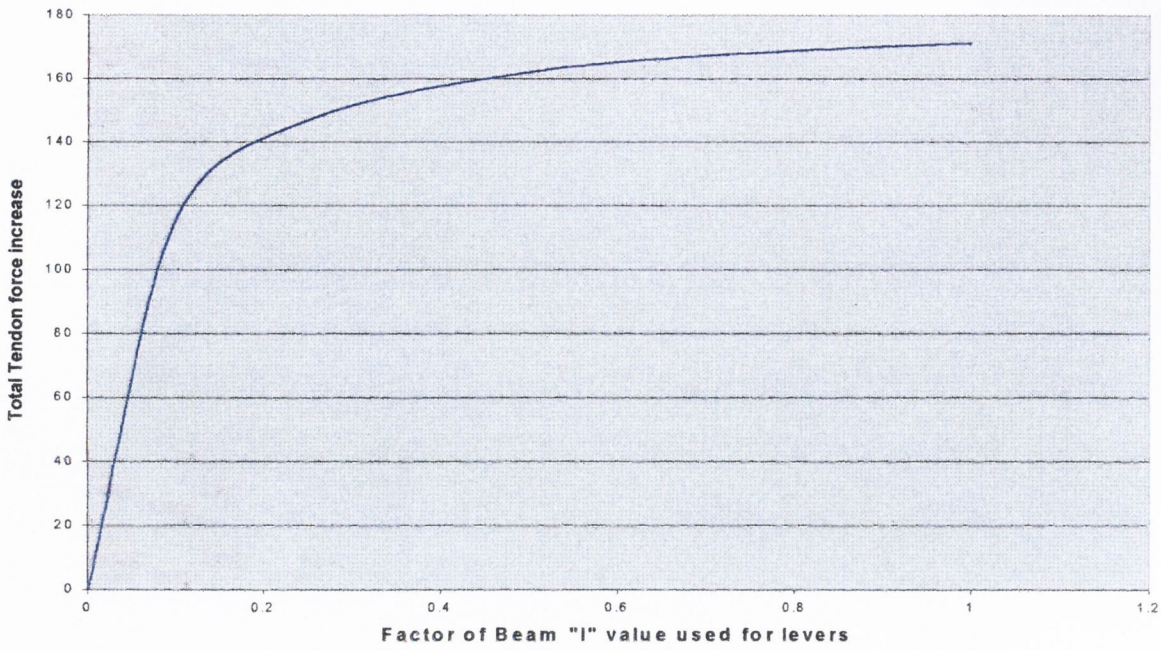

Figure 5.25: The relationship between tendon force increase and tendon lever flexibility with a constant tendon eccentricity of 0.51m from a base "I" value of 225.40×10^6 mm^4.

increases until a point is reached, in this case 0.51m, where further increase in tendon eccentricity is not beneficial. Further increase past this optimum value (for this lever section size) results in an increasing overall member depth with a diminishing beneficial passive tendon force, and thus, a diminishing beneficial self-counter moment application.

As the tendon levers increase in length, they behave more like flexible cantilevers in flexure and less like corbels in shear. The increasing flexibility reduces the overall extension of the passively engaged tendons, thus reducing total tendon force increase with respect to the central concentrated load application. Therefore, the interaction between tendon force and lever flexibility is non-linear one, such that the delivery of counter moment to the beam is not necessarily linear with respect to tendon eccentricity. The response of beam to load is, therefore, geometrically non-linear by virtue of the lever flexibility. The plot in figure 5.25 concurs with Equation 3.18 presented in the parametric study included in Chapter 3.

5.12 Active analysis

These analyses were carried out on the same modelled beam as that in the passive analyses. The active analyses involved pre-tensioning the tendons to a prescribed tendon force such that, on application of a given loading, the final resulting total tendon force would be 360kN (that is, the maximum available pre-tension force for the two 15.7mm diameter super strands used in the laboratory test discussed in chapter 7). The active analyses carried out were as follows;

- Active analysis with no loading
- General active analysis with 100kN and 200kN applied points loads
- Optimum active analysis

Active analysis with no central concentrated load applied

This analysis was carried out to compare with the results from the recorded data in the laboratory testing described in chapter 7. The tendons were pre-stressed in this analysis to the full available tendon capacity (that is, 360kN) in the absence of central concentrated load. Figure 5.26 shows a diagram of total stress at the mid-span section, together with the component stress diagrams.

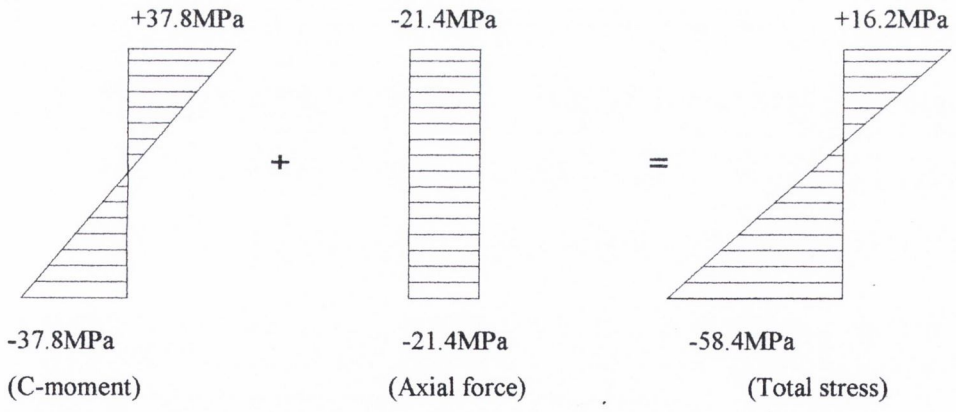

Figure 5.26: Mid-span section stresses with no point load and with a total tendon force of 360kN for the active case.

The lower flange stress with the total stress diagram is greater than the upper flange, as expected, with counter moment applied and without loading present. The analysis yielded a final counter moment of 61.2kNm with a tendon force of 360kN applied to the beam. The maximum deflection was 4.2mm (upwards) at mid-span, which was a positive value of (upward) deflection of 4.2mm. The results of this analysis allowed the tendon eccentricity to be calculated as 170mm (as expected).

Active analysis with a 100kN central concentrated load

With this analysis, the initial pre-tension forces had to be calculated. The passive analysis predicted an increase in the total tendon force of 56kN due to the application of a 100kN central concentrated load. This force was subtracted from the final allowable force of 360kN to yield an initial total tendon force of 304kN.

The results of this analysis gave an applied counter moment of 60.3kNm with a final axial force in the beam of 358.9kN. The maximum resulting stresses in the upper and lower flange at the mid-span section of the beam were –76.2MPa and +33.4MPa respectively.

The final deflection at the mid-span was 5.4.mm. This was the expected downward deflection at mid-span given that a tendon force of 360kN produced an upward pre-camber of 4.2mm and a 100kN central concentrated load applied to the beam with no tendons attached produced a downward mid-span deflection of 9.4mm. This deflection represented a 40% reduction compared to the neutral case.

Active analysis with a 200kN central concentrated load

This analysis was carried out to confirm the assumption made for the passive analysis that there is a linear relationship between the increase in total tendon force and the increase in central concentrated load for a particular tendon eccentricity. This analysis was carried out with a central concentrated load of 200kN applied to the beam. The

tendon force, prior to loading, was 250kN, based on the earlier observation about r_t. The analysis yielded a final tendon force of 360kN with a central concentrated load of 200kN applied. The tendon force increase under loading was 110kN. The maximum resulting stresses in the upper and lower flange at mid-span were –168.6.MPa and +125.8MPa respectively as shown in figure 5.27. The mid-span stresses in the passive analysis, with a 200kN load applied, were –180.8MPa in the upper flange and +168MPa in the lower flange. This implies that applying the tendon force of 360kN has provided an additional bending stress capacity of +/-10.4MPa at the critical mid-span section.

The downward mid-span deflection was 14.5mm which demonstrated again that the deflection can be calculated as the algebraic difference between the upward pre-camber arising from the final post-loaded total tendon force, and the downward deflection due to the application of a central concentrated load. For this tendon configuration, a 360kN tendon force produces an upward pre-camber of 4.2mm and a 200kN central concentrated load without tendons attached to the levers produces a downward deflection of 18.7mm, thus yielding a predicted mid-span deflection of 14.6mm, which is within 1% of the above deflection for this analysis.

The maximum mid-span stress of –168.6MPa represents a 9% reduction and the 14.5mm mid-span deflection represents a reduction of 22.5% in the un-strengthened beam maximum stress and deflection respectively under a 200kN central concentrated load.

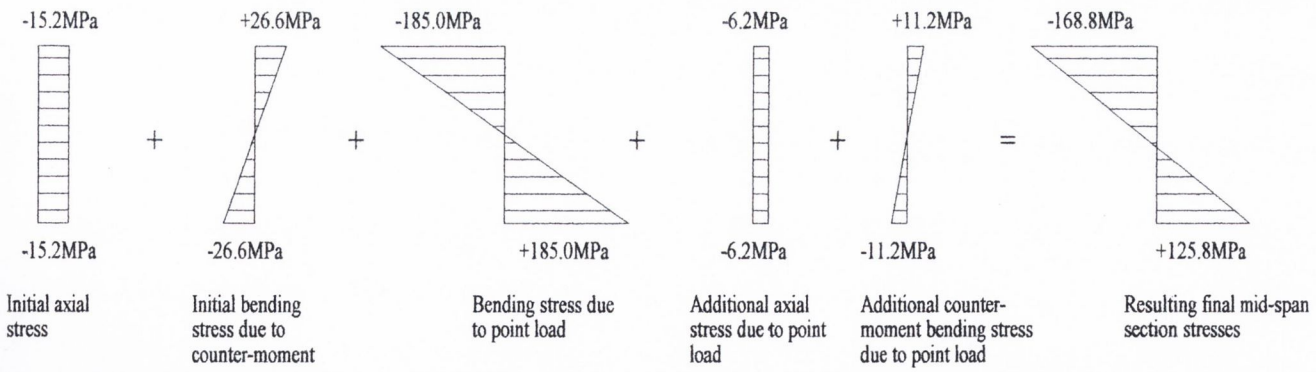

Figure 5.27: Mid-span section stresses with active tendons and a 200kN central concentrated load.

The resulting applied counter moment, calculated from the mid-span section stresses, was 61.3kNm from which the eccentricity of 170mm was calculated (that is, counter moment divided by axial force).

The increase in tendon eccentricity yields a substantially higher ratio of induced tendon force to load (r_t = 0.525kN/kN) than in the previous within-flanges tendon configuration. This implies that greater counter moment can be applied at the pre-loaded stage and greater self- counter moment will result under loading, thus, improving overall beam load bearing capacity. With all the active analyses, the predicted r_t rate was exactly the same as the value calculated using equation 3.18. These calculations, therefore, provide independent confirmation of the accuracy of that equation.

5.13 Beam linear analysis with imposed limiting stress

Further analysis was carried out to establish the theoretical maximum load the modelled beam could withstand with the revised lower tendon configuration. In applying the theoretical maximum load it was assumed that an adequate number of tendons were attached to the beam to apply the full capacity counter-moment (that is, that the constraint of the two 15.9mm diameter tendons no longer existed). For the laboratory testing phase of this research, the tendon force (360kN) and the central concentrated load (200kN) were limited for the purposes of re-testing (that is, tested within the elastic range) and safety. An assumed maximum allowable stress of +/-185MPa was used in this analysis.

A maximum pre-loaded counter moment was calculated such that the resulting maximum stress in the lower flange, in the portion of the beam between the application of the counter moments, was –185MPa. The pre-loaded counter moment was calculated as 191kNm with a pre-loaded tendon force, P_i , of 1125kN. A central concentrated load of 261kN can be applied to deliver peak stresses on loading, as calculated using the equations for beam improvement derived in chapter 3. The analysis yielded a final beam axial force of 1256.6kN with an applied counter moment of 213.3kNm.

The subsequent application of this 261kN central concentrated load indeed yielded a maximum stress of –185MPa in the upper flange of the mid-span beam section. The lower flange maximum stress at the same section was +34.8MPa. Figure 5.28 shows the total mid-span total section stresses together with the component section stresses. It was noted that, with the above configuration, a stress of +/-241.7MPa would result for the un-strengthened beam if the 261kN central concentrated load were applied.

The beam in this analysis yielded an improvement in capacity of 32.5% with a maximum applied counter-moment of 213.3kNm. The un-strengthened beam, when stressed to +/-185MPa, can carry a central concentrated load of 200kN, however, the mid-span deflection will be 28mm and in excess of the limiting criteria of span/360 (that is, 16.7mm). The central concentrated load that will yield the maximum allowable deflection of 16.7mm is 175kN, which yields the stated percentage improvement.

Figure 5.29 shows the resulting bending moment diagram of the beam with the lower tendon arrangement and a central concentrated load of 261kN applied. The final moment at the mid-span was 178.6kNm (sagging) with the final axial beam force of 1256.6kN. Figure 5.30 shows the stress contours of the beam in which it can be seen that the stress distribution at the tendon anchor points is less concentrated than with the previous tendon configuration and the counter-moment is applied over a wider region, thus, removing the need for stiffening and as demonstrated by the local analyses of the earlier

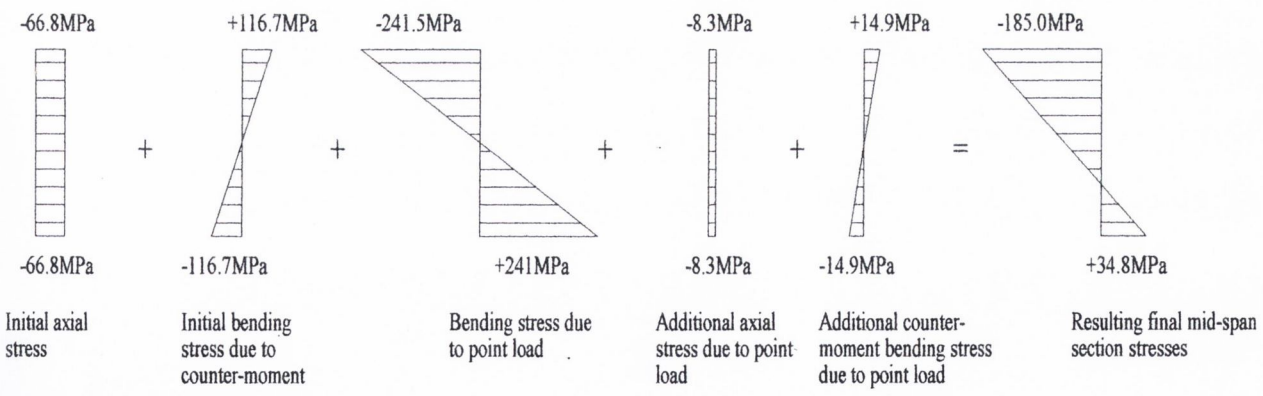

Figure 5.28: Figure showing the mid-span stresses of the beam with a 1256kN total tendon force applied and a central concentrated load of 261kN.

configuration in chapter 4 (see figure 4.3) and by the local analysis in this chapter (see figure 5.18).

The maximum deflection in this case was a downward deflection at mid-span of 9.8mm. This defection was expected and demonstrated that the relationship between applied tendon force and upward pre-camber was linear and that the relationship between applied central concentrated load and downward deflection (with a tendon force applied) was linear. The upward mid-span pre-camber (under the applied 1256kN tendon force) was 14.7mm and is 3.5 times greater than the 4.2mm, which was the upward deflection with a 360kN total tendon force. Similarly, for the downward mid-span deflection, the same proportional relationship existed.

The final mid-span deflection represented a 24% reduction when compared to the un-strengthened beam. This revised tendon configuration has allowed a load capacity improvement of 30.5% for a relatively low increase in overall beam depth (50mm). The improved capacity and deflection reduction implies that this method of strengthening has good potential for retrofitted strengthening methods or for section size reduction in new construction.

The analyses of the first configuration demonstrated that the concept was valid. However, owing to the low tendon eccentricity, relatively larger tendon forces are required to apply counter-moments and, as a consequence, flexural capacity is reduced.

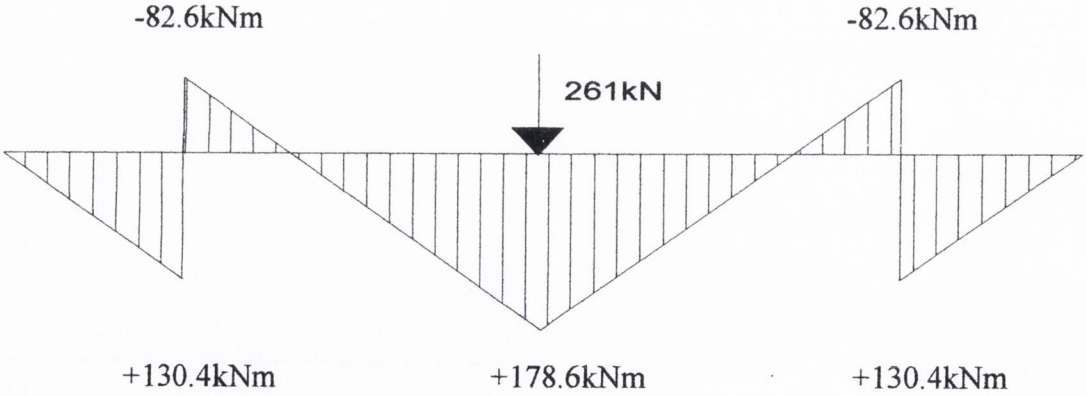

Figure 5.29: Final bending moment diagram resulting from the full capacity analysis with the maximum 261kN load applied.

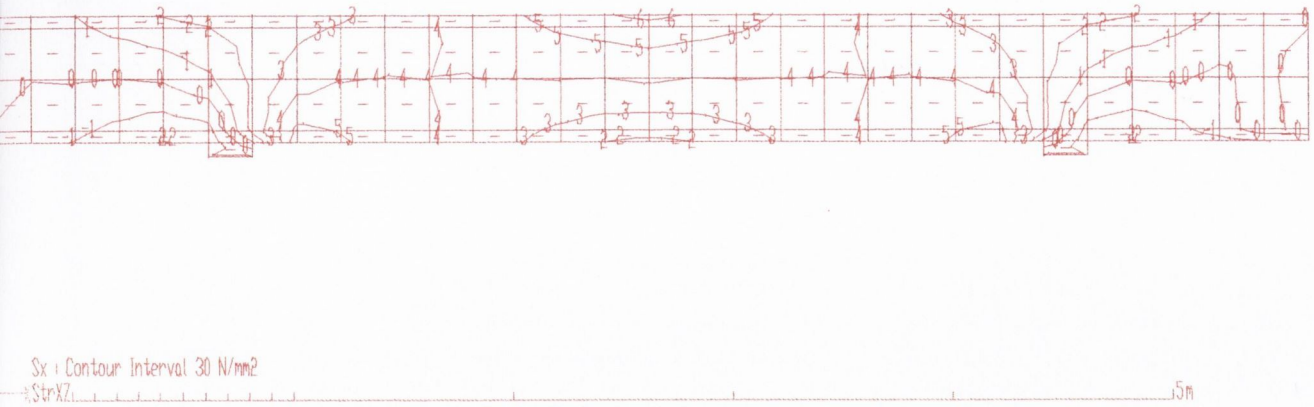

Figure 5.30: Stress contours with a 261kN central concentrated load and with a tendon force of 1256kN applied in the full capacity analysis. (Multiply contour factors by 30MPa).

With the second configuration, a greater eccentricity resulted in a more efficient system where more counter-moment can be applied per unit tendon force. This implies that lower tendon forces are required, and, thus, greater flexural capacity is available.

5.14 Conclusions

A tendon eccentricity of 98mm was predicted from an FE analysis of the first horizontal tendon and lever configuration. An analysis with the tendons attached directly to the web of the beam with the above eccentricity, yielded almost the same counter moment (within 1% difference) and pre-camber (within 2% difference) as the tendon and lever configuration. The local web stress, however, with the tendons attached directly to the beam were far greater than in the case where the tendon levers were attached to the upper flange. Table 5.1 shows a summary of all the predictions of the FE analyses for the tendon configuration contained within the overall depth of the beam.

Type of analysis	Mid-span deflection (mm)	Mid-span section stresses (N/mm^2)	
All under 200kN load		Top flange	Bottom flange
Hand calculations for un-strengthened beam	19.1	-184.6	184.6
2-D FEA for un-strengthened beam	19.4	-183.6	183.6
3-D FEA for un-strengthened beam	19.4	-184.8	184.8
3-D FEA Beam with lever stiffeners attached only (no tendons)	18.8	-184.8	184.8
3-D FEA Beam with tendons passively engaged and no loading	18.6	-185.2	182.4
3-D FEA Beam with tendons actively engaged and no loading	-0.8	0.6	-43.2
3-D FEA Beam with tendons actively engaged and loading applied	pre-camber -0.8 and post loaded 17.8	-184.7	141.9

Table 5.1: Summary for all analyses under a 200kN load

It was found that the tendon eccentricity was only slightly greater than the minimum for improvement (that is, e>Z/A) for this case and the constraint of not exceeding the overall depth of the beam yielded a poor overall improvement. A revised configuration was considered.

Revised tendon configuration

Further analyses were carried out on a revised configuration whereby the tendons ran under the lower flange and were fixed at the optimum location for counter-moment application with thick-wall tubes. The overall beam depth with this configuration increased by 60mm compared to that of the previous configuration (that is, the outer diameter of the thick-wall tube). For this increase of depth of 60mm an increase in tendon eccentricity was gained from 98 to 170mm. Table 5.2 shows a summary of the analyses for the revised configuration.

Type of Analysis	Load (kN)	Deflection (mm)	Upper flange mid-span section stress (MPa)	Lower flange mid-span section stress (MPa)	Tendon force (kN)
Neutral with thick wall tubes attached	200	18.7	-184.9	184.9	0
Neutral without thick wall tubes attached	200	18.8	-184.8	184.9	0
Passive	100	8.6	-90.3	83.7	54
Passive	200	17.6	-180.8	168.8	108
Active	No Load	-4.2	16.2	-58.4	360
Active	100	5.4	-76.2	33.4	358.9
Active	200	14.5	-170.4	125.8	360
Full elastic capacity analysis	261	9.8	-185	35.4	1256.6

Table 5.2: Summary of the results of FE analyses with thick wall tubes attached to the underside of the lower flange.

Owing to the increase in tendon eccentricity, the improvement in the rate of counter-moment application per unit tendon force (from 0.105kN/kN to 0.525kN/kN) was noted. The self-counter moment performance of the thick-wall tube configuration was therefore improved. Analysis predicted that a 200kN central concentrated load would induce a 110kN tendon force, which would give rise to an 18.7kNm self counter-moment. The previous configuration had a predicted self counter-moment of 2.2kNm with the same loading.

With the revised tendon configuration an improvement in load carrying capacity of 30.5% was predicted when considering ultimate limit state loads and an improvement of 49% was predicted when considering serviceability limit state loads. A reduction in deflection of 24.3% was achieved when compared to the un-strengthened beam.

CHAPTER 6
NON-LINEAR ANALYSES

6.1 Non-linear plastic capacity analysis of beam with the tendon and thick-wall tubes

In order to establish the ultimate strength of the beam and tendon configuration with the thick-wall tubes attached to the beam soffit, a FE plastic analysis using ANSYS was undertaken. The plastic analysis was necessary to establish the interaction between beam and tendons when plastic deformations occurred. The analysis would also allow the typical mode of failure to be examined for steel beams with external tendons.

6.1.1 Modelling

The beam was modelled with the elements described in section 4.9, which are tetrahedral shaped elements that model solid body distortion under loading. The element had nodes with three translational degrees of freedom (dof) as discussed in section 4.8, and had provision for elastic and plastic material properties attributes (plastic yield at 265MPa). The tendons had "beam23" elements that require cross-sectional beam input data. These elements respond as would a beam under loading (that is, three translational dof), and also have provision for elastic and plastic deformation. The tendon steel was modelled with a yield stress of 1300N/mm^2 (BS 3617, 2002). Figure 6.1 shows the stress versus strain model of the beam and tendon modelled steel.

For the configuration considered here, with the elastic analyses, the magnitude of deflections were such that the beam's soffit and tendons did not come into contact. Plastic modelling, however, required that contact be made between the underside of the beam's lower flange and the tendons, due to much greater mid-span deflections post yield. Some difficulty was encountered modelling this contact as no element selected for the tendons could accommodate (axial) plastic deformation, initial strain and with contact elements attached. The problem was overcome by providing "soft links" at mid-span

between the underside of the lower flange and the tendons. The soft links were elements that had a negligible elastic modulus (5MPa) that was sufficiently low to not effect the flexural behaviour of the beam up to a strain of 0.99 (that is, practically, the point were contact is made with the tendon under beam deflection). When a strain of 0.99 was reached a modulus of $200x10^9$GPa was prescribed so that at this point loading rigid contact could be modelled between the beam and tendons. Figure 6.2 shows the idealised stress versus strain plot for the material used with the soft links. Figure 6.3 shows the modelled beam with the tendons just making contact with the beam's lower flange. The clearance between the tendons and the lower flange prior to loading is 22mm.

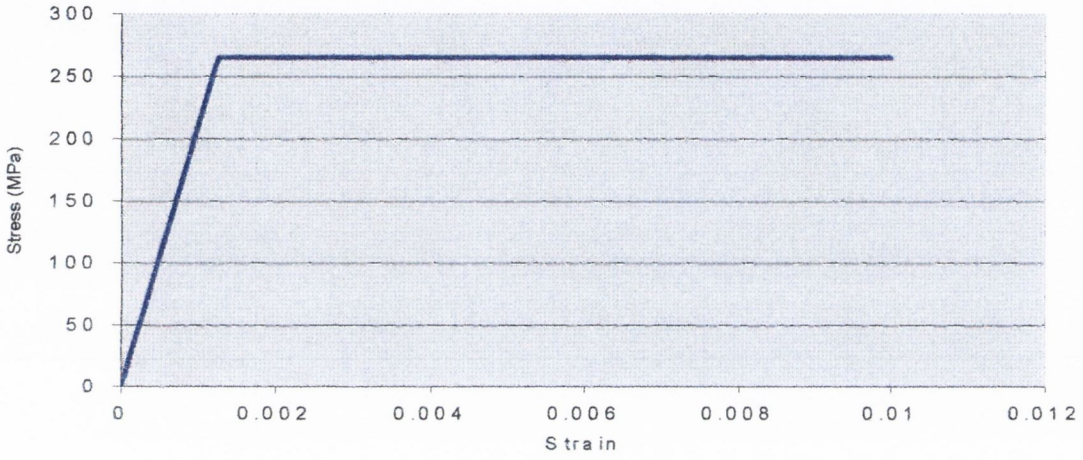

(a)

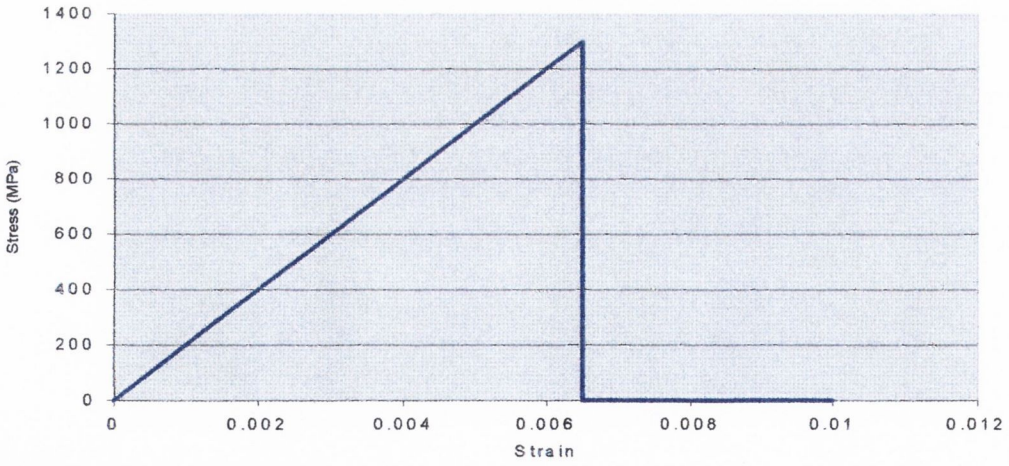

(b)

Figure 6.1: Plots of idealised stress versus strain for (a) beam steel and (b) tendon steel.

When incremental loading is applied, the beam deflects (while the tendons remain straight) until the gap between the tendon and beam's lower flange is almost entirely closed, at which point the soft link element's elasticity greatly increases and contact is recognised.

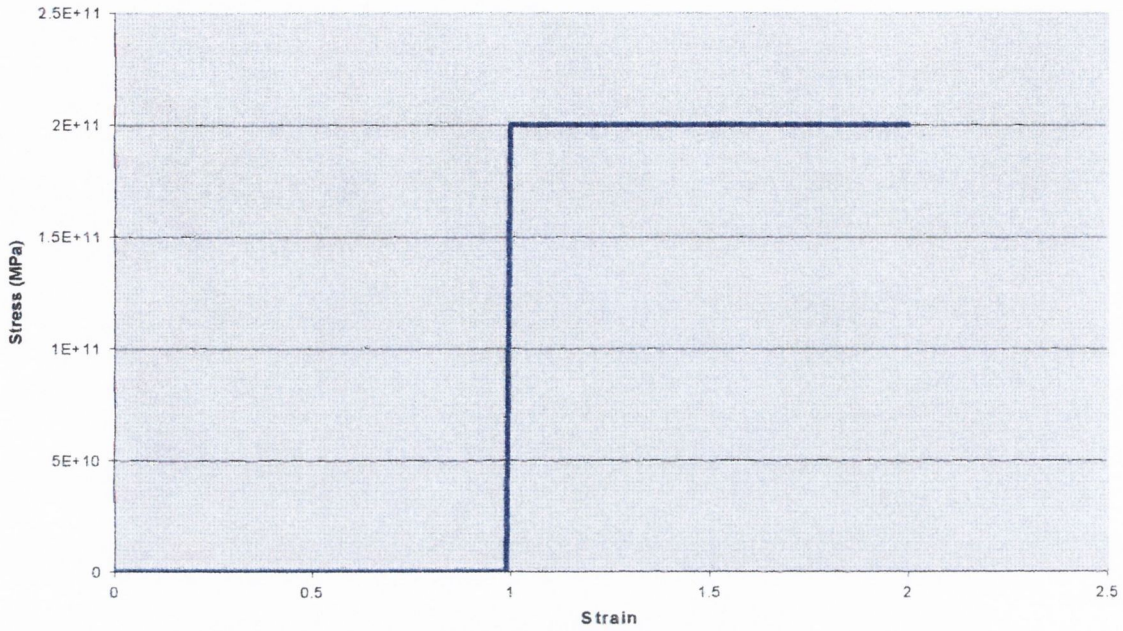

Figure 6.2: Idealised material model used with soft link.

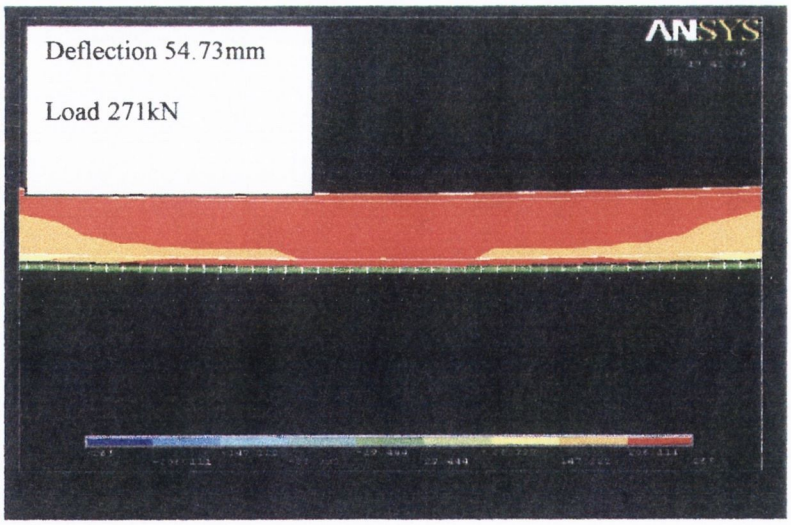

Figure 6.3: Under a plastic response, contact is recognised between tendon and beam's lower flange using a "soft" link.

6.2 Un-strengthened beam plastic analysis

This analysis was carried out to compare the ultimate strength of the beam with that of a similar beam strengthened with the tendon configuration as shown in figure 5.17. The beam was modelled, as in previous analyses, with "solid92" tetrahedral elements and with no tendons or levers attached. A plastic hinge formed at the beam's mid-span when a central concentrated load of 231kN was applied. Figure 6.4 shows a 3D view of the stress contours of the beam under this load at which point the deflection was 32.3mm with a fully developed plastic hinge at mid-span.

6.2.1 Unloaded beam pre-camber of strengthened beam

An elastic analysis with an initial pre-tension (initial strain) only was carried out and compared to the earlier analysis (Chapter 5) which had a similar loading but without the soft links attached. The tendons had a prescribed tendon force of 1240kN, resulting in a counter moment of 210.8kNm. The analysis demonstrated that the addition of the soft links had no significant effect on the elastic flexural behaviour of the beam. A pre-camber of 16.82mm resulted, which was within 0.1% of the resulting pre-camber in the earlier analysis, where no link connection existed between the underside of the lower flange and the tendons. Figure 6.5 shows a magnified displacement plot of the pre-cambered beam which incorporated the soft link located at mid-span.

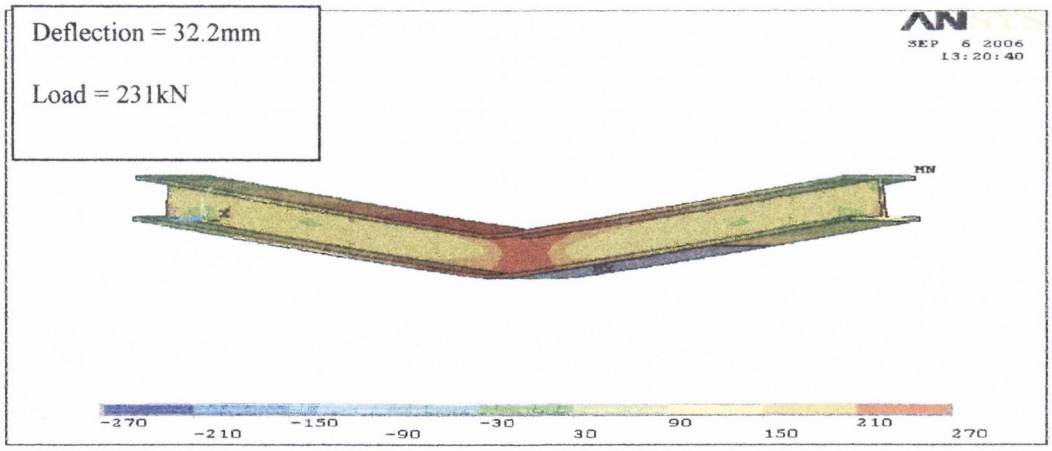

Figure 6.4: Plastic hinge formed in un-strengthened beam, as shown by a contour plot, with a load of 231kN applied

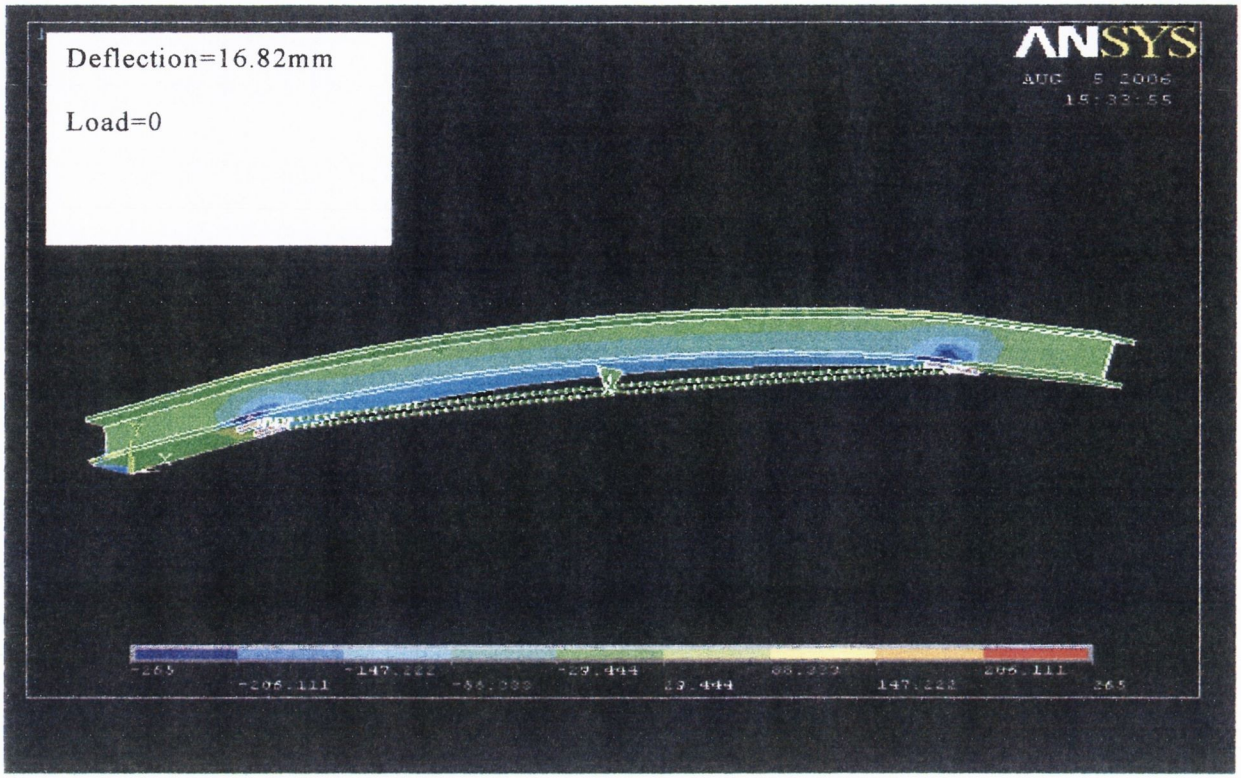

Figure 6.5: Exaggerated pre-cambered beam with soft links attached at mid-span

6.3 Ultimate strength

This analysis was carried out to predict the loading at failure and the mode of failure. The behaviour of the beam to failure under monotonic load can be divided into four stages, as follows:

(a) Elastic behaviour of both beam and tendons up to plastic hinge development in beam.

(b) Plastic hinge at the beam's mid-span with tendon stresses remaining within their elastic range.

(c) With further deflection, the tendons touch the underside of beam which develops further resistance to loading due to the tendon axial deformation (while still elastic).

(d) Widened plastic zone propagating from the beam's mid-span until tendon rupture.

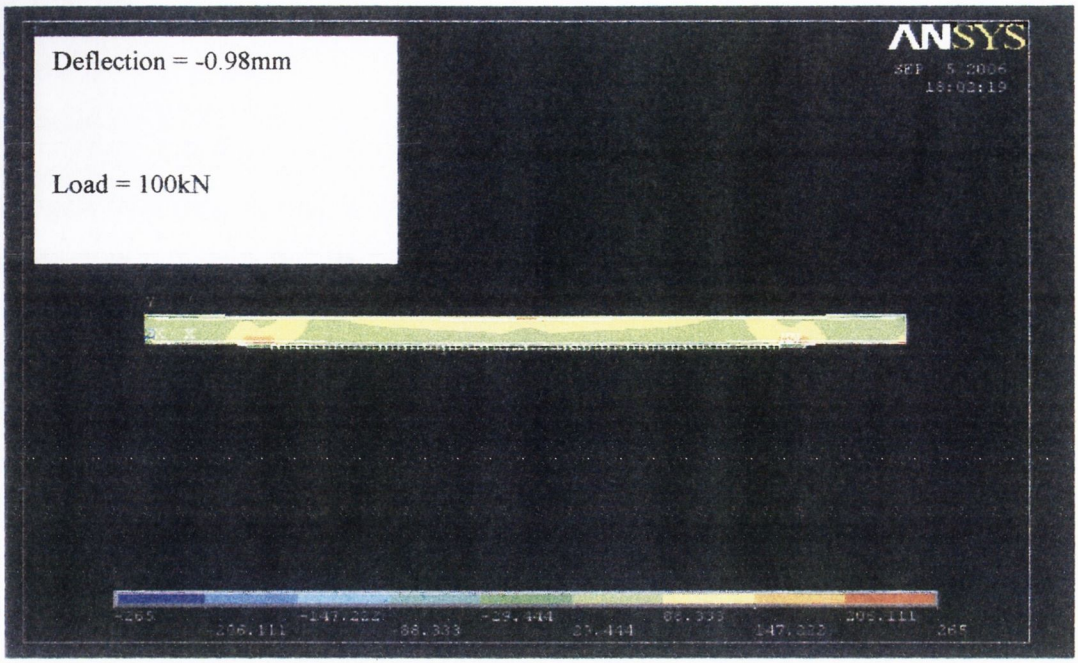

Figure 6.7: Stress contours with both the beam and tendons within their elastic stress range.

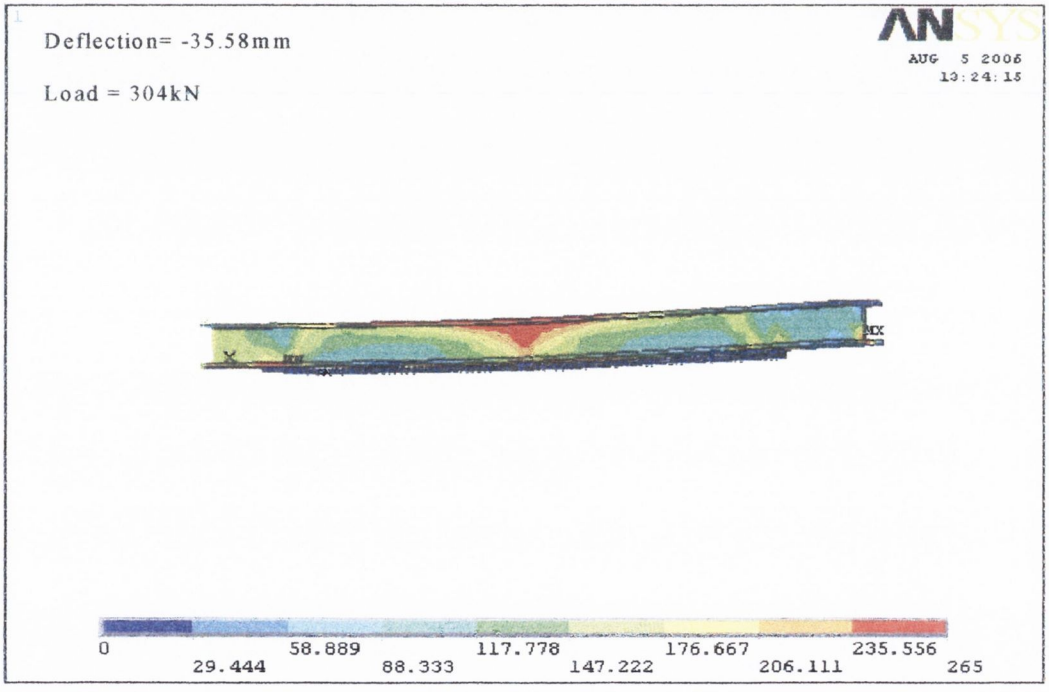

Figure 6.8: Development of a plastic hinge at mid-span and with tendons in elastic stress range.

In the first stage, both beam and tendon are in the elastic stress range. The mid-span stresses, deflection and the r_t rate are as discussed in the previous elastic analysis (Chapter 5), up to just when a plastic hinge forms at mid-span.

Figure 6.6 shows the mid-span deflection of the beam over the four different stages to failure. The deflections in the first phase were as in the earlier analysis for both the beam and tendon elastic responses to loading.

Figure 6.7 shows the stress diagrams with a central concentrated load of 100kN applied giving rise to a mid-span deflection of –0.98mm (that is, beam is in stage 1 of deflection plot shown in figure 6.6). This was within 1% of the value resulting from the calculated deflection using equation 3.23 with the same loading, tendon force and span.

The rate of deflection is greater in the second stage than the first and can be attributed to the formation of a plastic hinge. The plastic hinge occurred under a central concentrated load of 304kN, which represents a 31.6% increase in the un-strengthened load, with a mid-span defection of –35.38mm and marks the beginning of the second stage of beam behaviour. At mid-span, plastic stresses develop firstly within the upper flange due to both compressive axial and maximum bending stresses at mid-span (see 3D view in figure 6.8).

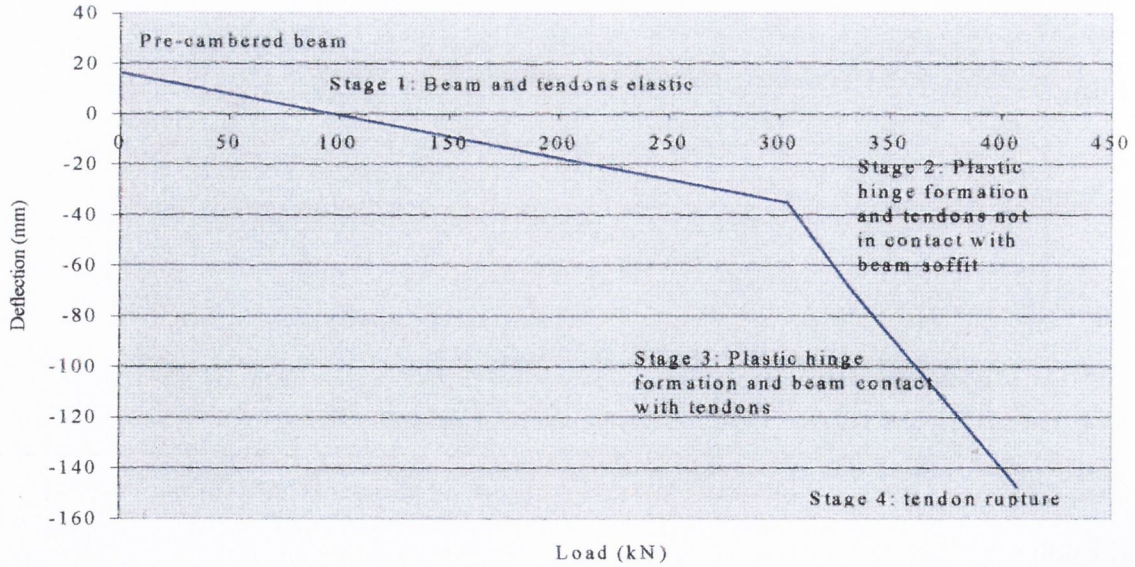

Figure 6.6: Deflection of beam over four stages to ultimate strength.

The plastic stresses propagate down towards the lower flange under increased loading until a full plastic hinge develops whereupon a normal plastic rotation occurs. The tendon force at this stage is 1425kN. The mid-span deflection of 35.4mm at this stage is far in excess of the serviceability limit of span/360 (that is, 16.67mm for a 200kN load).

In the second phase, as further central concentrated is applied at 35.4mm deflection, the plastic region continues to propagate outward from the mid-span and the rate of deflection is greater in this phase than in the previous, as shown in figure 6.6. Under a central concentrated load of 394kN, resulting in a mid-span deflection of –139.0mm, now contact was made between the beam soffit and tendons and marked the beginning of the third stage of deflection. Now, the rate of tendon force increase with respect to central concentrated is greater than in the previous two phases and is due to the mechanism by which the tendon force is applied, as shown in figure 6.9.

The rate of deflection in this phase slows down slightly due to a stiffer system in load resistance. It can be seen from figure 6.9 that the mechanism is effectively a cable supported structure with a full developed plastic hinge at mid-span that has a resistence to rotation equal to the plastic moment capacity (M_p) of the section. The vertical load is now predominantly resisted by the tensile forces in the tendons and the residual compressive strength of the beam.

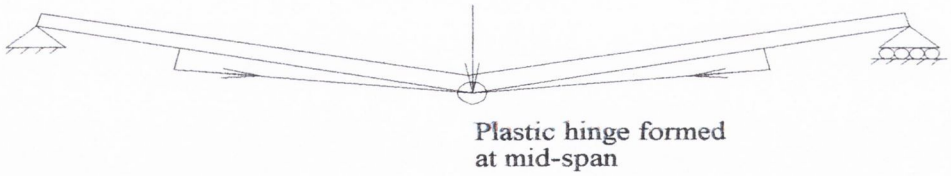

Figure 6.9: Plot shows mechanism applies tendon force due to load application.

The beam displayed a predominantly ductile response just to the point of ultimate loading whereupon tendon rupture occurs. However, the strengthened beam must undergo substantial deflection (150.9mm) prior to failure, thus, giving abundant warning (see figure 6.10).

The stress contour plot of the beam with a 394kN central concentrated load and a tendon force of 1671kN (the tendon yield force) is shown in the figure. It can be seen that the plastic region has propagated outward from mid-span with increased loading. This outward propagation is due to axial compressive stress with increasing load as in the case with the elastic stress. However the rate r_t predicted with the plastic analysis (0.97kN tendon force/ kN load) is almost twice that of the elastic value. The ultimate failure load of 408kN was an improvement of 43% when compared to ultimate load of a similar un-strengthened beam. Further, the failure load is 35% greater than the maximum elastic load for the un-strengthened beam. It can also be seen that the beam undergoes substantial deflection prior to tendon rupture (145mm), thus, a yielding a predictable ductile response.

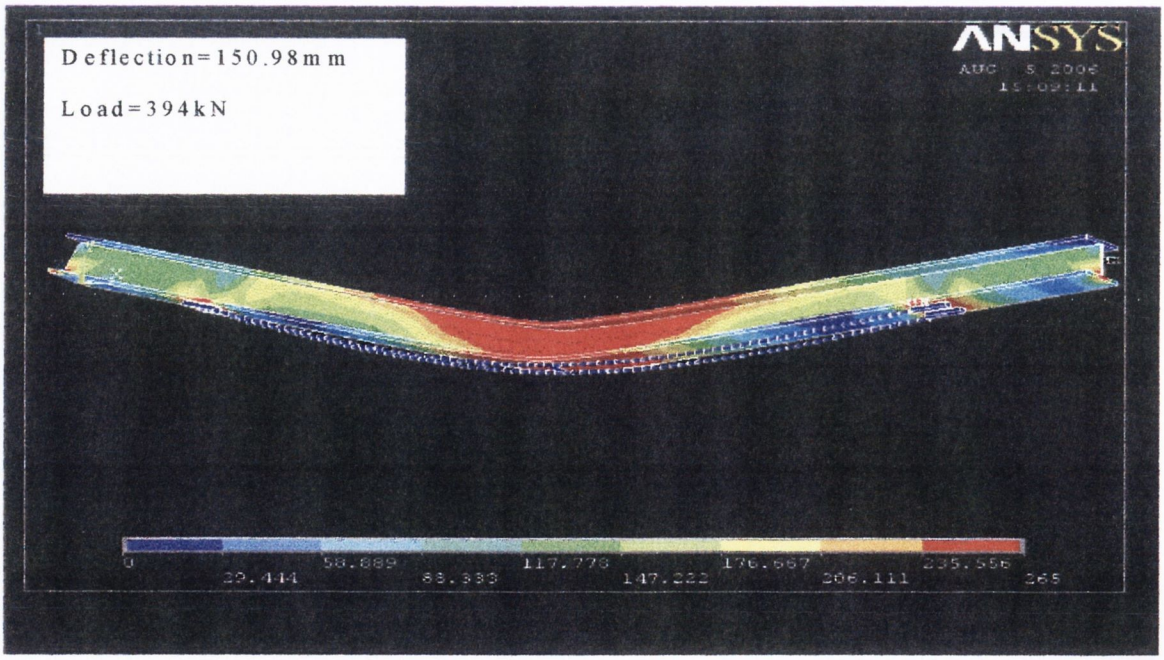

Figure 6.10: Contour plot with ultimate load applied.

6.4 Comparative analyses

An analytical study of three other methods of beam strengthening was carried out in order to make comparison between them and the method proposed with this research. The two types of strengthening methods were as follows:

1. Pulley and tendon method
2. Steel plates welded to the lower flange of the steel beam (Albrecht et al. 1988).
3. CFRP pre-stressed plates bonded to the lower side of the lower flange (Sebatian 2005).

6.4.1 Full capacity analysis of pulley and tendon method of strengthening for comparison

Pre-loaded analysis

The use of external tendons bent around pulleys to provide beneficial upward thrust to reduce the maximum moment was described in chapter 2. An analysis of a configuration considered by Khairallah et al. (1997) and as shown in figure 6.11, was compared with that of the tendon configuration shown in figure 5.17. Using the same beam, overall member

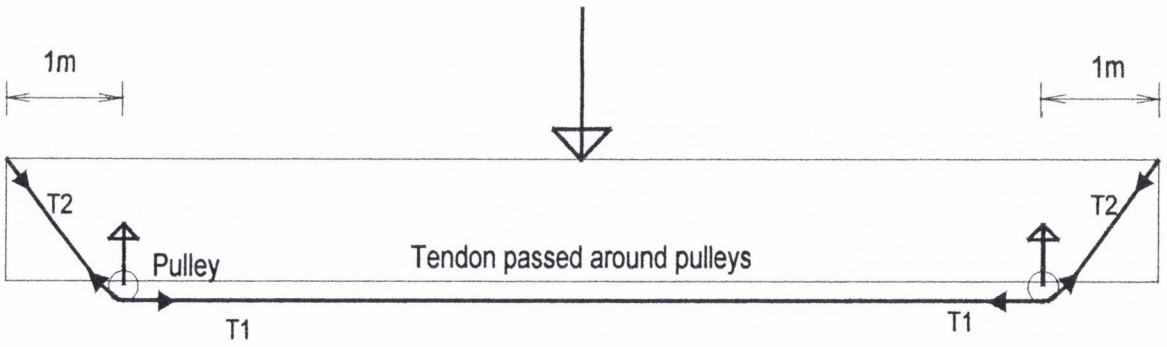

Figure 6.11: The tendon configuration used for comparison with the revised lower tendon configuration in this research.

depth and limiting stress of +/-185MPa, the pulley system configuration was analysed. The pulleys were located below the beam such that the tendon eccentricity was the same as that in the configuration shown in figure 5.17 (that is, 170mm below the neutral axis). In practice, the tendon pulleys would have to be located outside each side of the lower flange to allow the tendons to pass to a depth below the lower flange and anchorage for the tendons at each end of the beam would have to be provided on the outer faces of the flanges to ensure the tendons were straight in the beam longitudinal direction (see figure 6.12).

The beam and tendon forces were modelled, as in the previous FE analyses, with the same tetrahedral elements, making use of a provision with the tendon elements to prescribe an initial strain. In practice, the tendon forces at each side of the pulley should be same. The pulleys were modelled by providing three separate members for each tendon (that is, two inclined members at each end of the tendon and a horizontal member between them). The three members were all pinned at their ends on the underside of the lower flange at the location of the tendon pulleys, which provided the required tendon eccentricity. This implied that the forces in the members modelled as tendons would not have balanced forces, as would be the case were tendons passed around pulleys which are free to rotate. A number of trial analyses were carried out and the initial strains in the tendons were "tweaked" until the forces in each of the members were the same as would be the case with the continuous tendon passed around the (assumed frictionless) pulleys.

Elastic analysis of the pre-loaded beam demonstrated that an initial pre-tension force of 1195kN applied a beneficial moment of 184kNm with a maximum mid-span section stress of –185.0MPa. (see figure 6.13). The tendon configuration shown in figure 5.17 applied a pre-loaded counter moment of 191kNm with a pre-tension of 1125kN. The effective eccentricity of this former configuration is 170mm based on the above figures. The rate of applied counter-moment per unit tendon force, r_t, for the pulley configuration shown in figure 6.12 is 0.153kNm/kN.

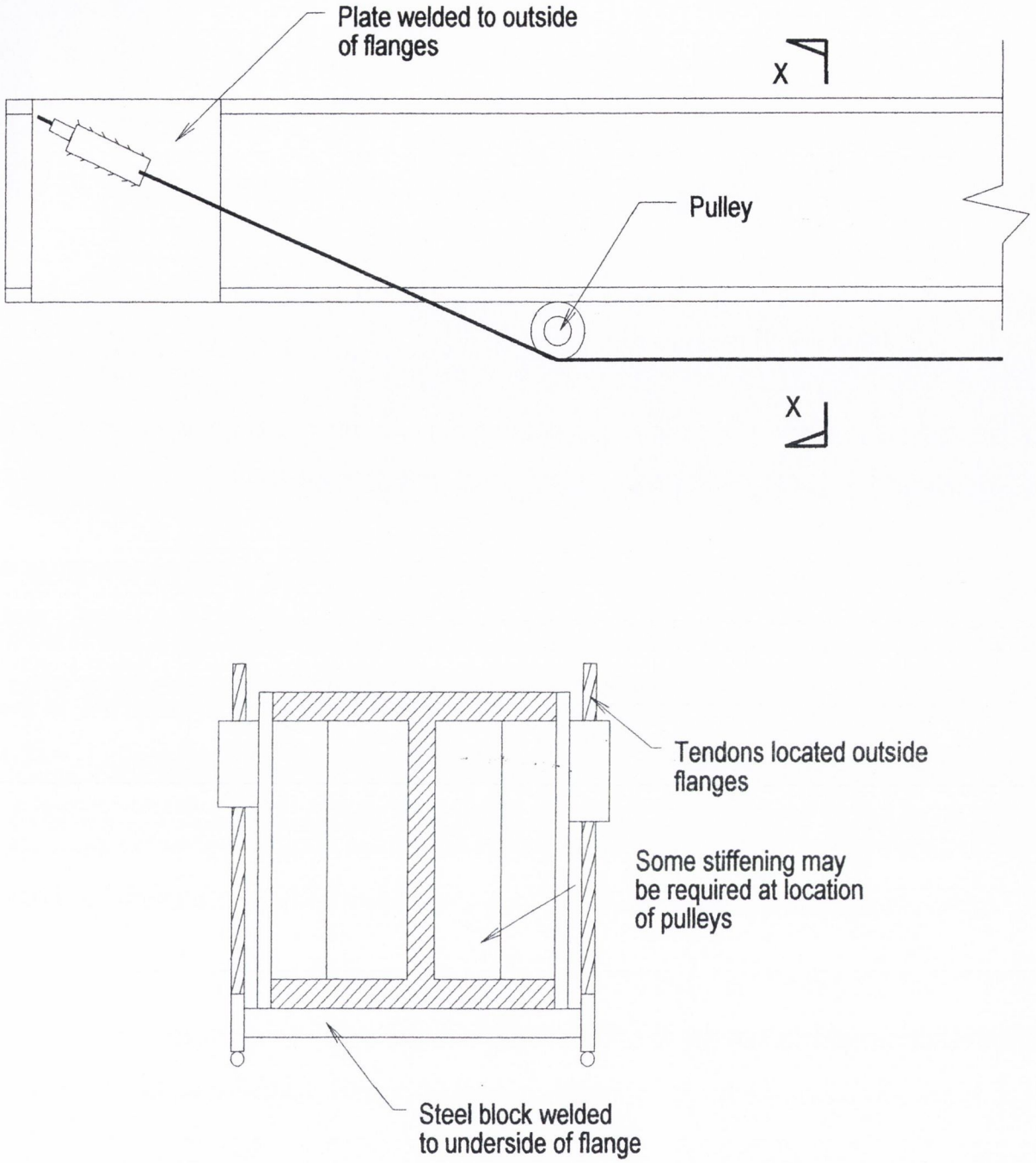

Figure 6.12: How the tendon configuration shown in figure 4.54 would pass outside the flanges of beam.

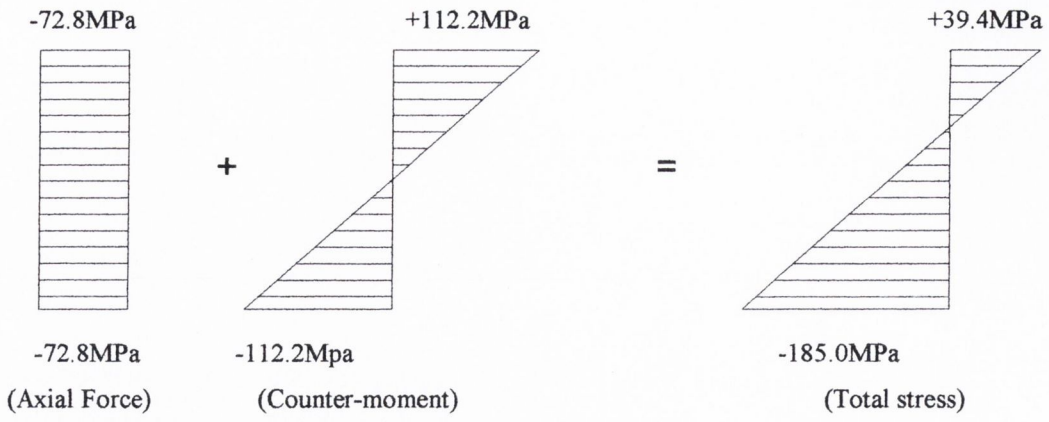

Figure 6.13: The mid-span section stresses for the pulley configuration with the pre-tension force of 1195kN applied and with no central concentrated load.

This 11% increase is not a considerable improvement in performance, however, as will be seen in the next section, the self counter-moment application was significantly greater for the configuration shown in figure 5.17. The low self counter-moment can be attributed to the pulley not allowing additional tendon forces to develop due to lower flange tensile strain under loading (that is, forces in tendon were balanced ($T_1 = T_2$) in analysis either side of pulley to model actual response). The FE analysis predicted an upward pre-camber for the configuration, shown in figure 6.12, of 12.4mm which represented a 15.6% reduction in the 14.7mm achieved with the configuration shown in figure 5.17.

Analysis with loading applied

With the 1195kN pre-tension force in place, a 230kN central concentrated load was applied to the beam. As in the first analysis the forces were balanced. This load resulted in a maximum mid-span section stress of –184.7MPa in the upper flange. The final post loaded mid-span section stresses are shown in figure 6.14. The application of the 230kN central concentrated load resulted in a final tendon force of 1250kN being induced. This was an increase of 55kN, which, when compared to the increase of 126kN in the configuration in figure 5.17, represents a 56% reduction in the induced tendon force. This represents a reduction in the self counter-moment application, that is, from 11.4kNm

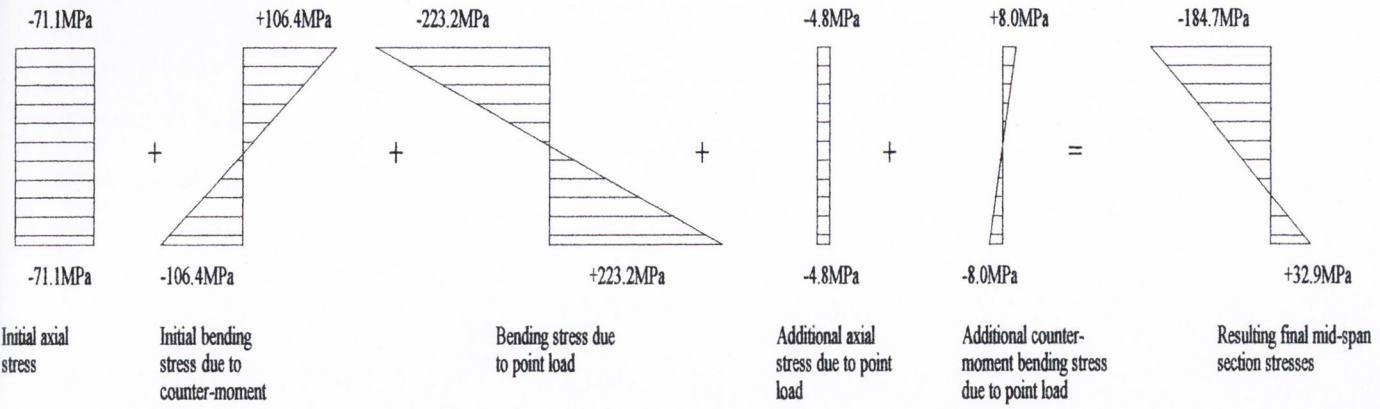

Figure 6.14: Figure showing the mid-span section stresses with the final central concentrated load of 230kN applied.

with this configuration compared to 22.7kNm with the configuration in figure 5.17. The mid-span deflection at failure was 37.8mm under a 272kN central concentrated load. The mode of failure was ductile with a mid-span plastic hinge and no tendon interaction as is the case for the configuration shown in figure 5.17 (that is, the tendons do not make contact with the beams' soffit). Under a 200kN load (for comparison) the deflection was 11.8mm. The former configuration (in figure 5.17) yields a significantly lower deflection of 1.2mm under a similar loading. The thick-wall tube application is in practice, a more straightforward method of application than the configuration proposed in figure 6.11, which would require greater expense to fabricate. In addition to the anchor points for the tendons, the tendon pulleys would also require plating to distribute the high concentrations of stress associated with external tendon applications.

The pulley configuration analysis yielded a maximum load that was 41% (272kN) lower than the tendon configuration shown in figure 5.17 (408kN). The counter moment application rate for the pulley configuration was 0.525kN/kNunit of tendon force and the rate for the configuration shown in figure 5.17 was 0.525kN/kN which is more efficient than with the pulley configuration by some 343%.

6.4.2 Steel plate welded to the lower flange of a steel beam.

This method of strengthening has been in practice for many decades and involves welding or bolting steel plates to increase the flexural strength in areas of higher bending stresses. A 6m beam similar to that used with the tendon strengthening system was considered here. The beam had a 25mm thick steel plate, 250mm wide, fixed to the lower flanges as shown in Figure 6.15.

The plate was curtailed at 1000mm from each simple support and was assumed to act monolithically with the beam section (that is, adequately welded throughout its length so at to provide full stress development under flexure).

A lateral torsional buckling load of 253.2kN was found to be the maximum load that the strengthened plated beam could carry (see appendix H). This load represented an increase of 3.3% when compared to the un-strengthened beam. When compared to the ultimate strength of the beam with external tendons (394kN), the ultimate strength of the steel plated beam is 46% less.

The mid-span deflection for a central concentrated load of 200kN was calculated using equation 3.23 and was found to be 12.6mm. The load of 200kN was chosen for both

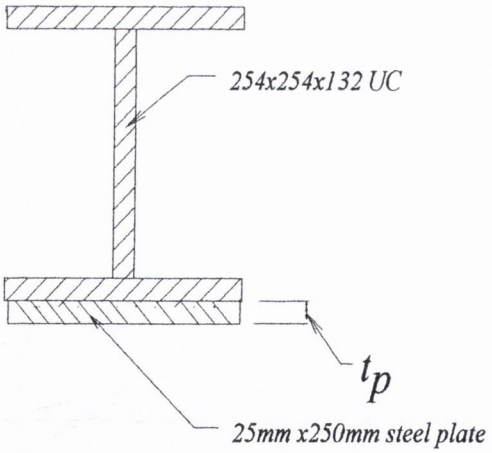

Figure 6.15: Location of plate on member section.

methods of strengthening as both methods respond elastically under such loading. When compared to the un-strengthened beam, this represents a 49% reduction in mid-span deflection. However, when compared to the external tendon strengthened beam (6.6mm), it represents a 92% increase for the same mid-span loading (excluding additional self-weight deflection).

With regard to the overall depth of the beam, the steel plated beam had an overall depth saving of 25mm when compared to the external tendon beam. However, the member self-weight increase of the steel plated beam is 49kg/m as compared to an increase of just 6.2kg/m with the external tendon application. This represents a significant increase in self-weight bending stress and peak deflection (1.24mm).

6.4.3 Strengthening with pre-stressed CFRP plates.

The method of strengthening with pre-stressing CFRP plates involves bonding the plate in its stressed state to the member and allowing the adhesive to cure before releasing the applied tensile plate forces, as discussed in chapter 2. Figure 6.16 shows the layout of the strengthening CFRP bonded plate, which will be analysed for comparative purposes.

The CFRP plates used in the ultimate load capacity analysis were Diversified Composites custom high modulus pultruded strips (henceforth referred to as DC-1 strips) with an elastic modulus of 229kN/mm^2 and a plate thickness of 3.2mm (Schnerch et al., 2005).

According to the technical report of the UK concrete society (EU Report No. 55(11)) the maximum material design stress for the CFRP plate is given by the following expression.

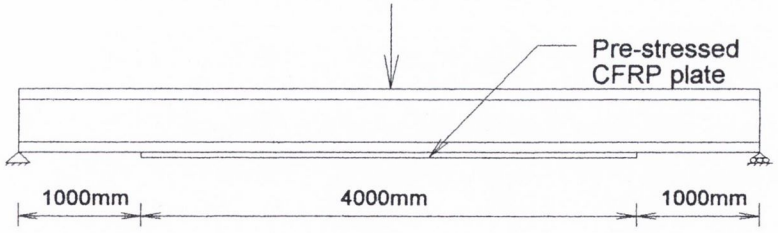

Figure 6.16: Configuration of pre-stressed CFRP plate on beam

$$f_{fd} = \frac{f_{fK}}{\gamma_{mf} \cdot \gamma_{mm} \cdot \gamma_{mfe}} \qquad (6.1)$$

where:

γ_{fK}= material characteristic failure stress (2800N/mm^2).

γ_{mm}= safety factor which depends on the method of installation (in this case 1.4 for wet laid CFRP plates.

γ_{mf}= safety factor dependant on the method of manufacture of the material (1.4 for CFRP plates).

γ_{mfe}= partial safety factor (1.15) for CFRP plates (see table 2, EU report No. 55(11)).

Using equation 6.1, the maximum design stress is 1242N/mm^2. Adequate cross-sectional area was provided for the CFRP plate (576mm^2) such that its ultimate strength was the same as for the steel tendon's ultimate strength (that is, 1671kN).

As discussed in chapter 2, Sebastian (2005) proposes a method of analysis for strengthening steel members with CFRP bonded plates. The author points out that some considerations that apply to strengthened concrete structures do not apply when designing strengthened steel members. De-bonding plate failure due to material flexural cracking and end peel plate failure due to shear cracking are not considered in the case of steel strengthened members. However, adhesive and plate material failure rather than parent material failure are more likely to occur with CFRP strengthened steel members.

The following assumptions are made with the proposed method of analysis:

- The steel is assumed to be elastic –perfectly plastic
- The CFRP plate is assumed to linear elastic to failure.
- The adhesive is assumed to be linear with a shear stress distribution that peaks at mid-span and decreases moving towards each CFRP plate end.

An expression to predict the bond shear stress distribution between the CFRP plate/lower flange interface within the yield zone at mid-span at a distance, x, from the mid-point of the beam was developed (see equation 2.4). It was suggested that further investigation

was necessary to establish correction factors between the proposed method that assumed no interfacial slip and subsequent non-linear FE analysis that modelled interfacial slip. As a conservative value and as recommended by CFRP plate adhesive manufacturers (Sikadur Epoxy Adhesives 2001), the limiting adhesive bond shear stress was assumed to be 4MPa.

When calculating the ultimate moment capacity of the plastic section (see equation 2.2) the yield stress must be increased to allow for additional capacity provided by pre-stressing. When pre-stressing is applied to the unloaded beam the resulting upper flange net beneficial stresses have less value than in the beneficial stresses in the lower flange. Thus, with increased central concentrated loading, the upper flange will reach yield stress first. It is for this reason that net beneficial stress resulting in the upper flange is taken as the increased yield stress in equation 2.2 when calculating the ultimate moment capacity.

With a pre-tension plate force of 640kN applied to the bonded CFRP plate at the pre-loaded stage and assuming linear strain throughout the depth of the section, a beneficial bending moment of 88.4kNm is applied and the resulting theoretical mid-span section stresses are shown in figure 6.17.

It can be seen from the theoretical mid-span stresses that an upper flange net beneficial stress of 16.1MPa results thus giving an effective increase stress capacity of 281.1MPa (that is, 265+16.1MPa). This value is used in equation 2.2 to calculate (M_{ult}) the ultimate moment value of 38kNm which implies an ultimate central concentrated load of 254.6kN.

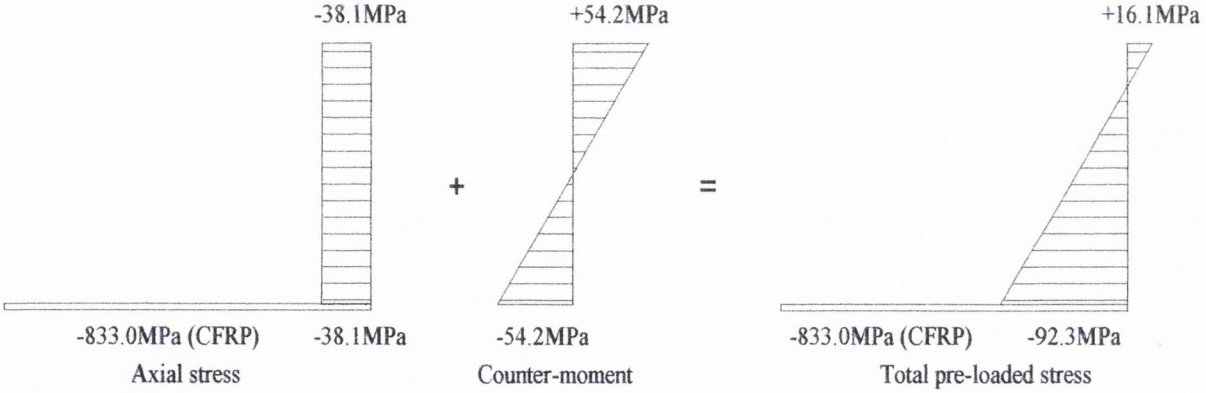

Figure 6.17: Mid span section stresses of pre-loaded beam with pre-stressed CFRP plate.

6.4.4 FE plastic analysis of beam strengthened with pre-stressed CFRP plates

A non-linear FE analysis was carried out to verify the calculated ultimate load and to predict the bond shear stress distribution on the plate/flange interface. The beam and CFRP plate were also modelled with solid elements "solid92" and with bi-linear material properties (for plastic analysis). The plate was assumed to be glued to the modelled beam as in figure 6.16 and the pre-stressing force applied via a thermal (negative temperature) load. Figure 6.18 shows the unloaded beam with pre-stressing applied to the CFRP plate.

The analysis predicted a tensile stress of 833MPa at the plate centre and 774MPa at the plate ends. The stress in the lower and upper flanges were –90.6MPa and +15.2MPa

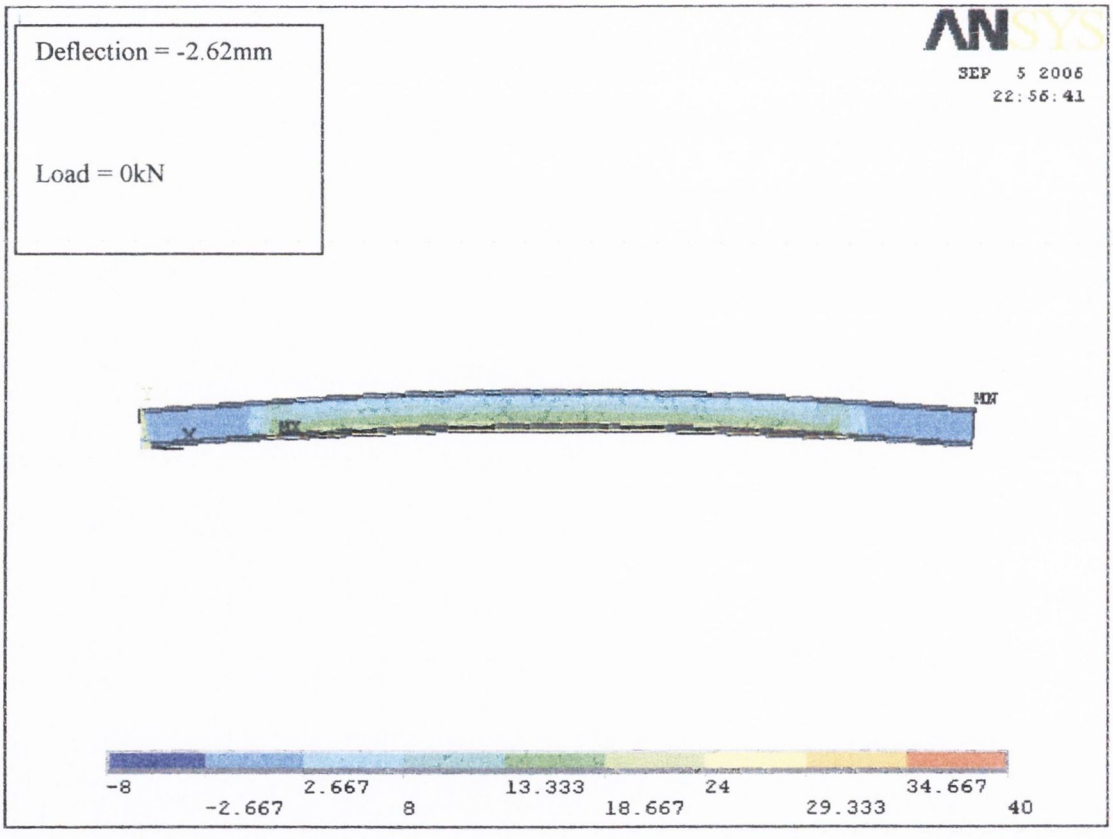

Figure 6.18: Pre-cambered unloaded beam with CFRP pre-stressed.

respectively and compared closely to the stresses calculated by hand (within 3% difference). The mid-span pre-camber was 2.62mm with a mid-span pre-stress force of 640kN.

With pre-stressing applied to the CFRP, a full plastic hinge at mid-span formed under a central concentrated load of 244kN. The mid-span deflection under this loading was 31.7mm. Figure 6.19 shows the stress contours of the beam with a post loaded CFRP tensile force of 816kN at mid-span and 736kN close to the plate ends under this ultimate load of 244kN.

The FE plastic analysis demonstrated that when compared to the un-strengthened beam ultimate loading (220kN), the improvement in ultimate strength with the pre-stressed CFRP plate system was 10.9%. The analysis also demonstrated that, owing to the variation in bond shear stress on the CFRP/flange interface, the beneficial direct stress and applied beneficial moment (via the CFRP plate), varied along the length of the plate

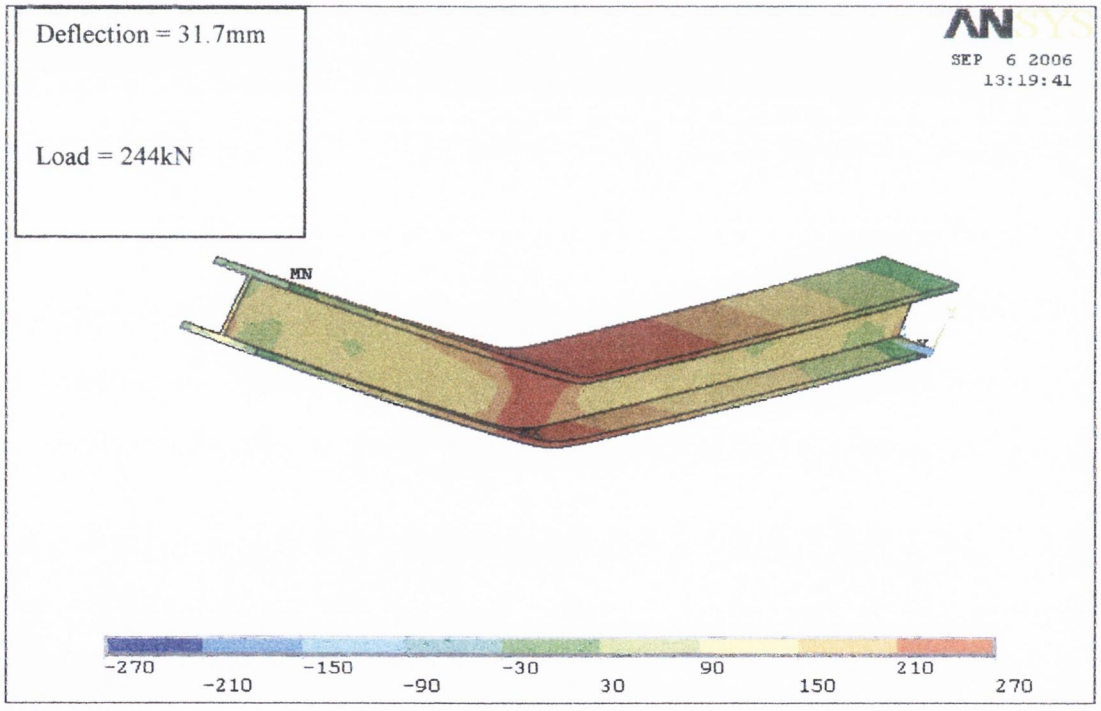

Figure 6.19: Development of plastic hinge in CFRP plated beam.

(that is, peak beneficial moment at mid-span of 130.5kNm reducing to 117.7kNm close to each plate end). The overall member depth was only increased by 4.2mm which is a 45.2mm saving in overall member depth compared to the external tendon strengthening system. However, the ultimate strength gain of 10.9% is considerably less than the 32% gain when making comparisons between both of the predicted non-linear FE analysis ultimate loads for the two cases. It is not possible to apply concentrated counter moments with externally bonded pre-stressed CFRP plates (as in the case of external tendons) and, thus, it is impossible to optimise the bending moment diagram. If sufficient counter moment is applied at the optimum locations, too much is applied at mid-span or if sufficient counter moment is applied at mid-span, to little is applied at the optimum locations.

When a central concentrated load of, say, 200kN is applied to the pre-stressed CFRP plated beam (that is, a load at which the beam responds elastically) a mid-span deflection of 16.1mm was noted. This deflection was greater than in the case of the beam strengthened with external tendons which responded with a deflection of 9.3mm at the mid-span under the same loading conditions. The deflection with the CFRP plated beam represents a 73% increase when compared to the external tendon strengthened beam.

6.5 Conclusions

Non-linear analyses were carried out on the revised configuration to establish the ultimate strength and mode of failure. The analyses demonstrated that the strengthened beam could bear a 43% greater ultimate load than with a similar un-strengthened beam. The analyses also highlighted the four phases of deflection up to ultimate loading. The first was an elastic response of both beam and tendons until the second phase where a plastic hinge forms at mid-span. Deflection continues (at a greater rate) under further loading until contact is made between the tendons and beam soffit which marks the beginning of the third phase of deflection (at a lower rate than the previous phase due to an increase in

effective stiffness). The end of the third phase of deflection occurs with tendon failure and beam collapse.

In order for the beam to respond as described, an adequate cross-sectional area of tendons must be provided to ensure that a plastic hinge develops prior to tendon failure. The designer must first establish the rate of tendon force increase with respect to load application, r_t , for the configuration under consideration. Knowing r_t will allow the designer to ensure that the tendon stresses remain sufficiently below their characteristic breaking strength when a plastic hinge forms in the beam. This will allow a ductile response to occur with substantial deflection before tendon failure.

Comparative analyses were carried out for three methods of strengthening on a similar beam to that used with the external tendons (that is, steel plated beam and pre-stressed CFRP plated beam). For both methods of strengthening examined, moment is applied, at varying amounts, to the member throughout the length of the plate/tendon. When applying counter moments it is essential that concentrated moments are applied at optimum locations in order to optimise the member being strengthened and, also, for efficient use of the pre-stressing method. Strengthening with external tendons is an efficient method, as moments of specific magnitude can be applied at specific locations so as to optimise the bending moment diagram and efficiently use pre-stressing forces. This creditable performance by the external tendon/counter-moment system proposed in this research can be justified by referring to table 6.2 which shows a summary of similar strengthening systems applied to a 254x254x132kG/m UC.

Method	Ulimate load (kN)	Mode of Failure	Mid-span deflection under 200kN load	Deflection at Failure	Self-weight/m
Steel plated beam	253.2	ductile	16.1mm	42.2mm	181kg/m
CFRP plated beam	244	ductile until plate rupture	16.6mm	31.7mm	132.2kg/m
Tendon and Pulley system	272	ductile	11.8mm	37.8mm	133.1kg/m
External tendons (thick-wall tubes)	394	ductile until tendon rupture	7.2mm	150.9mm	138kg/m

Table 6.2 Comparison of strengthening methods considered.

The external tendon system has an ultimate load that was 44.8% higher than the next best alternative system (tendon and pulley system) with a maximum mid-span deflection that was 43% less in the elastic range.

CHAPTER 7

LABORATORY TESTING OF A BEAM WITH COUNTER-MOMENTS APPLIED BY EXTERNAL TENDONS

The horizontal tendon configuration described in chapter 4 gave a rate of counter moment applied per kN of tendon force of 0.019kNm. To verify the predicted behaviour, it is necessary to carry out laboratory testing on a 254x254x132kg/m U.C. spanning 6m with simple supports. It can be shown, using the theory in section 3.1 that a counter-moment of 200kNm is required to produce the typical five equal peaked optimum bending moment diagram when a 200kN central concentrated load is applied to this beam. However, it was not possible to achieve the optimum bending moment diagram on application of a 200kN central concentrated load as the capacity of the available tendons restricted the maximum applied counter moment to 35kNm. It was decided to proceed with the laboratory testing for the earlier configuration, firstly, to verify the FE analysis results and, secondly, to serve to gain a more complete understanding of the tendon, lever and beam interaction with a view to testing a revised lower tendon configuration. As it was required to carry out a number of tests on the beam, the central concentrated was restricted to 100kN such that the total stresses (that is, bending and axial) were kept well within the elastic range. The outcome of the laboratory testing for the revised lower tendon configuration is also discussed in this chapter.

7.1 Test beam design and fabrication

Levers and plates were welded to the underside of the upper flange of the beam, together with stiffening plates welded to the outside edge of the flanges as described in section 4.2. Two cables of super-strand 15.7mm core diameter, high tensile tendons were available for use. These tendons had a characteristic breaking strength of 265kN for a single strand (PSC Freyssinet 1986). It was decided to use a working load of 70% (180kN) of the breaking strength per tendon, which is within the recommended 80% value. This meant that when the tendons were fully tensioned, the beam would have a total axial force of 360kN, with 180kN being applied by each tendon lever either side of the web.

7.2 Lever design

The tendon levers had a horizontal force capacity of 600kN each (see Appendix G). The upper flange had been analysed locally, close to the optimum location for counter moment application (that is, 1m in from each support). Based on the results of the local FE analyses of the stiffening upper flange plates and the outer edge flange plates discussed in chapter 4, it was considered that both the upper and lower flanges could be engaged to dissipate the high local concentration of axial, shear, and bending stresses induced by the action of the levers with the tensioned tendons attached. At least 500mm of 18mm fillet weld was used to weld the upper flange plate and the vertical lever plates. A 12mm fillet weld was used for the 300mm long 60mm diameter thick-wall tubes as shown in figure 7.1 (see Appendix G for weld design calculations).

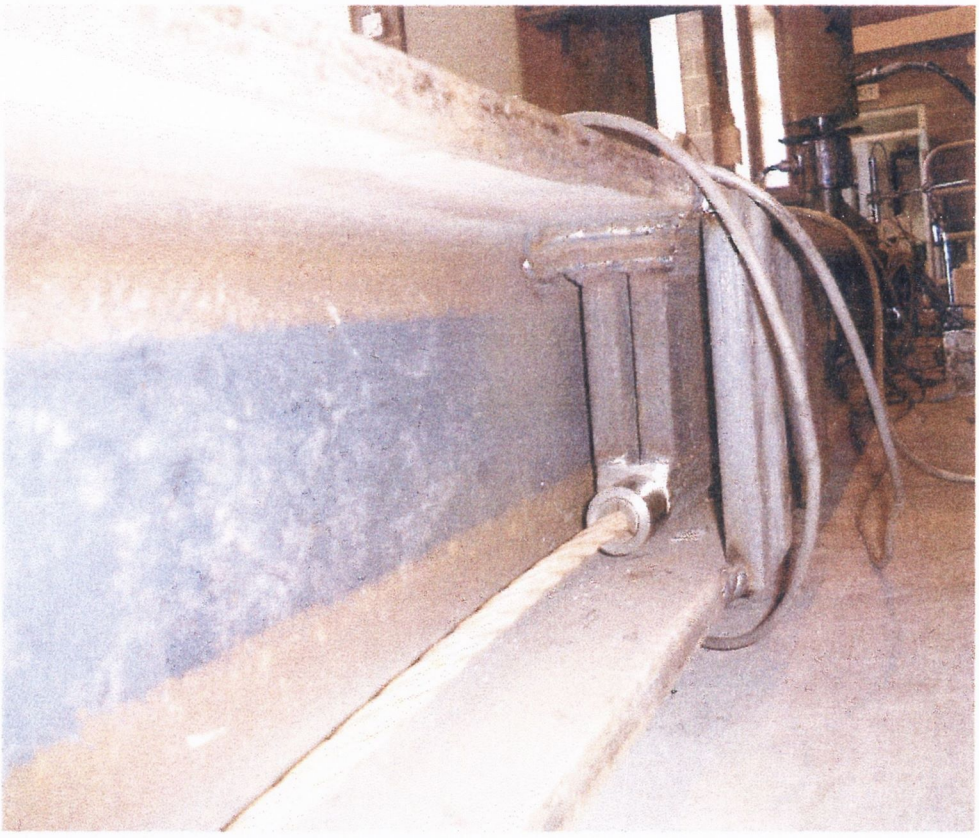

Figure 7.1: The fabricated tendon and lever configuration with flange stiffeners.

All the tendon lever welds were designed using B.S. 5950:part 1 (using grade 43 steel). The 12mm fillet weld, with a throat thickness of 8.4mm and 450mm long, provided a working shear transmission capacity of 436kN. The vertical plates welded to the thick-wall tube were checked for horizontal shear and with an assumed working stress of not more than 125MPa (BS 5950) on the principal plane, yielded a working capacity of 975kN. The local tendon lever FE analyses predicted a maximum stress of 53MPa in the 25mm thick vertical plates used as the tendon levers. Based on the hand calculations of local crushing and buckling of the 25mm thick plates, the plates were considered strong enough to safely transmit the maximum tendon forces arising during the laboratory testing, to the beam. With an assumed working stress of 185MPa (well below the recommended 250MPa in BS 5950 part 1) and an outside diameter of 60mm with a wall thickness of 20mm, the axial capacity of the thick-wall tube was 465kN per tube. The working stress, predicted by the FE local analyses, in the vertical stiffeners welded to the outside edges of the upper and lower flanges at both sides of the beam at the location of the application of the counter moment was 36MPa in axial stress, giving an axial force of 87kN. Fillet welds 165mm long of 12mm depth were provided at each end of the vertical stiffeners, giving a shear capacity of 160kN (with a shear stress of 115MPa) per stiffener and an axial capacity of 640kN (using an axial stress of 155MPa from BS 5950 part 1). The two external stiffeners at each side of the lever locations provide an overall shear capacity of 640kN and an overall axial capacity of 2560kN. The axial stiffener capacity referred to here is the axial strength of the external stiffeners that transmit forces from the upper flange to the lower flange to assist in the dissipation of high local stresses by engaging both the upper and lower flange. The predicted maximum stress in the tendon levers occurred in the thick wall tube and was a compressive stress of 87.4MPa.

7.3 Tendon configuration and jacking

As mentioned earlier, it was decided to use the horizontal tendon configuration. The tendons were located as closely as possible to the upper face of the lower flange to maximise tendon eccentricity and as closely as possible to the web to minimise eccentricity about the vertical Y-Y axis. It was suggested that the tendon eccentricity be minimised in the Y-Y plane to avoid bending stresses (see figure 7.2), in the event of the

tendons being tensioned up separately or at different rates. The system of jacking used, however, did not give rise to differential tension in the tendons, a matter that will be discussed later in this chapter. Each tendon is locked off at one end and jacked to a prescribed force at the other end, and this is done at opposite ends of the beam either side of the web.

Two practical problems needed to be resolved with regard to applying the tension forces to the tendons, as follows:

1. The conventional hand held jacks employed in concrete post-stressing required a minimum clearance of 60mm measured from the centre of the tendon to the nearest surface. This clearance applies to the smallest hand-held hydraulic jack used in pre or post tensioning.

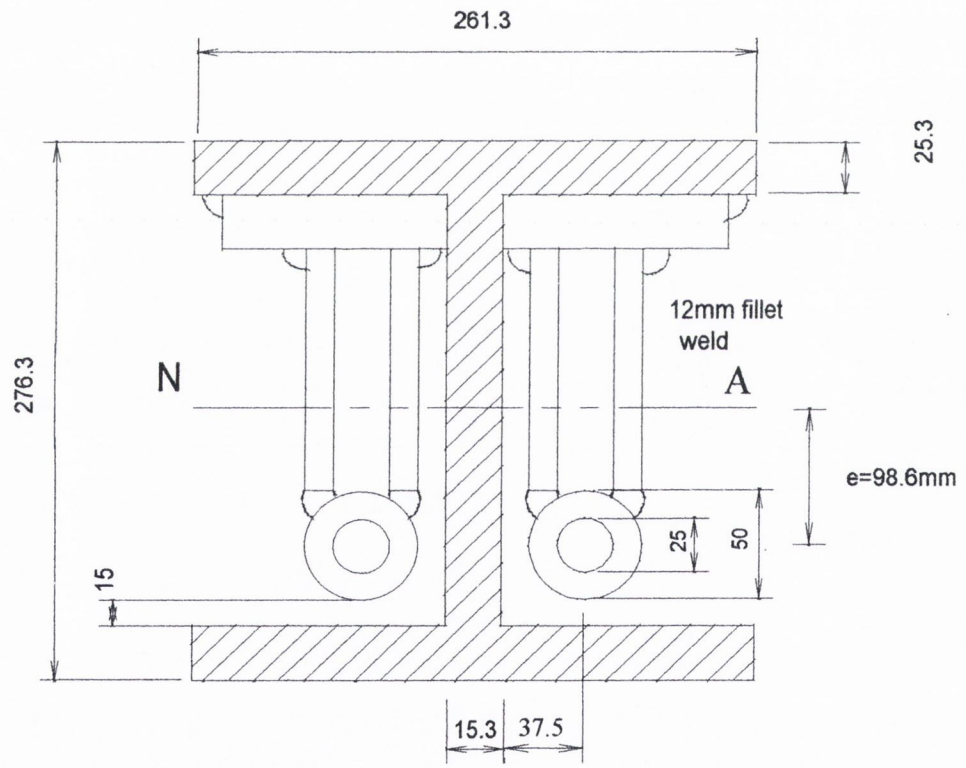

Figure 7.2: Cross section of the beam with the tendon and levers with the thick-wall tubes attached.

2. As many tests were to be carried out on the beam, this required the tendons to be tensioned to varying forces and, sometimes, with no force. Consequently, a safe method of stressing and de-stressing the tendons had to be devised.

With regard to the first problem, it was decided to locate the centre of the thick-wall tube centre 40mm from the upper surface of the lower flange (that is, 15mm clearance from the outer surface of the tube to the upper surface of the lower flange). This meant that the conventional post stressing hand-held hydraulic jacks could not be used to stress the tendons at the location of the thick-wall tubes welded on the beam. It was decided to employ two lengths of the same thick-wall tube, 1100mm long, to allow jacking to take place outside the ends of the beam. This was achieved by transmitting the jack forces to the face of the thick-wall tube, thus, providing a reaction against which the tendons could be tensioned (see figure 7.3). It was suggested that these thick-wall sleeves could serve a dual purpose in that they could also be used, with adequate calibration and strain gauges fitted, as load cells as a check on the load cell readings of the tendon tensile forces. This proved to be an invaluable check on the tendon forces as some difficulty was encountered with the laboratory equipment, as discussed later in this chapter.

With regard to the second problem, one of de-stressing, it was found that no facility exists in conventional hand-held post-tensioning jacks to relieve or totally release stresses that have been locked in place by the barrel and wedge mechanism employed in tendon stressing.

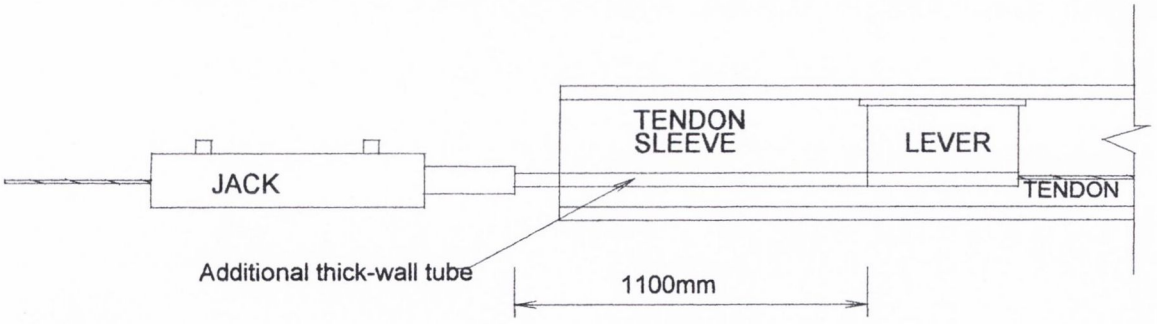

Figure 7.3: The jacking arrangement at one end of the test beam.

A method was devised, therefore, that would allow the tendons to be repeatedly fully tensioned and incrementally and completely reduced back to zero stress. A free-standing hydraulic pump was used to power two reversible 50 tonne capacity hydraulic jacks, located at opposite ends of the beam, (as not enough clearance was available to operate both jacks at the same end of the beam) one on each tendon. This allowed the jacks to tension the tendons to the required force and, when reversed, to slacken the tendons to a lower force or to totally release the stress. The procedure for stressing and de-stressing is as follows (see figure 7.4):

1. The two tendons were cut to a length of 10m. This allowed enough length for the tendons to travel the length of the beam and allowed for an adequate additional length required for the reversible hydraulic jacks.

2. A locking barrel and wedge was fitted to one end of each tendon. The tendons were passed through the thick-wall tubes at either side of the web, each starting from an opposite end of the beam. When both tendons were pulled through the thick-wall tubes as far as the barrel and wedge, the additional length of tendon for each lay at opposite ends of the beam.

3. The two 1100mm lengths of thick-wall tube were placed on the free end of each tendon and moved down the tendon until the end of each sleeve butted against the face of the thick-wall tube welded to the down-stand levers.

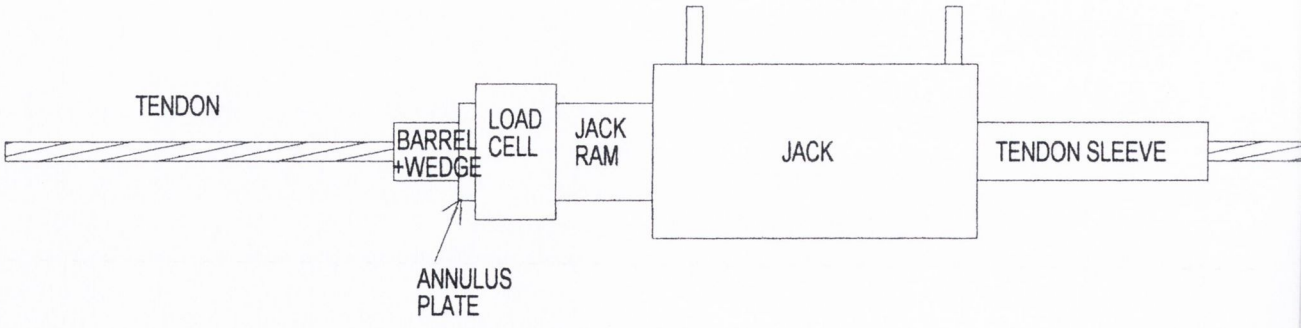

Figure 7.4: The configuration for jacking and releasing the tendon forces

4. The two reversible jacks were then placed on the free end of each tendon and moved into position behind the thick-wall sleeves. The jack ram lies on the outside of the cable (see figure 7.3). Before the jacks were placed, the direction of travel of each was checked to see if they were both moving in the same direction.

5. Two 25 tonne load cells were then placed on each tendon in front of the hydraulic jacks. These load cells were used to calibrate the tendon thick-wall tubes.

6. 25mm thick circular annulus plates were then placed on the free end of each tendon. The outside diameter was large enough to receive the hydraulic jack ram (100mm) and the inside diameter was small enough to receive a barrel and wedge locking clamp (20mm).

7. Finally, a barrel and wedge clamp was then placed over the annulus plate on the free end of each tendon. The location of the barrel and wedge clamps needed some consideration in view of the fact that there was a need to be remove them safely to further test and, ultimately, to dismantle the test beam. The barrel and wedge clamps needed to be located at mid-point of the travel of the jack-rams to allow the barrel and wedges to be removed when the jacks were fully retracted.

Figure 7.5 shows a digital image of the above configuration set up in the laboratory. The picture shows, moving inwards along the tendon, the barrel and wedge grip, an annulus plate, a load cell, the ram on the jack, a reversible 50 tonne bottle jack in front of which is the tendon sleeve.

As mentioned earlier, the problem of applying different tendon forces either side of the web, thus giving rise to bi-axial bending, did not arise with this jacking system. The two reversible jacks were powered from the same hydraulic reservoir ensuring that at any

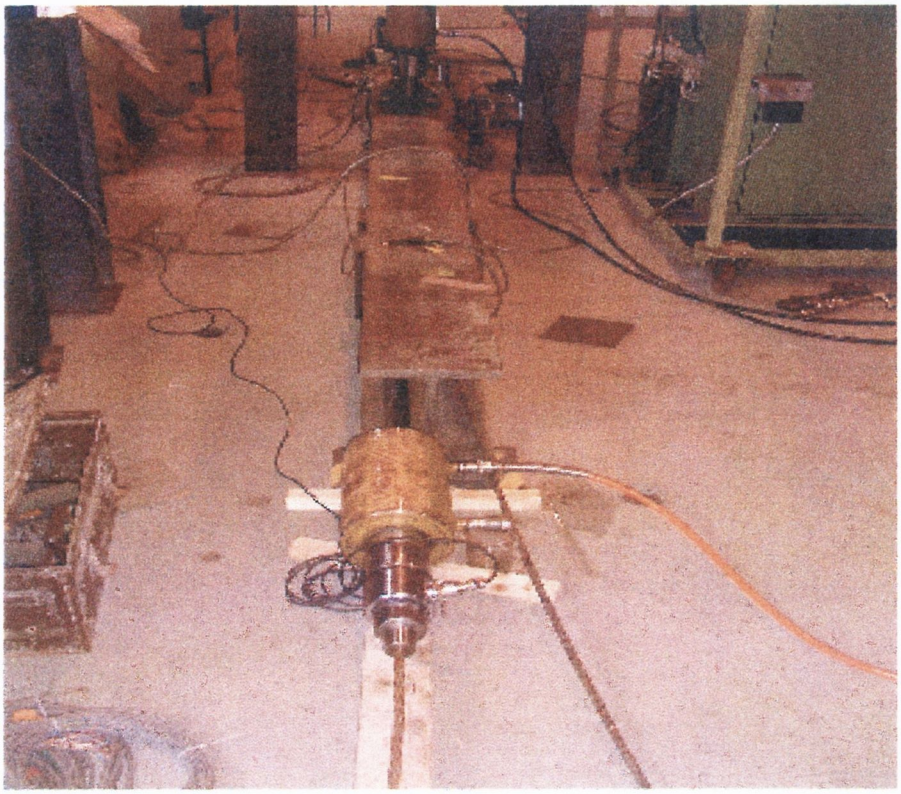

Figure 7.5: The reversible tendon jacking configuration.

stage during the jacking procedure, the pressure, and thus the force, in both jacks was the same (see figure 7.6). The flow in the hydraulic pipes could be alternated in either direction to control the direction of travel in both of the hydraulic jacks. As the barrel and wedge clamps were placed on the portion of tendon outside the jacks (that is, not lying between the jack and the beam), as in the case for conventional jacking methods, this allowed the tendons to be safely de-stressed as the jacks were retracted.

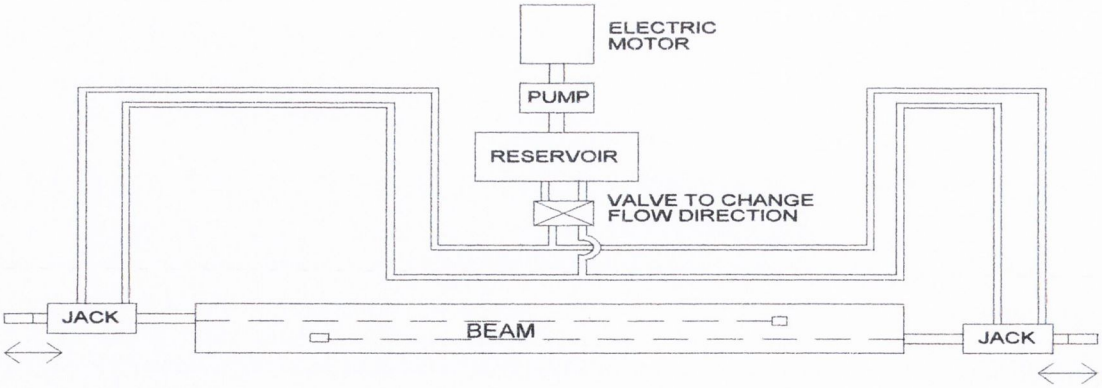

Figure 7.6: Schematic plan view of jacking system used to stress and de-stress tendons.

7.4 Central concentrated beam loading, beam supports and data logging

The simple supports were fabricated using 50mm diameter solid mild steel bars that were 350mm long and welded to a 400mm square, 25mm thick plate. The simple supports were placed on the heavily reinforced concrete floor of the test hall to give a clear span of 5950mm. The beam placed on the simple supports gave a clearance from the under side of the lower flange to the laboratory floor of 75mm. This clearance was adequate as the results of the FE analysis gave an expected maximum deflection of 10mm at mid-span.

The central concentrated load was applied via a hydraulic jack that was powered by a hydraulic pressure system independent of that for the tendon jacks. The jack that applied the central concentrated load was fixed to a loading frame located at the mid-span of the beam. The loading frame consisted of a cross-beam bolted to two vertical struts at either side of the beam, standing 1.2m apart from centre to centre. The vertical struts were 1.4m high and were 254x254x73kg/m U.C.s. The cross beam consisted of two deep channel sections that were 432x102x65kg/m in size. The channels were welded "back to back" with a space between them of 60mm to allow two 50mm diameter high tensile solid threaded bar (Macalloy bars) to pass through at either end of the cross-beam. The high tensile bars were passed through the 900mm deep laboratory floor, via prefabricated holes, and anchored to the slab soffit. The load jack for the concentrated load was fixed to the cross-beam of the loading yoke which allowed the jack to apply the downward vertical load. Figures 7.7 and 7.8 show the configuration of the loading frame and the loading frame in operation in the laboratory respectively.

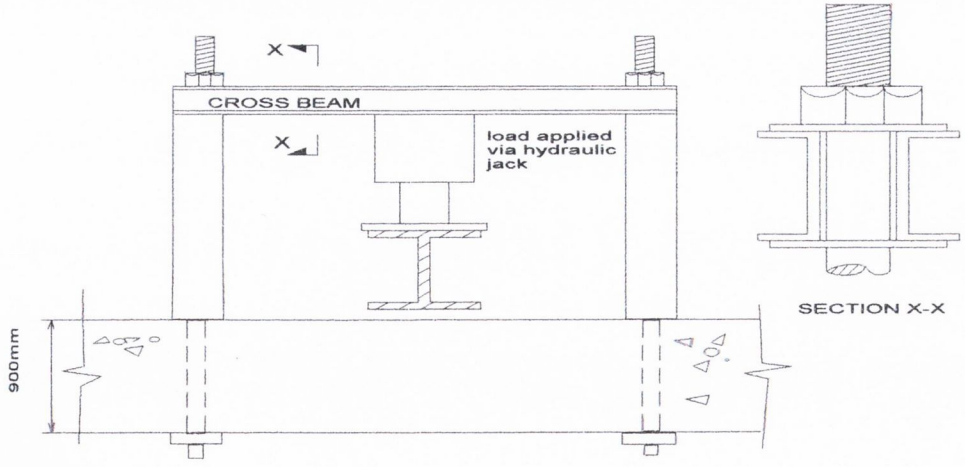

Figure 7.7: loading arrangement for central concentrated load (not to scale).

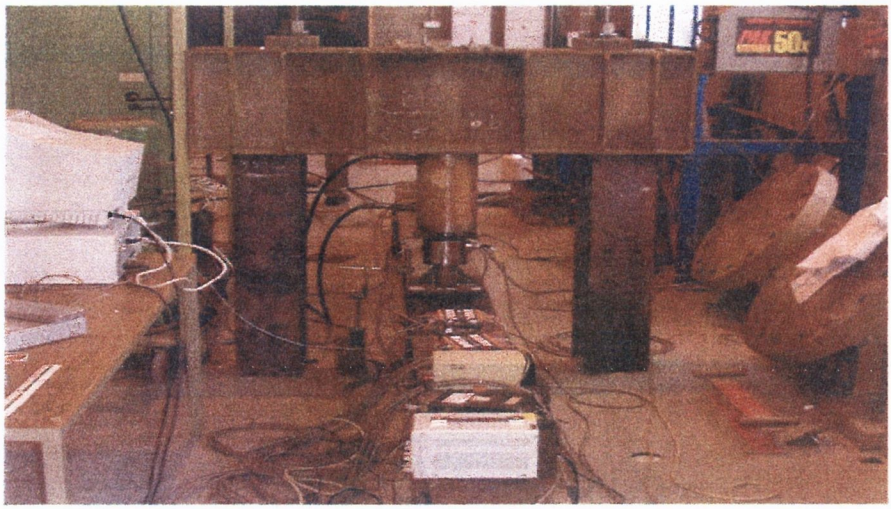

Figure 7.8: Photograph of the loading frame employed for the test beam

7.4.1 Strain and deflection monitoring apparatus

Quarter bridge strain gauges were used to monitor the strains at prescribed locations on the beam. Figure 7.9 shows a diagram of the test beam with the location of the strain gauges numbered 1 to 12. Strain gauges 13-16 were fitted to the tendon sleeves.

A pair of strain gauges was placed at either side of the location of application of the counter moments, with one of each pair on the upper surface of the upper flange (gauges 1 and 3) and the other on the lower face of each flange (gauges 2 and 4). These gauges were placed to monitor if the beam transmitted the counter moments to the beam. In theory, a finite point of application of counter moment is assumed when calculating the moment in the optimised beam, as discussed in chapter 3. Stress contours in the FE analysis suggested that, at the application of a counter moment, the transition from positive to negative bending occurred over a length of the order of 0.4m – 0.6m, depending on the magnitude of counter moment applied. Strain gauges were also placed on the web of the beam at the neutral axis at mid-span (gauge 6) and between the central concentrated load and support. Four strain gauges (9-12) were located on the flnages at mid-span. Two each were located near the outer edge of the lower face of the lower and upper flanges.

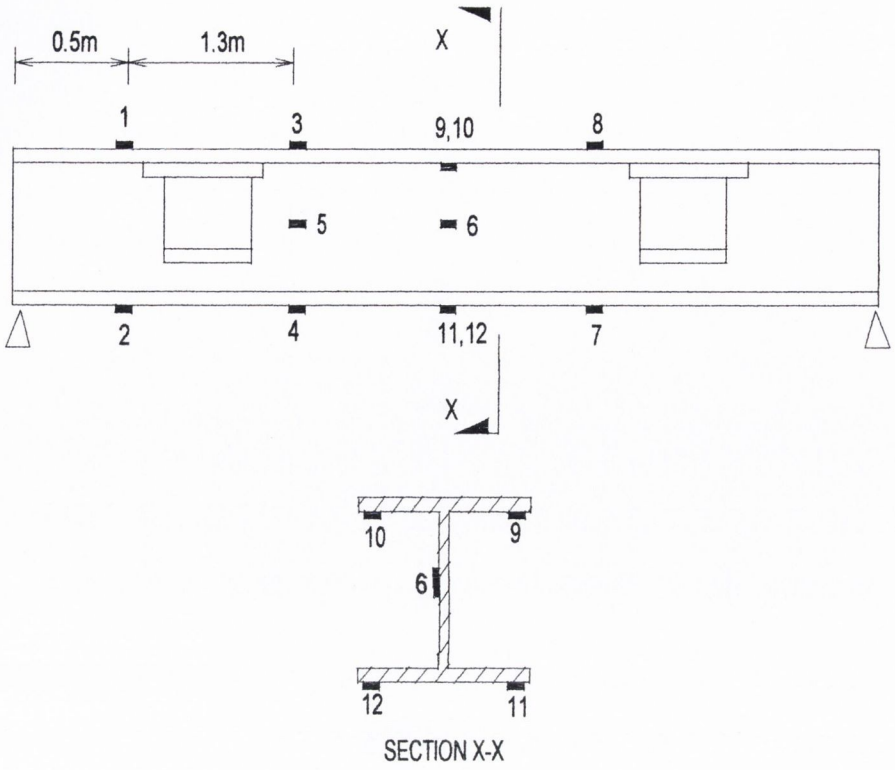

Figure 7.9: The location of the quarter-bridge strain gauges on the test beam

As a check for symmetry and consistency, two strain gauges were "mirrored" about the centre of the beam at the location of the opposite counter moment lever (gauges 7 and 8). It was necessary to place the latter strain gauges underneath the top flange because the hydraulic jack that applied the central concentrated load required a spreader plate to be placed on the upper face of the upper flange, to prevent high local stresses when the loading was applied. When plotting the stress diagrams at mid-span, the readings for the strain gauges located on the lower face of the upper flange were used to calculate the strains on the upper face of the upper flange (using similar triangles).

The tendon sleeves discussed earlier in this chapter also had strain gauges placed on them. These strain gauges (13-16) were used to monitor the force in each tendon and especially to detect tendon force "take-up" when the central concentrated load is applied. The term take-up here refers to the increase in tendon force, and thus counter-moment, when the central concentrated load is applied.

The readings from the load cells placed at the end of each tendon were compared with the readings of the strain gauges located on the tendon sleeves. The strains were recorded using a data logging software (System 5000) which has provision for deflection recording also. An LVDT was used to measure the deflection at mid-span. The logging system can measure at prescribed time intervals and a setting of 10 readings per second was employed.

7.5 Laboratory Testing

A testing regime was set out for the test beam, with the horizontal tendon configuration discussed in chapter 4, as follows:

Neutral test

A central concentrated load is applied with no tendons attached to the beam.

- Passive test

  A central concentrated load is applied to the beam with the tendons passively engaged

- Active test

  A central concentrated load is applied to the beam with the tendons actively engaged.

7.5.1 Neutral beam test

The function of this control test was to provide a baseline of results to compare with subsequent testing. This test was carried out with no tendons in place and was also used to verify the results of the FE analysis for this configuration. Hand calculations of the deflection of the 6m span test beam (with a central concentrated load of 100kN) predicted a deflection of 9.5mm at the mid-span of the beam. The results of the FE analysis predicted a deflection of 9.2mm at the mid-span, which suggested that the tendon levers and stiffeners might have a slight effect on the overall stiffness of the beam.

The measured maximum deflection during the test was at the mid-span and was 9.5mm. The deflection in this test was used to estimate the value of the Young's modulus of the beam (shear deformations were neglected) and was calculated as 208.5GPa (see appendix I). The deflection predicted from hand calculations and FE analysis were derived using a Young's modulus value of 210.0GPa. The revised value of 208.5Gpa was used to carry out an FE analysis, which yielded a mid-span deflection of 9.5mm.

The Young's modulus value of 208.5GPa extracted from this test was used to calculate the stresses from the measured strains in the beam for the laboratory testing outlined in this chapter.

7.5.2 Passive test

This test involved attaching the tendons to the beam with the barrel and wedge grips, the tendon sleeves, and the hydraulic jacks in place, as discussed earlier in this chapter. The purpose of this test was to establish the magnitude of force induced in the tendons upon the application of a 100kN central concentrated load. It was necessary to first apply a "seating" force to the tendons (of the order of 50kN in each tendon) owing to the barrel and wedge mechanism. The barrel and wedge grips needed to be tightened onto the tendons to ensure that no slippage, and thus no loss of tension force, would occur when trying to determine the magnitude of force taken up by the tendons upon the application of the central concentrated load. With the barrel and wedge locking mechanism in place (that is, when, after some 10 minutes, no reduction in the tendon forces was noticed) the seating forces were removed.

With the slack taken up on the tendons, any further increment in tendon force would register on the load cells placed on each tendon. The beam axial forces were measured from the stress diagrams at the mid-span section. The total stress diagram was first calculated and then the component bending and axial stress diagrams were deduced. The mid-span stress diagrams were derived from the strain gauges located on the lower face of the lower flange and the lower face of the upper flange, as discussed earlier. Hence, an

adjustment was made to calculate the stresses at the upper face of the upper flange. Table 7.1 shows a table of measured strains at the locations of the gauges numbered in figure 7.9

It can be seen in table 7.1 that the readings in strain gauges 1 and 2 have approximately the same absolute value of 76 microstrain, as expected, to give a stress of 15.4MPa. The stress is due to a 25kNm bending moment, with no axial force present outside the zone of application of the counter-moments. Little difference exists between the absolute value of the readings of the strain gauges 3 and 4 as only a small tendon force was induced with this tendon configuration. This will be discussed later in this chapter. Similarly, for strain gauge readings 7 and 8, the bending moment and small axial force present produced readings with little difference in the absolute values. There is good correspondence between gauges 3 and 8 and 4 and 7, as would be expected. The readings of strain gauges 5 and 6 were close to zero and again are what would be expected with a small axial force present (<11kN), given both strain gauges are located on the neutral axis.

Figure 7.10 shows the mid-span stress diagrams as deduced from stresses measured in the passive test. The average measured strain from strain gauges 9 and 10 was -443$\mu\varepsilon$ (compressive strain) in the upper flange, to give a stress of –92.5MPa and the average strains from gauges 11 and 12 was +440$\mu\varepsilon$ (tensile strain) in the lower flange to give a stress of +91.2MPa.

The results of the testing showed that, when a 100kN central concentrated load was applied, a tendon tensile force of approximately 11kN was induced in the tendons. A plot of the 100kN central concentrated load against the tensile force induced in the tendons is shown in figure 7.11.

Strain gauge no.	1	2	3	4	5	6	7	8	9	10	11	12
Reading (microstrain)	-76	75	-184	179	-3	-4	177	-183	-441	-446	438	442

Table 7.1: The measured strains on test beam with a 100kN central concentrated load and tendons passively engaged.

The results of this test demonstrated that this particular tendon configuration was not efficient. When applying counter moments to improve beam performance, the more "self" counter moment that can be applied (that is, counter moment induced due to an increase in tendon force upon application of a given loading), the greater will be the efficiency of the beam in question. Nonetheless, it was decided to continue with the testing regime and to consider later a more efficient tendon configuration with overall member depth still a constraint.

Strain gauges 3 and 4 to the right of the tendon levers had recorded strains of -184$\mu\varepsilon$ and +179$\mu\varepsilon$, which yield stresses of -38.5MPa and +37.3MPa respectively. Figure 7.12 shows the stress diagram at this section, together with the component stress diagrams. Strain gauge 8, which mirrored strain gauge 3 about the centre-line of the beam in figure 7.9, had a recorded strain of -183$\mu\varepsilon$ giving a stress of -38.5MPa and strain gauge 7, which mirrored strain 4, had a recorded strain of +177$\mu\varepsilon$ giving a stress of 37.3MPa.

It can be seen from figure 7.12 that little tendon force is induced and, thus, very little counter moment is applied with the horizontal tendon configuration. The beam overall depth has been kept to a minimum (that is, the tendons and levers are kept within the

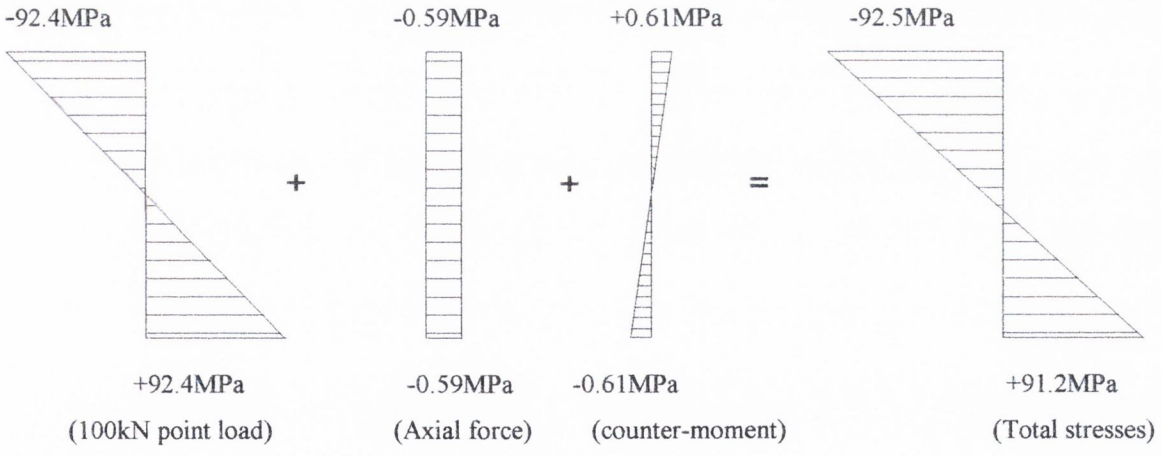

Figure 7.10: The mid-span stresses due to a 100kN central concentrated load with tendons passively engaged.

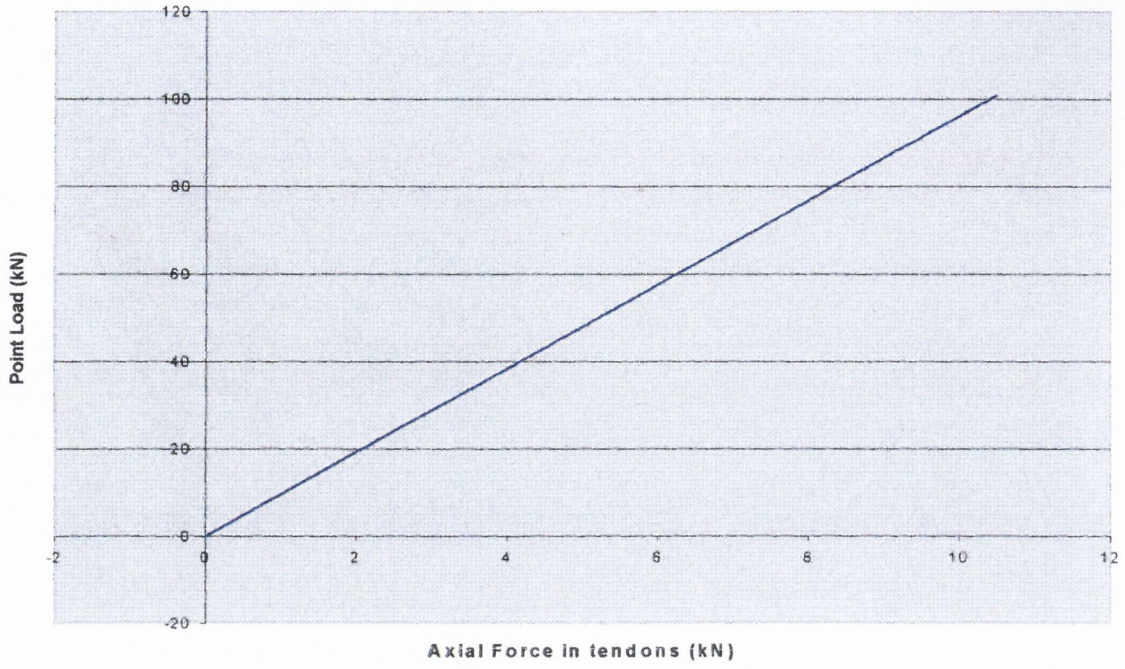

Figure 7.11: A plot of tendon force increase with respect to central concentrated load application for passive test (3000 readings at 10 per second).

flanges), and the price being paid for this is that practically all of the tendon force required to apply the optimum counter moments will have to be applied prior to loading. The constraint to applying pre-loaded counter moment is the hogging capacity of the beam.

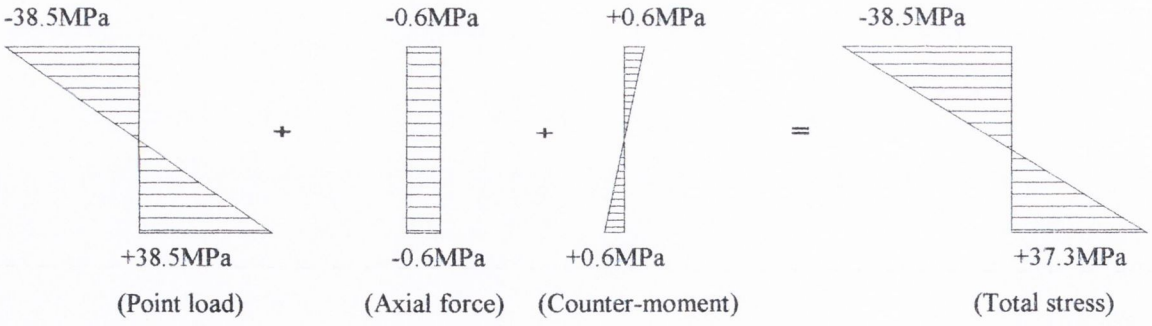

Figure 7.12: Figure showing section stresses at the location of strain gages 3 and 4 in passive test.

Figure 7.13 shows the deflection response of the test beam in the passive test as the 100kN central concentrated load was applied. There is a linear relationship between central concentrated load and deflection, as expected. The maximum deflection recorded at the mid-span of the beam in the passive test was 8.8mm. The FE analysis of this test yielded a mid-span deflection 9.2mm, which was within 4.5% of the predicted value.

If the increase in tendon force due to the application of the central concentrated load had been greater, the downward deflection would have been less, due to the hogging effect of the induced counter-moments. Were a pre-loaded tendon force to be applied, it would cause an upward pre-camber in the beam but does not reduce the gross beam downward displacement due to a given loading. However, the net final deflection will be less in the active test.

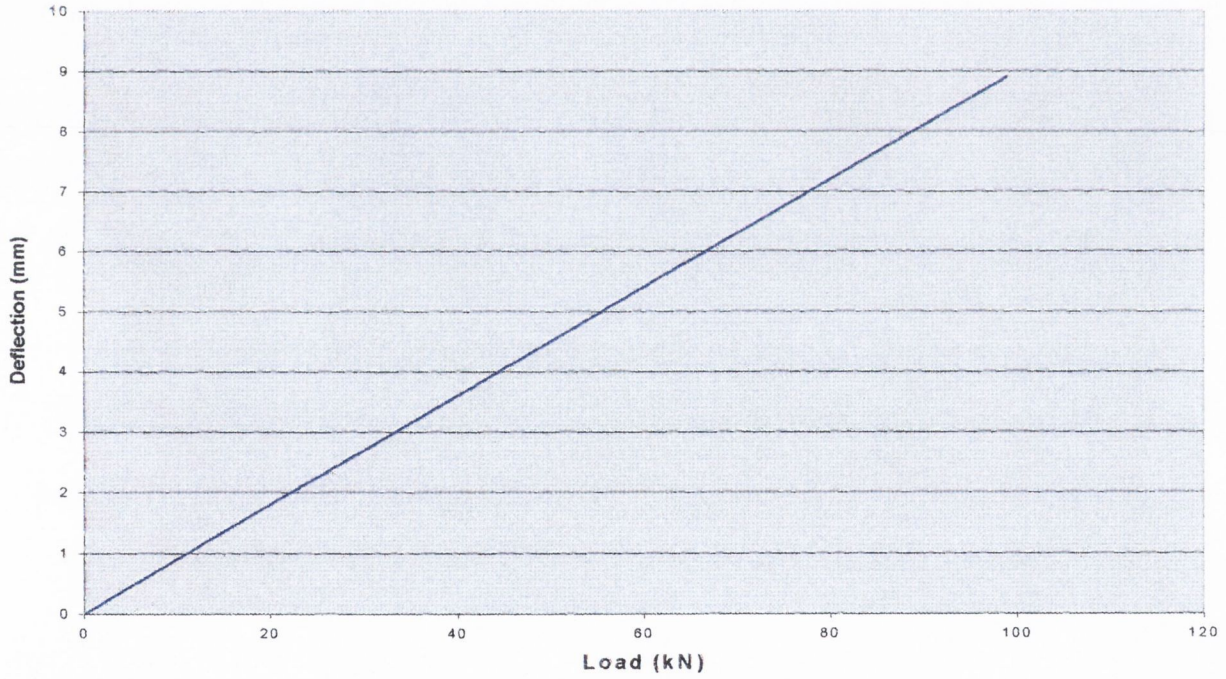

Figure 7.13: The linear relationship between load and deflection for the passive test, with a 100kN central concentrated load applied.

7.5.3 Active tests

The next type of test involved actively engaging the tendons to a prescribed overall tendon force prior to applying a central concentrated load. The passive testing established that practically all of the required counter moment, with the current tendon configuration, must be applied prior to loading the test-beam. As discussed earlier, the two super-strand tendons could only apply a total tendon force of 360kN and this was the maximum active tendon force that could be applied throughout the active testing regime. There were two types of active testing, namely, a general active test and an optimum active test.

Active test with no central concentrated load applied.

This laboratory test was carried out to investigate the magnitude of the applied pre-loaded counter moment that arises from applying a total tendon force of 300kN. The tendon force was restricted to this value so as allow ample additional tendon force capacity (the expected value was 11kN based on the passive test with a 100kN load) when a 100kN central concentrated load was applied. With the tendon jacking system set up as described earlier, the tendons were tensioned up to this tendon force and the resulting applied counter moment was deduced (from the strain readings) to be 29.8kNm. The maximum upward deflection was 2.1mm. The maximum resulting stress of 32.6MPa was in the lower flange at mid-span of the beam compared to the upper flange stress of 0.6MPa. The upward deflection of the beam was linear with respect to tendon force. Figure 7.14 shows the mid-span stress diagrams.

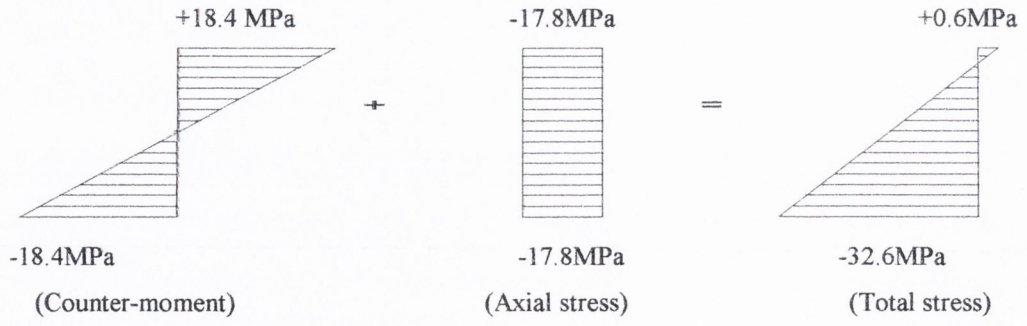

Figure 7.14: The mid-span section component stresses with 300kN tendon force and no loading

Active test with a 100kN central concentrated load

This test involved applying a 100kN central concentrated load to the beam while applying as much counter moment as possible within the allowed range of total tendon force (360kN). This test was carried out to observe the improvement that could be achieved in the bending moment diagram with the counter moments and central loading applied to the test beam, as compared with that of the bending moment diagram of the original beam with the (same) central concentrated load only. The test was also carried out to examine the increase in tendon force due to the application of the 100kN central load following the application of a pre-tensioned tendon force of 300kN. It was also necessary to establish whether the increase in tendon force due to the loading observed in the passive test (that is, 11kN), was a function of the initial pre-stressed tendon force or whether the process was linear.

The increase in tendon force during the test beam loading was carefully monitored in the unlikely event that the tendons would exceed the recommended safe working stresses (that is, 80% of characteristic breaking force of 265kN per tendon). The FE analysis had predicted that, for this test beam and tendon configuration, the deflection was linear (that is, an equal increment of force produced an equal increment of deflection).

The plot in figure 7.15 shows the negative deflection, or upward pre-camber, of 2.1mm due to the application of the tendon force and also the deflection arising from the subsequent application of a 100kN central concentrated point load. The beam was confirmed to behave linear elastically.

Figure 7.16 shows a comparison of the above plot (shifted along the x axis to the right for clarity) together with a plot of the beam in the neutral test with no tendons attached. It can be seen from the plot that, while in both tests the beam behaves linearly elastically, the rate of deflection, and thus the overall deflection, is reduced by the presence of the counter moments. In effect, the stiffness of the beam is enhanced by the tendons.

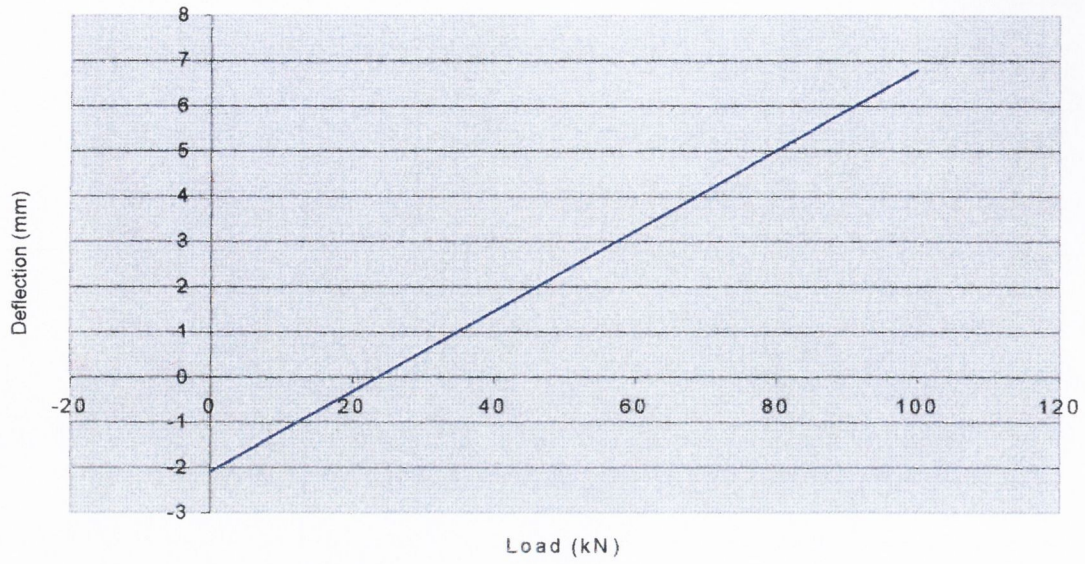

Figure 7.15: The initial pre-camber of 2.1mm in the unloaded beam and the final deflection of 6.8mm, with a linear response.

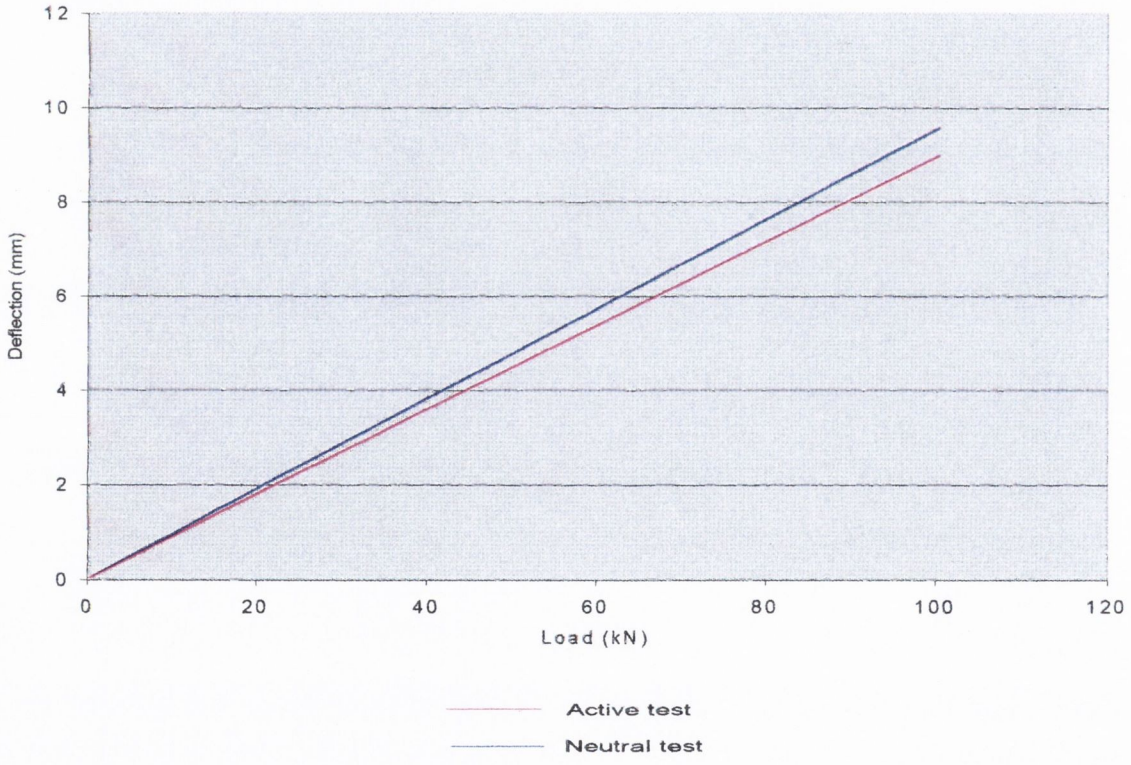

Figure 7.16: Figure shows the different rates of deflection of the test beam with and without counter moments under a 100kN central concentrated load.

The mid-span section stress component diagrams for the active test with a 300kN axial force in the beam and no central concentrated load applied are shown in figure 7.16, as derived from the measured strains. The applied counter moment is calculated as 29.8kNm. This was very close to the expected value, as the FE analysis of this test predicted a counter moment of 30.0kNm and the value recorded in the previous test with a tendon force of 300kN was also 29.8kN.

The stress component diagrams (also derived from the strain measurements) for the active test with a 100kN central concentrated load and a final tendon force of 311.4kN are shown in figure 7.17, for the mid-span section of the beam.

The stress diagrams demonstrate that, with the application of the concentrated load, the counter moment increases from 29.8kNm to 30.7kNm, which represents a 1.1% increase. The tendon configuration did not perform efficiently, in that, practically all (98.8%) of the required counter moment required would have to be applied at pre-loaded stage. The test demonstrated that the increase in tendon force of 11.4kN, when a 100kN central concentrated load was applied in this active test, was close to the original tendon force increase in the passive test (that is, 11.0kN).

The poor efficiency of the beam is due to a small tendon eccentricity (98mm) and the implications of this are as follows:

- When applying the pre-loaded counter moment, relatively large tendon forces must be applied, which give rise to high axial beam stresses between the points of application of the counter moments. The high compressive axial stresses reduce the available bending capacity which limit the maximum possible compressive bending stress (due to pre-loaded counter moment) that can be applied to the lower flange
- A low eccentricity implies that the beam will induce a small self-counter moment under loading. The greater the proportion of self-counter moment that can be applied the lesser the pre-loaded tendon force that needs be applied to achieve a required final post-loaded counter moment.

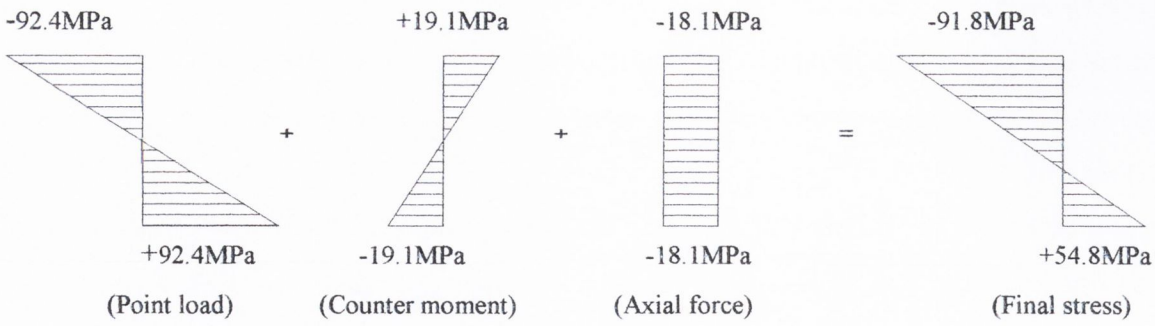

Figure 7.17: The mid-span section component stresses with 300kN tendon force and a 100kN central concentrated load applied.

The ideal is not to have to apply any pre-loaded tendon forces (that is, for the tendons to be passively engaged only) and for the beam's self-counter moment to be 100% of the required post-loaded optimum counter moment. This case would require a much greater tendon eccentricity (utilising levers) and is often not practical in building construction.

It was found that once the magnitude of the tendon force increase was established for a given loading, in this case 11.4kN for a 100kN central concentrated load, this additional increase could be subtracted from the final required tendon forces to give the initial pre-loading tendon forces. Figure 7.18 shows a plot of how the tendon force varies as the subsequent 100kN central concentrated load is applied to the beam.

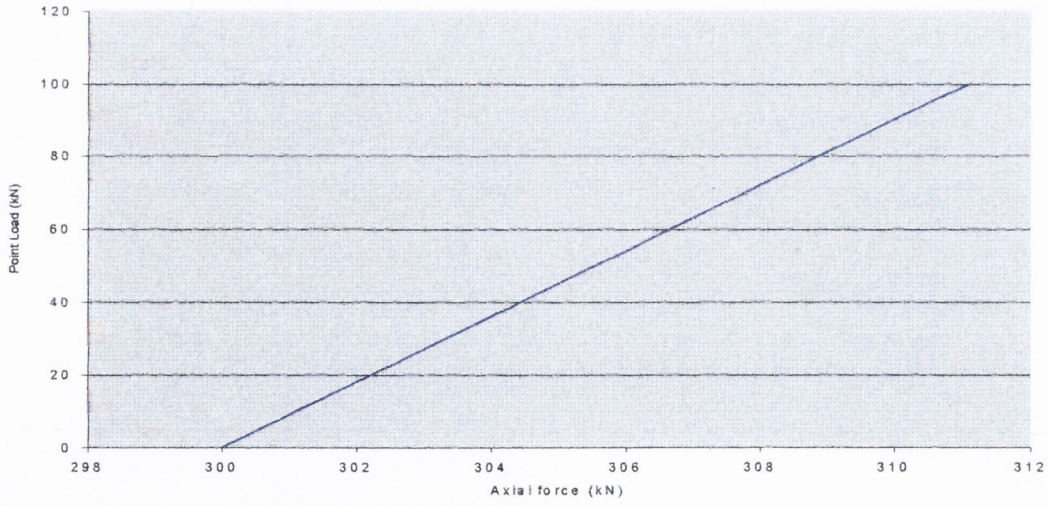

Figure 7.18: Plot of the tendon force increase in the active test when a 100kN central concentrated load is applied.

The slope of the line in this plot is the same as the slope of the line in the passive test case (that is, the rate of tendon force increase due to load application). Given that the slopes of the lines in each of the above cases is the same, the two tests demonstrated that the amount of tendon force increase induced by a given loading is independent of the initial pre-tension tendon forces, and the relationship is linear.

A tendon force of 300kN was recorded from the load cell readings on the hydraulic jacks. The tendon force of 300kN was found, form the strain gauges, to apply a counter moment of 30.12kNm. If the counter-moment is a product of Pe (where P is the tendon force and e is the tendon eccentricity), then, as P is known, e in this case must be 98mm. This calculation confirms exactly the predictions of the 3-D finite element study.

Figure 7.19 shows a plot of how the total counter-moment is achieved. The initial tendon force is applied to the beam, inducing a counter moment of 29.9kNm. Upon the application of the central concentrated load, an increase in that counter moment (to 31.8kNm) arises. The ideal path of counter-moment application with respect to central concentrated load has also been plotted on the above graph. Here 100% of the resulting

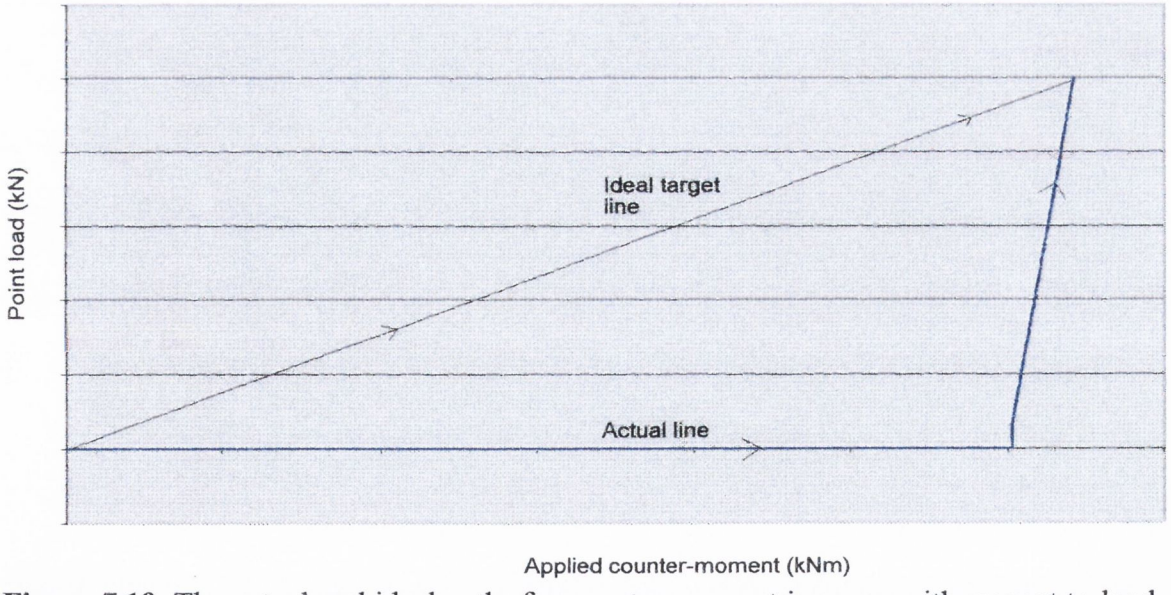

Figure 7.19: The actual and ideal paths for counter moment increase with respect to load increase.

counter-moment has been produced as a result of applying the central concentrated load and would remove the need for any pre-tension tendon forces. In this ideal case, the beam is totally self-regulating with regard to counter-moment.

Active test producing optimum shape bending moment diagram

The objective of this next test was not to investigate the maximum possible loading but, rather, to show, in principle, that it is possible to produce an optimised bending moment diagram shape (given the maximum available tendon force of 360kN) and, thus, to achieve the maximum counter moment of approximately 35kNm. The rate of increase of tendon force attributable to the central concentrated load application was found to be linear and this allowed the initial pre-loading tendon forces to be calculated. If 35kNm of counter moment is the maximum amount that can be applied to the beam, and if the counter moment (for one pair of counter moments applied) must be two-thirds the value of the original maximum bending moment for a simply supported beam with a central concentrated load, then the original maximum bending moment must have a value of 52.5kNm (that is, 3/2x35kNm). This implies that, for a 6m simply supported span, the central concentrated load must be 35kN in order to achieve the optimum bending moment diagram, with a maximum positive or negative value of 17.5kNm.

The central concentrated load for this test was, therefore, selected as 35kN and the increase in total tendon force due to the application of that load was calculated as 4.0kN. The pre-loaded applied counter moment was to be 34.4kNm (that is, 98.8% of 35kNm) because, as discussed earlier, practically all of the required counter moment had to be pre-applied to the beam, owing to the poor efficiency of the tendon configuration. The remainder of the required counter moment was provided by self-counter moment under a 35kN load.

In the test, the initial pre-loaded total tendon force was 355.4kN following which a central concentrated load of 35kN was applied. The total tendon force increased by 4.6kN to 360kN, which applied a post-loaded counter-moment of 35.1kNm. The section

strains for this test are shown in Table 7.2, from which the section stresses and, thus, the final bending moment diagram were produced. The final mid-span deflection was 1.2mm (compared to an un-strengthened deflection of 3.2mm, representing an improvement of more than 265%).

The test demonstrated that the "post loaded" optimum bending moment diagram was achievable with this tendon configuration and is shown in figure 7.20. However, it is recognised that the optimum bending moment diagram referred to here is the typical five-peaked diagram, which was obtained with a reduced load, which was limited by the maximum amount of counter-moment that could be applied due to a limitation in the tendon capacity. Clearly if the tendon capacity was raised, it would be possible to apply much higher counter-moments and, hence, higher concentrated loads for this "optimum" bending moment diagram.

The maximum stress resulting in the beam was at the pre-loaded stage and was a compressive stress of -42.8MPa with the total tendon force of 351.8kN applying a counter-moment of 34.1kNm. The highest stress resulting in the post-loaded stage was –31.8MPa with a central concentrated load of 35kN applied.

FE analysis showed that the beam could only have a relatively low improvement in load capacity, of the order of less than 2%, due to the low effective tendon eccentricity. Large tendon forces must be applied in order to apply the counter moments required for beam improvement, which, with this tendon configuration, take up almost 50% of the beam stress capacity.

Strain gauge no.	1	2	3	4	5	6	7	8	9	10	11	12
Reading (microstrain)	-53	51	-48	-156	-103	-101	-153	-47	-152	-156	-51	-49

Table 7.2: Strain gauge reading for the optimum shape bending moment diagram test. The locations of the strain gauges are given in figure 7.9.

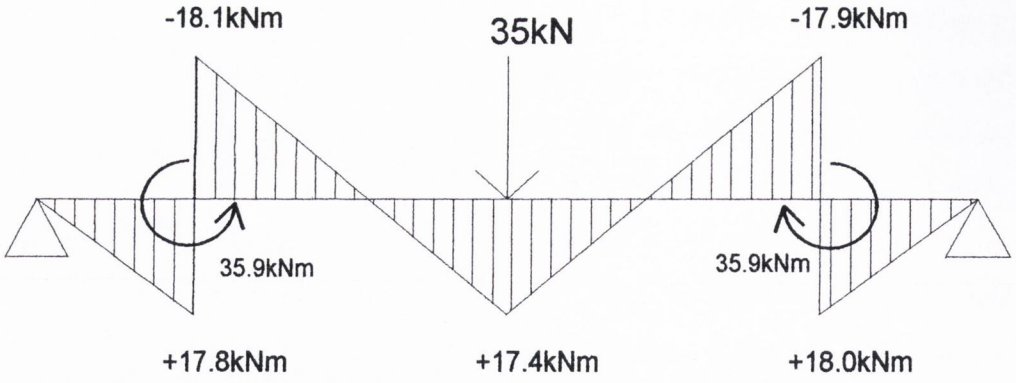

Figure 7.20: The optimum five-peaked shape bending moment diagram with a 35.kN central concentrated load applied.

The testing demonstrated that the counter-moments can be induced in the beam over a narrow range about the anchor points attached to the beam underside.

Greater tendon eccentricities will result in less P_i being required to apply given pre-loaded counter moments, otherwise P_i uses up a large portion of the beams' capacity. The testing demonstrated that the concept of using counter-moments to reduce bending moment is valid. A second configuration tested, which is more efficient than the first, will now be discussed.

7.6 Laboratory testing with a revised lower horizontal tendon configuration

Analyses carried out on the beam with the lower tendon configuration have indicated that this beam is more efficient in applying self-counter moment. The beam tested earlier had a tendon force increase to applied central concentrated load ratio, r_t, of 0.102kN/kN. The theoretical analyses of the beam with the revised lower tendon configuration yielded a tendon force increase to applied central concentrated load ratio of 0.525kN/kN. With this improved efficiency, more loading could be applied, in theory. However, no previous laboratory testing has been carried out on the beam with the lower tendon configuration and it was decided, therefore, to carry out both passive and active tests in the laboratory with a maximum central concentrated load of 100kN. This maximum load was used to allow a large scope for additional tendon force without overstressing the test beam.

7.6.1 Test beam and tendon design and fabrication

It was decided to use the beam that been tested previously in the laboratory, except with the tendons now attached to the underside of the lower flange via thick-wall tubes. The overall beam capacity had been checked previously with the earlier tendon configuration. It was established in the earlier neutral laboratory test that the levers had no significant effect on the flexural behaviour of the beam. The tendon levers welded to the upper flange were, therefore, left in place. Local analyses of the thick-wall tubes, welded to the underside of the lower flange at the optimum counter moment location, had shown that no additional stiffening was required in this area (see chapter 4).

7.6.2 Thick-wall tube design

The axial capacity of the thick-wall tubes had been checked earlier and, as the same tendon forces were to be used in the second testing regime, it was decided to use the same length of tube with the lower tendon configuration (that is, 300mm long thick-wall tube). Two runs of 12mm fillet welds, 300mm long, were provided each side of each tube. Figure 7.21 shows the beam section with the tendon thick-wall tubes fixed to the lower flange. This provided a shear transmission capacity, between the tube and the lower face

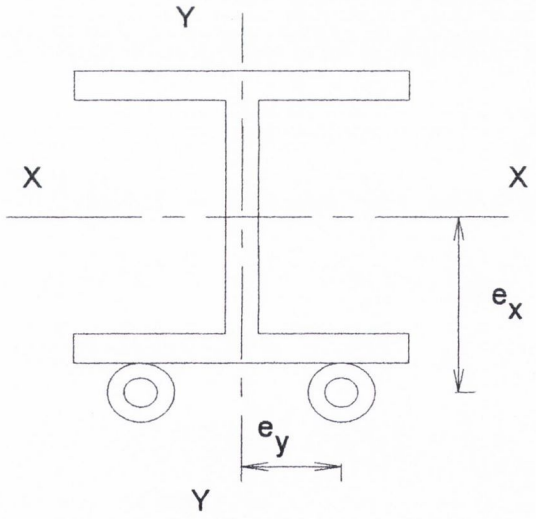

Figure 7.21: The tendon eccentricities from the section "X-X " and "Y-Y" axes.

of the lower flange, of 510kN per tube assuming a shear weld strength of 115MPa (B.S. 639). With the 60mm outside diameter tubes welded to the underside of the lower flange, a tendon eccentricity, e_x, of 170mm was achieved. The eccentricity, e_y, from the vertical (Y-Y) axis of the beam was kept to a minimum distance of 50mm. This allowed a 12mm fillet weld to pass along the inside edge of the thick-wall tube. This distance was minimised as a precautionary measure against differential tendon force giving rise to undesirable bending moments about the Y-Y axis. It was considered unlikely that the method of jacking would give rise to significant differential tendon forces.

7.6.3 Tendon configuration and jacking

The same hydraulic system was employed with this tendon configuration as with the previous configuration (see figure 7.22). Therefore, as discussed in section 7.3 no differential tendon forces would arise.

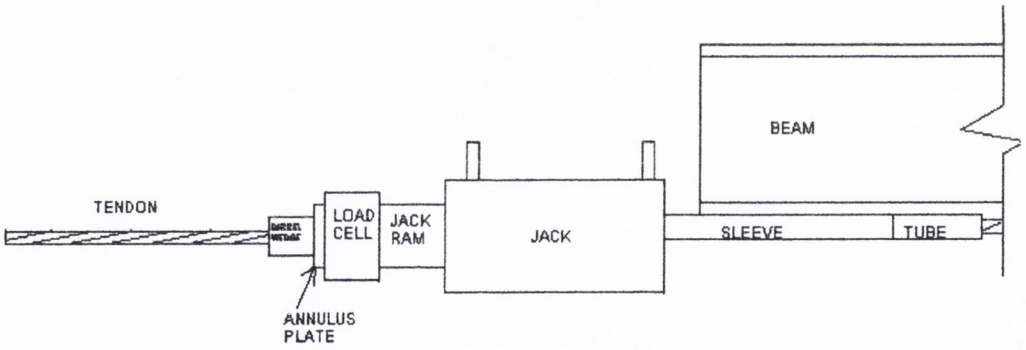

Figure7.22: The hydraulic jacking arrangement for the revised tendon configuration.

7.6.4 Monitoring apparatus

The strain gauges were located as in the earlier testing programme, numbered 1-12 (see figure 7.9). The tendon sleeves had two strain gauges fitted to each and were numbered 13-16.

It was decided not to remove the external stiffeners welded to the outer edges of the upper and lower flanges for the last test series, but to cut them at mid-height. A "tell-tale" gauge was place on one cut stiffener at each end of the test beam. The tell-tale gauges were used to monitor the displacement between the upper and lower halves of the cut stiffeners. It was suggested that the measured displacement, if any, could be used to calculate the forces which would have been induced in the original uncut stiffeners, were the beam to have a counter moment and central concentrated load applied.

7.6.5 Beam supports and central concentrated loading

The 6m spanning beam was supported, as in the last testing regime, on a 50mm diameter solid bar welded to 400mm square 25mm thick plated placed on the laboratory floor at either end of the beam. These supports provided enough clearance for the expected beam deflection at mid-span and also for strain gauge cables to pass under the beam (that is, the 10mm diameter cables could pass under the beam to the strain gauges fixed on the lower flange).

The central concentrated load was applied via the same hydraulic jack and loading rig described with the earlier tendon configuration testing. The beam loading hydraulic jack had an independent hydraulic system and could have no effect on the pressures present, if any, on the tendon jacking system.

7.7 Laboratory testing

A testing regime was set out for the revised beam with the lower tendon configuration. The results of this testing were used in a comparison with the FE analysis described in the last chapter. The testing regime was as follows:

- Neutral beam test
- Passive test with a 100kN central concentrated load
- Active test with a 100kN central concentrated load
- Active test producing the optimum bending moment diagram
- Active test with optimum load for an applied counter moment of 61kNm

7.7.1 Neutral beam test

This test was carried out to establish whether the introduction of the thick wall tubes had any effect on the flexural behaviour of the beam. The data recorded from this test could also be compared with the results of the FE simulation of this test. A 100kN central concentrated load was applied with the thick-wall tubes attached to the underside of the lower flange and the tendons were not in place. The maximum deflection was 9.5mm and was recorded at the mid-span of the beam. This concurred with the previous passive test results reported in section 7.5.1. This test demonstrated that neither the addition of the thick-wall tubes nor the cutting of the outer stiffening plates had any reasonable effect on the beam deflection.

The two strain gauges placed on the top surface of the upper flange at mid-span (that is, strain gauges 9 and 10) yielded readings of -442$\mu\epsilon$ and -441$\mu\epsilon$ giving an average value of compressive stress of 92.1MPa. The lower flange strain gauges (strain gauges 11 and 12) gave readings of 440$\mu\epsilon$ and 443$\mu\epsilon$ giving an average value of tensile stress of 92.1MPa.

7.7.2 Passive test with a 100kN central concentrated load

This test involved placing the tendons on the beam, and passively engaging them and applying a central concentrated load of 100kN. The function of this test was to observe the increase in total tendon force when the concentrated load was applied. The data extracted from this test could be compared with the results of the simulated FE analysis of this test. It would also confirm the actual eccentricity of the new configuration.

A total tendon force increase of 52.8k N was observed with a 100kN central concentrated load applied (that is, 26.4kN/tendon). The maximum recorded strains were at the mid-span and were -434$\mu\varepsilon$ and -438$\mu\varepsilon$ in strain gauges 9 and 10 respectively, in the upper flange. These gauges yielded an average value of strain of -436$\mu\varepsilon$ to give a value of compressive stress of -91.1MPa in the upper flange. Similarly, the resulting strains in the lower flange were +402$\mu\varepsilon$ and +398$\mu\varepsilon$ in strain gauges 11 and 12 respectively, to give an average strain of +400$\mu\varepsilon$, which yielded a tensile stress in the lower flange of +83.4MPa. The value of Young's modulus assumed for this beam was, as discussed in chapter 4, 208.5GPa.

The resulting maximum stresses at mid-span are shown in figure 7.23 together with the component stresses. These stresses showed that an axial force of 52.8kN acted at the mid-portion of the beam (that is, between the points of application of the self-counter moment). The recorded strains in the thick-wall tendon sleeves were 77$\mu\epsilon$,+/-3$\mu\epsilon$. Knowing the cross-sectional area of the tubes allowed the compressive forces to be calculated as 26.4kN. A counter moment of 8.9kNm was determined with the axial force of 52.8kN present. This allowed the actual tendon eccentricity to be calculated as 0.17m, as predicted.

The maximum deflection was 8.9mm (that is, a downward deflection at the mid-span). When this deflection is compared with the neutral test beam deflection with the same 100kN central concentrated load, by superposition, this would indicate that a total pre-tension force of 53kN would produce an upward pre-camber of 0.6mm. Further laboratory testing would confirm this by linear interpolation, as it was found that deflection was linear with respect to load application.

The simulated FE analysis for this laboratory test predicted a total tendon force increase of 56kN when a 100kN central concentrated load was applied. The predicted deflection was an 8.6mm downward deflection at mid-span. The FE predictions compared closely to the actual results (8.9mm) achieved in the laboratory.

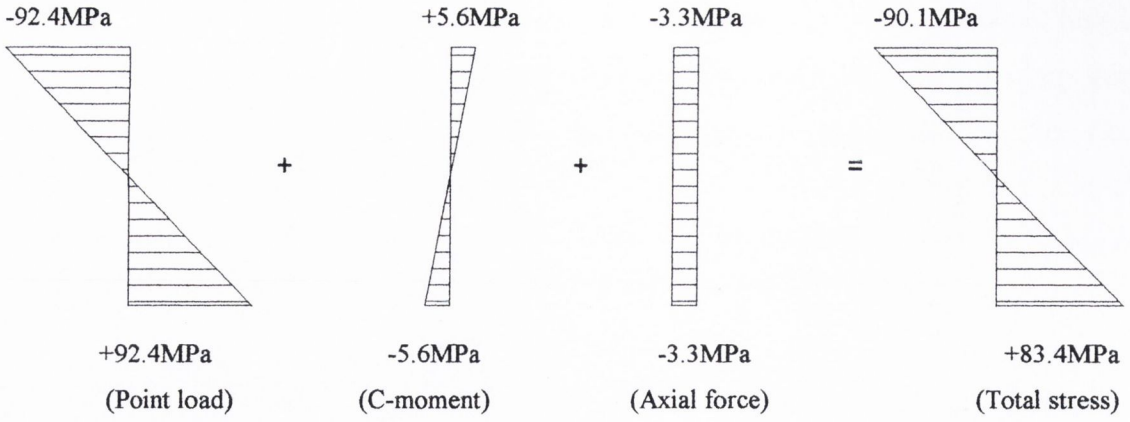

Figure 7.23: Mid-span stresses for the passive test with a 100kN central concentrated load applied on the new tendon configuration.

The resulting stresses at the mid-span section of the FE analysis were, again, good predictions of the stresses calculated from the strain gauge readings in the test. The mid-span section upper flange stress was predicted by the FE analysis as being -90.1MPa (compressive) and the test results yielded an upper flange mid-span section stress of -90.1MPa also. The lower mid-span section stress was predicted as being +83.7MPa (tensile) by the FE analysis and the test results yielded a lower mid-span section stress of 83.4MPa (that is, within 0.5%).

A plot of the beam axial force versus central concentrated load application and a plot of the measured self-counter moment versus the central concentrated load application are shown in figures 7.24 and 7.25 respectively. The central concentrated load was applied over a period of approximately 2 minutes and strain gauge readings were taken at a rate of 5 per second, giving approximately 300 points which are plotted on the graphs of the these figures.

The plots show the linear relationship between the measured tendon force increase and applied central concentrated load and similarly the linear relationship between self-counter moment and applied central concentrated load. From these figures, the rate of tendon force increase with respect to central concentrated load increase is 0.528kN/kN

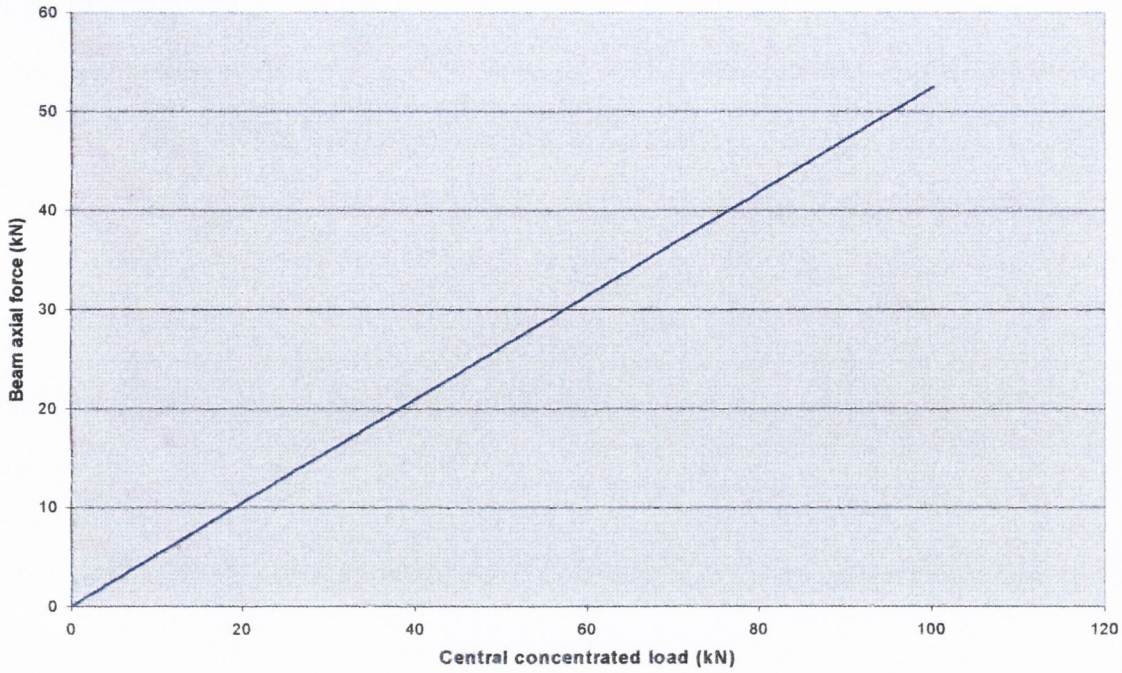

Figure 7.24: The increase in beam axial force as central concentrated load is applied for the passive test with a 100kN central concentrated load for the thick-wall tube tendon configuration.

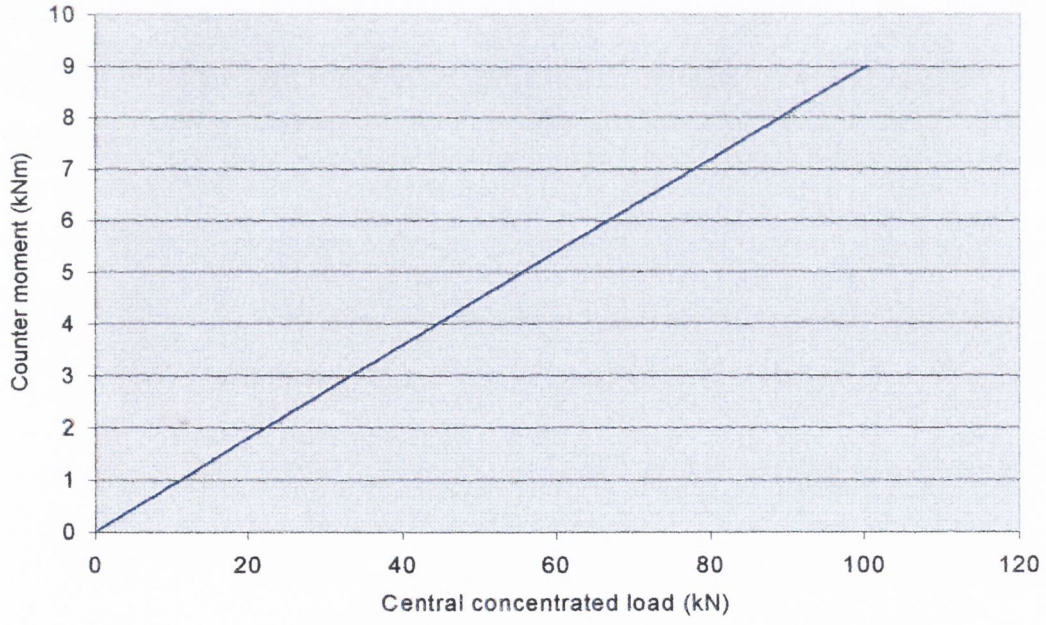

Figure 7.25: The increase in counter-moment application with respect to central concentrated load application for the passive test with a 100kN central concentrated load for the thick-wall tube tendon configuration.

and compares favourably with the predicted rate in section 5.12 (that is, 0.525kN/kN). This test confirmed that the rate of increase of tendon force with respect to central concentrated load increase is linear, irrespective of the magnitude of the tendon eccentricity from the beam section neutral axis.

7.7.3 Active testing

As with the active testing of the beam with the previous tendon configuration, the greatest counter moment that the two 15.7mm core diameter super strands could apply was employed (that is, a post-loaded total tendon force of 360kN). Having established the rate of total tendon force increase with respect to central concentrated load increase, the initial pre-loaded tension forces could be applied to the beam, as appropriate.

Active test with no central concentrated load

The function of this test was to establish the magnitude of counter moment that could be applied with a total tendon force of 360kN. The resulting axial beam force was 360kN, and the tendons applied a counter moment of 61kNm and the relationship was linear. The maximum beam stresses predicted from the FE analysis were at the mid-span section and were –59.2MPa in the lower flange and +16.4MPa in the upper flange. The maximum stresses recorded in this test at the mid-span were +16.3MPa (tensile) in the upper flange and –58.6MPa (compressive) in the lower flange, and were all within 1% error of the results yielded from the analysis. Figure 7.26 shows the total stress and component stress diagrams of the mid-span section.

The predicted values of deflection from the FE analysis was 4.2mm upwards pre-camber comparing well with the 4.1mm arising from this test.

In the previously discussed passive test, with a central concentrated load of 100kN applied, a downward deflection of 8.8mm was observed with a tendon force increase of 52.4kN.

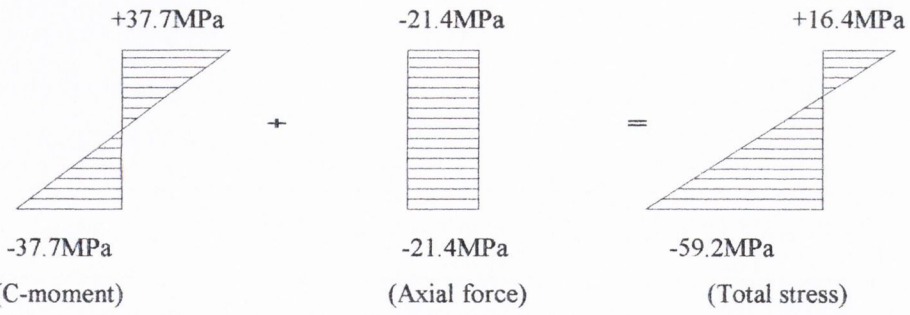

Figure 7.26: The mid-span section stresses of the active test with a tendon force of 360kN applying counter-moments of 61kNm for the lower tendon configuration.

Figure 7.27 shows plots of the deflection of the beam at mid span with respect to tendon force increase induced by central concentrated load application, and mid span deflection with respect to tendon force increase induced by hydraulic jack. Note the difference in the rate of deflection with respect to tendon force in each. The rates of deflection differ due to the loading patterns. The 8.8mm downward deflection is due to an applied point loading with some reduction due to the passively engaged tendons. The upward deflection is due solely to the tendon force increase applied by hydraulic jacking

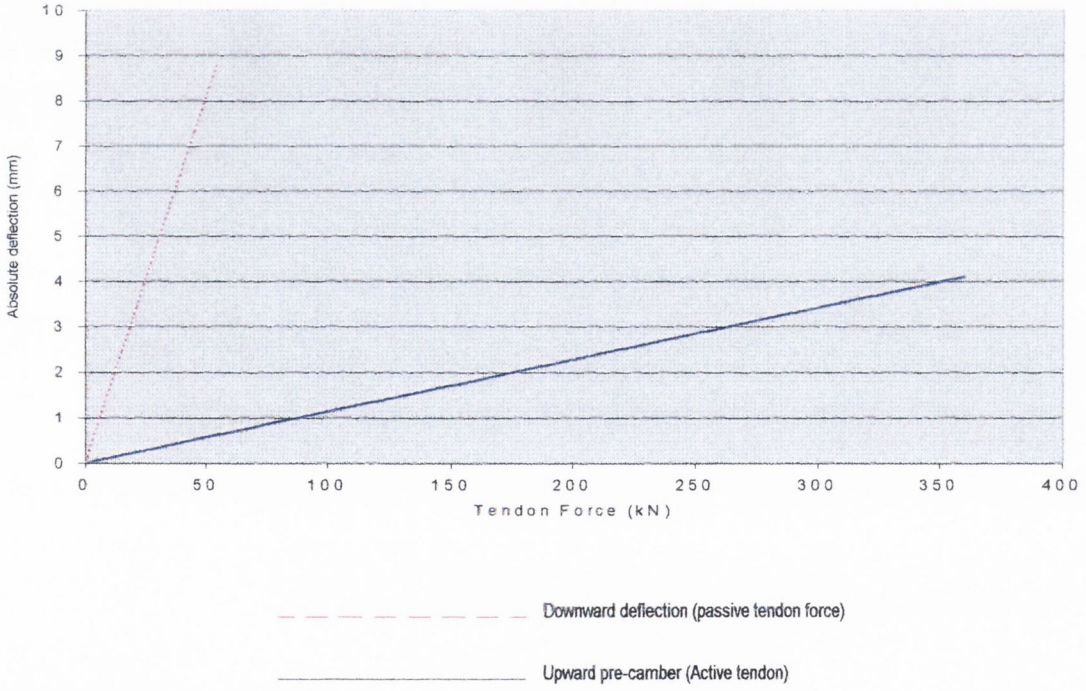

Figure 7.27: The rates of deflection for the passive and active test with a 100kN central concentrated load applied in each.

If equation 3.24 is applied to the beam with an applied load of 100kN this gives a final deflection, Δ, of 8.83mm. This value is within 0.3% error of the deflection measured in this test. Equation 3.24 indicates what improvement in deflection will exist, and the final deflection will depend on components γ_r and r_t (as determined by the tendon eccentricity, e) and P_i.

Active test with a 100kN central concentrated load

The objectives of this laboratory test was to investigate the tendon force increase when a 100kN central concentrated load was applied to the beam in conjunction with an initial pre-tension force applied to the tendons. The total tendon force increase, due to the application of a 100kN central concentrated load in the passive test, was measured to be 52.4kN. The final required post-loaded, or "target", tendon force with this test, was conservatively, 300kN.

This test could also confirm the results of the passive test with the 100kN central concentrated load. The passive test yielded a total tendon force increase of 53kN for the 100kN load. This yielded 247kN as the initial pre-loaded total tendon force. With this pre-loaded tendon force and the 100kN central concentrated load applied the final axial load present in the beam was, indeed, 300kN. The bending moment at mid-span was 98.4kNm and the applied counter moment was 50.8kNm. The FE analysis predicted a counter-moment of 50.9kNm with a 300kN tendon force present and no beam loading, which compares well with the test pre-loaded counter-moment.

This test demonstrated that the rate of change of tendon force with respect to an applied central concentrated load remains linear and proportional, irrespective of the initial pre-tension tendon force when compared with the 100kN passive test.

Figure 7.28 shows the initial total tendon force of 247kN and the rate of change of tendon force with respect to the central concentrated load of 100kN. The FE analysis predicted a final downward deflection of 8.1mm with a final tendon force of 360kN. If a linear

relationship is assumed between the tendon force and the upward pre-camber of the beam, and, if a tendon force of 360kN produces an upward deflection of 4.1 mm, then one would expect an upward pre-camber of 3.5mm for a tendon force of 300kN. Applying equation 3.24 for final mid-span deflection for an initial tendon force of 247kN and a post-loaded tendon force of 300kN (with an applied central concentrated load of 100kN) gives a predicted value of downward deflection of 6.4mm at the mid-span section. A maximum downward deflection of 6.4mm was recorded at the mid-span section.

The plot in figure 7.29 shows the deflection at mid-span versus tendon force. This plot is an amalgamation of the two types of deflection shown earlier. The first stage of deflection shows the upward pre-camber due to the initial pre-tension force of 247kN and the second stage is the application of the 100kN central concentrated load. Again, here the two different rates of deflection with regard to total tendon force can be seen. This is due to the two different loading conditions, giving rise to two different bending moment diagrams experienced by the beam.

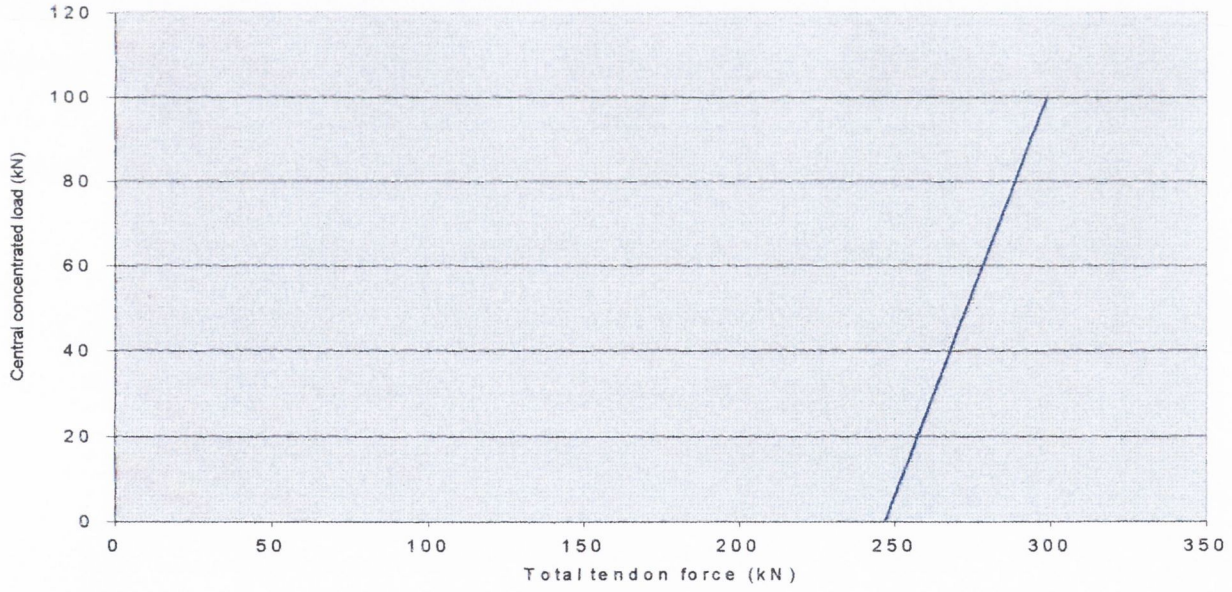

Figure 7.28: Plot of an initial pre-loaded tendon force of 247kN and a linear increase of tendon force to 304kN due to the application of a 100kN central concentrated load.

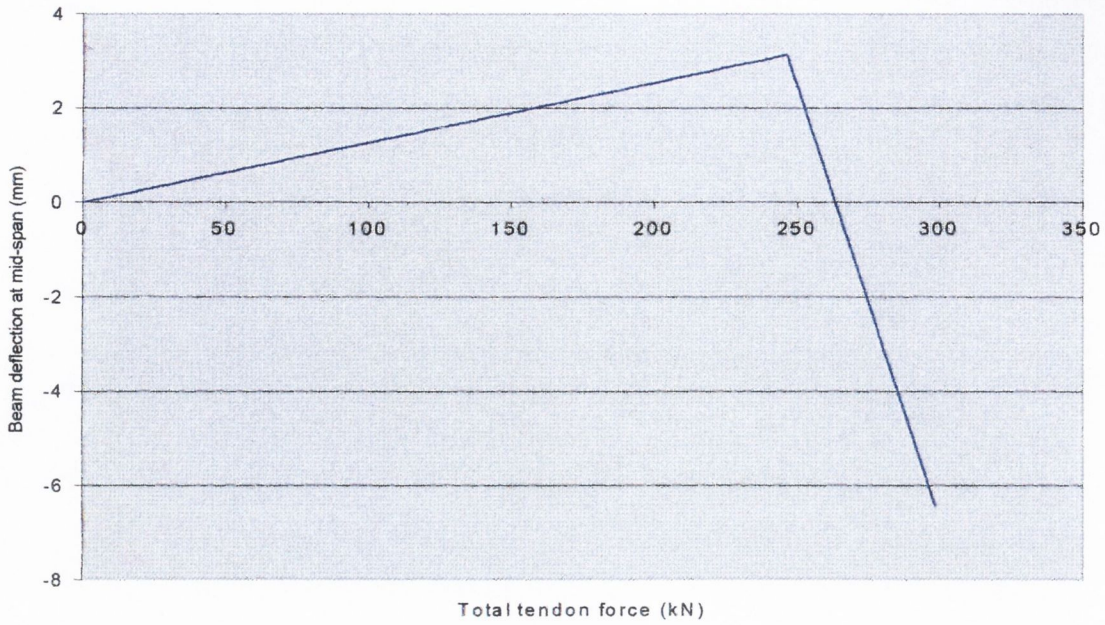

Figure 7.29: A plot of the initial pre-camber due to the pre-stressing and the downward deflection due to the application of the 100kN load.

The test also demonstrated that the rate of deflection of the beam with respect to tendon force increase is dependant on the method of tendon force application (i.e. whether by jacking or by central concentrated load application). The self-induced counter moment is preferable as the beam response is stiffer. This test was the second occasion in which the tendon sleeves were used to record the tendon forces due to load cell inconsistencies. It was confirmed that the calculated forces arising from the tendon thick-wall mild steel tubes were the same as the resulting beam axial forces. The rate of strain per unit force applied to the thick-wall tubes was calculated and used to adjust the tendon jacks to achieve the required tendon forces. Subsequent testing with the load cells were used to calibrate and confirm the strains corresponding to the required tendon forces.

7.8 Conclusions

Initial configuration

The passive tests demonstrated that the ratio r_t of tendon force increase to applied central concentrated load was linear. The testing also demonstrated that the amount of increase for a given applied central concentrated load was independent of the initial pre-loaded

total tendon forces. The active tests proved that the deflection of the beam was also linear with respect to central concentrated load application and was dependent on the amount of initial pre-loaded tendon forces.

It was found that in the active test the gross downward displacement was the same for a given central concentrated load as it was in the passive test, however, the final net downward deflection was dependent on the initial upward deflection due to the pre-loaded tendon forces. The second order effects are negligible as the relative displacement between the anchor points and mid-span is very small (that is, the anchor points deflect with the beam and, also, beam rotation occurs at the anchor points which further reduces mid-span deflection).

The testing confirmed the accuracy of results of the FE analysis, principally that the actual tendon eccentricity was lower than had been originally planned. The testing demonstrated the actual eccentricity was 98mm. It had been thought that extending the lever from the underside of the upper flange to as close as possible to the upper face of the lower flange would result in a tendon eccentricity greater than the above value.

The overall efficiency of the beam with the first tendon and lever configuration was poor with an actual load improvement (for a comparative load of 200kN) of less than 2% to that of the un-strengthened case and it was decided that a more efficient tendon configuration was required. Table 7.4 shows a summary of the test results for the initial configuration.

Case	Load	Final Tendon Force	Laboratory Testing	Laboratory Testing	Deflection
	(kN)	(kN)	Top Flange Stress (MPa) at mid-span	Lower Flange Stress (MPa) at mid-span	(mm)
Neutral	100	0	-92.8	92.8	9.5
Passive	100	11	-92.5	91.5	8.8
Active	0	300	0.6	-32.6	-2.1
Active	100	311.4	-91.6	54.8	6.8
Active (optimum)	35	360	-31.8	-10.8	1.2

Table 7.4: Summary of the test results of the beam with the original tendon configuration.

Revised tendon configuration

The results of the neutral beam test for the revised lower tendon configuration yielded a mid-span deflection of 9.45mm, which compares favourably to the predicted FE value of 9.4mm (that is, within 1%).

The passive test with a 100kN central concentrated load applied yielded a tendon force increase of 52.8kN with a final mid-span deflection of 8.9mm. The FE analysis predicted a tendon force increase of 54kN, which gave a difference within 2.4% between the predicted and test values. The predicted mid-span deflection of 8.6mm compares well to the test result and is within a 4% difference. The passive test confirmed that the predicted eccentricity of 170mm was accurate. The passive testing also confirmed that the relationship between tendon force increase and central concentrated load increase is linear and that the rate is 0.525kN/kN. This represents a substantial improvement on the original configuration. The configuration delivers much improved proportion of self-counter moment on loading (that is, 17% greater than with the previous tendon configuration for the same tendon cross-sectional area).

The active test with a 100kN central concentrated load and a 300kN tendon force yielded a final applied counter moment of 50.8kNm, which was within 0.5% of the predicted FE value of 50.9kNm. This prediction was interpolated from a linear chart of tendon force increase to counter moment application based on the results of the FE analyses of the revised tendon configuration. The tendon force was restricted to 300kN to allow a margin of safety with the tendon force increase due to the application of the 100kN central concentrated load. The test results demonstrated that the relationship between tendon force and applied counter moment was linear and that values could be interpolated with reasonable accuracy.

For the active test with a 100kN central concentrated load and an initial pre-tension force of 247kN, equation 3.24 predicted a final mid-span deflection of 6.34mm. The test mid-span deflection was 6.3mm, which was within a 0.5% difference and confirmed that this expression could be used to predict the mid-span deflection with reasonable accuracy.

Table 7.5 show a summary of the test results for the revised tendon configuration.

Case	Load	Final Tendon Force	Laboratory testing	Laboratory testing	Deflection
	(kN)	(kN)	Top Flange Stress (MPa) at mid-span	Lower Flange Stress (MPa) at mid-span	(mm)
Neutral	100	0	-92.1	92.1	9.5
Passive	100	56	-91.1	83.4	8.9
Active	0	360	16.3	58.6	-4.1
Active	100	300	-78.9	43.3	6.4

Table 7.5: Summary of test results of the beam with the revised lower tendon configuration.

The results of the testing verified the FE analysis predictions and demonstrated that further FE analyses for similar strengthened beams would predict accurate deflection, stresses and maximum loading. The testing confirmed the accuracy of the FE predicted tendon force increase and, thus, the r_t rate for both tendon eccentricities. The FE analysis also predicted a linear relationship between load and deflection which the testing also confirmed.

The revised tendon configuration had a significant increase in performance of self counter-moment application, with relatively little increase in overall member depth when compared to the previous tested configuration. The testing verified that counter-moments can be induced with pre-tensioned tendons and this method is a viable method for member strengthening with regard to both retrofit and new construction.

CHAPTER 8

CONCLUSIONS

8.1 Review

Previous research carried out by the author investigated the concept of optimum counter moment application (Maher, 1998). The theory outlined in chapter 3 was principally concerned with establishing whether it was possible to achieve an optimum bending moment diagram for a pair or pairs of counter moments applied to a variety of beams.

A number of methods of beam repair and strengthening were reviewed in chapter 2. While methods of repair or retrofitted tendons were principally examined, this current research was carried out with a view to using the regime for new construction (that is, applying tendons in the workshop to pre-fabricated beams).

With the plate bonding methods of strengthening applied to concrete members, the member performance can be improved somewhat and the primary application is to reinstate the original member capacity. With steel plates bonded to steel members the capacity can be improved in the order of 10-20% of the original and, again, the primary application is structural repair. External tendons fitted retrospectively to steel beams can improve beam performance, however, most applications reviewed were primarily concerned with repair.

Equations were developed for the application of counter moments that considered simply supported and fixed end beams with central concentrated loads and with asymmetrical concentrated loads, and two-span beams with central and asymmetrical concentrated loads applied.

An arbitrary case of a 6m single span beam with a 200kN central concentrated load was selected. Hand calculations showed that a 686x254x125 UB with an overall depth of 615mm, was required to carry a 200kN central concentrated load. A 254x254x132 UC, with an overall depth of 276.3mm, was selected as the beam to be strengthened for the

above loading and span. Two types of tendon configuration were considered for strengthening.

With the first tendon and lever configuration, the tendon was contained within the beam flanges, the resulting tendon eccentricity was low (99mm) and slightly above the minimum required for beam improvement (96.4mm). A second configuration was considered with the tendon attached to the underside of the beams' lower flange via thick-wall tubes. This configuration was considerably more efficient in performance (with an eccentricity of 170mm) and delivered greater pre and post-loaded counter-moment per unit tendon force than the first configuration tested.

Beam testing verified the strengthening method and demonstrated that initial pre-tension force gave rise to pre-camber and reduced final deflection un-loaded and loaded beam respectively. The testing also demonstrated that the increase in tendon force due to load application was independent of initial tendon force.

Independent finite element analyses confirmed the experimental findings.

8.2 Ultimate capacity analysis

The ultimate capacity analyses demonstrated that the strengthened beam could bear a 48% greater ultimate load compared to a similar un-strengthened beam. The analyses also highlighted the four phases of deflection up to ultimate loading, as discussed in chapter 4.

In order to ensure the predominantly ductile response described, an adequate cross-sectional area of tendons must be provided to ensure that a plastic hinge develops prior to tendon failure. The designer must first establish the rate of tendon force increase with respect to load application, r_t , for the configuration under consideration. Knowing r_t will allow the designer to ensure that the tendon stresses remain sufficiently below their

characteristic breaking strength when a plastic hinge forms in the beam. This will allow a ductile response to occur with substantial deflection before tendon failure.

8.3 Principal conclusions

The testing demonstrated that the tendon force increase and calculated section stresses due to load application was as predicted by the FE analyses (that is, not greater than 2% difference). This was also the case for all subsequent tests. With this testing, the tendon force increase due to load application was low and the tendon configuration did not perform efficiently with regard to self-counter moment application. The revised tendon configuration, however, yielded a substantial improvement in tendon force increase.

The series of active tests with horizontal tendon configuration within the overall depth of the beam demonstrated that the tendon force increase was independent of the initial tendon force. As with the passive testing, the active testing demonstrated that the performance was poor and little counter moment was applied for a relatively high tendon force. The application of the subsequent tendon configuration, which resulted in a 12% increase in overall beam depth, yielded a strengthened beam that could withstand a 48% increase in ultimate capacity compared to the un-strengthened beam.

The principal objective of this research was to establish a method of strengthening that allows a substantial overall beam depth reduction and provides a member with at least the same flexural strength and deflection as the original deeper un-strengthened beam required for the same span and loading .

Tendon configuration employed with this research demonstrated that is possible to strengthen a member with applied counter-moments and to significantly increase ultimate capacity (up to 48%) and reduce deflection (up to 46%). Similar or better performances could be achieved for other beam arrangements, depending on the ability to achieve higher tendon eccentricities.

Future work on this external tendon application could include considering different loading for simply supported beams (that is, static uniformly distributed load), or dynamic loading) and also the fatigue strength of the tendon configuration could be explored. Continuous beams could be examined with both static and dynamic loading applied. The effect of unloaded spans in continuous beams with regard to applied counter moments could be explored in three or more span beams.

The area of external tendons applied to portal frames could be explored further. Long spanning portals could be achieved, particularly where there is no restricted headroom and tendon levers could be longer than in the case of beams. Research into the static and dynamic responses of steel portal frames strengthened with external tendons could also be carried out.

It can be concluded that the tendon system employed is a viable method of strengthening and has the potential to substantially improve load-bearing capacity. Substantial increase in capacity and member depth can be achieved with the strengthening system. The use of external tendons is the only known viable and an efficient method applying specific concentrated moments at specific location to optimise the bending moment diagrams of loaded members. Deflection can be significantly reduced with this strengthening method and in cases where serviceability predominates, deflection can be controlled by prescribed initial tendon force.

References

1. Abdelrahmen, A. and Rizkalla, S. H., "Deflection control of concrete beams pre-tensioned by CFRP reinforcements", *Journal of Composites for Construction,* Vol.3 No.2, may 1999, 55-62.
2. Aeberhard, H.V., Bvergi, P., Ganz, H., Marti, P., Matt, P. and Sleber, T., *External post tensioning,* VSL International Ltd. Publications, 1989.
3. Albrecht, P., "Fatigue strength of adhesively bonded plates", *Journal of Structural Engineering,* June 1987, Vol. 113, No. 3, 1236-1249.
4. Allen, A. H., *An Introduction to Prestressed Concrete,* Cement and Concrete Association, 1986.
5. Al-Mayah, A., Soudki, K. A. and Plumtree, A., "Experimental and Analytical Investigation of a Stainless Steel Anchorage for CFRP pre-stressing tendons", *PCI Journal*, March-April 2001, Vol. 46. No. 2, 88-100.
6. Andra, H. P. and Maier, M., "Post-strengthening of reinforced concrete structures by pre-stressing externally bonded carbon fibre reinforced polymer (CFRP) strips" Conference Proceedings: Structural Faults and Repair, 1999.
7. Arduini, M. and Nanni, A., "Behaviour of pre-cracked RC beams strengthened with CFRP sheets", *Journal of Composites for Construction,* ASCE, January 1997, Vol. 1, No. 2, 63-70.
8. AS4100, *Steel Structures,* Standards Australia, Sydney Australia, 1998.
9. Balvac Ltd. *M8 Kingston Bridge, Glasgow: External post-tensioning installation,* Balfour Beatty Publications, 2001.
10. Brosens, K., Ahmed, O. and Van Gement, D., "Strengthening of concrete structures with externally bonded reinforcement: Design philosophy and practical applications", Department of Civil Engineering, KU, Leuven, Belgium, 2000.
11. British Standards Institute, BS4: Part 1 (1980), *Specification for hot rolled sections.*
12. British Standards Institute, BS 5950: Part 1 (2000), *Code of practice for design in simple and continuous construction: Hot rolled sections.*

13. British Standards Institute, BS 5950: Part 2 (2000), *Specification for materials, fabrication and erection: Hot rolled sections.*

14. British Standards Institution, BS 639: Sections 1 and 2 (1988), Covered electrodes for the manual metal-arc welding of mild steel and medium-tensile steel.

15. Brown, A. R. G., "Corrosion of CFRP to metal couples in saline environments" , Proceedings of the 2nd International Conference on Carbon Fibres, London, February, 18-20, 230-241.

16. Brozzetti, J. "Design development of steel-concrete composite bridges in France", *Journal of Constructional Steel Research*, Vol. 55, 2000, 229-243.

17. Busel, J. P. (editor), "Product Selection Guide: FRP Composite Products for Bridge Applications", MDA, The Market Development Alliance of the Composites Industry, First Edition, 2000, 264.

18. CEB-FIP *(fib bulletin 35)*, "Rettrofitting of concrete structures by externally bonded FRPs", May 2006.

19. Chajes, M., Swinehart, M., Richardson, D. and Wenczel, G. "Bridge rehabilitation using advanced composites: Ashland bridge SR-82 over Red Clay Creek", Faculty of Civil Engineering, University of Delaware, Newark, DE, 2002.

20. Chan, T. K., Cheong,H. K. and Nguyen, D. M., "Experimental investigation on delamination failure of CFRP strengthened beams" Conference Proceedings: (ICCMC/IBST *International conference on advanced technologies in design, construction and maintenance of concrete structres*) 2001.

21. Choqueuse, D., Davies, P. Mazeas, F. and Baizeau, R., "Aging of composites in water: Comparison of five materials in terms of absorption kinetics and evolution of mechanical properties" High Temperature and Environmental Effects on Polymeric Composites 2nd Volume, ASTM Special Technical Publication, 1302, Thomas S. Gates and Abdul-Hamid Zureick, eds., American Society for Testing and Materials, 73-96.

22. Colloti, V. and Speadea, G., "Shear strengthening of RC beams with bonded steel plates", *Journal of Structural Engineering,* April 2000, Vol.127, No. 4, 367-373.

23. Darby, J., Skwarski, A., Brown, P. and Haynes, M., "Pre-stressed advanced composite plates for the repair and strengthening of structure", Conference Proceedings: Structural Faults and Repair, 1999.
24. Deuring, M. "Strengthening of RC with pre-stressed fibre reinforced plastic sheets" EMPA Research Report 224, Dubendorf, Switzerland. (published in german).
25. Dolan, C. W., Bakis, C. E. and Nanni, A., "Design recommendations for concrete structures pre-stressed with FRP tendons", FHWA – DTFH61-96-C-00019, Final Report , August 2001.
26. European Concrete Research Action Group, *New materials and systems for pre-stressed concrete,* December 2002.
27. El-Hacha, R., Gren, M. and Wight, G. "Concrete beams post-strengthened with pre-stressed carbon fibre reinforced polymer sheets", Conference Proceedings: Structural Faults and Repair, London, June 2001(a).
28. El-Hacha, R., Gren, M. and Wight, G. "Concrete beams post-strengthened with pre-stressed carbon fibre reinforced polymer sheets", Conference Proceedings: Structural Faults and Repair, London, June 2001(b).
29. El-Hacha, R., Gren, M. and Wight, G. "Innovative System for Pre-stressing Fiber-Reinforced Polymer Sheets" *ACI Structural Journal,* May-June 2003, 305-313.
30. Fam, A. Z., Rizkalla, S. and Tadros, G., "Behaviour of CFRP for pre-stressing and shear reinforcement of concrete highway bridges", *ACI Structural Journal*, Vol. 94, No.1, Jan-Feb, 1997, 77-86.
31. Francis, R., "Bi-metallic Corrosion: Guides to good practice in corrosion control" , National Physical Laboratory, Teddington, Middlesex, 15P.
32. GangRao, V.S. and Vijay, P.V. "Bending behaviour of beams wrapped with carbon fabric", *Journal of Structural Engineering,* July 1998, Vol.124, No. 1, 3-10.
33. Garden, H. N. and Hollaway, L. C. "An experimental study of the failure modes of reinforced concrete beams strengthened with pre-stressed carbon composite plates" *Composites (Part B)* 1998, 411-424.
34. Ghali, A. and Neville, A. M., *Structural Analysis,* E and FN Spon, London and New york, 1997.

35. Hamilton, H. R., Wheat, H. G., Breen, J. E. and Frank, K.H. "Corrosion testing grout for post-tensioning ducts and stay cables", *Journal of Structural Engineering,* February 2000, Vol.126, No. 2, 163-170.

36. Hancock, G. J. and Trahair, N. S., "Distortional buckling of web steel members" *Proceedings from Theodore V. Galambos Symposium.*, Structural Stability Research Council. Lehigh University, Bethlehem, 85-96.

37. Harada, T., Matsuda, H., Tokumitsu, S., Enomoto, T. and Idemitsu, T., "Developments of non-metallic anchoring devices for FRP tendons", Non Metallic (FRP) Reinforcement for Concrete Structures, Edited by L. Taerwe, ISBN 0 419 20540 3, 43-48.

38. Harajli, M., Khairallah, N. and Nassif, H., " Externally pre-stressed members: Evaluation of second order effects", *Journal of Structural Engineering,* October 1999, Vol. 125, No. 10, 1151-1161.

39. Hewson, R. N., "The use of external tendons for the Bankok second stage expressway" *The Structural Engineer,* December 1993, Vol. 71, No. 23, 412-420.

40. Hook, J. and Cooper, J., "Applications of CFRP composites for bridge rehabilitation and strengthening in the USA", Federal Highway Administration Publications, Department of Transport, 2001.

41. Jungwirth, D. and Windisch, A., "Tendons made of non-metallic materials, requirements and economic application", Non-metallic (FRP) Reinforcement for Concrete Structures, Edited by L. Taerwe, ISBN:0 419 20540 3, 34-40.

42. Kemp, A. R., "Designing for Ductility", *The Structural Engineer,* March 18, 2003, Vol. 81, No. 6, 13-14.

43. Khairallah, N., and Harajili, M. H. "Experimental evaluation of the behaviour of reinforced concrete T beams strengthened using external prestressing", Proc., *International Conference on Rehabilitation and Development of Civil Engineering Infrastructure Systems, American University of Beirut, Beirut, Lebanon.* October 1997, Vol. 2, 1282-1293.

44. Kreyszig, E., *Advanced Engineering Mathematics-(7^{th} edition),* John Wiley & Sons INC., 1993.

45. Li, A., Assih, J. and Delmas, Y., "Shear strengthening of RC beams with externally bonded steel plates", *Journal of Structural Engineering,* April 2001, Vol.127, No. 4, 374- 380.

46. Li, W., Albrecht, P., Saadatmanesh, H. and Bull, W., "Behaviour of pre-stressed beams strengthened with external tendons", *Journal of Structural Engineering,* December 1995, Vol. 121, No. 12, 1842-1849

47. Luke, P. S., Leeming, M. B. and Skwarski, A. J. "ROBUST results for carbon fibre" Concrete Engineering International, 2, vol. 2, 19-21.

48. London Underground Ltd. *Under-bridge Assessment*, Engineering standard E3314, 1984.

49. Maher, I., *The use of external tendons for beam improvement*, BAI Dissertation, Trinity College, 1998.

50. McBagonluri, F., Garcia, K., Hayes, M., Verghese, N. and Lesko, J. J., "Characterisation of Fatigue and Combined Environment on Durability Performance of Glass/Vinyl Ester Composites for Infrastructure Appications", *International Journal of Fatigue,* Vol. 22, No. 1, January 2000, 53-64

51. Mc. Bride, H., *The optimisation of portal frames using counter moments and plastic limit synthesis, M. Sc. dissertation, Trinity College*, Dublin, August 2001.

52. McKay, K. S. and Erki, M. A., "Flexural behaviour of concrete beams pre-tensioned with Arimid Fibre Reinforced tendons", *Canadian Journal of Civil Engineering,* Vol. 20, 1993.

53. Meier, U., Deuring, H. and Schwegler, G., "Strengthening of structures with CFRP laminates: Research and application in Switzerland" , Advanced Composites in Bridges and Structures, Edited Neale, K. W. and Labossiere, P., 1992.

54. Miki, C., Ito, Y. and Sasaki, E., "Fatigue strength and repair cases in steel bridges", Tokyo Institute of Technology, Tokyo, 2000.

55. Miriyala, S. K., Tucker, W. C., Rockett, T. J. and Brown, R., "Degradation of carbon reinforced polymer composites under galvanic coupling conditions", Proceedings of the 33rd AIAA/ASME/ASCE/AHS/ASC Structures, Structural Dynamics and materials Conference, Dallas, Texas, April, 13-15, 3036-3045.

56. Miyamoto, A., Tei, K., Nakamura, H. and Bull, W., "Behaviour of pre-stressed beams with external tendons", *Journal of Structural Engineering,* September 2000, Vol. 126, No. 9, 1033-1044.

57. Mohamad, A., Oehkers, D. J. and Bradford, .M. A., "Shear peeling of steel plates bonded to tension faces of RC beams", *Journal of Structural Engineering,* December 2001, Vol. 127, No. 12, 1453-1459.

58. Mutsuyoshi, H., Machida, A. and Sano, M., "Behaviour of pre-stressed concrete beams using FRP as external cable", Japan Concrete Institute, Vol. 13, 1991.

59. Nanni, A., Bakis, C. E., O'Neill, E. F. and Dixon, T., "Performance of FRP tendon-anchor systems for pre-stressed concrete structures", *PCI Journal*, January-Febuary 1996.

60. Nguyen, D. M., Chan, T. K. and Cheong, H. K., "Brittle failure and bond development length of CFRP –concrete beams", *Journal of Composites for Construction,* Aug. 2000, 1242-1253.

61. Nordin, H., Carolin, A. and Taljsten, B., "Concrete beams strengthened with prestressed near surface mounted reinforcement (NSMR)" International Conference on FRP Composites in Civil Engineering CICE 2001 Ed. J.G. Teng, Hong Kong, ISBN: 0-08-0439445-4, 1067-1075.

62. Nordin, H., "Strengthening structures with externally pre-stressed tendons", Lulea University of Technology: Technical Report, 2005. ISSN: 1402-1536.

63. Norris, T., Saadatmanesh, H. and Ehsani, R., "Shear and flexural strengthening of RC beams with Carbon Fibre Sheets", *Journal of Structural Engineering,* July 1997, Vol.123, No.7, 903-911.

64. Oehlers, D. J., Mohamad Ali, M. S. and Weimin Lou, "Upgrading continuous concrete beams by gluing steel plates to their tension faces", *Journal of Structural Engineering,* March 1998, Vol. 124, No. 3, 224 – 232.

65. Oehlers, D. J., "Development of design rules for retrofitting by adhesive bonding or bolting either FRP or steel plates to RC beams or slabs in bridges and buildings", *Composites (Part A) - Applied Science and Manufacturing*, 2001, Vol.32. No. 9, 1345-1355.

66. Phares, B. M., Wipf, T. J., Klaiber, F. W., Hawash, A. A. and Lee, Y. S., "Strengthening of steel girder bridges using CFRP", Civil and Structural Engineering Department, Iowa state University, Iowa. 2000.

67. Picard, A., Massicotte, B. and Bastien, J., "Relative efficiency of external pre-stressing", *Journal of Structural Engineering,* December 1995, Vol.121, No. 12, 1832-1841.

68. Picard, A., Massicotte, B. and Bastien, J., "Analysis of continuous beams pre-stressed with localised tendons", *Journal of Structural Engineering,* February 2000, Vol. 126, No. 2, 262-265.

69. Pisani, M. A., "A numerical survey on the behaviour of beams pre-stressed with FRP cables" *Construction and building materials*, 1998, Vol. 12, 221-232.

70. Quantrill, R. J. and Hollaway, L. C. "The flexural rehabilitation of reinforced concrete beams by the use of pre-stressed advanced composite plates" *Composites Sciences and Enchology,* 58, 1998, 1259-1275.

71. Rahimi, H. and Hutchinson, A., "Concrete beams strengthened with externally bonded FRP plates", *Journal of Composites for Construction,* ASCE, November 2001, Vol. 119, No. 6, 214 - 219.

72. Ritter, M. A., *Bridge design, Construction, Inspection and Maintenance,* United States Department of Agriculture Publications, 1990.

73. Rogpwsky, D., Harder, J. and Demitt, A., "Investigation protocol for the evaluation of post-tensioned buildings", Department of Civil/Structural Engineering, University of Alberta, July 2003.

74. Rombach, P., "Pre-cast segmental box girder bridges with external pre-stressing: Design and Construction" Technical University Hamburg, July 2000.

75. Ryu, H., Shim, C., Chang, S. and Chung, C., "Inelastic behaviour of externally pre-stressed continuous composite box-girder bridge with prefabricated slabs", *Journal of Constructional Steel Reaserach,* Vol. 60, 2004, 989-1005.

76. Saadatmanesh, H. and Malek, A. M., "Design guidelines for flexural strengthening of RC beams with FRP plates", *Journal of Composites for Construction,* November 1998, Vol. 2, No. 4, 158 – 164.

77. Schnerch, D., Dawood, M., Sumner, E. A. and Rizkalla, S., "Behaviour of Steel-Concrete beams strengthened with un-stressed and pre-stressed high modulus CFRP strips" The fourth middle East Symposium on Structural Composites for Infrastructure Applications, Alexandria, Egypt, May 20-23, 2005.
78. Sebastian, W. M., "Significance of mid-span de-bonding failure in FRP beams", *Journal of Structural Engineering,* July 2001, Vol.127, No. 7, 792 – 798.
79. Sebastian, W. M., "Design of strengthening in metal yield zones" Proceedings from the Institution of Civil Engineers: Structures and buildings, October 2005, Issue SBS, 303-310.
80. Sen, S., Shahawy, M., Sukumar, S. and Rosas, J. "Durability of Carbon pre-tensioned Elements in a Marine Environmnet", *ACI Structural Journal*, November-December 1998, 716-724.
81. Sikadur Ltd. "Bridge Strengthening with the Sika Stresshead pre-stressing System" International Case studies, No.9, 2004.
82. Steel Construction Institute, *Steel Designers Manual,* (edited by Davison, B. and Owens, G. W.) Blackwell Publishings, 2005, ISBN-10: 1-4051-3412-7.
83. Stoll, F., Saliba, J. E. and Casper, L. E. "Experimental study of CFRP pre-stressed high-strength concrete beams", *Composite Structures,* Vol. 49, March 2000, 191-200.
84. Sumito, S. and Wang, M. L., *Sustainable structural health monitoring systems,* Keisoku research consultants technical publications, Tokyo, 2003.
85. Taljsten, B., "FRP strengthening of existing concrete structures – Design guidelines" ISBN: 91-89580-03-6
86. Tan, K. H. and Ng, C. K., "Effects of deviators and tendon configuration on the behaviour of externally pre- stressed beams", *Journal of Structural Engineering,* 1997, Vol. 94, No. 1, 13 - 24.
87. Tavakkolizadeh, M., Mohammadreza, A. and Saadatmanesh, H.,"Galvanic corrosion of carbon and steel in aggressive environments", *Journal of Composites for Construction*, Vol. 5, No. 3, August 2001, 200-202.
88. Tavakkolizadeh, M., and Saadatmanesh, H., "Strengthening of steel-concrete composite girders using carbon fiber reinforced ploymer sheets", *Journal of Structural Engineering*, ASCE, Vol. 129, No. 1, January 2003, 30-40.

89. Trahair, N. S., "*Flexural torsional buckling of structures*" E & FN Spon London 1993.

90. Trahair, N. S. and Hancock, G. J., "Steel member strength by inelastic lateral buckling", *ASCE Journal of Structural Engineering*, January 2004, Vol. 130 No. 1,64-68.

91. Triantafillou, T. C. and Deskovic,, N. "Innovative Pre-stressing with FRP Sheets: Mechanics of short-term Behaviour" *Journal of Engineering Mechanics*, 1991, Vol. 117, 1652-1672.

92. Triantafillou, T. C., Deskovic, N.,"Strengthening of concrete structures with pre-stressed fibre reinforced plastic sheets" *ACI Structural Journal,* 89, Vol.3, 235-244.

93. The Highway Agency, (DMRB) *The Design Manual for Roads and Bridges,* 2001.

94. Valentino, J. Pi, Y. L. and Trahair, N. S., "Inestalic buckling of steel beams with central torsional restraints", *ASCE Journal of Structural Engineering*, September 1997, Vol. 123, No. 9, 1180-1186.

95. Valentino, J. and Trahair, S. N., "Torsional restraint against lateral buckling", *ASCE Journal of Structural Engineering*, October 1998, Vol.124, No. 10, 1217-1225.

96. Viroguex, M., *External post-stressing*, Institute of transport and public transport publication, France 1983.

97. West, R. P. Lecture notes from MSc. course C6 Structural optimisation, Trinity College, Dublin 2000.

98. Wight, R. G., Green, M.F. and Erki, M. A. "Post strengthening concrete beams with pre-stressed FRP sheets", Non-metallic (FRP) Reinforcement for concrete structures, 1995, ISBN 0 419 20540 3.

99. Yura, J. A., "Fundaments of beam bracing" *Proceedings from the Structural Stability Res. Council Conference,* Lehigh University, Bethlehem, 1993, 1-19.

100. Zarnic, R., Bosiljkov, V. and Bokan-Bosiljkov, V. "*Improvement of bending and load bearing capacity by externally bonded plates*", Thomas Telford Publications, 1999.

101. Zhang, J. P., "Diagonal cracking and shear strength of reinforced concrete beams", *Magazine of Concrete Research,* March 1997, Vol. 49, No. 178, 55-65.

Appendix A

Derivation of expressions for counter-moment location and magnitude for various cases

A.1 Symmetrical loading on simply supported beam

Consider the bending moment diagram of a simply supported beam with a central concentrated load (moment diagram inverted for clarity) and the same beam with a pair of counter moments applied and no concentrated load.

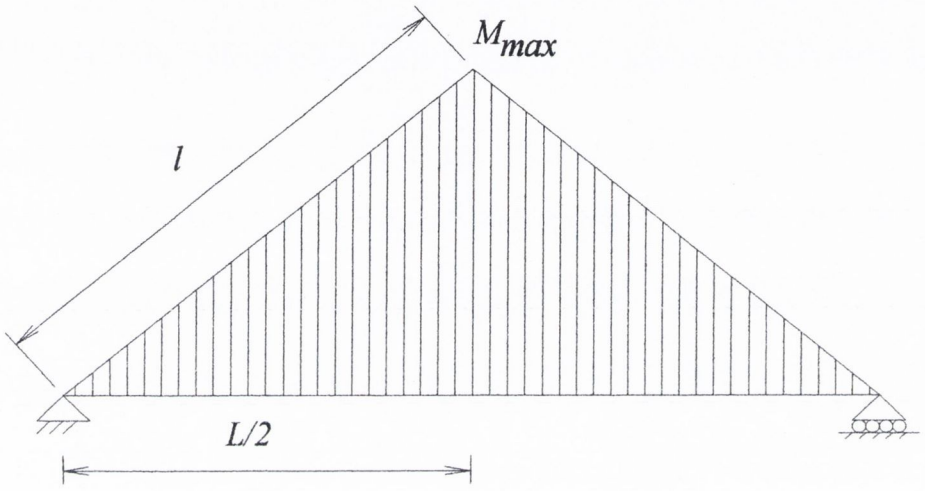

(a)

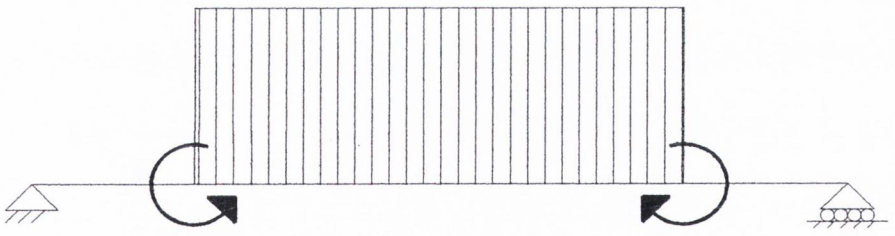

(b)

Figure A.1: Bending moment diagram of (a) concentrated load applied to a simply supported beam (b) a pair of counter moments applied to a simply supported beam.

Figure A.2 shows the combined bending moment diagram (BMD) of part (a) and (b) in figure A.1. Considering the geometry of the BMD the location of the counter moment "x_1" on the left (and right, mirrored about the location of the concentrated load) must equal the slope distance *l/3* projected onto the horizontal base, if all net peaks m_{max} are equal.

Therefore, by similar triangles, x_1 can be expressed as follows:

$$x_1 = \frac{L/2}{l} \bullet \frac{l}{3} = L/6 \tag{A.1}$$

and it can be seen that the magnitude of the applied pair of counter moments must be:

$$2m_{\max} = \frac{2M_{\max}}{3} = m_{co} \tag{A.2}$$

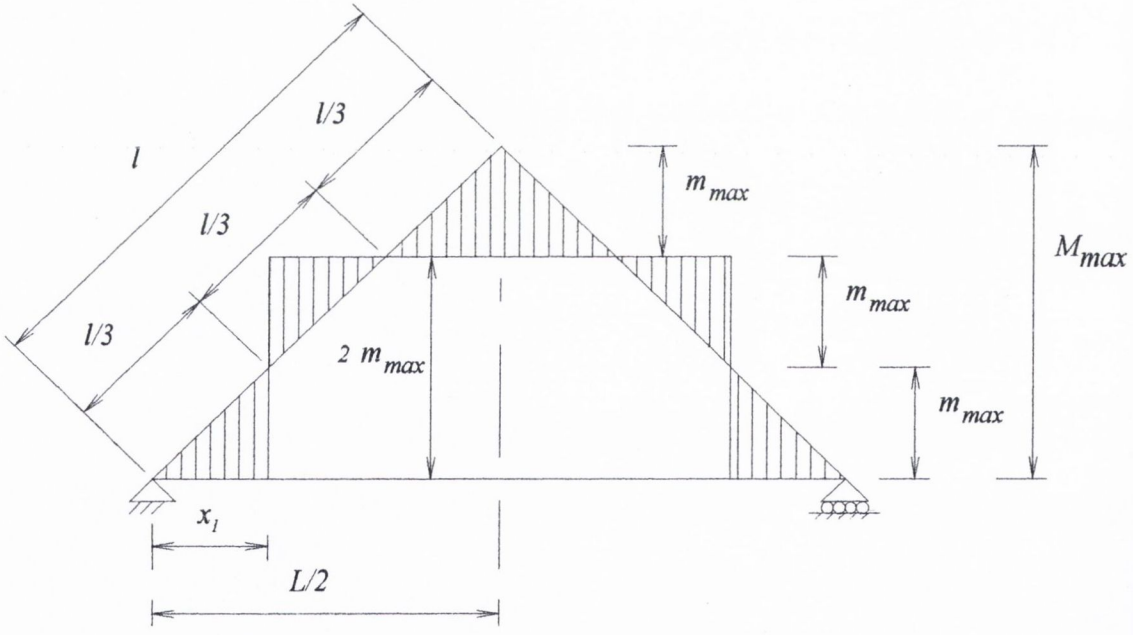

Figure A.2: Net bending moment diagram (that is, moment due to concentrated load +ve and moment due to counter moments (–ve)).

Similarly, if two pairs of counter moment are applied to the beam, the net bending moment diagram results as shown in figure A.3. It can be seen by geometry that for all net peaks m_{max} to be equal, the locations x_1 and x_2 for the two pairs of counter moments must be as follows (the same dimensions apply, measured from the right support):

$$x_1 = \frac{L/2}{l} \bullet \frac{l}{5} = \frac{L}{10} \tag{A.3}$$

and,

$$x_2 = \frac{L/2}{l} \bullet \frac{3l}{5} = \frac{3L}{10} \tag{A.4}$$

Again, by geometry the magnitude of each pair of counter moments, m_{co} , must be $2m_{max}$, (if $5m_{max} = M_{max}$) and can be expressed as follows:

$$2m_{\max} = \frac{2M_{\max}}{5} = m_{co} \tag{A.5}$$

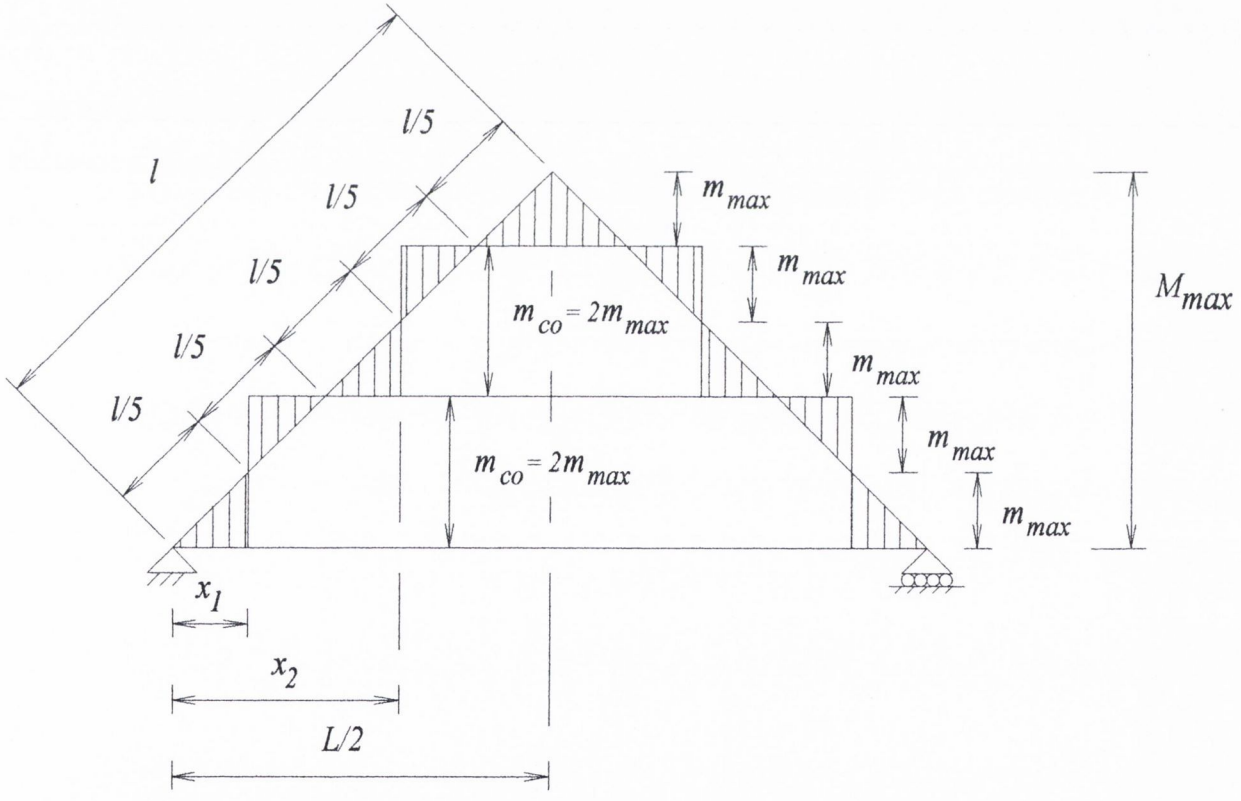

Figure A.3: Net bending moment diagram with two pair of counter moments applied.

Thus, for any number of pairs of counter moments, m, the location of each pair of counter moments, x_n (Where i ranges from 1 to m) from the left support can be expressed as follows (Maher 1998):

$$x_i^* = \frac{L(2i-1)}{2(2m+1)} = \frac{L(2i-1)}{(4m+2)} \tag{A.6}$$

and the location from the right support is:

$$x_i^{*'} = l - x_i^* \tag{A.7}$$

The magnitude of each pair of counter moments can be expressed as (Maher 1998):

$$|m_{\max}| = \frac{|M_{\max}|}{2m+1} \tag{A.8}$$

A.2 Asymmetrical loading on simply supported beam

In the case of an asymmetrical concentrated load on a simply supported beam, as shown in figure A.4, the dimension $L/2$ can be replaced in equation A.6 by the dimension "a" when locating counter moments from the left support. Similarly, $L/2$ can be replaced by the dimension "b" when locating moments from the right support . Equation A.7 will apply when calculating the magnitude of the counter moments for an asymmetrical concentrated load on a simply supported beam.

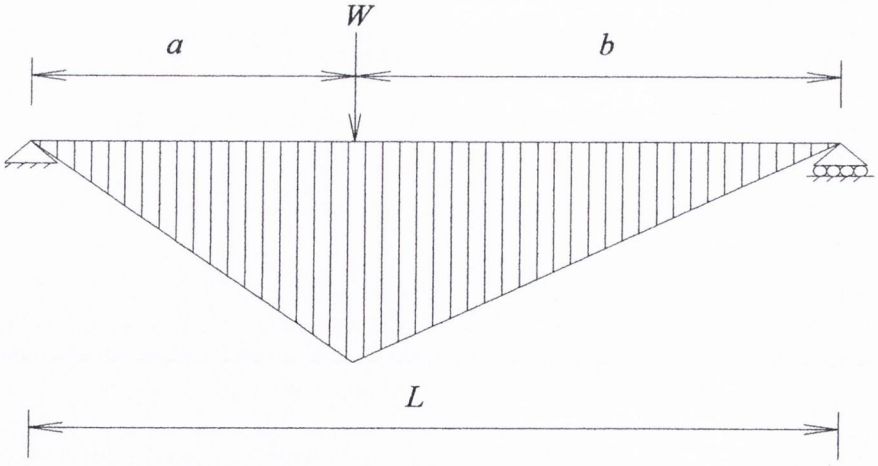

Figure A.4: Asymmetrical concentrated load applied to simply supported beam.

The following expressions will apply for asymmetrical loading on a simply supported beam with m number of pairs of counter moment located at each x_i where i ranges from 1 to m.

For counter moment locations, $x_i^{'}$, to the left of the concentrated load measured from the left support,

$$x_i^{'} = \frac{a(2n-1)}{(2m+1)} \tag{A.9}$$

For counter moment locations, $x_i^{''}$, to the right of the concentrated load measured from the right support,

$$x_i^{''} = \frac{b(2n-1)}{(2m+1)} \tag{A.10}$$

Again, as in the previous case the maximum moment with counter-moments applied can be expressed using equation A.8.

A.3 Uniformly distributed load on a simply supported beam

Consider the case of one pair of counter moments applied to a simply supported beam with a uniformly distributed load as shown in figure A.5. The locations from the left support must be at the ordinates in the bending moment diagram where the values are $M_{max}/3$ for the optimum bending moment diagram to be achieved. The magnitude of the pair of counter moments must also be $2M_{max}/3$ for the optimum bending moment diagram to be achieved.

If $M_{\max} = \frac{wL^2}{8}$

then,

$$\frac{M_{\max}}{3} = \frac{wL^2}{24}$$

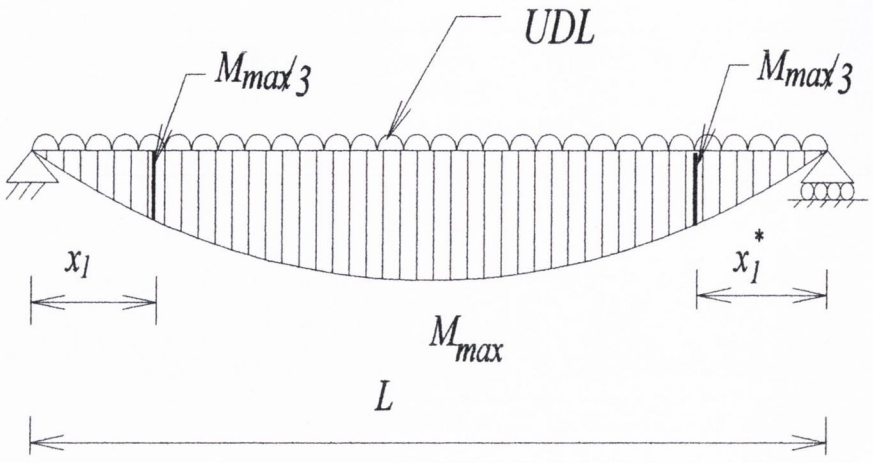

Figure A.5: UDL applied to simply supported beam.

The location of the counter moments can be derived by solving the moment quadratic equation $Mf(x) = \frac{wL}{2}x - \frac{wx^2}{2} = \frac{wL^2}{24}$ to yield:

$$x_i^* = L\left(\frac{1}{2} - \frac{1}{\sqrt{6}}\right) \tag{A.11}$$

If m number of pairs of counter moments are applied, their locations can be expressed as solutions to the quadratic bending moment equation where the values of the bending moment on the un-strengthened beam are $M_{max}(2i-1)/2m+1)$ (where i ranges from 1 to m). That is, if $m=2$, location of counter moments on the beam shown in figure A.5 will be at the moment ordinates $M_{max}/5$ and $3M_{max}/5$ for the inner and outer counter moments respectively at each side of the peak moment, M_{max} . The expression for the location of counter moments is as follows (Maher 1998):

$$x_i = \frac{L}{2}\left(1 - \sqrt{\left(1 - \left(\frac{2i-1}{2m+1}\right)\right)}\right) \tag{A.12}$$

for the location of the counter moments to the right of the peak moment M_{max} :

$$x_i^{*'} = L - x_i^* \tag{A.13}$$

Equation A.8 can then be used to calculate the magnitude of the counter moments.

A.4 Fixed end beam with central concentrated load

Consider the bending moment diagram for the fixed end beam with a central concentrated load shown in figure A.6. If one pair of counter moments are applied to the beam with no central concentrated load the bending moment diagram shown in figure A.7 results.

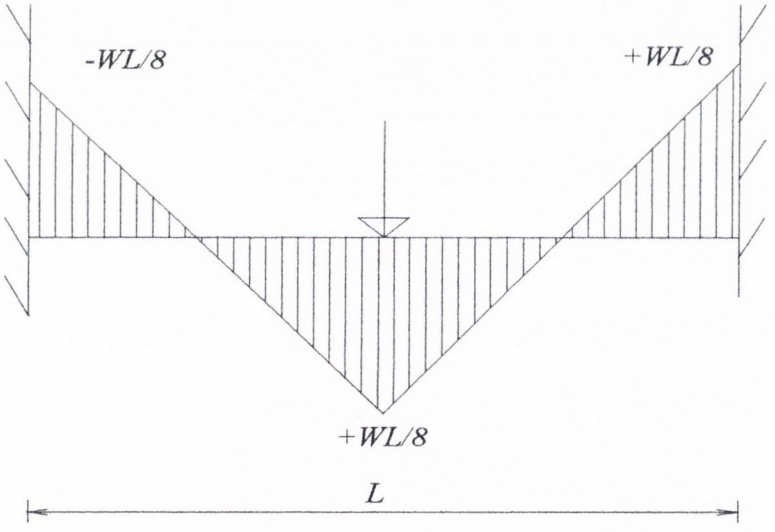

Figure A.6: Fixed end beam with central concentrated load.

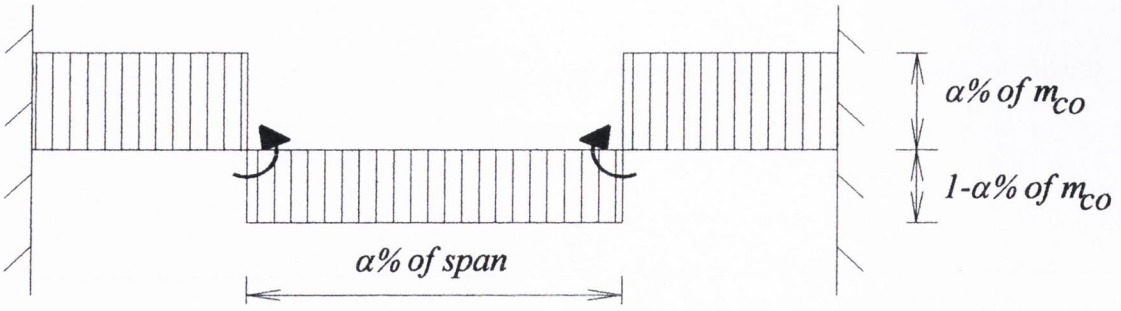

Figure A.7: Pair of counter moments of magnitude m_{co} applied to a fixed end beam.

Let the distance between the counter moments be α% of the span, L. Provided the counter-moments are applied symmetrically about the centre of the span, The percentage of each counter-moment carried to each support will be same percentage, α%. If one considers a concentrated moment applied to a fixed end beam as shown in figure A.8 the fixed end moments can be expressed as follows (Ghali et al. 1997);

$$m_l = \frac{m_{co}a}{L}\left(2 - \frac{3a}{L}\right) \tag{A.14}$$

where,

m_l = the fixed end moment at the left support

$$m_r = \frac{m_{co}}{L}\left(2 - \frac{3b}{L}\right) \tag{A.15}$$

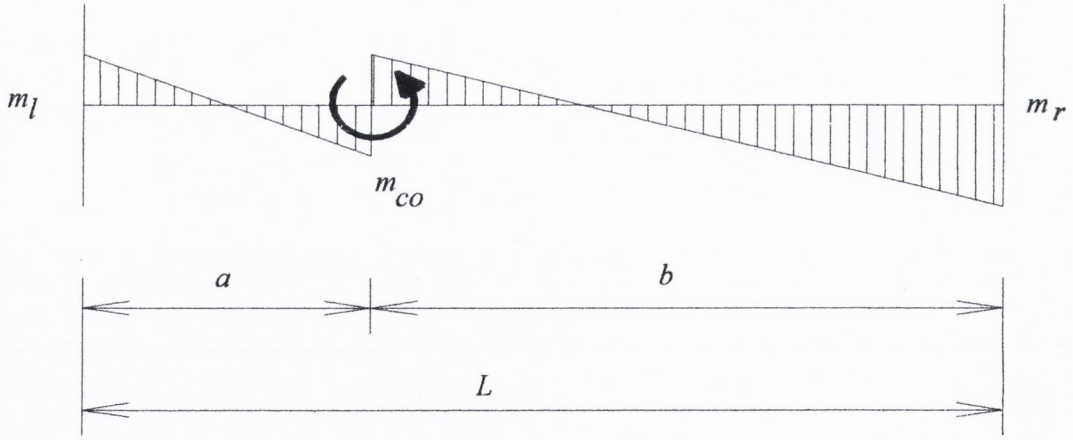

Figure A.8: Concentrated moment applied to fixed end beam

If, for example, a fixed end beam had a span of 10m and two such moments (100kNm) shown in figure A.8 were applied with opposite sign and located 2m from each support (that is, the distance between the counter-moments is 6m). The fixed end moment induced at the left support is due to a contribution from both concentrated moments and can be calculated using equation A.14 which yields a value of 60kNm (that is, 60% of each counter-moment). It can be seen that 60% of the span is between the location of the counter-moments as shown in figure A.9.

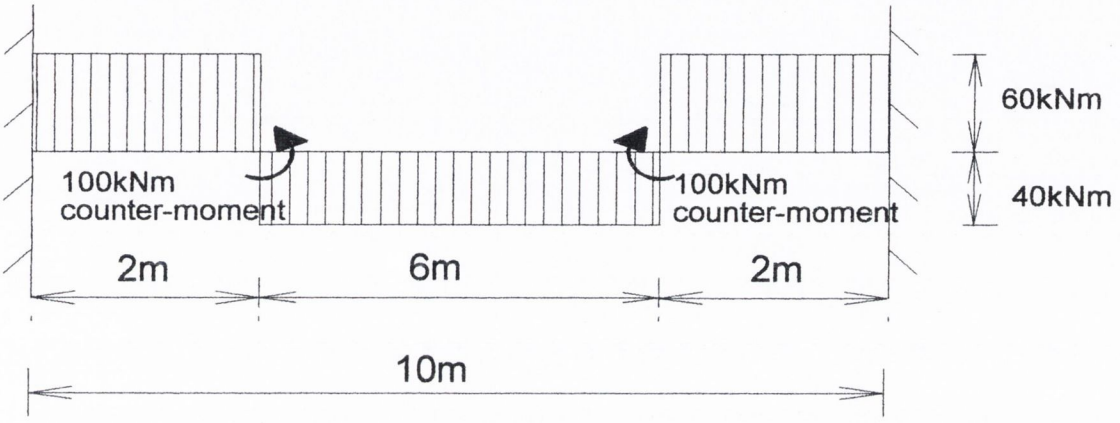

Figure A.9: Fixed end beam with 100kNm counter-moments applied.

It can be seen by geometry that for one pair of counter moments the optimum location must be at the points of contra-flexure on the diagram in figure A.6 (that is, $x_1^* = L/4$ and $x_1^{*'} = 3L/4$). Also, for optimality, the magnitude of the counter moments, m_{co} must be $WL/8$, to yield the bending moment diagram. Similarly, for multiple counter moments applied, the maximum resulting moment on the optimised moment diagram will be (Maher 1998):

$$|m_{\max}| = \frac{M_{\max}}{n+1} \tag{A.7}$$

and the locations to the left of the concentrated load can be expressed by (Maher 1998):

$$x_i^* = \frac{iL}{2(n+1)} \tag{A.8}$$

and the locations to the right of the concentrated load can be expressed by (Maher 1998):

$$x_i^{*'} = L - x_1^* \tag{A.9}$$

APPENDIX B

Equations used in software to calculate moments on a two span continuous beam

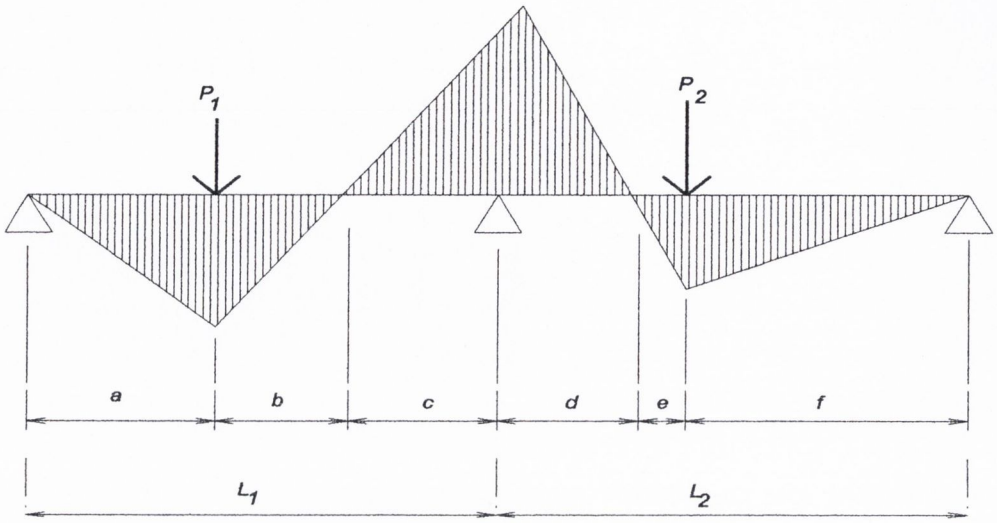

Figure B1: Figure showing the variables P_1, P_2, L_1, L_2 and *a-f*.

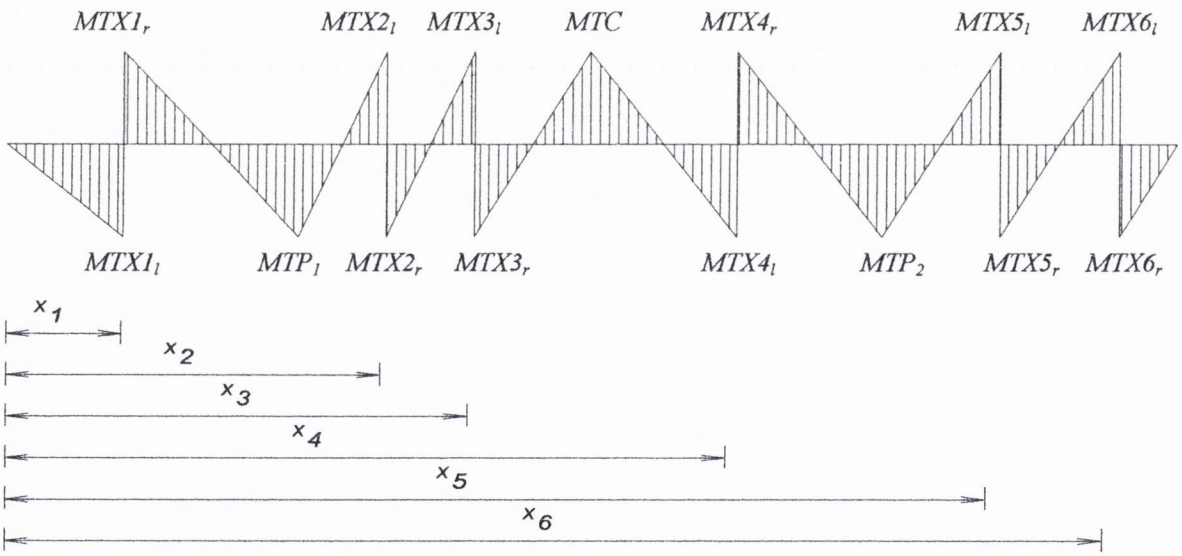

Figure B2: Figure showing the location of the moments calculated in equations B1-B15 together with the dimensions x_1-x_6.

As, discussed in chapter 3, if a single counter-moment is applied to the two span continuous beam shown in figure B1, the bending moment diagram results as shown in figure 3.11 and reproduced in here in figure B.3. The moment just to the left and right of the counter-moment, m_l , and m_r , can be expressed by equations B.1 and B.2 respectively.

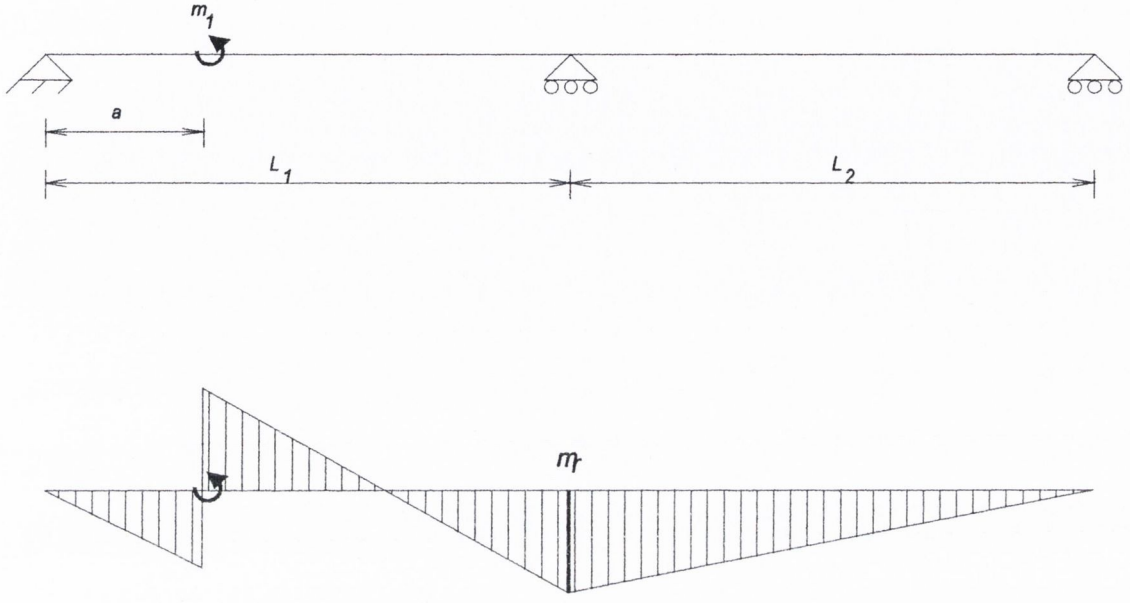

Figure B.3: single counter-moment applied to two span continuous beam.

$$m_1^- = \left[\frac{am_1L_1}{2L_2(L_1+L_2)}\right]\left[\left[\frac{3a^2}{L_1^2}\right]-1\right] \qquad [B.1]$$

$$\left|m_1^+\right| = \left|m_1\right| - \left|m_1^-\right| \qquad [B.2]$$

$$MTX1_l = -\frac{x_1m_1}{L_1} + \frac{m_1x_1}{2(L_1+L_2)}\left(\frac{3x_1^2}{L_1^2}-1\right) - \frac{m_2x_1}{L_1} + \frac{m_2x_1}{2(L_1+L_2)} + \left(\frac{3x_2^2}{L_1^2}-1\right) - \frac{m_3x_1}{L_1}$$
$$+ \frac{m_3x_1}{2(L_1+L_2)}\left(\frac{3x_3^2}{L_1^2}-1\right) - \frac{m_4x_1L_2}{2L_1(L_1+L_2)}\left(\frac{3x_4^2}{L_2^2}-1\right) - \frac{m_5x_1L_2}{2L_1(L_1+L_2)}\left(\frac{3x_5^2}{L_2^2}-1\right) \qquad [B.3]$$
$$- \frac{m_6x_1L_2}{2L_1(L_1+L_2)}\left(\frac{3x_6^2}{L_2^2}-1\right) + R_lx_1$$

$$MTX1_r = MTX1_l - m_1 \qquad \text{[B.4]}$$

$$MTX\,2_l = -\frac{x_2 m_1}{L_1} + \frac{m_1 x_2}{2(L_1+L_2)}\left(\frac{3x_1^{\,2}}{L_1^{\,2}} - 1\right) - \frac{m_2 x_2}{L_1} + \frac{m_2 x_2}{2(L_1+L_2)}\left(\frac{3x_2^{\,2}}{L_1^{\,2}} - 1\right) - \frac{m_3 x_2}{L_1}$$
$$+ \frac{m_3 x_2}{2(L_1+L_2)}\left(\frac{3x_3^{\,2}}{L_1^{\,2}} - 1\right) - \frac{m_4 x_2 L_2}{2L_1(L_1+L_2)}\left(\frac{3x_4^{\,2}}{L_2^{\,2}} - 1\right) - \frac{m_5 x_2 L_2}{2L_1(L_1+L_2)}\left(\frac{3x_5^{\,2}}{L_2^{\,2}} - 1\right) \qquad \text{[B.5]}$$
$$- \frac{m_6 x_2 L_2}{2L_1(L_1+L_2)}\left(\frac{3x_6^{\,2}}{L_2^{\,2}} - 1\right) + m_1 + m_2 + R_l x_2 - P_1(x_2 - a)$$

$$MTX2_r = MTX2_l - m_2 \qquad \text{[B.6]}$$

$$MTX3_l = -\frac{x_3 m_1}{L_1} + \frac{x_3 m_{13}}{2(L_1+L_2)}\left(\frac{3x_1^{\,2}}{L_1^{\,2}} - 1\right) - \frac{x_3 m_2}{L_1} + \frac{x_3 m_2}{2(L_1+L_2)}\left(\frac{3x_2^{\,2}}{L_1^{\,2}} - 1\right) - \frac{x_3 m_3}{L_1}$$
$$+ \frac{x_3 m_3}{2(L_1+L_2)}\left(\frac{3x_3^{\,2}}{L_1^{\,2}} - 1\right) - \frac{x_3 L_2 m_4}{2L_1(L_1+L_2)}\left(\frac{3x_4^{\,2}}{L_2^{\,2}} - 1\right) - \frac{x_3 L_2 m_5}{2L_1(L_1+L_2)}\left(\frac{3x_5^{\,2}}{L_2^{\,2}} - 1\right) \qquad \text{[B.7]}$$
$$- \frac{x_3 L_2 m_6}{2L_1(L_1+L_2)}\left(\frac{3x_6^{\,2}}{L_2^{\,2}} - 1\right) + m_1 + m_2 + m_3 + R_l x_3 - P_1(x_3 - a)$$

$$MTX3_r = MTX3_l - m_3 \qquad \text{[B.8]}$$

$$MTX4_l = \frac{x_4 L_1 m_1}{2L_2(L_1+L_2)}\left(\frac{3x_1^{\,2}}{L_1^{\,2}} - 1\right) + \frac{x_4 L_1 m_2}{2L_2(L_1+L_2)}\left(\frac{3x_2^{\,2}}{L_1^{\,2}} - 1\right) + \frac{x_4 L_1 m_3}{2L_2(L_1+L_2)}\left(\frac{3x_3^{\,3}}{L_1^{\,2}} - 1\right)$$
$$+ \frac{x_4 m_4}{L_2} - \frac{x_4 m_4}{2(L_1+L_2)}\left(\frac{3x_4^{\,2}}{L_2^{\,2}} - 1\right) + \frac{x_4 m_5}{L_2} - \frac{x_4 m_5}{2(L_1+L_2)}\left(\frac{3x_5^{\,2}}{L_2^{\,2}} - 1\right) + \frac{x_4 m_6}{L_2} - \frac{x_4 m_6}{2(L_1+L_2)}\left(\frac{3x_6^{\,2}}{L_2^{\,2}} - 1\right) \qquad \text{[B.9]}$$
$$- m_4 - m_5 - m_6 + R_r x_4 - P(x_4 - f)$$

$$MTX4_r = MTX4_l - m_4 \qquad \text{[B.10]}$$

$$MTX5_l = +\frac{x_5 L_1 m_1}{2L_2(L_1+L_2)}\left(\frac{3x_1^{\,2}}{L_1^{\,2}}-1\right)-\frac{x_5 L_1 m_2}{2L_2(L_1+L_2)}\left(\frac{3x_2^{\,2}}{L_1^{\,2}}-1\right)+\frac{x_5 L_1 m_3}{2L_2(L_1+L_2)}\left(\frac{3x_3^{\,2}}{L_1^{\,2}}-1\right)$$
$$+\frac{x_5 m_4}{L_2}-\frac{x_5 m_4}{2(L_1+L_2)}\left(\frac{3x_4^{\,2}}{L_2^{\,2}}-1\right)+\frac{x_5 m_5}{L_2}-\frac{x_5 m_5}{2(L_1+L_2)}\left(\frac{3x_5^{\,2}}{L_2^{\,2}}-1\right)+\frac{x_5 m_6}{L_2}-\frac{x_5 m_6}{2(L_1+L_2)}\left(\frac{3x_6^{\,2}}{L_2^{\,2}}-1\right) \quad [B.11]$$
$$-m_5-m_6+P_2(x_5-f)$$

$$MTX5_r = MTX5_l - m_5 \quad [B.12]$$

$$MTX6_l = +\frac{x_6 L_1 m_1}{2L_2(L_1+L_2)}\left(\frac{3x_1^{\,2}}{L_1^{\,2}}-1\right)-\frac{x_6 L_1 m_2}{2L_2(L_1+L_2)}\left(\frac{3x_2^{\,2}}{L_1^{\,2}}-1\right)+\frac{x_6 L_1 m_3}{2L_2(L_1+L_2)}\left(\frac{3x_3^{\,2}}{L_1^{\,2}}-1\right)$$
$$+\frac{x_6 m_4}{L_2}-\frac{x_6 m_4}{2(L_1+L_2)}\left(\frac{3x_4^{\,2}}{L_2^{\,2}}-1\right)+\frac{x_6 m_5}{L_2}-\frac{x_6 m_5}{2(L_1+L_2)}\left(\frac{3x_5^{\,2}}{L_2^{\,2}}-1\right)+\frac{x_6 m_6}{L_2}-\frac{x_6 m_6}{2(L_1+L_2)}\left(\frac{3x_6^{\,2}}{L_2^{\,2}}-1\right) \quad [B.13]$$
$$+R_r x_6$$

$$MTX6_r = MTX6_l - m_6 \quad [B.14]$$

$$MTP_1 = -\frac{am_1}{L_1}+\frac{am_1}{2(L_1+L_2)}\left(\frac{3x_1^{\,2}}{L_1^{\,2}}-1\right)-\frac{am_2}{L_1}+\frac{am_2}{L_2}\left(\frac{3x_2^{\,2}}{L_1^{\,2}}-1\right)-\frac{am_3}{L_1}+\frac{am_3}{2(L_1+L_2)}\left(\frac{3x_3^{\,2}}{L_1^{\,2}}-1\right) \quad [B.15]$$
$$-\frac{aL_2 m_4}{2L_2(L_1+L_2)}\left(\frac{3x_4^{\,2}}{L_2^{\,2}}-1\right)-\frac{aL_2 m_5}{2L_2(L_1+L_2)}\left(\frac{3x_5^{\,2}}{L_2^{\,2}}-1\right)-\frac{aL_2 m_6}{2L_2(L_1+L_2)}\left(\frac{3x_6^{\,2}}{L_2^{\,2}}-1\right)+R_l+m_1$$

$$MTC = +\frac{L_1 m_1}{2(L_1+L_2)}\left(\frac{3x_1^{\,2}}{L_1^{\,2}}-1\right)+\frac{L_1 m_2}{2(L_1+L_2)}\left(\frac{3x_2^{\,2}}{L_1^{\,2}}-1\right)+\frac{L_1 m_3}{2(L_1+L_2)}\left(\frac{3x_3^{\,2}}{L_1^{\,2}}-1\right) \quad [B.16]$$
$$-\frac{L_2 m_4}{2(L_1+L_2)}\left(\frac{3x_4^{\,2}}{L_2^{\,2}}-1\right)-\frac{L_2 m_5}{2(L_1+L_2)}\left(\frac{3x_5^{\,2}}{L_2^{\,2}}-1\right)-\frac{L_2 m_6}{2(L_1+L_2)}\left(\frac{3x_6^{\,2}}{L_2^{\,2}}-1\right)+R_l L_1-P_1 b$$

$$MTP_2 = +\frac{fL_1m_1}{2L_2(L_1+L_2)}\left(\frac{3x_1^{\,2}}{L_1^{\,2}}-1\right)+\frac{fL_1m_2}{2L_2(L_1+L_2)}\left(\frac{3x_2^{\,2}}{L_1^{\,2}}-1\right)+\frac{fL_1m_3}{2L_2(L_1+L_2)}\left(\frac{3x_3^{\,2}}{L_1^{\,2}}-1\right)$$

$$+\frac{fm_4}{L_2}-\frac{fm_4}{2(L_1+L_2)}\left(\frac{3x_4^{\,2}}{L_2^{\,2}}-1\right)+\frac{fm_5}{L_2}-\frac{fm_5}{2(L_1+L_2)}\left(\frac{3x_5^{\,2}}{L_2^{\,2}}-1\right)+\frac{fm_6}{L_2}-\frac{fm_6}{2(L_1+L_2)}\left(\frac{3x_6^{\,2}}{L_2^{\,2}}-1\right) \quad \text{[B.17]}$$

$$-m_6+R_rf$$

Appendix C

Flow chart for program to solve counter moment application for two span continuous beam.

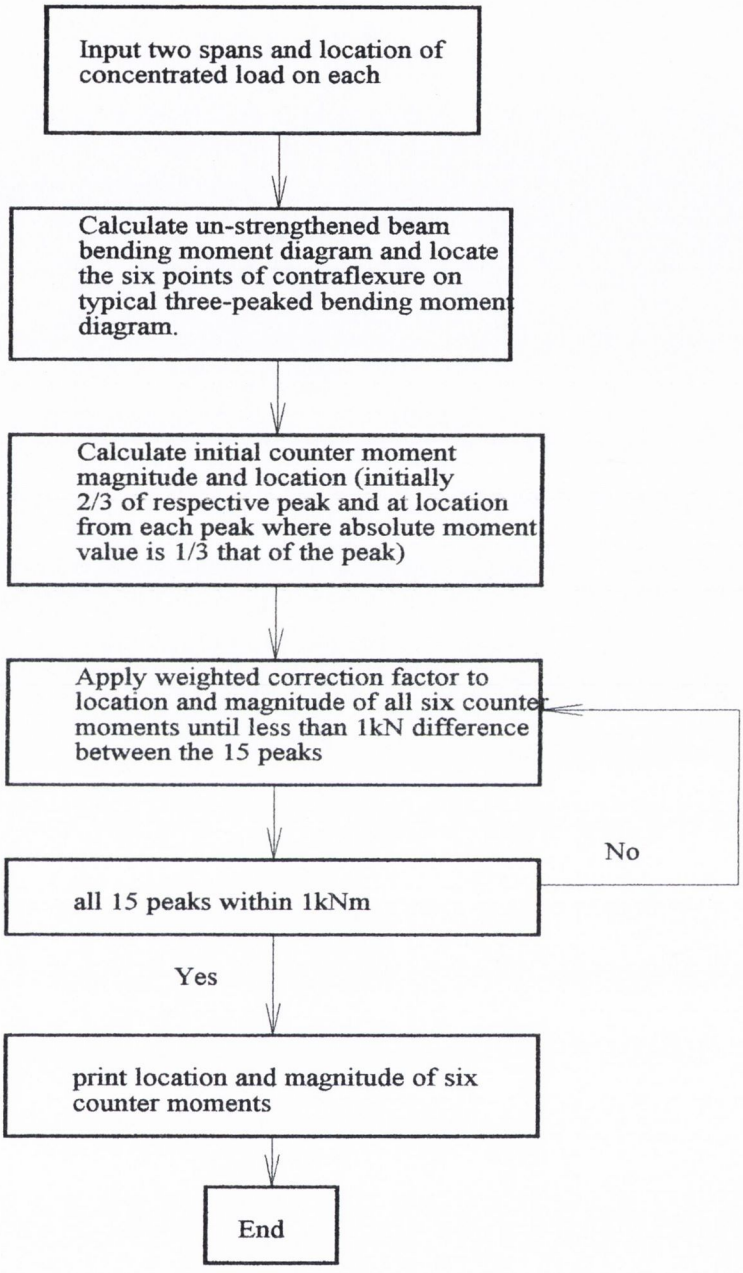

Figure B.1: Flow chart for program to calculate optimum counter moments for a two-span continuous beam

Appendix D

Expression for r_t

It is required to develop an expression for the rate of tendon force increase with respect to central concentrated load application, r_t.

Consider the strengthened beam as a statically indeterminate structure to one degree of indeterminacy, as shown in figure D.1.

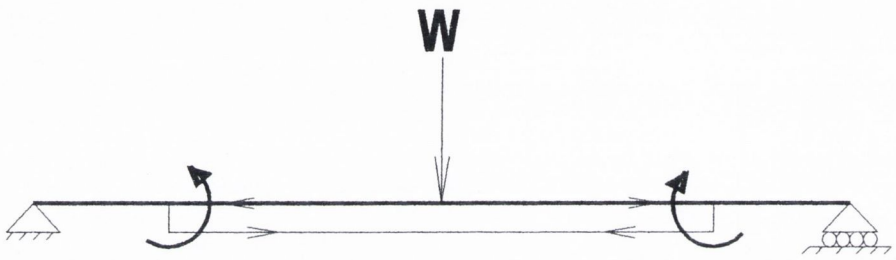

Figure D.1: Configuration of statically indeterminate strengthened beam.

By cutting the tendon, consider the "released" structure, as shown in figure D.2.

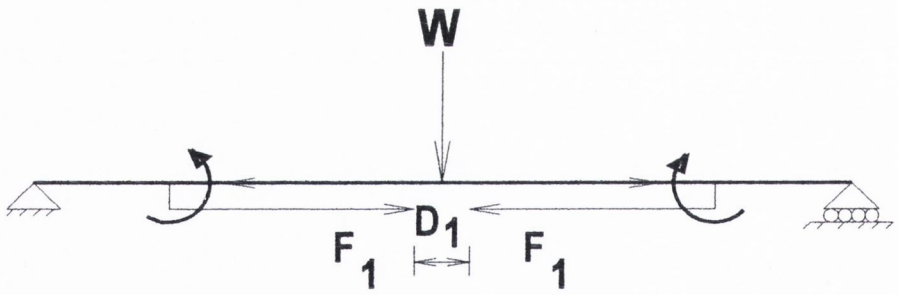

D_1= the discontinuity of the cut tendon arising from the central concentrated load W

F_1= the redundant force in the tendon.

Figure D.2: Configuration of the released structure.

The discontinuity, D_1, will be due to the strain that exists when on a plane extending down to the eccentricity of the tendons.

Consider Navier's equation (Morely, 1938),

$$\frac{M}{I} = \frac{E}{R} = \frac{\sigma}{y_{\max}} = \frac{\sigma}{e} \qquad \text{(D.1)}$$

where:

M= the bending moment

I= the section moment of inertia

E= the material elastic modulus

R= the radius of curvature of the beam

σ= the flexural bending stress

y_{max} = the outermost fibre from the beam's neutral axis

e = the tendon eccentricity from the beam's neutral axis.

or

$$\sigma = \frac{Me}{I} \qquad \text{(D.2)}$$

But, from Hook's law (Morley, 1938)

$$\varepsilon = \frac{\sigma}{E} \qquad \text{(D.3)}$$

Where:

ε = the strain of the material (that is, change in length/original length)

combining equations D.1 and D.3 gives

$$\Rightarrow \varepsilon = \frac{Me}{EI} \qquad \text{(D.4)}$$

Consider the case of a simply supported beam under a central concentrated load shown in figure D.3.

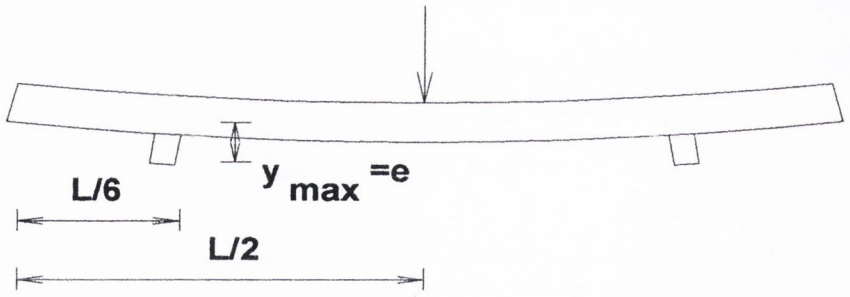

Figure D.3: Dimension for strain calculation at tendon eccentricity between the tendon levers (D_1).

As the configuration is symmetrical, the total strain at the beam soffit between the tendon levers can be expressed as twice the strain between L/6 and L/2 as shown in figure D.3: In the following expression, use substitution from equation D.4.

$$D_1 = 2\int_{\frac{l}{6}}^{\frac{l}{2}} \varepsilon .dx = 2\int_{\frac{L}{6}}^{\frac{L}{2}} \frac{Me}{EI}.dx$$

and,

$$M = \frac{W}{2}x$$

$$D_1 = \frac{We}{EI}\int_{\frac{L}{6}}^{\frac{L}{2}} x.dx$$

$$D_1 = \frac{WeL^2}{9\,EI} \qquad \text{(D.5)}$$

Now calculate F_1, the force required to "close" the gap on the released tendons, apply a unit force at the cut tendons (both redundant force directions are considered positive) as shown in figure D.4.

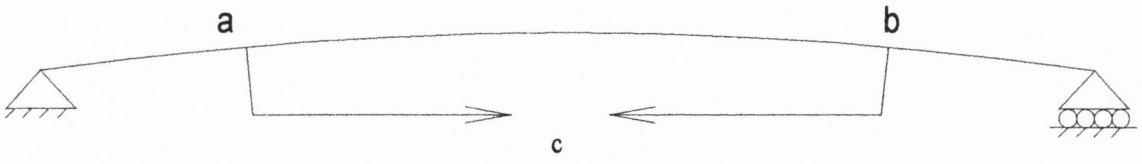

Figure D.4: Unit force applied to released structure.

Considering, f_{11}, the displacement at "c" due to a unit force. Four components are considered for this displacement, as follows:

1. Axial extension of tendons under a unit load

$$\frac{L_t}{E_t A_t} \tag{D.6}$$

where L_t = length of tendons, E_t = Elastic modulus of tendons and A_t = the cross-sectional area of tendons.

2. Axial shortening of the beam under a unit load (between the tendon levers only)

$$\frac{L_t}{E_b A_b} \tag{D.7}$$

where E_b = the elastic modulus of the beam and A_b = cross-sectional area of the beam.

3. Considering a rigid body at the levers, the horizontal lever displacement due to rotational displacement at "a" and "b" as shown in figure D.4 are θ_a and θ_b respectively.

   Using the general expression for the bending moment (Morely, 1938);

   $$\frac{-M}{EI} = \frac{d^2y}{dx^2}$$

   where M is a constant and equal to $P_t e$.

   Integrating once for the slope, $\frac{dy}{dx}$,

   $$\frac{dy}{dx} = \frac{-1}{EI}[Mx + A]$$

Let position "a" in figure D.4 be the origin, thus, at mid-span (L/3) the slope is zero which gives:

$$A = \frac{ML}{3EI}$$

at the origin, $x=0$, (that is, at the tendon lever) the slope is:

$$\frac{dy}{dx} = \frac{ML}{3EI}$$

in this case, $M=1.e$, (that is, a unit force applied to the tendons), therefore,
The slope at a (and also equal and opposite at b) is:

$$\theta_a = \frac{eL}{3\ EI} = -\theta_b \qquad \text{(D.8)}$$

where the symbol, θ, is the slope of beam (subscript denotes the location along the beam)

considering both tendon lever ends where the tendon is attached, the total horizontal component of displacement (that is, the rigid body extension induced in the tendons), δ_h, is:

$$2\delta_h = 2e \sin \theta_a = 2e \sin \frac{el}{3EI} \qquad \text{(D.9)}$$

where l is the lever length.

4. The cantilever displacement of the tendon levers for a unit force is given by,

$$\frac{2\ L_l^3}{3\ E_l I_l} \qquad \text{(D.10)}$$

where L_l= the length of the tendon lever, E_l = the modulus of elasticity of the tendon lever steel and I_l = the second moment of area of the tendon's cross section.

By letting (in this case) L_t = 2L/3 and using equations D.5-D.9, f_{11} (that is, the displacement at ordinate 1 (D1) due to a unit force (F1) as shown in figure D.2) can be expressed as follows:

$$f_{11} = \frac{2L}{3E_t A_t} + \frac{2L}{3E_b A_b} + 2\left\{ e\sin\left(\frac{eL}{3E_b I_b}\right) + \frac{L_l^3}{3E_l I_l}\right\} \tag{D.11}$$

The general flexibility equation is (Ghali, et al. 1997)

$[f]\{F\} = \{D\}$

where:

$[f]$ = the flexibility matrix

$\{F\}$= the force vector

$\{D\}$ = the displacement vector

then

$F_1 = [f_{11}]^{-1}\{D\} = P_f$

where P_f is the resulting tendon force arising from a central concentrated load,

$\Rightarrow$ (in the case when the initial tendon force, P_I , =0)

$$P_f = \frac{\dfrac{WeL^2}{9E_b I_b}}{\dfrac{2L}{3E_t A_t} + \dfrac{2L}{3EA} + 2\left\{ e\sin\left(\dfrac{eL}{3EI}\right) + \dfrac{l_l^3}{3E_l I_l}\right\}}$$

and when W=1$^{\#}$ (a unit force) this yields the expression for r_t (the rate of tendon force increase with respect to central concentrated load application as follows:

$$r_t = \frac{\dfrac{eL^2}{9E_b I_b}}{\dfrac{2L}{3E_t A_t} + \dfrac{2L}{3E_b A_b} + 2\left\{ e\sin\left(\dfrac{el}{3E_b I_b}\right) + \dfrac{L_l^3}{3E_l I_l}\right\}} \tag{D.12}$$

Appendix E

Mid-span deflection due to counter-moments

In order to calculate the mid-span deflection with a central concentrated load and counter-moments applied, it is required that an expression be developed for the component of deflection due to counter-moments.

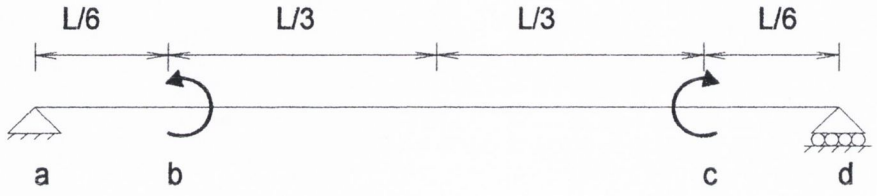

Figure E.1: Notation used for pre-camber deflection calculations.

Let b = origin:

$$\phi_1 = \left[M_{(x)} = 0\right] for\ , a \leq x < b$$

$$\phi_2 = \left[M_{(x)} = -M\right] for\ , b \leq x \leq c$$

$$\phi_3 = \left[M_{(x)} = 0\right] for\ , c < x \leq d$$

$$\frac{d^2y}{dx^2} = \frac{-M}{EI} = \int_b^a 0 .dx + \int_b^c M .dx + \int_c^d 0 .dx$$

$$\int_b^c \frac{d^2y}{dx^2}.dx = \frac{-1}{EI}\int_b^c M .dx$$

$$\frac{dy}{dx} = \frac{-1}{EI}\left[Mx\right]_0^{L/3} \Rightarrow \frac{dy}{dx} = \frac{-ML}{3EI} \qquad \text{(E.1)}$$

which is, the slope of the beam at the tendon levers

$$\int \frac{dy}{dx}.dx = y = \frac{-M}{EI}\left[\frac{Lx}{3}\right]_0^{L/3} = \frac{-ML^2}{9EI} \qquad \text{(E.2)}$$

which is, the component of deflection at mid-span due to the counter-moments.

Appendix F.1: Design checks for 686x254x125UB

Design calculations to BS 5950: parts 1 and 2

F.1.1 Lateral torsional buckling load of un-strengthened beam

Assume laboratory conditions: Beam rests on simple supports under a central concentrated load applied to the top flange with no bolted end connections and no lateral restraint between supports. All subsequent terms in square brackets are references extracted from the BS5950:parts 1 and 2 design codes for steel sections.

Destablizing load:

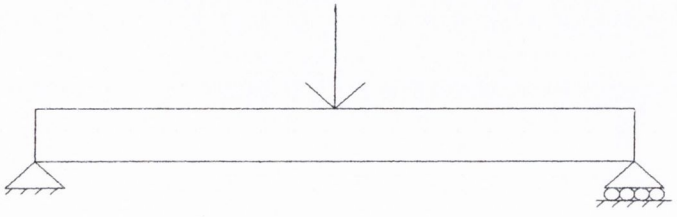

$$L_{LE} = 1.4L_{LT} + 2D = 9756mm \qquad \text{[table 13]}$$

Classify section: [table 11]

$$p_y = 265N/mm^2 \quad \text{[table 9]} \qquad \text{[3.1.0]}$$

$$\varepsilon = \sqrt{\frac{275}{p_y}} = 1.018$$

$$\frac{b}{T} = \frac{120.65}{16.2} = 7.44 < 9\varepsilon$$
$$\frac{d}{t} = \frac{615.1}{11.7} = 52.6 < 80\varepsilon \qquad \text{[table 11]}$$

Hence, section is plastic.

F.1.2 Lateral torsional buckling moment

$$M_b = p_b S_x \qquad \text{[4.3.6.4]}$$

where,

$S_x = 3994cm^3$

p_b= the permissible bending stress.

and:

$$\lambda_{LT} = uv\lambda_y\sqrt{\beta} \qquad [4.3.6.7]$$

β=1 (plastic section) [4.3.6.9]

$\Rightarrow \lambda_{LT} = uv\lambda_y$

$$\lambda_y = \frac{L_E}{r_y} = \frac{9756}{52.4} = 186.2$$

$u = 0.862$ (section tables)
$v = 0.85$ [table 19]

$\lambda_{LT} = 0.862x0.85x186.2x1.018 = 138.8$

$p_b = 76mm^2$ [table17]

$M_b = 76x3994000 = 303kNm$

If $M = \frac{WL}{4} \Rightarrow W_{ult} = 202.7kN$

F.1.3 Section shear capactiy

$$F_v \prec 0.6P_v \qquad [4.2.3]$$

where,
F_v= the maximum shear force due to loading
P_v= the section shear capacity

$P_v = 0.6p_y tD = 0.6x265x16.2x677.9 = 1746kN$

$F_v = \frac{202.7}{2} = 101.35 < 1746kN$ O.K. (low shear)

F.1.4 Local web bearing capacity

<u>At mid-span:</u>

$$P_{bw} = (b_1 + nk)t.p_{yw} \qquad [4.5.2.1]$$

where,

$n = 5$
k = T+r =16.2+15.2 =31.4mm
b_1 = t+1.6r+2T = 68.4mm [4.5.1.3]
p_{yw} = 265N/mm^2

$$P_{bw} = (68.4 + 5x31.4)x117\ x265 = 698\ kN > 202.7kN \quad \text{O.K.}$$

No stiffeners required as web bearing capacity is greater than applied load (202.7kN).

At end supports:

Again,

$$P_{bw} = (b_1 + nk)t.p_{yw}$$

where,

$n = 2 + 0.6b_e / k$ and must be < or = 5 [4.5.2.1]

where,

b_e= 0 (that is, the length of the stiff bearing to the closest end of the beam)

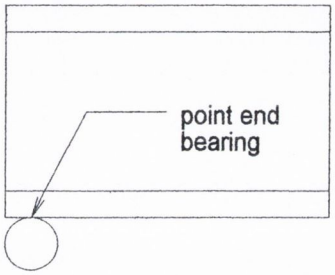

Figure F.1: Detail of end support bearing.

Therefore, n =2.

$P_{bw} = (68.4 + 2 + 2x31.4)x11.7x265 = 406.7kN > 110kN$

No stiffeners required as bearing capacity is greater than W/2 (101.35kN).

F.1.5 Local buckling stiffness of web

At end supports:

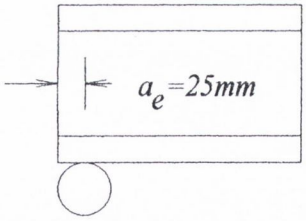

Figure F.2: Detail of end support distance, a_e.

$a_e < 0.7d = 157.9mm$

$$\Rightarrow P_x = \frac{a_e + 0.7d}{1.4d} \bullet \frac{25\varepsilon.t}{\sqrt{(b_1 + nk)d}} \bullet P_{bw} = 218kN > 101.35kN \quad [4.5.3.1]$$

No stiffeners required local web bearing capacity is greater than W/2.

At mid-span:

$a_e = 3000mm > 0.7d = 157.9mm$

$$\Rightarrow P_x = \frac{25\varepsilon t}{\sqrt{(b_1 + nk)t}} \bullet P_{bw} = 325kN > 220kN \qquad [4.5.3.1]$$

No stiffeners required as local web bearing capacity at mid-span is greater than W.

Appendix F.2: Design checks for 254x254x132UC

Design calculations to BS 5950: parts 1 and 2

F.2.1 Lateral torsional buckling load of un-strengthened beam

Assume laboratory conditions: Beam rests on simple supports under a central concentrated load applied to the top flange with no bolted end connections and no lateral restraint between supports. All subsequent terms in square brackets are references extracted from the BS5950:parts 1 and 2 design codes for steel sections.

Destablizing load:

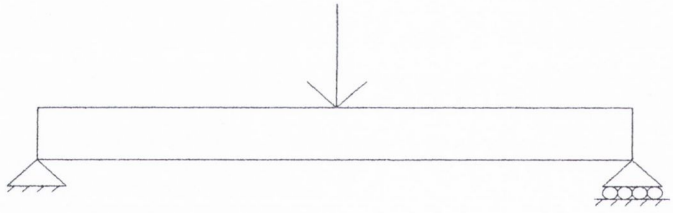

$$L_{LE} = 1.4L_{LT} + 2D = 8953mm \qquad [table\ 13]$$

where ;
L_{LT} , is the laterally unrestrained span
D , is the overall depth of the member

Classify section: [table 11]

$$p_y = 265N/mm^2 \qquad [table\ 9] \qquad [3.1.0]$$

$$\varepsilon = \sqrt{\frac{275}{p_y}} = 1.018$$

$$\frac{b}{T} = \frac{123}{25.3} = 4.86 < 9\varepsilon$$
$$\frac{d}{T} = \frac{225.7}{15.3} = 14.75 < 80\varepsilon$$ [table 11]

Hence, section is plastic.

F.2.2 Lateral torsional buckling moment

$$M_b = p_b S_x$$ [4.3.6.4]

where,

$S_x = 1870cm^3$

p_b= the permissable bending stress.

and:

$$\lambda_{LT} = uv\lambda_y\sqrt{\beta}$$ [4.3.6.7]

β=1 (plastic section) [4.3.6.9]

$\Rightarrow \lambda_{LT} = uv\lambda_y$

$$\lambda_y = \frac{L_E}{r_y} = \frac{8953}{66.9} = 133.8$$

$u = 0.85$ (section tables)

$v = 0.57$ [table 19]

$\lambda_{LT} = 0.85x0.57x133.8x1 = 64.8$

$p_b = 197N/mm^2$

$M_b = 197x1870000 = 368.4kNm$

If $M = \frac{WL}{4} \Rightarrow W_{ult} = 245kN$

The maximum buckling load is 245kN for the un-strengthened beam.

F.2.3 Section shear capactiy

$$F_v \prec 0.6P_v$$ [4.2.3]

where,

F_v= the maximum shear force due to loading
P_v= the section shear capacity

$$P_v = 0.6 p_y t D = 0.6x265x15.3x276.3 = 1120kN$$

$$F_v = \frac{220.7}{2} = 110.35 < 1120kN \quad \text{O.K. (low shear)}$$

F.2.4 Local web bearing capacity

At mid-span:

$$P_{bw} = (b_1 + nk)t.p_{yw} \qquad [4.5.2.1]$$

where,

$n = 5$
$k = T+r = 25.3+12.7 = 38mm$
$b_1 = t+1.6r+2T = 86.2mm$ [4.5.1.3]
$p_{yw} = 265N/mm^2$

$P_{bw} = (86.2 + 5x38)x15.3x265 = 1119kN > 220kN$ O.K.

No stiffeners required web bearing capacity is greater than applied load (220kN).

At end supports:

Again,

$$P_{bw} = (b_1 + nk)t.p_{yw}$$

where,

$n = 2 + 0.6b_e / k$ and must be < or = 5 [4.5.2.1]

where,

b_e= 0 (that is, the length of the stiff bearing to the closest end of the beam)

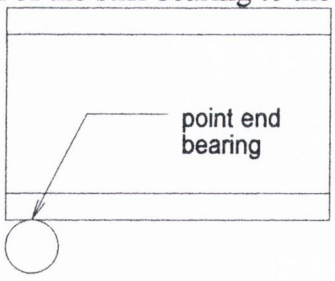

Figure F.3: Detail of end support bearing.

Therefore, n =2.

$P_{bw} = (86.2 + 2x38)x15.3x265 = 657kN > 110kN$

No stiffeners required as bearing capacity is greater than W/2 (110kN).

F.2.5 Local buckling stiffness of web

At end supports:

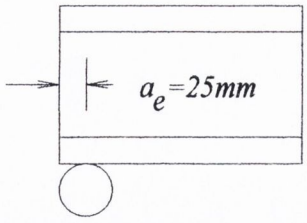

Figure F.4: Detail of end support distance, a_e.

$a_e < 0.7d = 157.9mm$

$$\Rightarrow P_x = \frac{a_e + 0.7d}{1.4d} \bullet \frac{25\varepsilon.t}{\sqrt{(b_1 + nk)d}} \bullet P_{bw} = 581kN > 110kN \qquad [4.5.3.1]$$

No stiffeners required local web bearing capacity is greater than W/2.

At mid-span:

$a_e = 3000mm > 0.7d = 157.9mm$

$$\Rightarrow P_x = \frac{25\varepsilon.t}{\sqrt{(b_1 + nk)t}} \bullet P_{bw} = 1714kN > 220kN \qquad [4.5.3.1]$$

No stiffeners required as local web bearing capacity at mid-span is greater than W.

F.2.6 Local section capacity:

Assume a tendon force of 1200kN (that is, the tendons are within their elastic stress range) with a maximum allowable load applied to the beam:

$$\frac{F_c}{A_g} + \frac{M_x}{M_{cx}} + \frac{M_y}{M_{cy}} \leq 1 \qquad [4.8.3.2]$$

Where,
F_c = the tendon force
A_g = the gross cross-sectional area of the section
p_y = the yield stress
M_x= the moment about the major axis
M_y = the moment about the minor axis
M_{cx} = the major axis moment capacity
M_{cy} = the minor axis moment capacity

$M_{cx} = p_y S_x$ and $M_{cy} = p_y S_y$ (low shear) [4.2.5.2]

and must be less than $1.2 p_y Z = 513 kNm$ about major axis and $183.2 kNm$ about minor axis (simple supports) [4.2.5.1]

$M_{cx} = 265x1870000 = 495.5 kNm < 513 kNm$

$M_{cy} = 265x7530000 = 199.5 kNm > 183.2 kNm$ (use $183.2 kNm$).

$$\frac{1200x10^3}{16800x265} + \frac{M_x}{495.5x10^6} + \frac{0}{183.2x10^6} \leq 1 \qquad [4.8.3.2]$$

$\Rightarrow M_x$ (maximum net moment) $= 362.8 kNm$

The tendons will provide a beneficial moment of 205.3kNm (that is, $1200kN$ x 0.17m), thus, the available local section moment capacity about the major axis is:

$362.8 + 205.3 = 569 kNm$

$$M = \frac{WL}{4} \Rightarrow W_{ult} = 378.6 kN$$

$P_i = 1200 - 0.525x378.6 kN = 1001.2 kN$

where, $r_t = 0.525$kN/kN

F.2.7 Member buckling resistance (exact method)

In plane buckling:

Considering firstly the section with moments about the major axis (that is, no tendon rupture which would induce a moment about the minor axis also.)

For major axis in plane buckling :

$$\frac{F_c}{P_{cx}} + \frac{m_x M_x}{M_{cx}} \left(1 + \frac{F_c}{P_{cx}} \right) \leq 1 \qquad [4.8.3.3.2]$$

where,

P_{cx} = the member compression resistance considering buckling about the major axis only
m_x = the reduction factor for major axis flexural buckling

Calculate P_{cx}:

$$L_E = 1.0L = 6000mm \qquad [table 22]$$

$r_x = 116mm$

$$\lambda_x = \frac{6000}{116} = 51.7$$

$P_{cx} = p_c A_g$

$p_c = 235N/mm^2$ [table 24, curve a]

$P_{cx} = 235x16800 = 3948kN$

$m_x = m_y = 0.9$ [table26] [4.8.3.3.4]

$$\frac{425x10^3}{3948x10^3} + \frac{0.9xM_x}{M_{cx}}\left(1 + \frac{1425x10^3}{3948x10^2}\right) \leq 1 \qquad [4.8.3.3.2]$$

$\Rightarrow M_x \leq 258.4kNm$ (maximum net moment),

Available moment capacity for the tendons within the overall beam depth is (allowing for counter moment of 139.6kNm):

$258.4 + 139.6 = 389kNm$

$\Rightarrow W_{ult} = 265.3kN$

Available moment capacity for the thick-wall tube and tendon application is (allowing for counter moment of 242.3kNm):

$258.4 + 205.3 = 463.7kNm$

$\Rightarrow W_{ult} = 309.2kN$

Out-of-plane buckling:

For out of plane bucking the following equation must be satisfied:

$$\frac{F_c}{P_{cy}} + \frac{m_{LT}M_{LT}}{M_b} \leq 1 \qquad [4.8.3.3.3]$$

Calculate P_{cy}:

$$\lambda_y = \frac{L_E}{r_y} = \frac{6000}{66.9} = 89.6$$

$p_c = 161N/mm^2$ (table 24, curve b)

$P_{cy} = 161x16800 = 2704kN$

$m_{LT} = 0.85$ (table 18) [4.8.3.3.4]

Therefore, moment capacity (net) about the major axis is:

$$\frac{1425x10^3}{2704x10^3}+\frac{0.85M_{LT}}{331x10^6}\leq 1 \qquad [4.8.3.3.3]$$

$\Rightarrow M_{LT} \leq 184.3kNm$ (net moment capacity)

Available moment capacity for the tendons within the overall beam depth is (allowing for counter moment of 139.6kNm):
$184.2+139.6=323.8kNm$

$\Rightarrow W_{ult}=215.8N$

and

$P_i = 1425 - 0.105\,x215.8 = 1403.3kN$

Available moment capacity for the thick-wall tube and tendon application is (allowing for counter moment of 242.3kNm):
$184.2+242.3=389.5kNm$

$\Rightarrow W_{ult}=284.3kN$

and

$P_i = 1200 - 0.525\,x284.3 = 1050.7kN$

F.2.8 Tendon rupture:

The ultimate moment capacity of the two sections shown in figure H.3 were considered after tendon rupture. With both cases the beam has axial compressive force with moments about major and minor axes.

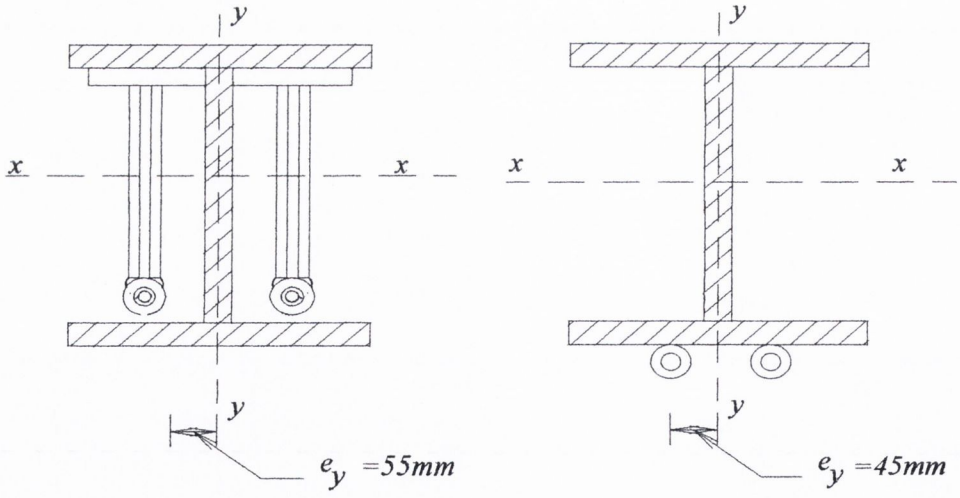

(a) Earlier configuration (b) Revised configuration

Figure F.5: The two tendon configurations considered.

Lateral torsional buckling about minor axis with moment about both axes

The following equation must be satisfied when checking minor axis lateral torsional buckling capacity with compressive axial force and moments about both axes are present.

$$\frac{F_c}{P_{cy}} + \frac{m_{LT}M_{LT}}{M_b} + \frac{m_y M_y}{M_{cy}}\left(1 + 0.5\frac{F_c}{P_{cy}}\right) \leq 1 \qquad [4.8.3.3.3]$$

$M_{cy} = 265x878000 = 232.6kNm$

$F_c = \frac{1200}{2} = 600kN$

For the tendon and lever within the overall beam depth application:

$M_{(tendon)x} = \frac{1200x0.098}{2} = 58.8kNm$

$M_{(tendon)y} = \frac{1200x0.055}{2} = 33kNm$

$$\frac{600x10^3}{2704x10^3} + \frac{0.85M_{LT}}{331x10^6} + \frac{0.9x33x10^6}{232.6x10^6}\left(1 + \frac{0.5x600x10^3}{2704x10^3}\right) \leq 1 \quad [4.8.3.3.3]$$

$\Rightarrow M_{LT} = 248.1kNm$ (net)

Available moment capacity allowing for counter moment (69.8kNm)

$248.1 + 68.9 = 306.9kNm$

$\Rightarrow W_{ult} = 204.6kN$

For the revised tendon configuration:

$M_{(tendon)x} = \frac{1200x0.17}{2} = 102kNm$

$M_{(tendon)y} = \frac{1200x0.045}{2} = 27kNm$

$$\frac{600x10^3}{2704x10^3} + \frac{0.85M_{LT}}{331x10^6} + \frac{0.9x27x0.045x10^6}{232.6x10^6}\left(1 + \frac{600x10^3}{2704x10^3}\right) \leq 1 \qquad [4.8.3.3.3]$$

$\Rightarrow M_{LT} = 301.1kNm$ (net)

Available moment capacity allowing for counter moment (121.1kNm)

$301.1 + 102 = 403.1kNm$

$\Rightarrow W_{ult} = 268.7kN$

In the event of a tendon rupture both configurations are adequate to withstand the loading to be applied in the laboratory testing (200kN maximum).

Appendix G

Weld designs for stiffeners and tendon levers

Any reference in square brackets in this appendix, refer to BS5950:part 1: 2000 and references in parenthesis for this appendix refer to the Steel Designers' Manual (2005).

Considering the lever weld design subjected to a moment and shear force applied. The design code for welding states that when considering weld design, the sum of all stresses due to forces and moments transmitted by welds must not exceed the design stress, p_w , [6.8.7.2]. Figure G.1 shows the tendon lever welds considered.

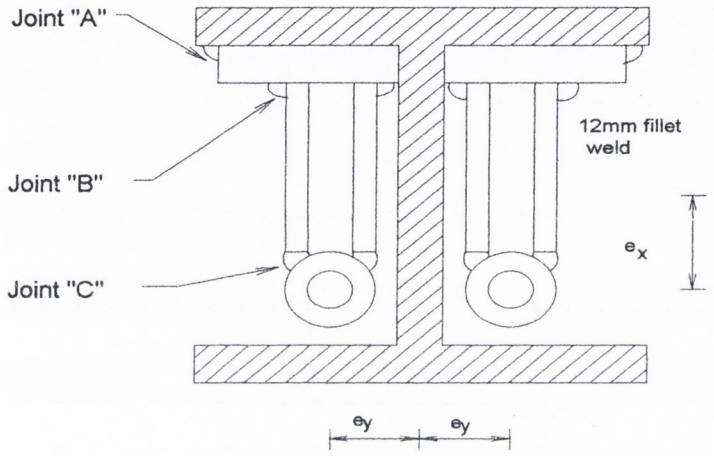

Figure G.1: Weld joints A, B, and C considered in lever design.

Assume tendon force per lever of 600kN (in excess of tendon strength). Figure G.2 shows an elevation of the stiffening plate welded to the underside of the upper flange at the levers.

Design strength for weld: $p_w = 220\text{N/mm}^2$ [table 37]

G.1: Upper flange stiffening plate.

Calculate shear stress:

$$\tau = \frac{600x10^3}{(500+2x100)x12.6} = 39.7N/mm^2$$

Calculate bending stress: (the moment imparted to the plate via the tendon lever about X-X, M_w , 0.19x600=114kNm)

Modulus of weld about axis X-X; (Steel Designers' Manual (2005): from appendix entitled "*capacities for fillet welds*")

$$Z_{xx} = 630 + 578 = 1208cm^3 \qquad \text{(table: welds in plane of force)}$$

$$\sigma = \frac{M_w}{Z_{xx}} = 99.4N/mm^2$$

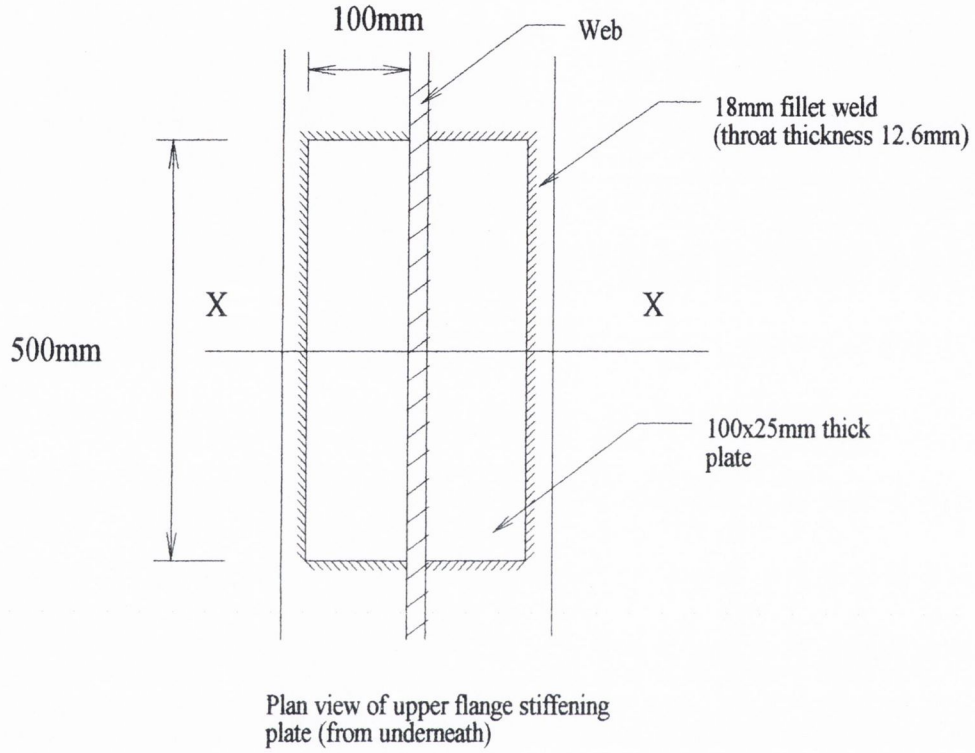

Plan view of upper flange stiffening plate (from underneath)

Figure G.2: Plan view of upper flange stiffening plate.

Therefore:

$\tau + \sigma = 139.1N/mm^2 \prec 220N/mm^2$ (sum of stresses is less than p_w) [6.8.7.2]

G.2: Vertical plates connecting upper flange plate to thick-wall tubes.

Figure F.3 shows a plan sectional view through the vertical lever plates with 15mm fillet welds joining them to the upper flange plate.

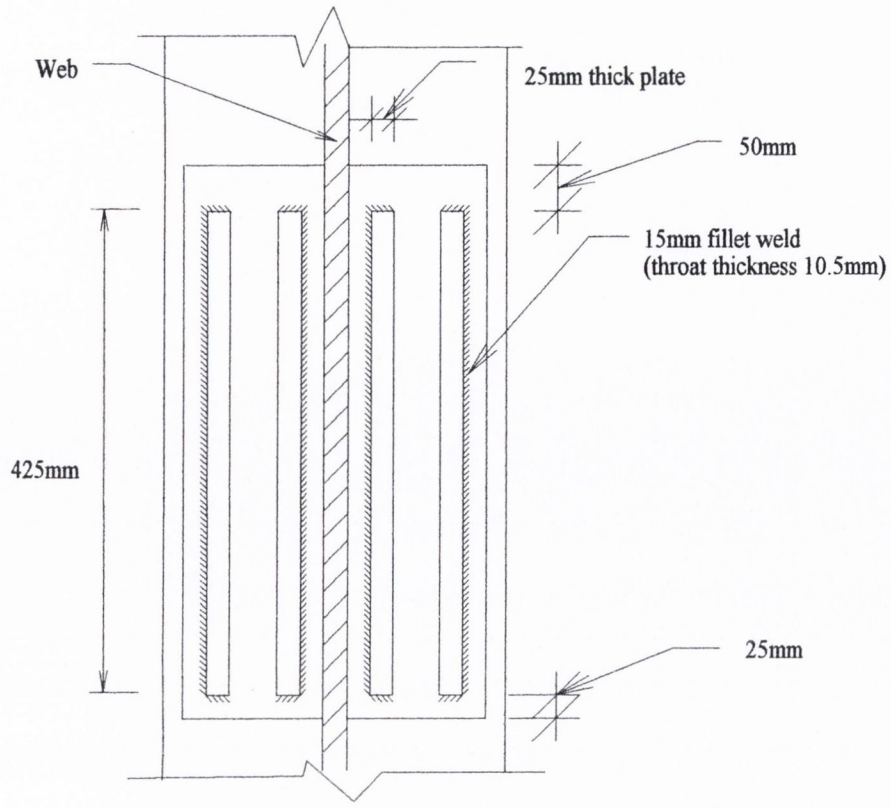

Figure G.3: Section through vertical lever plates connected to the upper flange plate.

Calculate shear stress in welds:

$$\tau = \frac{600x10^3}{(2x425 + 4x25)x10.5} = 60.1N/mm^2$$

Calculate maximum bending stress:

$Z_{xx} = 632.1 + 223.6 = 855.7cm^3$ (table: welds not in plane of force)

Moment imparted to upper flange plate from vertical levers (see figure G.4):

Therefore:

$$M_w = 0.165x600 = 99kNm$$

$$\sigma = \frac{M_w}{Z_{xx}} = 115.7N/mm^2$$

$\tau + \sigma = 175.8N/mm^2 \prec 220N/mm^2$ (OK, sum of stresses is less than p_w). [6.8.7.2]

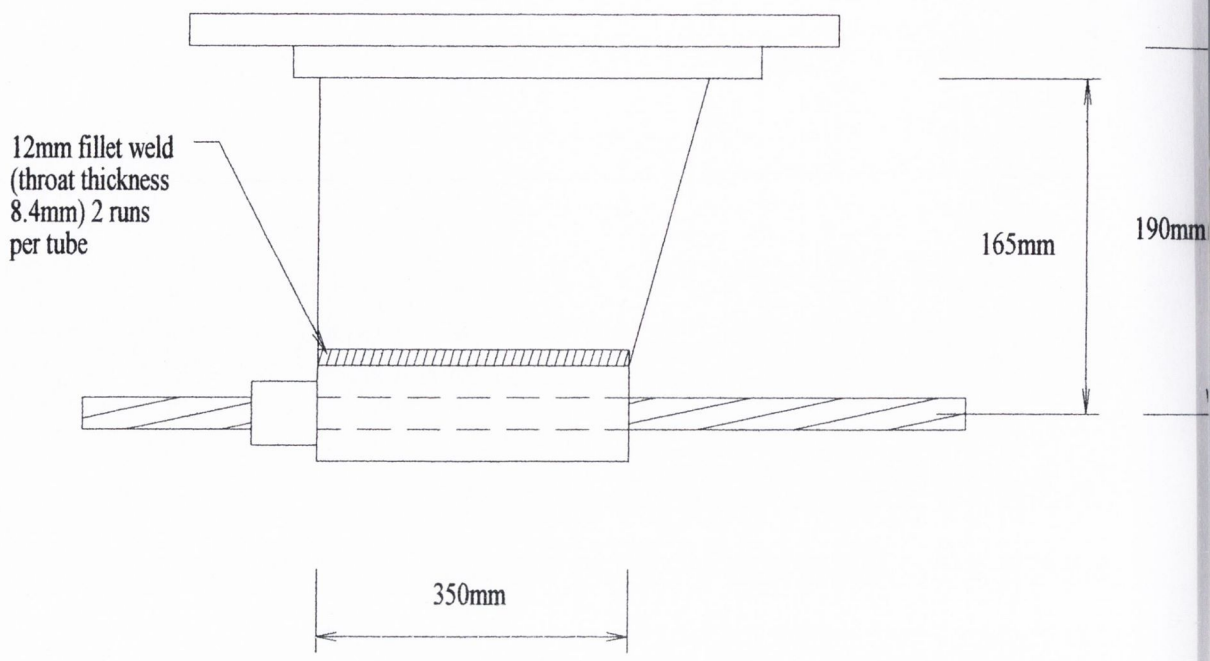

Figure G.4: Side elevation of lever configuration

G.4 Longitudinal welds joining thick-wall tube to vertical lever.

Calculate longitudinal weld capacity:

P_w= 220N/mm^2 [table 37]

Weld capacity = $2x350x220x8.4 = 1293.6kN \succ 600kN$

G.3 Outer edge flange stiffeners

Outer edge flange stiffeners required to engaged both flanges in counter moment distribution.

Figure G.5 shows a view of the distorted upper flange without the external stiffeners. The moment generated by the tendon lever is resisted by the couple shown acting on the upper flange. Consider the moment transferred to the upper flange plate (120kNm) due to the tendon lever acting on the elevated view shown in figure G.5. The resultant couple transferred to the plate is a couple of magnitude 480kNm acting at a lever arm of 250mm (that is, the pressure centroids lie above and below the elevated plate neutral axis as shown in figure G.6)

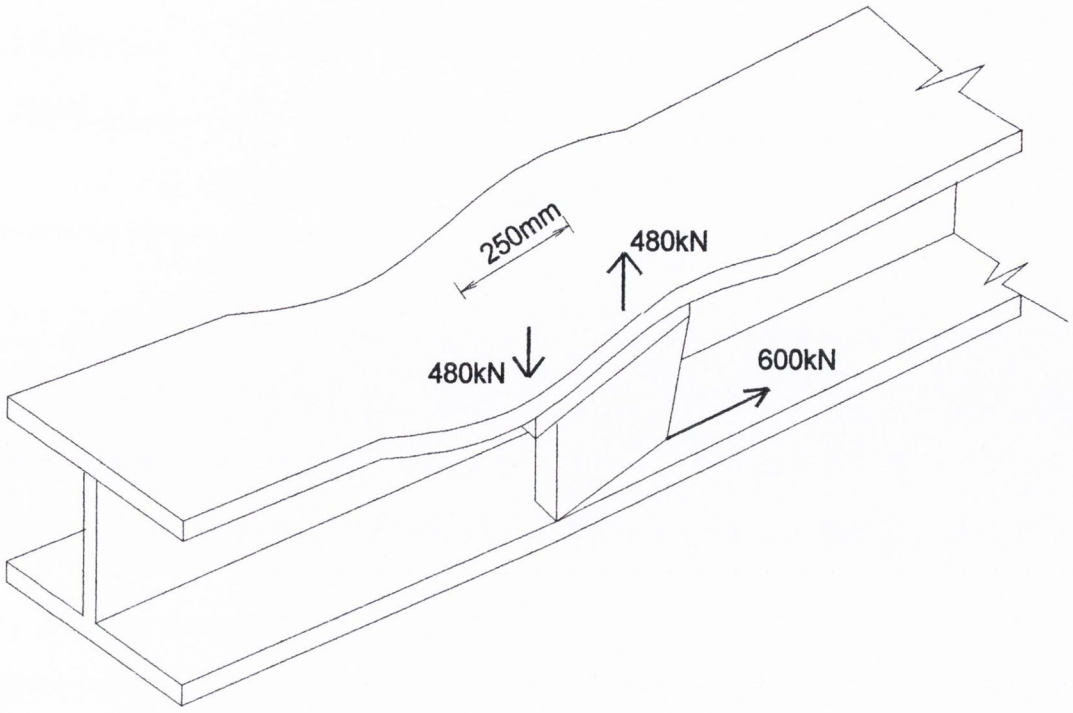

Figure G.5: Couple acting on upper flange due to tendon lever moment.

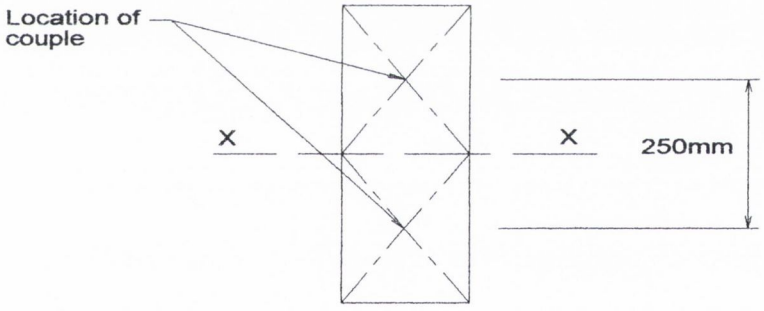

Figure G.6: View of elevated upper flange plate showing the location of the resulting couple acting on the plate due to the moment generated by the tendon lever.

Therefore: force to be resisted by each stiffener is 480kN
Using 100mmx25mm outer plates:

Calculate axial capacity of stiffener,

$p_y = 265 N/mm^2$ [table 9]

$150x25x265 = 993kN \succ 480kN$ (axial capacity of stiffener OK)

Weld capacity for weld at stiffener ends

p_w= 220N/mm^2 [table 37]

Therefore, as shown in Figure G.7:

$(150+18x2)x220x12.6 = 515.6kN \succ 480kN$ (weld at plate ends OK).

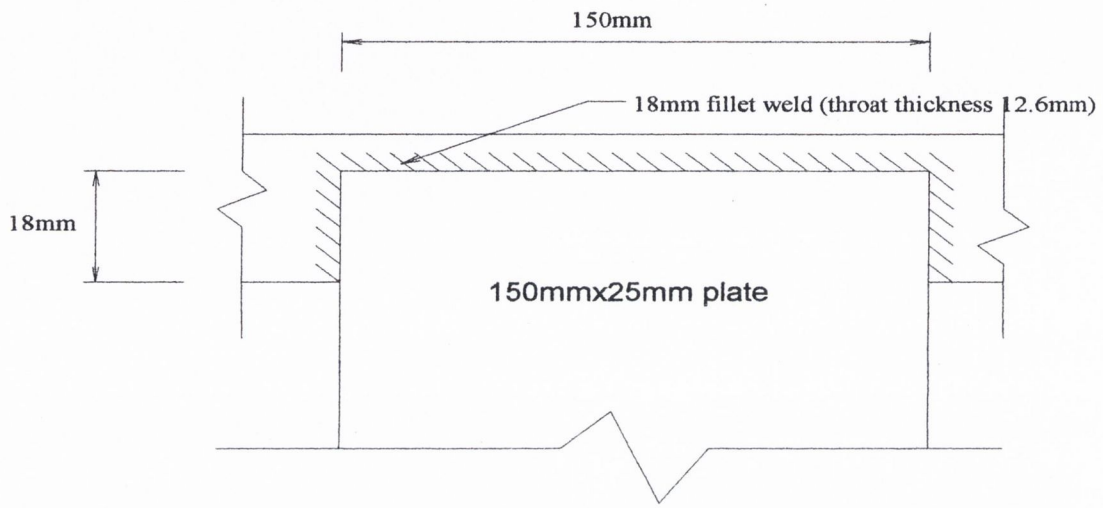

Figure G.7: Outer edge flange stiffening plate end weld details.

Appendix H

H.1 Calculate I_x and I_y of plated section:

y_e=the distance from the lowermost section fibre to the location of the elastic neutral axis.

Consider the section in figure X.1,

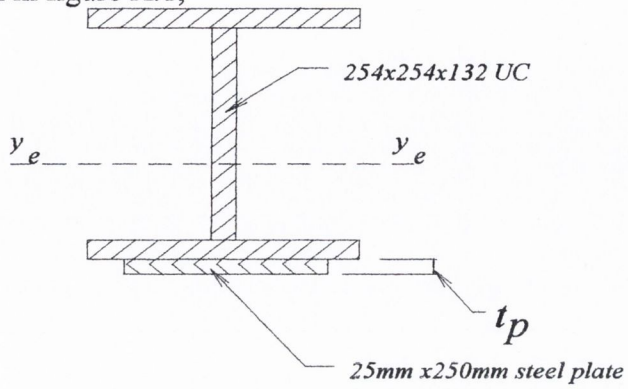

Figure H.1: Steel plated section with elastic neutral axis.

Using first moments of area it can be shown that y_e=99.8mm, (and A=23050mm^2) from which, the second moment of area, I_{xx} , can be calculated as 34153cm^4 . Similarly the second moment of area about the minor axis, I_{yy} , can be calculated as 10785cm^4.

Calculate r_y (radius of gyration about minor axis)

(Steel Construction Institute-Designers' manual)

$$r_y = \left[\frac{I_y}{A}\right]^{\frac{1}{2}} = 6.84cm \qquad \text{(H.1)}$$

H.2 Calculate plastic section modulus about major axis, S_x:

The location of the plastic section neutral axis will be lower than the elastic (see figure I.2).

Calculate, Y_p the plastic neutral axis.

A_g= the gross cross-sectional area of the section

A_p= the cross-sectional area of the plate

$A_g = 16800 + (25x250) = 23050mm^2$

Calculate half the area less the area of the stiffening plate:

$\frac{23050}{2} - 250x25 = 5275mm^2$ (giving the area that lies beneath the plastic neutral axis in the lower flange)

Therefore, the location of the neutral axis measuring from the bottom of the beams' lower flange is,

$\frac{5275}{261.3} = 20.2mm$ (261.3=width of flange)

The axis that divides the sectional area into two equal amounts is 45.2mm from the strengthened beam soffit.

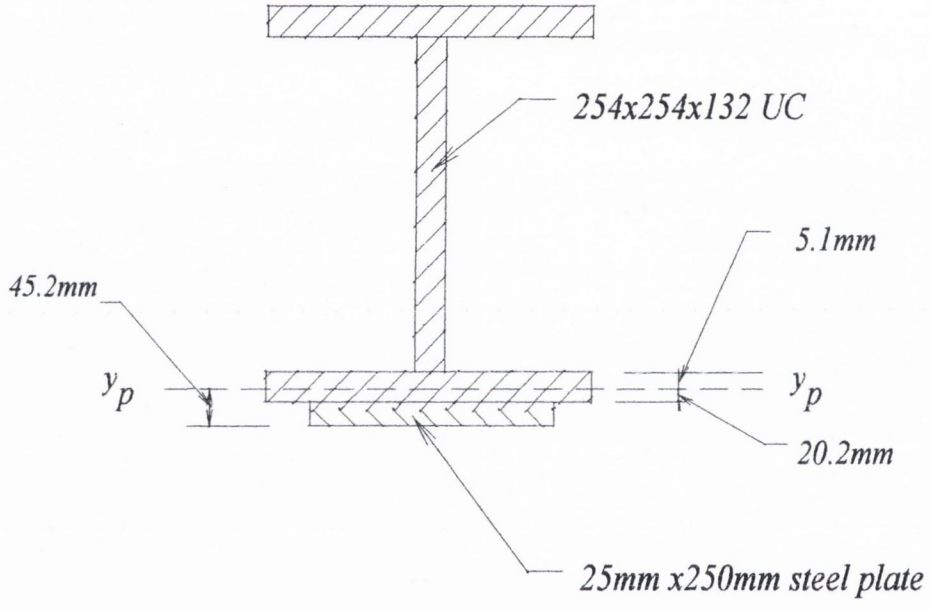

Figure H.2: Steel plated section with plastic neutral axis.

$$y_p = 45.2mm \tag{H.2}$$

CalculateS_x:

$$S_x = \left\{ \int_0^{130.65} \int_{230.8}^{257.17} y.dy.dx + \int_0^{7.65} \int_{4.5}^{230.8} y.dy.dx + \int_0^{130.65} \int_{-20.8}^{4.5} y.dy.dx + \int_0^{125} \int_{-45.18}^{-20.8} y.dy.dx \right\}$$

$$S_x = 2\left\{130.65\left[\frac{257.17^2}{2} - \frac{230.8^2}{2}\right] + 7.65\left[\frac{230.8^2}{2} - \frac{4.5^2}{2}\right] + 130.65\left[\frac{4.5^2}{2} - \frac{20.8^2}{2}\right] + 125\left[\frac{-20.8^2}{2} - \frac{45.18^2}{2}\right]\right\}$$

$$S_x = 2281cm^3 \qquad \text{(H.3)}$$

H.3 Ultimate load for steel plated beam

As in the case of the un-strengthened beam the governing criteria for ultimate loading is lateral torsional buckling at mid-span (BS 5950:part 1:2000). Using a permissible stress of $p_y = 265\text{N/mm}^2$ [table 9] this implies that the section is plastic [table 11] and also a de-stabilising load is applied [table 13].

$$L_E = 1.4L_{LT} + 2D = 9003mm \qquad \text{[table 13]}$$

$$M_b = p_b S_x \qquad \text{[4.3.6.4]}$$

$$\lambda_{LT} = uv\lambda_y\sqrt{\beta} \qquad \text{[4.3.6.7]}$$

where:

$\beta = 1$

$v = 0.64$ [table 19]

For flanged sections symmetrical about minor axis only,

$$u = \left[I_y S_x^2 \gamma / A^2 H\right]^{\frac{1}{4}} \qquad \text{(Steel construction institute- Designers' manual)}$$

where:

$$\gamma = \left[1 - \frac{I_y}{I_x}\right] = 0.684$$

H= the warping constant from section tables is 1.19 dm^6

Therefore,

$$\underline{u = 0.93}$$

$\lambda_y = \frac{L_E}{r_y} = 131.6$. Hence $\lambda_{LT} = 77.5$ [4.7.2]

$p_b = 166.5N/mm^2$ [table 16, rolled sections] and, $M_b = p_b S_x = 379.8kNm$ [4.8.3.3.1]

$M_b = \frac{W_{ult}L}{4} \Rightarrow W_{ult} = 253.2kN$ (maximum central concentrated load)

$\Rightarrow 14.7\%$ increase in un-strengthened load (220kN).